Bioleaching of refractory primary copper sulfides using the metal/carbon catalysts

小山, 恵史

KYUSHU
UNIVERSITY

Bioleaching of refractory primary copper sulfides using the metal/carbon catalysts

by

Keishi OYAMA

Department of Earth Resources Engineering
Graduate School of Engineering
Kyushu University
Fukuoka, Japan

A thesis submitted to Kyushu University
for the degree of Doctor of Engineering

March 2020

Abstract

Recent serious depletion in copper (Cu)-grade of ore and increase in the contamination of arsenic (As) becomes an increasingly serious problem in the Cu mining industry, requiring the development of Cu exploitation process from As-bearing refractory copper minerals such as enargite (Cu_3AsS_4). Bioleaching, using the microbiological activity to extract metals from minerals, is considered as one of the promising technique, while this process still needs to be improved due to the slow Cu dissolution kinetics. This suggests the necessity of reaction accelerator such as a catalyst for faster Cu solubilization in order to satisfy the economic feasibility. This thesis is, therefore, consisted of two main purposes: screening of useful catalysts for bioleaching of refractory copper sulfides (**chapters 4**, **5**, and **6**; fundamental studies) and its application to practical conditions (**chapter 7**; application study).

In **chapter 1**, the background of enargite bioleaching using mesophiles/moderate thermophiles or thermophiles was overviewed. Siver-/Carbon-assisted bioleaching of chalcopyrite ($CuFeS_2$), which is also recognized as the refractory minerals, were also summarized to propose the possible catalyst that is assumed useful for enargite bioleaching.

In **chapter 2**, methodologies used in this work were described.

Prior to the bioleaching experiment, in **chapter 3**, the inhibitory effect of Cu and iron (Fe) ions on molybdenum blue method (usually employed as the colorimetric As determination method) was tested for the development of As detection method that is applicable to Cu sulfide leachate. The co-presence of solo metal (e.g. Fe^{2+}, Fe^{3+}, or Cu^{2+}) showed no inhibition to the As determination, while the large amount of mixed metals ions (25 mM Fe^{2+}, 25 mM Fe^{3+}, and 50 mM Cu^{2+}) slightly oxidized the As(III) to As(V), resulting in the underestimation of As(III) concentration. This oxidation ratio, however, remained negligibly small amount (only 4%), suggesting the applicability of the molybdenum blue method to Cu sulfide leachate for the analysis of the changes in As(III) concentration. In the following chapters, As(III) concentration was thus determined by this molybdenum blue method.

In **chapter 4**, the catalytic effect of silver on bioleaching of enargite concentrate was evaluated, and its underlying mechanisms were elucidated. Increasing addition of silver sulfide (Ag_2S) as a silver catalyst facilitates enargite dissolution, achieving 96% final Cu recovery in the presence of 0.04% Ag_2S. On the other hand, the dissolution of pyrite, co-existing in enargite

concentrate, was suppressed with the addition of Ag_2S due to (i) the E_h-reduction along with Ag_2S addition and (ii) preferential subjectivity of Ag_2S to the oxidation by Fe^{3+}, rather than pyrite, based on the difference in rest potential. Arsenic immobilization was also enhanced by Ag_2S addition, resulting in 56% immobilization of once-dissolved As from enargite as ferric arsenate. Solid residue analyses and thermodynamical calculation revealed that enargite dissolution was promoted via the combination of two different mechanisms: (i) the replacement of Cu in enargite structure with Ag ion in the solution, and (ii) enargite transformation into easily soluble intermediate, chalcocite (Cu_2S). These observations confirmed the utility of Ag as a catalyst for bioleaching of enargite concentrate. Although an alternative catalyst with similar catalytic property was not found, it was expected the possibility of an economically feasible process by the reuse of added silver.

In **chapter 5**, catalytic effect of activated carbon (AC) on bioleaching of enargite concentrate was evaluated and its underlying mechanisms were elucidated. Along with AC addition, final Cu recovery was improved from 36% (0% AC) to 53% (0.2% AC), confirming the usefulness of the AC catalyst. Lowered E_h with AC addition was observed, which was attributed to the Fe^{3+}-reduction coupled with RISCs oxidation on the AC surface, clarified by abiotic experiment. This lowered E_h led to the suppression of pyrite dissolution, eventually resulting in the prolonged enargite dissolution without Fe passivation. Accompanying with Cu solubilization, As dissolved from enargite was successively immobilized as ferric arsenate, while it starts to re-solubilize, triggered by pyrite dissolution. Overall, control of pyrite dissolution by AC-catalyzed E_h-reduction was found a key factor of Cu solubilization and As immobilization during bioleaching of enargite concentrate.

In **chapter 6**, the physicochemical properties determining the E_h-reduction ability of AC was clarified through the comparison of various AC with different surface characteristics to find optimal AC for bioleaching of enargite concentrate. Series of abiotic experiment and Raman analysis found that the well-developed graphene structure formed via the chemical-activation process significantly promoted coupling reaction (Fe^{3+}-reduction coupled with RISCs oxidation), which is the result of its superiority in E_h-reduction ability. On the other hand, the abundant surface functional groups on the steam-activated carbon derived from well-developed defect structure seemed to be suitable for the oxidative reaction rather than the coupling reaction. Same trend was confirmed even in the bioleaching experiment, and rather, powder AC enabled to retain faster enargite dissolution. As a result, it was concluded that the

powder-type chemical-activated carbon is the most desirable for E_h-control and enhanced Cu solubilization in bioleaching of enargite concentrate.

In **chapter 7**, the catalytic effect of AC was tested in bioleaching of As-bearing copper concentrate at the high pulp density in the stirred tank reactor for further process development and future implementation into the mining industry. Pulp density of bioleaching successfully increased up to 10% (w/v) by subsequently transferring the pre-grown culture at lower pulp density to that at higher pulp density. AC addition to this high pulp density bioleaching improved Cu recovery from 80% (0% AC) to almost 100 % (0.05% and 0.5% AC), by accelerating the dissolution of chalcopyrite and enargite via (i) optimal potential achievement by AC-catalyzed E_h-control and (ii) enhanced galvanic reaction though the frequent contact between AC and minerals. Moreover, As immobilization as Fe-As precipitates were also facilitated, confirming the utility of AC even in the practical condition (high pulp density, complex mineralogy, and reactor scale).

In **chapter 8**, whole findings were summarized as a conclusion, and the recommendations for future work were provided.

要旨

近年の銅生産の現場における、鉱石中銅品位の低減化、それに伴う砒素含有率の増加は深刻な問題となっており、enargite (Cu_3AsS_4)を始めとした砒素含有銅鉱物中からの銅回収プロセスの発展が熱望されている。微生物反応を利用したバイオリーチングは有効な技術として注目を集めているが、銅浸出速度に依然として課題があり、触媒等、反応促進要因の必要性が示唆されている。本博士論文では、難処理硫化銅鉱物のバイオリーチングにおける有用触媒の探求および比較 （**第 4、5、6 章**;基礎研究）、さらに、より実践的条件への適応（**第 7 章**;応用研究）で構成される。

第 1 章では、砒素含有鉱物として従来研究対象とされてきた enargite のバイオリーチングに関して総括した。さらに、enargite と並んで難処理性が認識されている chalcopyrite ($CuFeS_2$)のバイオリーチングにおいて、有用性が示唆されている銀触媒および炭素触媒に関してまとめ、enargite のバイオリーチングにも適応可能な候補を提示した。

第 2 章では、本博士論文中の実験における一般的手順および分析方法等について記述した。

第 3 章では、実験の前段階として、砒素含有鉱物のバイオリーチング中において重要となる、砒素の定量法に関する検討を行った。具体的には、従来砒素定量に利用されてきた吸光光度法であるモリブデンブルー法の銅および鉄イオンによる阻害を議論し、銅浸出溶液中の砒素定量が同法によって可能か検討した。各種イオンが単独で砒素と共存する際は定量への阻害は確認されなかったが、多量の鉄および銅イオンが共存する際には、As(III)の As(V)への酸化が確認され、サンプル中の As(III)濃度を過小評価する結果となった。しかし、その酸化割合は 4%程度に留まったため、ほぼ無視できる程度の誤差と考えられ、モリブデンブルー法が As(III)濃度変化の傾向評価に利用できることが示された。以後の章において、As(III)濃度は、このモリブデンブルー法によって定量した。

第 4 章では、enargite 精鉱のバイオリーチングにおける銀触媒添加の影響を評価し、代替触媒探求のためにメカニズム解明に取り組んだ。銀触媒として硫化銀を添加するに伴い、バイオリーチング中での enargite からの銅浸出が促進され、0.04% (w/v)の硫化銀存在下で、72 日後に 96%の最終銅浸出率を達成した。一方で、enargite 精鉱中に共存する pyrite (FeS_2)の溶解は(i) 硫化銀の添加に伴う溶液電位の低減化および(ii) 硫化銀自身の低い静止電位に起因する選択的酸化よって抑制された。銀の添加に伴い、非晶質の ferric arsenite として最大 56%の砒素が不動化していることも認められた。種々の固体残渣分析および熱力学的考察により、enargite の溶解は(i) 溶液中の銀イオンと enargite 結晶中の銅イオンの置換による銅浸出、および、(ii) 中間体 Cu_2S を介した銅浸出の 2 つのメカニズムによって進んでい

ることが推察された。以上より、enargite 精鉱のバイオリーチングにおける銀触媒の極めて高い有用性が確認された。同様のメカニズムで作用する安価な代替触媒の発見には至らなかったが、添加した銀触媒の回収により、経済的なプロセス実現の可能性が示唆された。

第 5 章では、enarigte 精鉱のバイオリーチングにおける活性炭添加の影響を評価し、そのメカニズム解明に取り組んだ。活性炭添加に伴い 36% (0% AC)であった最終銅回収率が 53% (0.2%)へと向上し、活性炭の有用性が示された。活性炭添加に伴う溶液電位の低減化が確認され、化学実験により、活性炭表面での Fe^{3+}還元と RISCs（Reduced inorganic sulfur compounds; 無機還元型硫黄化合物）酸化のカップリング反応が、その要因であると判明した。これに伴い、高電位で高速溶解する pyrite の溶解も抑制され、これが、鉄被膜が存在しない状態での息の長い enargite の溶解に繋がることにより、最終銅浸出率が向上したと予想された。砒素は enargite の溶解に伴い随時 ferric arsenate として沈殿していたが、pyrite の溶解に伴い沈殿が溶解、液中に再溶出した。以上を踏まえ、活性炭による電位低減化により、pyrite の溶解をコントロールすることが、enargite 精鉱のバイオリーチングでの銅浸出および砒素不動化において極めて重要であると判明した。

第 6 章では、種々の活性炭を比較検討することにより、活性炭の電位低減化能を決定する物性を解明し、enargite 精鉱のバイオリーチングに最適な活性炭の選定を行った。結果として、薬品賦活炭が有する発達したグラフェン構造により、Fe^{3+}還元－RISCs 酸化カップリング反応が促進され、最も優れた電位低減化効果を示すことが判明した。一方で水蒸気賦活炭はそのディフェクト構造の豊富さから表面官能基を多く有し、カップリング反応よりも酸化反応の影響が顕著に見受けられた。バイオリーチングにおいても同様に薬品賦活炭が優れた溶液電位低減化効果を示し、さらに粉状の活性炭を用いると、溶液電位低減化による enargite の溶解の低速化を打ち消すように銅浸出が促進されることも確認された。結果として、粉状の薬品賦活炭が enargite 精鉱のバイオリーチングにおいて最も適していると結論付けた。

第 7 章では、産業化を視野に入れたプロセスの発展のために、リアクターを用いた高パルプ濃度砒素含有銅精鉱バイオリーチングでの活性炭の影響評価を行った。中度好熱性微生物叢を高パルプ濃度の系に段階的に継代することにより、最終的に 10%までパルプ濃度を向上させることに成功した。ここに活性炭を添加したところ、活性炭無添加では易溶解性鉱物の溶解が中心的で80%に留まった銅浸出が、活性炭の(i) 溶液電位の低減化効果および(ii) 高接触頻度によるガルバニック反応促進効果により、enargite および chalcopyrite の溶解を著しく促進、ほぼ全ての銅溶出につながった。また、砒素－鉄沈殿としての砒素不動化効率も活性炭の存在により向上し、より実践的な実験条件下（高パルプ濃度、複雑組成銅精鉱利用、リアクタースケール）においても活性炭の有用性を確認することができた。

第 8 章では、上記検討結果を総括して結論とし、将来的な研究への提言を記した。

Contents

List of Tables

List of Figures

Abbreviations

ABS	Acidophilic basal salts
AC	Activated carbon
Ac.	*Acidianus*
Am.	*Acidimicrobium*
AMD	Acid mine drainage
At.	*Acidithiobacillus*
As(III)	Arsenite (H_3AsO_3)
As(V)	Arsenate ($H_2AsO_4^-$)
ATR-FTIR	Attenuated total reflection-Fourier transform infrared spectroscopy
BET	Brunauer–Emmett–Teller
Cu^{2+}	Cupric copper
EPMA	Electron probe micro analyzer
EPS	Extracellular polymeric substances
HBS	Heterotrophic basal salts
ICP-OES	Inductively coupled plasma optical emission spectrometry
Lp.	*Leptosprillum*
Ms.	*Metallosphaera*
MLA	Mineral liberation analyzer
Fe^{2+}	Ferrous iron
Fe^{3+}	Ferric iron
Fm.	*Ferrimicrobium*
PCR	Polymerase chain reaction
Sf.	*Sulfolobus*
Sb.	*Sulfobacillus*
SEM	Scanning electron microscope
w/v	weight per volume
XRD	X-ray diffraction

Chapter 1

Introduction

1.1 Introduction

1.1.1 Copper

Copper (Cu) is one of the essential metals for the daily life of human beings. Its high electrical and heat conductivity are applied for electric wires and cooking devices, respectively. The mixture of it with other metals (i.e. alloy) generate high quality materials, being able to apply for wider usages. Recent development of electronic devices also accelerates the consumption of copper as its components. This situation shows that stable copper supply is necessary for the future human society.

Chile is well-known as the best copper producer in the world to meet such a large amount of copper demand. The world copper production in 2011 was reported as 16,100,000 ton, and the copper production in Chile accounts for 34% of it as a major copper producer, followed by Peru, China, USA, Australia, Zambia, Russia, Indonesia, Canada, and Congo. On the other hand, the total minable reserve is considered as 690,000,000 tons in 2011, meaning that world copper might be exhausted approximately 30 years later based on brief calculation.

Majority of copper reserves are derived from porphyry copper deposit that accounts for 65% of world copper reserve. This type of deposit is composed of three types of layers: (i) copper oxides, (ii) secondary copper sulfides, and (iii) primary copper sulfides. A layer of copper oxides exist on the upper part of the deposit and show high copper-grade (> 1%), consisting of copper oxides such as cuprite (Cu_2O) and malachite ($Cu_2CO_3(OH)_2$). Under the oxides layer, there are secondary copper sulfides such as chalcocite (Cu_2S) and covellite (CuS). Although these secondary sulfides layer shows lower copper-grade (1-3%) than that of copper oxides, today, it is also used for copper production due to its high solubility into leaching solution. At the bottom part of the deposit, primary copper sulfides are present such as chalcopyrite ($CuFeS_2$), bornite (Cu_5FeS_4), and enargite (Cu_3AsS_4), showing the lowest copper-grade (< 1%) and refractory property.

The exploitation of these primary sulfides has hardly been conducted in the past decades due to its difficulty in application to real operation. However, researchers' attention has recently been shifted toward these primary minerals since (i) the reserve of oxides and secondary sulfides were continuously decreasing and (ii) they (i.e. primary sulfide minerals) account for 70% of the world copper reserve (Sillitoe, 2010).

This situation requires the development of technique to recover the copper from primary copper sulfides.

1.1.2 Arsenic

Arsenic (As) is the 20th most abundant element in the earth's crust, and it is basically used for semiconductor products such as gallium arsenide (GaAs), which usually compose light-emitting diode (LED) and high-speed transistor. However, arsenic shows high toxicity on the living things. Since arsenic is categorized as a carcinogen, environmental regulation for arsenic exposure is strictly set as 0.01 mg/L by the World Health Organization (WHO) in 1993 (Leist et al., 2000).

There are two types of As occurrence: (i) natural sources and (ii) anthropogenic sources. In the former case, arsenic in the mineral is released via rock weathering, including the effect of microorganisms' activity (Oremland and Stolz, 2005), while, in the latter case, it is derived from human activities, such as mining, manufacturing, industry and chemical weapon (Lièvremont et al., 2009). As a result, serious arsenic problems have been reported in many parts of the world such as Argentina, Bangladesh, Chile, China, Hungary, India (West Bengal), Mexico, Romania, Taiwan, Vietnam, and many parts of the USA (Smedley and Kinniburgh, 2002).

Arsenic is a common impurity in the metallurgical process because it is frequently associated with sulfur, iron, copper, silver, and gold. Current techniques to remove these arsenic contaminations are as below: ion exchange, adsorption on activated alumina and carbon, ultrafiltration, reverse osmosis, and co-precipitation or adsorption by metals (Leist et al., 2000). However, these techniques still have some problems with its cost and stability. The attention against arsenic treatment is therefore increasing, and it is necessary to improve the technique of arsenic removal and immobilization.

There are two predominant chemical oxidation states of arsenic in aqueous phase: trivalent arsenic (As(III)) and pentavalent arsenic (As(V)) (Riveros et al., 2001). Since it is well-known that trivalent arsenic is more toxic than pentavalent one, oxidation of trivalent to pentavalent is necessary as the first step of the arsenic treatment process (Matschullat, 2000).

1.1.3 Primary sulfide minerals

As mentioned above, primary sulfide minerals have increasingly been paid attention by researchers due to the harsh situation of future copper supply. In this section, as an example of primary sulfide minerals, chalcopyrite ($CuFeS_2$) and enargite (Cu_3AsS_4) are introduced.

1.1.3.1 Chalcopyrite

Chalcopyrite ($CuFeS_2$) is one of the primary sulfide minerals, showing golden yellow color, which is composed of copper, iron, and sulfur in the tetragonal crystal structure (Burdick et al., 1917). Since this mineral accounts for the majority of primary sulfide ore, researchers tend to employ chalcopyrite as an objective material. However, its refractoriness disturbs the economical operation of copper extraction from it.

1.1.3.2 Enargite

Enargite (Cu_3AsS_4) is also one of the primary sulfide minerals, showing black color. This mineral is composed of copper, arsenic, and sulfur in the orthorhombic crystal structure and well-known as semiconducting materials (Henao et al. 1994). Enargite has several properties in common with chalcopyrite: (i) sulfide mineral composed of copper and another metal and (ii) refractory behavior against leaching treatment. It is generally associated with chalcopyrite, however, its similar property with chalcopyrite prevents effective separation.

Moreover, arsenic, included in enargite structure, requires arsenic treatment process after the leaching process, which is inferior to chalcopyrite from the economic point of view. However, the potential of enargite as the copper resource is not negligible, thus requiring the development of a novel process for enargite treatment, where only copper can be extracted, but arsenic remains in the solid phase.

1.2. The application of bioleaching for efficient copper extraction from sulfide minerals

1.2.1 Pyrometallurgy and hydrometallurgy

Until now, a number of techniques to obtain metals from minerals have been proposed and improved. These techniques are able to be divided into two categories: (i) pyrometallurgy, and (ii) hydrometallurgy. The former techniques such as calcination, roasting, smelting, and refining, are applicable to only high Cu-grade ore because the heating process is economically infeasible for the application to low Cu-grade ore. On the other hand, the latter techniques such as bioleaching, acid leaching, pressure leaching, are effective in the exploitation of low Cu-grade ore due to its lower cost in terms of energy consumption. Especially, bioleaching is a promising process from economic and environmental points of view. In this section, the definition, general mechanism, advantages and disadvantages of bioleaching are summarized.

1.2.2. Bioleaching

Bioleaching is one of the biohydrometallurgical techniques to extract objective metals from minerals by using microorganisms. Various metals can be the candidate of the objective metals, such as copper (Yang et al., 2009), zinc (Deveci et al., 2004), lead (Nasernejad et al., 1999), gold (Curreli et al., 1997), silver (Frías et al., 2002) and cobalt (Olson et al., 1990).

1.2.2.1 General mechanism of bioleaching

During the bioleaching process, microbial reactions are key factors, contributed by iron-oxidizing and sulfur-oxidizing microorganisms.

When the biological reaction proceeds, three different bioleaching strategies are considered (Rodriguez et al., 2003);

(i) Indirect bioleaching, whereby the microbial action is restricted to re-generation of the bioleaching reagent (i.e. Fe^{3+})

(ii) Contact bioleaching, which entails attachment of microorganisms to the mineral surface and these organisms provide the medium and facilitate the mineral attack through an electrochemical dissolution involving Fe^{3+} contained in the microbe's extracellular polymeric substances (EPS)

(iii) Cooperative bioleaching, which entails cooperation between microorganisms attached to the mineral surface and free bacteria in solution. The attached microbes, through contact bioleaching, release chemicals to the solution that constitute the energy source for the organisms that are free in solution.

In order to comprehend the general mechanism of bioleaching, pyrite (FeS_2) was taken as an example, since it is general impurity of ores and dissolution of pyrite is the fundamental reaction of bioleaching.

At the beginning of the bioleaching reaction, pyrite is slightly oxidized by the oxygen when pyrite is exposed to the air. Under such condition, if those ores become wet by rainwater, pyrite starts to dissolve and release Fe^{2+} and sulfate.

$$2FeS_2 + 7O_2 + 2H_2O \rightarrow 4SO_4^{2-} + 2Fe^{2+} + 4H^+ \text{ (chemical reaction)} \qquad \text{(Eq. 1-1)}$$

Produced Fe^{2+} is then oxidized by iron-oxidizing microbes to Fe^{3+}.

$$4Fe^{2+} + O_2 + 4H^+ \rightarrow 4Fe^{3+} + 2H_2O \text{ (biological reaction)} \qquad \text{(Eq. 1-2)}$$

Oxidized iron (i.e. Fe^{3+}) is used for further oxidation of pyrite due to its property as strong oxidizer, producing Fe^{2+} and elemental sulfur.

$$FeS_2 + 2Fe^{3+} \rightarrow 3Fe^{2+} + 2S^0 \text{ (chemical reaction)} \qquad \text{(Eq. 1-3)}$$

Elemental sulfur formed by the above reaction is the main reaction-inhibitor for further dissolution of pyrite. In order to promote the reaction even after the formation of elemental sulfur, sulfur-oxidizing microbes oxidize it to sulfate and remove it from pyrite surface.

$$2S^0 + 3O_2 + 2H_2O \rightarrow 2SO_4^{2-} + 4H^+ \text{ (biological reaction)} \qquad \text{(Eq. 1-4)}$$

As a result, further dissolution of pyrite continuously proceeds. The summarized reaction of pyrite dissolution by microbiological oxidation is described as below;

$$FeS_2 + 14Fe^{3+} + 8H_2O \rightarrow 15Fe^{2+} + 2SO_4^{2-} + 16H^+ \quad \text{(Eq. 1-5)}$$

In the bioleaching process, these reactions must be strictly managed. If these reactions spontaneously occur, the serious environmental problem occur since the highly acidic water containing large amount of heavy metals is discharged into the river, which is called acid mine drainage (AMD).

In the case of enargite bioleaching, the basic reaction is almost same. However, in the case of enargite bioleaching, since enargite includes no iron in its composition, Fe^{3+} as oxidizing reagent should be externally supplied.

$$Cu_3AsS_4 + 11Fe^{3+}\ 4H_2O \rightarrow 3Cu^{2+} + 11Fe^{2+} + H_2AsO_4^- + 4S^0 + 6H^+ \quad \text{(Eq. 1-6)}$$

(chemical reaction)

As mentioned above, Fe^{2+} produced via the oxidation of enargite is re-oxidized to Fe^{3+} by iron-oxidizing microbes.

As a result, further dissolution of enargite is continuously proceeded as shown in Fig. 1.1.

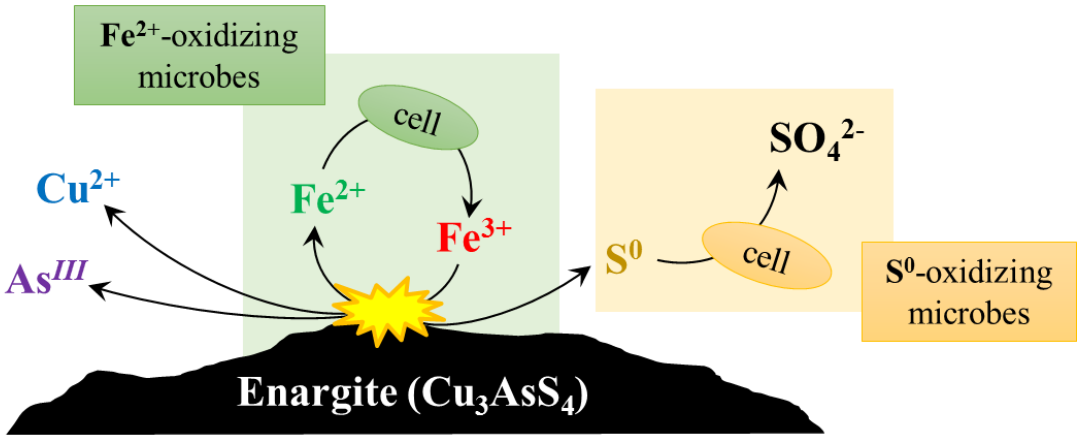

Fig. 1.1 The schematic image of enargite bioleaching.

1.2.2.2 Representative microorganisms used for bioleaching

At. (formerly *Thiobacillus*) *ferrooxodans*

At. ferrooxidans is an autotrophic, acidophilic, and moderately thermophilic bacterium, capable of growing on ferrous iron or sulfur compounds as the electron donor. In general, it grows optimally at pH 1.5-2.5 at 45-50°C. Therefore, it is commonly found in acid mine drainage containing various metal ions at low pH. Although it basically grows under aerobic conditions, it is able to grow under anaerobic conditions using ferric iron as the electron acceptor, instead of oxygen (Ohmura et al., 2002).

At. (formerly *Thiobacillus*) *thiooxidans*

At. thiooxidans is an autotrophic, acidophilic, and mesophilic bacterium, capable of growing on elemental sulfur as a primary electron donor under strictly aerobic conditions. The optimum temperature and pH for its growth are 28-30°C and less than 4.0, respectively. Additionally, it grows also on thiosulfate ($S_2O_3^{2-}$) and tetrathionate ($S_4O_6^{2-}$), but not hydrogen sulfide and sulfides (Waksman et al., 1922).

At. (formerly *Thiobacillus*) *caldus*

At. caldus is an mixotrophic, acidophilic, and moderately thermophilic bacterium, capable of growing on elemental sulfur and tetrathionate, but not on ferrous iron. The optimum temperature and pH for active growth of *A. caldus* are 45°C and 2.0-2.5, respectively (Hallberg et al., 1994).

Ac. brierleyi

Ac. brierleyi is a thermophilic and extremely acidophilic archaeon. It autotrophically grows on elemental sulfur and ferrous iron as the electron donor, at optimum pH of 1.5-2.0 and temperature of 70°C. It is able to also grow under anaerobic conditions by reducing sulfur (Segerer et al., 1986).

Lp. ferrooxidans

Lp. ferrooxidans is an obligately autotrophic, mesophilic, and acidophilic bacterium, capable of growing ferrous iron, but incapable of oxidizing elemental sulfur and RISCs (reduced inorganic sulfur compounds) (Hippe 2000). The optimum temperature and pH

for its growth are 25-35°C and 2.5-3.0, respectively. Therefore, *L. ferrooxidans* is often applied to bioleaching of sulfide minerals with *At. ferrooxidans* or *At. thiooxidans* (Bosecker, 1997).

Lp. ferriphilum

Lp. ferriphilum is an obligately autotrophic, moderately thermophilic, and acidophilic bacterium. It grows aerobically at optimum pH of 1.5 and temperature of 43°C. It obtains energy for growth by oxidizing ferrous iron as an electron donor. It was reported to grow on also pyrite, but not tetrathionate (Okibe et al., 2003).

Sb. thermosulfidooxidans

Sb. thermosulfidooxidans is a moderately thermophilic and acidophilic bacterium, capable of growing either heterotrophically or autotrophically on ferrous iron, tetrathionate, elemental sulfur, thiosulfate, and sulfide minerals (Pina et al., 2010; Xia et al., 2010). It is able to grow in a wide range of temperature and pH; at 20-60°C and pH 1.5-5.5, respectively. Optimum temperature and pH are 50-55°C and 1.9-2.4, respectively.

Sf. metallicus

Sf. metallicus is an extremely thermophilic, obligately autotrophic, and acidophilic archaeon. It grows aerobically at 50-75°C and pH 1.0-4.5 on elemental sulfur and sulfide (Huber et al., 1991; Gautier et al., 2008; Morales et al., 2011). Additionally, its growth via oxidation of pyrite and ferrous iron was also observed (Norris et al., 2000).

1.2.3 Enargite bioleaching

As mentioned above, recent depletion of high-grade copper ore has directed the researcher's attention toward low-grade and refractory sulfides such as chalcopyrite ($CuFeS_2$) and enargite (Cu_3AsS_4). In order to improve dissolution efficiency of these minerals, not only chemical leaching such as pressure leaching (Ruiz et al., 2011; Padilla et al., 2015) and acid leaching (Safarzadeh and Miller, 2014) but also biological leaching has been investigated by several research groups (Acevedo et al., 1998; Sasaki et al., 2009). Since enargite includes arsenic in its structure, researchers have tended to

engage in the study on chalcopyrite bioleaching, rather than enargite bioleaching, resulting in the limited number of studies involving in enargite bioleaching. However, according to the recent gradual increase of contamination of arsenic as an impurity in copper deposit, it has become no longer negligible to study involving in bioleaching of enargite. In this section, recent developments of techniques of enargite bioleaching are introduced.

1.2.3.1 Bioleaching of enargite by using thermophiles

Since enargite shows highly-refractory property during the leaching process, higher temperature conditions (60-70°C) are favorable for faster enargite dissolution, despite its economic infeasibility in real operation.

Escobar et al. (2000) conducted bioleaching of enargite at 70˚C using *Sulfolobus* BC, which is thermophilic and extremely acidophilic iron- and sulfur-oxidizing microorganisms. In the study, enargite was bioleached at 70˚C by *Sulfolobus* BC in shake-flasks experiments and 52% of copper extraction was obtained after 23 days of leaching at highest. In the absence of Fe^{3+} as an oxidizing reagent, *Sulfolobus* BC catalyzed the bioleaching of enargite possibly based on the direct mechanism, where microbe adheres onto the surface of enargite and attack it. In this case, since solubilized arsenic by microbial attack remained in the solution, 90% of inhibition of bacterial growth and activity was observed due to the toxicity of arsenic. On the other hand, in the presence of 1 g/L of Fe^{3+}, it was precipitated with arsenic as ferric arsenate to immobilize arsenic in the solid phase, preventing the presence of highly concentrated arsenic in the solution. As a result, no significant bacterial inhibition occurred, resulting in proceeding further dissolution of enargite. This arsenic behavior in the leaching solution is one of the key factors during bioleaching of enargite.

Muñoz et al. (2006) conducted bioleaching of enargite by using thermophilic archaeon, *Sf. metallicus*, at 68˚C. The results obtained in this study obviously showed that high-temperature condition (68˚C) is significantly effective on enargite dissolution: copper recovery reached over 84%. Additionally, the amount of iron precipitates formed on the surface of enargite increased at higher temperature, indicating that the immobilization of arsenic co-precipitated with iron was also enhanced with increase in temperature.

Lee et al. (2011) also conducted comparative bioleaching of enargite at ambient laboratory temperature and higher temperature, 65˚C. High copper recovery (> 81%) was also observed as same as the study conducted by Muñoz et al. (2006) at high temperature, while almost no copper extraction was seen at lower temperature conditions.

Takatsugi et al. (2011) and Sasaki et al. (2011) used *Ac. brierleyi* as iron- and sulfur-oxidizing microorganism during bioleaching of enargite at 70˚C. In these studies, over 90% of copper extraction was achieved within 27 days. Moreover, arsenic recovery was only 6%, while almost all copper was solubilized from enargite, indicating that the majority of solubilized arsenic was re-immobilized during the bioleaching period. They indeed confirmed the formation of scorodite ($FeAsO_4 \cdot 2H_2O$), which is one of the forms of ferric arsenate with high crystallinity and stability, and low iron requirement. These studies proposed the possibility of an ideal bioleaching process, where simultaneous achievement of both high copper extraction and arsenic immobilization can be realized. The studies of enargite bioleaching using thermophiles under different conditions, such as microbiological system, initial pH, temperature, and pulp density were summarized as below.

Table 1.1 The list of the previous studies in enargite bioleaching using thermophiles.

Microorganism(s)	Initial pH	Temp. (ºC)	Cu leached (%)	As leached (%)	Leaching periods (days)	Pulp density (%)	Enargite grade (%)	Volume	Conditions	Ref.
Sulfolobus BC	1.6	70	52	17	23	2	≈100	100 mL (△250 mL)	1.0 g/L Fe^{3+}	Escobar et al 2000
Sulfolobus BC	1.6	70	12	12	23	2	≈100	100 mL (△250 mL)	without Fe^{3+}	Escobar et al 2000
Sf. metallicus	1.8	68	84	N.D.	34	10	16	40 mL (△500 mL)	-	Munoz et al 2006
Sf. metallicus	1.8	70	98	N.D.	30	5	16.4	300 mL (△1000 mL)	Succcessively adapted culture	Astudillo et al 2008
Sf. metallicus	1.8	70	93	N.D.	30	10	16.4	300 mL (△1000 mL)	Succcessively adapted culture	Astudillo et al 2008
Sf. metallicus	1.8	70	65	N.D.	30	15	16.4	300 mL (△1000 mL)	Succcessively adapted culture	Astudillo et al 2008
Sf. metallicus	1.8	70	42	N.D.	30	20	16.4	300 mL (△1000 mL)	Succcessively adapted culture	Astudillo et al 2008
Sf. metallicus	1.8	70	36	N.D.	30	25	16.4	300 mL (△1000 mL)	Succcessively adapted culture	Astudillo et al 2008
Sf. metallicus	1.8	70	27	N.D.	30	30	16.4	300 mL (△1000 mL)	Succcessively adapted culture	Astudillo et al 2008

Microorganism(s)	Initial pH	Temp. (ºC)	Cu leached (%)	As leached (%)	Leaching periods (days)	Pulp density (%)	Enargite grade (%)	Volume	Conditions	Ref.
Sf. metallicus	1.8	70	61	N.D.	30	5	16.4	300 mL (△1000 mL)	Without adaptation	Astudillo et al 2008
Sf. metallicus	1.8	70	52	N.D.	30	10	16.4	300 mL (△1000 mL)	Without adaptation	Astudillo et al 2008
Sf. metallicus	1.8	70	29	N.D.	30	15	16.4	300 mL (△1000 mL)	Without adaptation	Astudillo et al 2008
Sf. metallicus	1.8	70	15	N.D.	30	20	16.4	300 mL (△1000 mL)	Without adaptation	Astudillo et al 2008
Sf. metallicus	1.8	70	11	N.D.	30	25	16.4	300 mL (△1000 mL)	Without adaptation	Astudillo et al 2008
Sf. metallicus	1.8	70	9	N.D.	30	30	16.4	300 mL (△1000 mL)	Without adaptation	Astudillo et al 2008
Acidianus, Metallospheara, Sulfolobus	1.8	70	96	N.D.	264	-	2.45% as Cu (4.2% as enargite)	Column leaching	Chalcocite dominant as Cu containing mineral	Lee et al 2011
Acidianus, Metallospheara, Sulfolobus	1.8	70	98	N.D.	475	-	5.62% as Cu (2.9% as enargite)	Column leaching	Chalcocite dominant as Cu containing mineral	Lee et al 2011
Acidianus, Metallospheara, Sulfolobus	1.8	70	88	N.D.	335	-	0.63% as Cu (12.8% as enargite)	Column leaching	Covellite dominant as Cu containing mineral	Lee et al 2011

Microorganism(s)	Initial pH	Temp. (℃)	Cu leached (%)	As leached (%)	Leaching periods (days)	Pulp density (%)	Enargite grade (%)	Volume	Conditions	Ref.
Acidianus, Metallospheara, Sulfolobus	1.8	70	95	N.D.	577	-	0.59% as Cu (20% as enargite)	Column leaching	Covellite dominant as Cu containing mineral	Lee et al 2011
Acidianus, Metallospheara, Sulfolobus	1.8	70	81	N.D.	335	-	0.73% as Cu (94.7% as enargite)	Column leaching	Enargite dominant as Cu containing mineral	Lee et al 2011
Acidianus, Metallospheara, Sulfolobus	1.8	70	90	N.D.	335	-	1.06% as Cu (95.9% as enargite)	Column leaching	Enargite dominant as Cu containing mineral	Lee et al 2011
Ac. brierleyi	1.5	70	62	12	76	1	88.1	50 mL (△200 mL)	0.9 g/L Fe^{2+}	Sasaki et al 2011
Ac. brierleyi	1.5	70	91	35	27	1	88.1	50 mL (△200 mL)	1.8 g/L Fe^{2+}	Sasaki et al 2011
Ac. brierleyi	1.5	70	91	6	27	1	88.1	50 mL (△200 mL)	2.7 g/L Fe^{2+}	Sasaki et al 2011
Ac. brierleyi	1.5	70	17	11	19	1	88.1	50 mL (△200 mL)	3.6 g/L Fe^{2+}	Sasaki et al 2011
Ac. brierleyi	1.5	70	83	N.D.	40	0.5	88.1	50 mL (△200 mL)	2.7 g/L Fe^{2+}	Sasaki et al 2011
Ac. brierleyi	1.5	70	91	N.D.	27	1	88.1	50 mL (△200 mL)	2.7 g/L Fe^{2+}	Sasaki et al 2011

Microorganism(s)	Initial pH	Temp. (ºC)	Cu leached (%)	As leached (%)	Leaching periods (days)	Pulp density (%)	Enargite grade (%)	Volume	Conditions	Ref.
Ac. brierleyi	1.5	70	81	N.D.	40	2	88.1	50 mL (△200 mL)	2.7 g/L Fe^{2+}	Sasaki et al 2011
Ac. brierleyi	1.5	70	91	6	27	1	88.1	50 mL (△200 mL)	2.7 g/L Fe^{2+}	Takatsugi et al 2011
Ms. hakonensis	2.0	75	15	N.D.	27	1	60	50 mL (△200 mL)	Pure culture	Ai et al 2017
Ms. sedula	2.0	75	60	N.D.	27	1	60	50 mL (△200 mL)	Pure culture (ARS50-2)	Ai et al 2017
Ms. sedula	2.0	75	62	N.D.	27	1	60	50 mL (△200 mL)	Pure culture (*cop* A mutant)	Ai et al 2017
Ms. sedula *Ms. hakonensis*	2.0	75	62	N.D.	27	1	60	50 mL (△200 mL)	Mixed culture (copA mutant)	Ai et al 2017
Ms. sedula *Ms. hakonensis*	2.0	75	35	N.D.	27	3	60	50 mL (△200 mL)	Mixed culture (copA mutant)	Ai et al 2017
Ms. sedula *Ms. hakonensis*	2.0	75	67	N.D.	27	1	60	50 mL (△200 mL)	Mixed culture (*cop* A mutant and ARS50-2)	Ai et al 2017
Ms. sedula *Ms. hakonensis*	2.0	75	62	N.D.	27	3	60	50 mL (△200 mL)	Mixed culture (*cop* A mutant and ARS50-2)	Ai et al 2017

1.2.3.2 Bioleaching of enargite using mesophiles and/or moderate thermophiles

Although high-temperature conditions enable the bioleaching of enargite to simultaneously achieve high copper recovery and low arsenic solubilization, the application of this process into real operation is unrealistic form economical point of view. Therefore, bioleaching of enargite at low-temperature conditions have also been conducted by several researchers.

Escobar et al. (1997) carried out chemical and biological leaching of enargite at 30˚C by using iron-and sulfur-oxidizing bacteria, *At. ferrooxidans*. Even though bioleaching achieved higher copper recovery than acid leaching as chemical leaching, its recovery was only 11% even after 32 days of the experimental period.

Bioleaching of enargite samples associated with arsenopyrite (FeAsS) (Corkhill et al., 2008) and pyrite (FeS_2) (Canales et al., 2002) have also been conducted at 30˚C. In both cases, not enargite but concomitant minerals were selectively attacked by microorganisms, confirming the refractoriness of enargite.

Sasaki et al. (2010) also conducted bioleaching of enargite under low temperature condition (25˚C) by using *At. ferrooxidans*. This study found that the formation of amorphous ferric arsenate but not scorodite, revealing that the arsenic precipitation formed during bioleaching at lower temperature is less crystallized and lack of stability as arsenic-bearing waste.

In each case, copper extraction was significantly lower than that under high-temperature conditions. Moreover, arsenic precipitates need to be further stabilized compared with that under high-temperature conditions. These results suggest the necessity of the reaction-accelerator such as a catalyst to achieve high copper extraction from enargite and form highly stable arsenic precipitation even at low temperature conditions.

The study of enargite bioleaching using mesophiles and/or moderate thermophiles under different conditions, such as microbiological system, initial pH, temperature, and pulp density were summarized below.

Table 1.2 The list of previous studies in enargite bioleaching using mesophiles/moderate thermophiles.

Microorganism(s)	Initial pH	Temp. (℃)	Cu leached (%)	As leached (%)	Leaching periods (days)	Pulp density (%)	Enargite grade (%)	Volume	Conditions	Ref.
At. ferrooxidans	1.6	30	9	6	32	5	46% as Cu	100 mL (△250 mL)	wihtout Fe^{3+}	Escobar et al 1997
At. ferrooxidans	1.6	30	11	8	32	5	46% as Cu	100 mL (△250 mL)	3.0 g/L Fe^{3+}	Escobar et al 1997
At. ferrooxidans	2.4	35	16	19	24	4	41	1.3 L (2 L fermenter)	air supply	Acevedo et al 1998
At. ferrooxidans	2.4	35	19	19	24	4	41	1.3 L (2 L fermenter)	1% CO_2	Acevedo et al 1998
At. ferrooxidans	2.4	35	19	24	24	4	41	1.3 L (2 L fermenter)	2% CO_2	Acevedo et al 1998
At. ferrooxidans	2.4	35	19	25	24	4	41	1.3 L (2 L fermenter)	3% CO_2	Acevedo et al 1998
At. ferrooxidans	2.4	35	18	21	24	4	41	1.3 L (2 L fermenter)	4% CO_2	Acevedo et al 1998

Microorganism(s)	Initial pH	Temp. (ºC)	Cu leached (%)	As leached (%)	Leaching periods (days)	Pulp density (%)	Enargite grade (%)	Volume	Conditions	Ref.
At. ferrooxidans	1.8	33	N.D.	2.5	8	6	8	3 L stirred tank reactor	-	Canales et al 2002
At. ferrooxidans	1.8	33	N.D.	< 0.1	8	18	8	3 L stirred tank reactor	-	Canales et al 2002
At. ferrooxidans	1.8	33	N.D.	< 0.1	8	24	8	3 L stirred tank reactor	-	Canales et al 2002
At. ferrooxidans	1.8	33	1 g/L as Cu	8	34	4	16	40 mL (△500 mL)	-	Muñoz et al 2006
Lp. ferrooxidans	1.8	30	8	9	32	1	≈100	250 mL (△250 mL)	40 mM Fe^{3+}	Corkhill et al 2008
At. ferrooxidans	2.38	22	6	5	65	3.3	≈100	75 mL (△300 mL)	Fe takeover from previous culture containing arsenopyrite	Fantauzzi et al 2009
At. ferrooxidans	2.34	22	7	7	157	3.3	≈100	75 mL (△300 mL)	Inoculated from above culture	Fantauzzi et al 2009

Microorganism(s)	Initial pH	Temp. (℃)	Cu leached (%)	As leached (%)	Leaching periods (days)	Pulp density (%)	Enargite grade (%)	Volume	Conditions	Ref.
At. ferrooxidans	2.34	22	2	1	44	3.3	≈100	75 mL (△300 mL)	Inoculated from above culture	Fantauzzi et al 2009
At. ferrooxidans	2	25	7	7	130	0.7	88.1	150 mL (△500 mL)	Arsenic adapted bacterial culture	Sasaki et al 2010
At. ferrooxidans	2	25	6	7	130	0.7	88.1	150 mL (△500 mL)	Non-adapted bacterial culture	Sasaki et al 2010
Acidithiobacillus, Leptospirillum	1.8	20-22	90	N.D.	301	-	2.45% as Cu (4.2% as enargite)	Column leaching	Chalcocite dominant as Cu containing mineral	Lee et al 2011
Acidithiobacillus, Leptospirillum	1.8	20-22	98	N.D.	653	-	5.62% as Cu (2.9% as enargite)	Column leaching	Chalcocite dominant as Cu containing mineral	Lee et al 2011
Acidithiobacillus, Leptospirillum	1.8	20-22	< 20	N.D.	241	-	0.63% as Cu (12.8% as enargite)	Column leaching	Covellite dominant as Cu containing mineral	Lee et al 2011
Acidithiobacillus, Leptospirillum	1.8	20-22	< 20	N.D.	637	-	0.59% as Cu (20% as enargite)	Column leaching	Covellite dominant as Cu containing mineral	Lee et al 2011

Microorganism(s)	Initial pH	Temp. (℃)	Cu leached (%)	As leached (%)	Leaching periods (days)	Pulp density (%)	Enargite grade (%)	Volume	Conditions	Ref.
Acidithiobacillus, Leptospirillum	1.8	20-22	< 20	N.D.	234	-	0.73% as Cu (94.7% as enargite)	Column leaching	Enargite dominant as Cu containing mineral	Lee et al 2011
Acidithiobacillus, Leptospirillum	1.8	20-22	< 20	N.D.	234	-	1.06% as Cu (95.9% as enargite)	Column leaching	Enargite dominant as Cu containing mineral	Lee et al 2011

1.3 Catalyst for bioleaching of sulfide minerals

Previous researches on bioleaching of enargite have suggested the necessity of some catalyst to enhance copper solubilization even under low temperature conditions. However, the number of studies using some catalysts on enargite leaching is limited. In order to obtain the valuable information of the possible catalyst that is useful for improvement of enargite bioleaching, studies investigating the effects of various catalysts on leaching of sulfide mineral, especially for chalcopyrite, are introduced.

1.3.1 Catalytic effect of metals

1.3.1.1 Catalytic effect of metals on chalcopyrite dissolution

A number of studies have investigated the effect of co-existing metal ions on the improvement of chalcopyrite dissolution. Muñoz et al. (2007) conducted chalcopyrite bioleaching in the presence of antimony (Sb), cobalt (Co), silver (Ag), bismuth (Bi), nickel (Ni), tin (Sn) and manganese (Mn). The results showed that only silver greatly enhanced chalcopyrite dissolution, but no other co-existing metals showed positive effects on it. Hiroyoshi et al. (2007) confirmed the positive effect of silver on accelerating copper extraction from chalcopyrite. In this study, bismuth was also found effective in enhancing chalcopyrite dissolution, which was not observed in the study conducted by Muñoz et al. (2007), since bismuth is likely to show inhibitory effect on microbial activity; bismuth is likely only useful in abiotic chemical leaching of chalcopyrite. Ballester et al. (1990) also tested various metal ions, Co, Bi, Ag, and mercury (Hg) in chalcopyrite bioleaching, observing the effectiveness of Hg as a catalytic metal as well as silver. However, considering its toxicity, it is inapplicable to real operation, suggesting that the silver is the only possible candidate for strongly enhancing the dissolution of refractory chalcopyrite.

1.3.1.2 Catalytic effect of silver on chalcopyrite dissolution

In order to investigate the reason of strong catalytic capability of Ag, underlying mechanism have been discussed in decades and several possibilities have been proposed: (i) improvement of electrical conductivity by the formation of silver sulfide inside elemental sulfur layer on chalcopyrite surface, (ii) silver atom diffusion into metal-deficient sulfur-rich layer formed on chalcopyrite surface and (iii) silver sulfide

formation which consumes hydrogen sulfide produced via chalcopyrite reduction, indirectly accelerating chalcopyrite dissolution .

The first theory, proposed by Nazari et al. (2011, 2012a, 2012b, 2012c), is based on the electron transfer catalyzed by silver-doped pyrite. In the presence of pyrite contacted with chalcopyrite, electron transfer between chalcopyrite and pyrite enable the corrosion of the chalcopyrite surface, resulting in the faster dissolution behavior of chalcopyrite. However, the formation of elemental sulfur via the dissolution of chalcopyrite inhibits the contact between the surface of chalcopyrite and pyrite, resulting in a weak galvanic effect. Instead of pure pyrite, silver-coated pyrite was employed to further enhance electron transfer between chalcopyrite and pyrite. In this process, the elemental sulfur formed on the surface of chalcopyrite can be transformed into Ag_2S, consequently retaining the electrochemical contact between chalcopyrite and pyrite with the intermediate of Ag_2S. As a result, chalcopyrite dissolution was dramatically accelerated, indicating that electron transfer between chalcopyrite grains and external regions (i.e. leaching solution, pyrite, and other materials) is assumed a key factor during silver-added leaching of chalcopyrite.

The second theory, proposed by Ghahremaninezhad et al. (2010, 2013, 2015), is based on the formation of metal-deficient sulfide film ($Cu_{1-x}Fe_{1-y}S_{2-z}$), which is considered as one of the passivation layers formed during chalcopyrite leaching. The existence of this layer possibly hinders the interaction between chalcopyrite and leaching solution, and diffusion of metal ions (i.e. Fe, Cu) passing through this layer rate-limits the dissolution of chalcopyrite. In the presence of silver, silver atom diffuses into the metal-deficient sulfide layer, resulting in the formation of silver sulfide (Ag_2S). As a result, electrical interaction between chalcopyrite and leaching solution is maintained with the intermediate of Ag_2S. In addition, oxidation of the silver sulfide is capable of releasing the silver atom into the solution and leaving behind porous elemental sulfur, which enables direct interaction between chalcopyrite and leaching solution. The most important point in this theory is diffusion of the silver atom into metal-deficient sulfide film, and reform of its structure.

The third theory, proposed by Hiroyoshi et al. (2000, 2001, 2002, 2004, 2008a, 2008b), is based on the redox potential of the leaching solution. In this theory, chalcopyrite dissolution is considered to be greatly enhanced within the certain range of redox

potential, which is determined by critical potential, E_c, and oxidation potential, E_{ox}: critical potential is the redox potential where reduction of chalcopyrite to more soluble copper sulfide (Cu_xS) occur, and oxidation potential is the redox potential where oxidation of Cu_xS to Cu^{2+} occur. In the presence of the silver, hydrogen sulfide (H_2S), produced via the reduction of chalcopyrite, is immediately consumed for the formation of silver sulfide by precipitating with silver ion in the leaching solution. As a result, chemical equilibrium is shifted toward the reaction for further chalcopyrite reduction. Consequently, chalcopyrite reduction to Cu_xS, followed by its oxidation to Cu^{2+}, is easily happened compared to the case in the absence of silver. The role of silver in this theory is the indirect contribution that consumption of hydrogen sulfide due to its high affinity with silver ion to form silver sulfide.

1.3.1.3 Catalytic effect of silver in chalcopyrite bioleaching

The catalytic advantage of Ag has also been actively tested not only in the abiotic acid leaching but also in bioleaching, even though its toxicity on the microbial activity is widely recognized. Various experimental conditions employed to evaluate the catalytic ability of Ag are listed in Table 1.3. Mesophiles such as *At. ferrooxidnas, At. thiooxidans, Lp. ferrooxidans* have been frequently used for those tests under relatively low temperature conditions. Even such harsh conditions for faster dissolution of chalcopyrite, higher Cu recovery (> 90%) has been indeed achieved in some cases (Yuehua et al., 2002; Muñoz et al., 2007; Abdollahi et al., 2015). These results indicate that silver is a promising catalyst for enhancing the dissolution of refractory copper sulfide even in the ioleaching process.

Table 1.3 The list of previous studies in silver-catalyzed chalcopyrite bioleaching.

Microorganism(s)	Initial pH	Temp. (ºC)	Cu leached (%)	Ag addition	Leaching periods (days)	Pulp density (%)	Chalcopyrite grade (%)	Volume	Conditions	Ref.
Acidithiobacilli	2	28	37	-	49	1.5	6	100 mL (△250)		Ahonen et al. 1990
Acidithiobacilli	2	28	39	9.5 mg Ag/L as Ag_2SO_4	49	1.5	6	100 mL (△250)		Ahonen et al. 1990
Acidithiobacilli	2	28	66	31.6 mg Ag/L as Ag_2SO_4	49	1.5	6	100 mL (△250)		Ahonen et al. 1990
Acidithiobacilli	2	28	5	8.9 mg Ag/L as Ag_2SO_4	40	5	13	100 mL (△250)		Ahonen et al. 1990
Acidithiobacilli	2	28	11	8.9 mg Ag/L as Ag_2SO_4	40	5	13	100 mL (△250)	Silver added after 5 days of leaching	Ahonen et al. 1990
Acidithiobacilli	2	28	35	29.6 mg Ag/L as Ag_2SO_4	40	5	13	100 mL (△250)	Silver added after 5 days of leaching	Ahonen et al. 1990
Acidithiobacilli	2	28	5	3 mg Ag/L as Ag_2SO_4	49	2	95	100 mL (△250)		Ahonen et al. 1990
Acidithiobacilli	2	28	10	3 mg Ag/L as Ag_2SO_4	49	2	95	100 mL (△250)		Ahonen et al. 1990
Acidithiobacilli	2	28	42	30 mg Ag/L as Ag_2SO_4	49	2	95	100 mL (△250)		Ahonen et al. 1990

Microorganism(s)	Initial pH	Temp. (℃)	Cu leached (%)	Ag addition	Leaching periods (days)	Pulp density (%)	Chalcopyrite grade (%)	Volume	Conditions	Ref.
Acidithiobacilli	2	35	90	30 mg Ag/L as Ag_2SO_4	16	5	7	300 mL (500 mL glass reactor)	Air and 1% CO_2(v/v) supply	Ballester et al. 1990
At. ferrooxidans, *Lp. ferrooxidans*	1.8	45	32	0.5 mg Ag/L as Ag_2SO_4	27	5	19% as Cu	100 mL (△250)		Gómez et al. 1999
At. ferrooxidans, *Lp. ferrooxidans*	1.8	45	59	1.5 mg Ag/L as Ag_2SO_4	27	5	19% as Cu	100 mL (△250)		Gómez et al. 1999
At. ferrooxidans, *Lp. ferrooxidans*	1.8	45	53	2.5 mg Ag/L as Ag_2SO_4	27	5	19% as Cu	100 mL (△250)		Gómez et al. 1999
At. ferrooxidans, *Lp. ferrooxidans*	1.8	50	27	1.5 mg Ag/L as Ag_2SO_4	26	5	19% as Cu	100 mL (△250)		Gómez et al. 1999
S-oxidizing bacterea	1.8	50	39	0.5 mg Ag/L as Ag_2SO_4	27	5	19% as Cu	100 mL (△250)		Gómez et al. 1999
S-oxidizing bacterea	1.8	50	66	1.5 mg Ag/L as Ag_2SO_4	27	5	19% as Cu	100 mL (△250)		Gómez et al. 1999
S-oxidizing bacterea	1.8	50	72	2.5 mg Ag/L as Ag_2SO_4	27	5	19% as Cu	100 mL (△250)		Gómez et al. 1999
S-oxidizing bacterea	1.8	50	47	2.5 mg Ag/L as Ag_2SO_4	26	5	19% as Cu	100 mL (△250)		Gómez et al. 1999

Microorganism(s)	Initial pH	Temp. (ºC)	Cu leached (%)	Ag addition	Leaching periods (days)	Pulp density (%)	Chalcopyrite grade (%)	Volume	Conditions	Ref.
At. ferrooxidans	1.3	25	58	135 mg/L as AgCl	20	2	20% as Cu	200 mL (△250)		Sato et al. 2000
At. ferrooxidans	1.3	25	62	665 mg/L as AgCl	20	2	20% as Cu	200 mL (△250)		Sato et al. 2000
At. ferrooxidans	1.3	25	65	1330 mg/L as AgCl	20	2	20% as Cu	200 mL (△250)		Sato et al. 2000
At. ferrooxidans	1.3	25	65	1330 mg/L as AgCl	20	2	20% as Cu	200 mL (△250)	with contact between chalcopyrite and silver chloride	Sato et al. 2000
At. ferrooxidans	1.3	25	18	1330 mg/L as AgCl	20	2	20% as Cu	200 mL (△250)	without contact between chalcopyrite and silver chloride	Sato et al. 2000
At. ferrooxidans, *At. thiooxidans*, *Lp. ferrooxidans*	2	30	73	100 mg/L as Ag_2S	28	5	≈100%	100 mL (△250)		Yuehua et al. 2002
At. ferrooxidans, *At. thiooxidans*, *Lp. ferrooxidans*	2	30	76	200 mg/L as Ag_2S	28	5	≈100%	100 mL (△250)		Yuehua et al. 2002
At. ferrooxidans, *At. thiooxidans*, *Lp. ferrooxidans*	2	30	39	10 mg/L as Ag_2S	20	5	0.33% as Cu	100 mL (△250)		Yuehua et al. 2002
At. ferrooxidans, *At. thiooxidans*, *Lp. ferrooxidans*	2	30	85	50 mg/L as Ag_2S	20	5	0.33% as Cu	100 mL (△250)		Yuehua et al. 2002

Microorganism(s)	Initial pH	Temp. (℃)	Cu leached (%)	Ag addition	Leaching periods (days)	Pulp density (%)	Chalcopyrite grade (%)	Volume	Conditions	Ref.
At. ferrooxidans, At. thiooxidans, Lp.ferrooxidans	2	30	91	100 mg/L as Ag_2S	20	5	0.33% as Cu	100 mL (△250)		Yuehua et al. 2002
Acidithiobacilli, Leptospirilli	2	35	94	9 mg/L as Ag	15	10	0.68% as Cu	80 mL (△250)		Muñoz et al. 2007
Acidithiobacilli, Leptospirilli	2	35	97	46 mg/L as Ag	44	2.5	0.68% as Cu	80 mL (△250)		Muñoz et al. 2007
Acidithiobacilli, Leptospirilli	2	35	92	91 mg/L as Ag	44	5	0.68% as Cu	80 mL (△250)		Muñoz et al. 2007
Acidithiobacilli, Leptospirilli	2	35	86	137 mg/L as Ag	44	7.5	0.68% as Cu	80 mL (△250)		Muñoz et al. 2007
Acidithiobacilli, Leptospirilli	2	35	84	182 mg/L as Ag	44	10	0.68% as Cu	80 mL (△250)		Muñoz et al. 2007
Acidithiobacilli, Leptospirilli	2	35	72	274 mg/L as Ag	44	15	0.68% as Cu	80 mL (△250)		Muñoz et al. 2007
Acidithiobacilli, Leptospirilli	2	35	97	9 mg/L as Ag	27	10	0.68% as Cu	80 mL (△250)		Muñoz et al. 2007
Acidithiobacilli, Leptospirilli	2	35	97	23 mg/L as Ag	27	10	0.68% as Cu	80 mL (△250)		Muñoz et al. 2007

Microorganism(s)	Initial pH	Temp. (℃)	Cu leached (%)	Ag addition	Leaching periods (days)	Pulp density (%)	Chalcopyrite grade (%)	Volume	Conditions	Ref.
Acidithiobacilli, Leptospirilli	2	35	97	36 mg/L as Ag	27	10	0.68% as Cu	80 mL (△250)		Muñoz et al. 2007
Acidithiobacilli, Leptospirilli	2	35	97	91 mg/L as Ag	27	10	0.68% as Cu	80 mL (△250)		Muñoz et al. 2007
Acidithiobacilli, Leptospirilli	2	35	89	137 mg/L as Ag	27	10	0.68% as Cu	80 mL (△250)		Muñoz et al. 2007
Acidithiobacilli, Leptospirilli	1.2	35	86	9 mg/L as Ag	14	10	0.68% as Cu	80 mL (△250)		Muñoz et al. 2007
Acidithiobacilli, Leptospirilli	1.5	35	91	9 mg/L as Ag	14	10	0.68% as Cu	80 mL (△250)		Muñoz et al. 2007
Acidithiobacilli, Leptospirilli	1.8	35	92	9 mg/L as Ag	14	10	0.68% as Cu	80 mL (△250)		Muñoz et al. 2007
Acidithiobacilli, Leptospirilli	2	35	89	9 mg/L as Ag	14	10	0.68% as Cu	80 mL (△250)		Muñoz et al. 2007
Acidithiobacilli, Leptospirilli	2.5	35	82	9 mg/L as Ag	14	10	0.68% as Cu	80 mL (△250)		Muñoz et al. 2007
Acidithiobacilli, Leptospirilli	3	35	26	9 mg/L as Ag	14	10	0.68% as Cu	80 mL (△250)		Muñoz et al. 2007

Microorganism(s)	Initial pH	Temp. (ºC)	Cu leached (%)	Ag addition	Leaching periods (days)	Pulp density (%)	Chalcopyrite grade (%)	Volume	Conditions	Ref.
Acidithiobacilli, Leptospirilli	2	35	67	9 mg/L as Ag	14	10	0.68% as Cu	80 mL (△250)	Deionized water	Muñoz et al. 2007
Acidithiobacilli, Leptospirilli	2	35	94	9 mg/L as Ag	14	10	0.68% as Cu	80 mL (△250)	1/10 0K medium	Muñoz et al. 2007
Acidithiobacilli, Leptospirilli	2	35	93	9 mg/L as Ag	14	10	0.68% as Cu	80 mL (△250)	0K medium	Muñoz et al. 2007
Acidithiobacilli, Leptospirilli	2	35	88	9 mg/L as Ag	14	10	0.68% as Cu	80 mL (△250)	Cl-free 0K medium	Muñoz et al. 2007
Acidithiobacilli, Leptospirilli	2	35	94	9 mg/L as Ag	14	10	0.68% as Cu	80 mL (△250)	without Fe^{3+}	Muñoz et al. 2007
Acidithiobacilli, Leptospirilli	2	35	95	9 mg/L as Ag	14	10	0.68% as Cu	80 mL (△250)	with 0.1 g/L Fe^{3+}	Muñoz et al. 2007
Acidithiobacilli, Leptospirilli	2	35	96	9 mg/L as Ag	14	10	0.68% as Cu	80 mL (△250)	with 0.25 g/L Fe^{3+}	Muñoz et al. 2007
Acidithiobacilli, Leptospirilli	2	35	96	9 mg/L as Ag	14	10	0.68% as Cu	80 mL (△250)	with 0.5 g/L Fe^{3+}	Muñoz et al. 2007
Acidithiobacilli, Leptospirilli	2	35	85	9 mg/L as Ag	14	10	0.68% as Cu	80 mL (△250)	with 1 g/L Fe^{3+}	Muñoz et al. 2007

Microorganism(s)	Initial pH	Temp. (ºC)	Cu leached (%)	Ag addition	Leaching periods (days)	Pulp density (%)	Chalcopyrite grade (%)	Volume	Conditions	Ref.
Acidithiobacilli, Leptospirilli	2	35	81	9 mg/L as Ag	14	10	0.68% as Cu	80 mL (△250)	with 3 g/L Fe^{3+}	Muñoz et al. 2007
Acidithiobacilli, Leptospirilli	2	35	95	9 mg/L as Ag	14	10	0.68% as Cu	80 mL (△250)	with 5 g/L Fe^{3+}	Muñoz et al. 2007
At. ferrooxidans, *Acidithiobicillus*-like isolate, *Lp. ferrooxidans*, *β-proteobacterium* isolate, *Fm. acidiphilum*, *Firmicute* isolate, *Sulfobacillus* isolate, *Thiomonas* sp., *At. thiooxidans*, *Acidiphilum* sp., *Acidocella* sp., *Acidobacterium* sp.	2	30	32	< 0.02 mg/L as Ag	30	2	50	100 mL (△250)		Johnson et al. 2008
At. ferrooxidans, *Acidithiobicillus*-like isolate, *Lp. ferrooxidans*, *β-proteobacterium* isolate, *Fm. acidiphilum*, *Firmicute* isolate, *Sulfobacillus* isolate, *Thiomonas* sp., *At. thiooxidans*, *Acidiphilum* sp., *Acidocella* sp., *Acidobacterium* sp.	2	30	27	0.52 mg/L as Ag	30	2	70	100 mL (△250)		Johnson et al. 2008

Microorganism(s)	Initial pH	Temp. (ºC)	Cu leached (%)	Ag addition	Leaching periods (days)	Pulp density (%)	Chalcopyrite grade (%)	Volume	Conditions	Ref.
At. ferrooxidans, *Acidithiobicillus*-like isolate, *Lp. ferrooxidans*, *β-proteobacterium* isolate, *Fm. acidiphilum*, *Firmicute* isolate, *Sulfobacillus* isolate, *Thiomonas* sp., *At. thiooxidans*, *Acidiphilum* sp., *Acidocella* sp., *Acidobacterium* sp.	2	30	87	16 mg/L as Ag	30	2	< 60	100 mL (△250)		Johnson et al. 2008
At. ferrooxidans, *Acidithiobicillus*-like isolate, *Lp. ferrooxidans*, *β-proteobacterium* isolate, *Fm. acidiphilum*, *Firmicute* isolate, *Sulfobacillus* isolate, *Thiomonas* sp., *At. thiooxidans*, *Acidiphilum* sp., *Acidocella* sp., *Acidobacterium* sp.	2	30	81	30 mg/L as Ag	30	2	45-50	100 mL (△250)		Johnson et al. 2008

Microorganism(s)	Initial pH	Temp. (ºC)	Cu leached (%)	Ag addition	Leaching periods (days)	Pulp density (%)	Chalcopyrite grade (%)	Volume	Conditions	Ref.
At. ferrooxidans, *Acidithiobicillus*-like isolate, *Lp. ferrooxidans*, β-*proteobacterium* isolate, *Fm. acidiphilum*, *Firmicute* isolate, *Sulfobacillus* isolate, *Thiomonas* sp., *At. thiooxidans*, *Acidiphilum* sp., *Acidocella* sp., *Acidobacterium* sp., *Lp. ferriphilum*, *Am. ferrooxidans*, *Ferroplasma* sp., *Fx. thermotolerans*, *Sb. thermosulfidooxidans*, *Sb. acidophilus*, *Sb. benefaciens*, *Firmicute* isolate, *At. caldus*, *Acidicaldus organivorans*, *Alicyclobacillus* isolate	2	37	64	< 0.02 mg/L as Ag	30	2	50	100 mL (△250)		Johnson et al. 2008

Microorganism(s)	Initial pH	Temp. (ºC)	Cu leached (%)	Ag addition	Leaching periods (days)	Pulp density (%)	Chalcopyrite grade (%)	Volume	Conditions	Ref.
At. ferrooxidans, *Acidithiobicillus*- like isolate, *Lp. ferrooxidans*, β-*proteobacterium* isolate, *Fm. acidiphilum*, *Firmicute* isolate, *Sulfobacillus* isolate, *Thiomonas* sp., At. *thiooxidans*, *Acidiphilum* sp., *Acidocella* sp., *Acidobacterium* sp., *Lp. ferriphilum*, *Am. ferrooxidans*, *Ferroplasma* sp., *Fx. thermotolerans*, *Sb. thermosulfidooxidans*, *Sb. acidophilus*, *Sb. benefaciens*, *Firmicute* isolate, *At. caldus*, *Acidicaldus organivorans*, *Alicyclobacillus* isolate	2	37	47	0.52 mg/L as Ag	30	2	70	100 mL (△250)		Johnson et al. 2008

Microorganism(s)	Initial pH	Temp. (ºC)	Cu leached (%)	Ag addition	Leaching periods (days)	Pulp density (%)	Chalcopyrite grade (%)	Volume	Conditions	Ref.
At. ferrooxidans, *Acidithiobicillus*-like isolate, *Lp. f errooxidans*, β-*proteobacterium* isolate, *Fm. acidiphilum*, *Firmicute* isolate, *Sulfobacillus* isolate, *Thiomonas* sp., *At. thiooxidans*, *Acidiphilum* sp., *Acidocella* sp., *Acidobacterium* sp., *Lp. ferriphilum*, *Am. ferrooxidans*, *Ferroplasma* sp., *Fx. thermotolerans*, *Sb. thermosulfidooxidans*, *Sb. acidophilus*, *Sb. benefaciens*, *Firmicute* isolate, *At. caldus*, *Acidicaldus organivorans*, *Alicyclobacillus* isolate	2	37	82	16 mg/L as Ag	30	2	< 60	100 mL (△250)		Johnson et al. 2008

Microorganism(s)	Initial pH	Temp. (℃)	Cu leached (%)	Ag addition	Leaching periods (days)	Pulp density (%)	Chalcopyrite grade (%)	Volume	Conditions	Ref.
At. ferrooxidans, *Acidithiobicillus*-like isolate, *Lp. ferrooxidans*, β-*proteobacterium* isolate, *Fm. acidiphilum*, *Firmicute* isolate, *Sulfobacillus* isolate, *Thiomonas* sp., *At. thiooxidans*, *Acidiphilum* sp., *Acidocella* sp., *Acidobacterium* sp., *Lp. ferriphilum*, *Am. ferrooxidans*, *Ferroplasma* sp., *Fx. thermotolerans*, *Sb. thermosulfidooxidans*, *Sb. acidophilus*, *Sb. benefaciens*, *Firmicute* isolate, *At. caldus*, *Acidicaldus organivorans*, *Alicyclobacillus* isolate	2	37	53	30 mg/L as Ag	30	2	45-50	100 mL (△250)		Johnson et al. 2008
Lp. ferriphilum, *Am. ferrooxidans*, *Ferroplasma* sp., *Fx. thermotolerans*, *Sb. thermosulfidooxidans*, *Sb. acidophilus*, *Sb. benefaciens*, *Firmicute* isolate, *At. caldus*, *Acidicaldus organivorans*, *Alicyclobacillus* isolate	2	37	60	< 0.02 mg/L as Ag	30	2	50	100 mL (△250)		Johnson et al. 2008

Microorganism(s)	Initial pH	Temp. (ºC)	Cu leached (%)	Ag addition	Leaching periods (days)	Pulp density (%)	Chalcopyrite grade (%)	Volume	Conditions	Ref.
Lp. ferriphilum, *Am. ferrooxidans*, *Ferroplasma* sp., *Fx. thermotolerans*, *Sb. thermosulfidooxidans*, *Sb. acidophilus*, *Sb. benefaciens*, *Firmicute* isolate, *At. caldus*, *Acidicaldus organivorans*, *Alicyclobacillus* isolate	2	37	59	0.52 mg/L as Ag	30	2	70	100 mL (△250)		Johnson et al. 2008
Lp. ferriphilum, *Am. ferrooxidans*, *Ferroplasma* sp., *Fx. thermotolerans*, *Sb. thermosulfidooxidans*, *Sb. acidophilus*, *Sb. benefaciens*, *Firmicute* isolate, *At. caldus*, *Acidicaldus organivorans*, *Alicyclobacillus* isolate	2	37	76	16 mg/L as Ag	30	2	< 60	100 mL (△250)		Johnson et al. 2008
Lp. ferriphilum, *Am. ferrooxidans*, *Ferroplasma* sp., *Fx. thermotolerans*, *Sb. thermosulfidooxidans*, *Sb. acidophilus*, *Sb. benefaciens*, *Firmicute* isolate, *At. caldus*, *Acidicaldus organivorans*, *Alicyclobacillus* isolate	2	37	31	30 mg/L as Ag	30	2	45-50	100 mL (△250)		Johnson et al. 2008

Microorganism(s)	Initial pH	Temp. (ºC)	Cu leached (%)	Ag addition	Leaching periods (days)	Pulp density (%)	Chalcopyrite grade (%)	Volume	Conditions	Ref.
At. ferrooxidans Acidithiobacillus sp.	2	30	38	0.5 mg/L as Ag	20	1	3	100 mL (△500)		Feng et al. 2013
At. ferrooxidans Acidithiobacillus sp.	2	30	50	2 mg/L as Ag	20	1	3	100 mL (△500)		Feng et al. 2013
At. ferrooxidans Acidithiobacillus sp.	2	30	48	10 mg/L as Ag	20	1	3	100 mL (△500)		Feng et al. 2013
At. ferrooxidans Acidithiobacillus sp.	2	30	52	50 mg/L as Ag	20	1	3	100 mL (△500)		Feng et al. 2013
At. ferrooxidans, *At. thiooxidnas*, *Lp. ferrooxidans*	1.6	32	84	30 mg/L as Ag	30	3	2.1	N.D.	10 g/L Fe^{2+} and 10 g/L S^0	Abdollahi et al. 2015
At. ferrooxidans, *At. thiooxidnas*, *Lp. ferrooxidans*	1.6	32	83	60 mg/L as Ag	30	3	2.1	N.D.	10 g/L Fe^{2+} and 10 g/L S^0	Abdollahi et al. 2015
At. ferrooxidans, *At. thiooxidnas*, *Lp. ferrooxidans*	1.6	32	96	120 mg/L as Ag	30	3	2.1	N.D.	10 g/L Fe^{2+} and 10 g/L S^0	Abdollahi et al. 2015
At. ferrooxidans, *At. thiooxidnas*, *Lp. ferrooxidans*	1.6	32	96	200 mg/L as Ag	30	3	2.1	N.D.	10 g/L Fe^{2+} and 10 g/L S^0	Abdollahi et al. 2015
At. ferrooxidans, *At. thiooxidnas*, *Lp. ferrooxidans*	1.6	32	99	400 mg/L as Ag	30	3	2.1	N.D.	10 g/L Fe^{2+} and 10 g/L S^0	Abdollahi et al. 2015

Microorganism(s)	Initial pH	Temp. (℃)	Cu leached (%)	Ag addition	Leaching periods (days)	Pulp density (%)	Chalcopyrite grade (%)	Volume	Conditions	Ref.
At. ferrooxidans, *At. thiooxidnas*, *Lp. ferrooxidans*	1.6	32	55	1000 mg/L as Ag	30	3	2.1	N.D.	10 g/L Fe^{2+} and 10 g/L S^0	Abdollahi et al. 2015
At. ferrooxidans, *At. thiooxidnas*, *Lp. ferrooxidans*	1.7	32	89	2 mg/L as Ag	8	1	≈100%	200 mL (△500)		Xia et al. 2018
At. ferrooxidans, *At. thiooxidnas*, *Lp. ferrooxidans*	1.7	32	89	5 mg/L as Ag	8	1	≈100%	200 mL (△500)		Xia et al. 2018
At. ferrooxidans, *At. thiooxidnas*, *Lp. ferrooxidans*	1.7	32	89	10 mg/L as Ag	8	1	≈100%	200 mL (△500)		Xia et al. 2018
At. ferrooxidans, *At. thiooxidnas*, *Lp. ferrooxidans*	1.7	32	64	20 mg/L as Ag	8	1	≈100%	200 mL (△500)		Xia et al. 2018

1.3.1.4 Catalytic effect of silver on enargite dissolution

As mentioned above, a number of researchers have engaged in the study on chalcopyrite leaching with catalyst, especially for silver-catalyzed chalcopyrite bioleaching. However, in the case of enargite, the number of studies investigating the effect of silver on enargite leaching is limited. Miki et al. (2016) performed the enargite leaching with the addition of silver as a catalyst, achieving higher copper extraction rate (75% of recovery within one day). The study assumed that the reactions proposed by Hiroyoshi also occurred during enargite leaching, however, the detailed mechanism of silver catalytic effect on enargite dissolution is still unclear.

1.3.1.5 The issues of Ag-application into the mining operation

As was mention in past decades, the utilization of Ag in real operation is economically infeasible. Nazari et al. (2011) proposed the application of Ag-doped pyrite to minimize the Ag-loss in the process by attaching the silver ion on the surface of pyrite, while its loss was inevitable (around 10% of silver was not recycled). This fact suggests the necessity of alternative catalyst, which is cheap and certainly disposable. Based on the previous study using silver as a catalyst, the required property for alternative instead of silver is as bellows: (i) high electrical conductivity, (ii) high affinity for sulfide formation, or (iii) lower ion tendency than copper. Even though mercury is likely thought one of the possibilities, it is also not able to be used as a catalyst due to its high toxicity from the environmental point of view. New insight to find the novel catalyst is thus desperately required for further development in the exploitation of primary copper sulfides.

1.3.2 Catalytic effect of carbon materials

Carbon materials have recently attracted researchers' attention due to their electrochemically catalytic effect on the dissolution of refractory copper sulfides. Originally, the utility of AC as one of the carbon materials has been reported in the chalcopyrite bioleaching experiment (Nakazawa et al., 1998; Zhang et al., 2007; Liang et al., 2010). In these studies, chalcopyrite dissolution was thought to be enhanced basically through galvanic interaction between electrically nobler AC and electrically poorer chalcopyrite. Olvera et al. (2013) tested its catalytic effect in enargite leaching by electrochemical study, suggesting its potential for the enhancement of enargite dissolution by causing galvanic effect as well as modifying semi-conductive surface property of enargite. Jahromi et al. (2016) indeed confirmed the effectiveness of AC in enargite leaching, where enargite dissolution was promoted based on (i) the oxidation of Fe^{2+} to Fe^{3+} (oxidant regeneration) and (ii) direct enargite oxidation by in-situ hydrogen peroxide production. These mechanisms were proposed by Ahumada et al. (2002), where the oxidation reactions occur on the surface of AC as follows;

$$2C_{red} + O_2 + 2H_2O = 2H_2O_2 + 2C_{ox} \quad \text{(Eq. 1-7)}$$

$$2Fe^{2+} + H_2O_2 + 2H^+ = 2Fe^{3+} + 2H_2O \quad \text{(Eq. 1-8)}$$

C_{red} and C_{ox} indicate that surface functional groups on the surface of AC. Eq. 1-7 shows the generation of hydrogen peroxide occurring on the surface of AC through the reaction of quinone or other oxidative functional groups such as carboxylic acid, anhydrides, hydroxyls, lactol groups, lactone groups, and phenol groups. This hydrogen peroxide is subsequently (i) consumed to directly oxidize enargite or (ii) used for the oxidation of Fe^{2+} to Fe^{3+} (Eq. 1-8), followed by enargite oxidation by produced Fe^{3+}. Modification of functional groups on the surface of AC with sulfuric acid, hydrochloric acid, or nitric acid was tested, confirming that the oxidation ability of AC was indeed varied with different acid treatments even in the leaching process (Jahromi et al., 2019).

On the other hand, it has been reported that the presence of AC suppress Eh rise during bioleaching process, implying that AC would also catalyze the Fe(III)-reduction

(Nakazawa et al., 1998; Zhang et al., 2007; Ma et al., 2017; Hao et al., 2018). This adverse catalytic effect of AC was confirmed in the chemical experiment conducted by Vargas et al. (2009), where Fe^{3+}-reduction to Fe^{2+} was able to be catalyzed by the AC. Liang et al. (2010) observed the decrease in Fe^{3+}/Fe^{2+} ratio with the addition of AC during chalcopyrite bioleaching, ensuring that Fe^{3+} was indeed catalytically reduced to Fe^{2+} by AC even in the presence of microorganisms. Although the reduction mechanism has yet been well-described, not only Fe^{2+}-oxidation but also Fe^{3+}-reduction have to be considered as the catalytic reaction caused by AC during the bioleaching process. Bioleaching of chalcopyrite catalyzed by carbon materials are summarized in Table 1.4.

Table 1.4 The list of previous studies in carbon-assisted chalcopyrite bioleaching.

Microorganism(s)	Initial pH	Temp. (℃)	Cu leached (%)	Carbon type	Carbon addition	Leaching periods (days)	Pulp density (%)	Chalcopyrite grade (%)	Volume	Conditions	Ref.
At. ferrooxidans	1.3	25	33	Activated carbon	0.5 g/L	19	2	20.39% as Cu	200 mL (△250)	-	Nakazawa et al. 1998
At. ferrooxidans	1.3	25	42	Activated carbon	2.5 g/L	19	2	20.39% as Cu	200 mL (△250)	-	Nakazawa et al. 1998
At. ferrooxidans	1.3	25	44	Activated carbon	2.5 g/L	38	2	20.39% as Cu	200 mL (△250)	−70+100 mesh	Nakazawa et al. 1998
At. ferrooxidans	1.3	25	52	Activated carbon	2.5 g/L	35	2	20.39% as Cu	200 mL (△250)	−200+280 mesh	Nakazawa et al. 1998
At. ferrooxidans	1.3	25	55	Activated carbon	2.5 g/L	35	2	20.39% as Cu	200 mL (△250)	−400 mesh	Nakazawa et al. 1998
At. ferrooxidans	1	25	73	Activated carbon	5 g/L	35	2	20.39% as Cu	200 mL (△250)	−400 mesh	Nakazawa et al. 1998
At. ferrooxidans	1.3	25	56	Activated carbon	5 g/L	35	2	20.39% as Cu	200 mL (△250)	−400 mesh	Nakazawa et al. 1998

Microorganism(s)	Initial pH	Temp. (℃)	Cu leached (%)	Carbon type	Carbon addition	Leaching periods (days)	Pulp density (%)	Chalcopyrite grade (%)	Volume	Conditions	Ref.
At. ferrooxidans	1.5	25	50	Activated carbon	5 g/L	35	2	20.39% as Cu	200 mL (△250)	−400 mesh	Nakazawa et al. 1998
At. ferrooxidans	1.7	25	41	Activated carbon	5 g/L	35	2	20.39% as Cu	200 mL (△250)	−400 mesh	Nakazawa et al. 1998
At. ferrooxidans	1.3	25	12	Activated carbon	2.5 g/L	35	2	20.39% as Cu	200 mL (△250)	−400 mesh without contact	Nakazawa et al. 1998
At. ferrooxidans	1.3	25	68	Activated carbon	2.5 g/L	35	2	20.39% as Cu	200 mL (△250)	−400 mesh with contact	Nakazawa et al. 1998
At. ferrooxidan, *At. thiooxidans*	1.2	30	64	Activated carbon	0.5 g/L	25	25	0.4% as Cu	100 mL (△250)	< 7.4 μm of AC	Zhang et al. 2007
At. ferrooxidan, *At. thiooxidans*	1.2	30	70	Activated carbon	2.0 g/L	25	25	0.4% as Cu	100 mL (△250)	< 7.4 μm of AC	Zhang et al. 2007
At. ferrooxidan, *At. thiooxidans*	1.2	30	79	Activated carbon	3.0 g/L	25	25	0.4% as Cu	100 mL (△250)	< 7.4 μm of AC	Zhang et al. 2007

Microorganism(s)	Initial pH	Temp. (℃)	Cu leached (%)	Carbon type	Carbon addition	Leaching periods (days)	Pulp density (%)	Chalcopyrite grade (%)	Volume	Conditions	Ref.
At. ferrooxidan, At. thiooxidans	1.2	30	60	Activated carbon	5.0 g/L	25	25	0.4% as Cu	100 mL (△250)	< 7.4 μm of AC	Zhang et al. 2007
At. ferrooxidan, At. thiooxidans	1.2	30	65	Activated carbon	3.0 g/L	25	25	0.4% as Cu	100 mL (△250)	< 7.4 μm of AC 0 day resting time	Zhang et al. 2007
At. ferrooxidan, At. thiooxidans	1.2	30	84	Activated carbon	3.0 g/L	25	25	0.4% as Cu	100 mL (△250)	< 7.4 μm of AC 1 day resting time	Zhang et al. 2007
At. ferrooxidan, At. thiooxidans	1.2	30	86	Activated carbon	3.0 g/L	25	25	0.4% as Cu	100 mL (△250)	< 7.4 μm of AC 2 day resting time	Zhang et al. 2007
At. ferrooxidan, At. thiooxidans	1.2	30	72	Activated carbon	3.0 g/L	25	25	0.4% as Cu	100 mL (△250)	< 7.4 μm of AC 4 day resting time	Zhang et al. 2007
At. ferrooxidan, At. thiooxidans	1.2	30	66	Activated carbon	3.0 g/L	25	25	0.4% as Cu	100 mL (△250)	< 7.4 μm of AC 6 day resting time	Zhang et al. 2007
Ac. manzaensis	1.5	65	90	Activated carbon	1.0 g/L	10	1	≈100%	100 mL (△250)		Liang et al. 2010

Microorganism(s)	Initial pH	Temp. (℃)	Cu leached (%)	Carbon type	Carbon addition	Leaching periods (days)	Pulp density (%)	Chalcopyrite grade (%)	Volume	Conditions	Ref.
Ac. manzaensis	1.5	65	94	Activated carbon	2.0 g/L	10	1	≈100%	100 mL (△250)		Liang et al. 2010
Ac. manzaensis	1.5	65	93	Activated carbon	3.0 g/L	10	1	≈100%	100 mL (△250)		Liang et al. 2010
Ac. manzaensis	1.5	65	88	Activated carbon	4.0 g/L	10	1	≈100%	100 mL (△250)		Liang et al. 2010
Ac. brierleyi *Ac. manzaensis* *Ms. sedula* *Sf. metallicus*	1.5	65	56	Activated carbon	2.0 g/L	8	1	33.69% as Cu	100 mL (△250)	37-74 μm of AC	Ma et al. 2017
Lp. ferriphilum, *At. caldus*, *Sb. thermosulfidooxidans*, *Fp. thermophilum*	1.8	45	77	Graphite	2.0 g/L	15	2	2.3% as Cu	100 mL (△250)	2 m^2/g in specific surface are < 75 μm in size	Hao et al. 2018
Lp. ferriphilum, *At. caldus*, *Sb. thermosulfidooxidans*, *Fp. thermophilum*	1.8	45	86	Activated carbon	2.0 g/L	15	2	2.3% as Cu	100 mL (△250)	400 m^2/g in specific surface are < 75 μm in size	Hao et al. 2018
Lp. ferriphilum, *At. caldus*, *Sb. thermosulfidooxidans*, *Fp. thermophilum*	1.8	45	95	Activated carbon	2.0 g/L	15	2	2.3% as Cu	100 mL (△250)	800 m^2/g in specific surface are < 75 μm in size	Hao et al. 2018
Lp. ferriphilum, *At. caldus*, *Sb. thermosulfidooxidans*, *Fp. thermophilum*	1.8	45	99	Activated carbon	2.0 g/L	15	2	2.3% as Cu	100 mL (△250)	1200 m^2/g in specific surface are < 75 μm in size	Hao et al. 2018

The addition of AC also shows a positive effect on the formation of scorodite ($FeAsO_4 \cdot 2H_2O$) as an immobilized form of once-dissolved As from enargite (Jahromi et al., 2018). This would attribute to the catalytic reaction on the surface of AC; As-oxidation was greatly enhanced in the presence of AC, possibly by hydrogen peroxide generated (Radzinski et al., 2016). The enhanced As-oxidation on the AC surface led to the As(V) supply for the in-situ formation of scorodite during enargite leaching, consequently promoting the immobilization of As in the solid phase (Jahromi et al., 2018).

Although the catalytic mechanism of AC in the leaching process is roughly summarized as (i) electrochemical reaction to accelerate the electron transfer (e.g. galvanic interaction and other redox reaction) and (ii) chemical reaction by surface functional groups to produce the oxidant (e.g. Fe(III) and hydrogen peroxide), further discussion is still necessary to reach a consensus among researchers. Moreover, the number of studies investigating the effect of AC on enargite bioleaching is still limited, while the addition of AC in chemical enargite leaching are shown effective in enhanced Cu dissolution and As immobilization.

1.4 The objective of this thesis

The objective of this thesis was set to seek a useful catalyst for the enhancement of Cu solubilization in enargite bioleaching. This work is divided into two parts; fundamental studies and application studies.

In the former part (fundamental studies), the catalytic effects of Ag and AC were evaluated in bioleaching of enargite concentrate and its catalytic mechanisms were elucidated. Prior to the bioleaching test, the applicability of molybdenum blue method to Cu sulfides leachate was tested for the determination of As(III) concentration in **chapter 3**. In **chapters 4 and 5**, the catalytic effect of Ag and AC was indeed tested in bioleaching of enargite concentrate using the mixed culture of moderately thermophilic microorganisms at 45ºC. Clarification of the underlying catalytic mechanism was the main purpose of these chapters. Based on the result obtained in **chapter 5**, the detailed catalytic mechanism of AC was further tested by comparing the various type of AC in **chapter 6**. The most appropriate AC was determined for the enhancement of Cu solubilization from enargite during the bioleaching process.

In the latter part (application studies), obtained information from fundamental studies were applied to As-bearing copper concentrate for the further development of AC-catalyzed bioleaching system. AC-catalyzed bioleaching of As-bearing Cu concentrate with high pulp density was conducted in the stirred tank reactor to evaluate the catalytic effect of AC in scale-up system (**chapter 7**).

Finally, whole phenomena in the presence of catalysts were summarized, and future research strategy was proposed for the further development of the enargite bioleaching system.

References

1. Abdollahi, H., Noaparast, M., Shafaei, S.Z., Manafi, Z., Muñoz, J.A. and Tuovinen, O.H., 2015. Silver-catalyzed bioleaching of copper, molybdenum and rhenium from a chalcopyrite–molybdenite concentrate. International Biodeterioration & Biodegradation 104, 194-200.
2. Acevedo, F., Gentina, J. and García, N., 1998. CO_2 supply in the biooxidation of an enargite-pyrite gold concentrate. Biotechnology Letters 20, 257-259.
3. Ahonen, L. and Tuovinen, O.H., 1990. Catalytic effects of silver in the microbiological leaching of finely ground chalcopyrite-containing ore materials in shake flasks. Hydrometallurgy 24, 219-236.
4. Ahumada, E., Lizama, H., Orellana, F., Suárez, C., Huidobro, A., Sepúlveda-Escribano, A. and Rodrıguez-Reinoso, F., 2002. Catalytic oxidation of Fe(II) by activated carbon in the presence of oxygen: Effect of the surface oxidation degree on the catalytic activity. Carbon 40, 2827-2834.
5. Ai, C., McCarthy, S., Liang, Y., Rudrappa, D., Qiu, G. and Blum, P., 2017. Evolution of copper arsenate resistance for enhanced enargite bioleaching using the extreme thermoacidophile *Metallosphaera sedula*. Journal of Industrial Microbiology & Biotechnology 44, 1613-1625.
6. Astudillo, C. and Acevedo, F., 2008. Adaptation of *Sulfolobus metallicus* to high pulp densities in the biooxidation of a flotation gold concentrate. Hydrometallurgy 92, 11-15.
7. Ballester, A., Gonzalez, F., Blázquez, M. and Mier, J., 1990. The influence of various ions in the bioleaching of metal sulphides. Hydrometallurgy 23, 221-235.
8. Bosecker, K., 1997. Bioleaching: metal solubilization by microorganisms. FEMS Microbiology Reviews 20, 591-604.
9. Burdick, C. L. and Ellis, J. H., 1917. The crystal structure of chalcopyrite determined by X-rays. Journal of the American Chemical Society 39, 2518-2525.
10. Canales, C., Acevedo, F. and Gentina, J.C., 2002. Laboratory-scale continuous bio-oxidation of a gold concentrate of high pyrite and enargite content. Process Biochemistry 37, 1051-1055.
11. Corkhill, C., Wincott, P., Lloyd, J. and Vaughan, D., 2008. The oxidative dissolution of arsenopyrite (FeAsS) and enargite (Cu_3AsS_4) by *Leptospirillum ferrooxidans*. Geochimica et Cosmochimica Acta 72, 5616-5633.
12. Curreli, L., Loi, G., Peretti, R., Rossi, G., Trois, P. and Zucca, A., 1997. Gold recovery enhancement from complex sulphide ores through combined bioleaching and cyanidation. Minerals Engineering 10, 567-576.
13. Deveci, H., Akcil, A. and Alp, I., 2004. Bioleaching of complex zinc sulphides

using mesophilic and thermophilic bacteria: comparative importance of pH and iron. Hydrometallurgy 73, 293-303.

14. Escobar, B., Huenupi, E. and Wiertz, J.V., 1997. Chemical and biological leaching of enargite. Biotechnology Letters 19, 719-722.
15. Escobar, B., Huenupi, E., Godoy, I. and Wiertz, J.V., 2000. Arsenic precipitation in the bioleaching of enargite by *Sulfolobus* BC at 70 C. Biotechnology Letters 22, 205-209.
16. Fantauzzi, M., Rossi, G., Elsener, B., Loi, G., Atzei, D. and Rossi, A., 2009. An XPS analytical approach for elucidating the microbially mediated enargite oxidative dissolution. Analytical and Bioanalytical Chemistry 393, 1931.
17. Feng, S., Yang, H., Xin, Y., Gao, K., Yang, J., Liu, T., Zhang, L. and Wang, W., 2013. A novel and highly efficient system for chalcopyrite bioleaching by mixed strains of *Acidithiobacillus*. Bioresource Technology 129, 456-462.
18. Frías, C., Díaz, G., Ocaña, N. and Lozano, J., 2002. Silver, gold and lead recovery from bioleaching residues using the PLINT process. Minerals Engineering 15, 877-878.
19. Gautier, V., Escobar, B., Vargas, T., 2008. Cooperative action of attached and planktonic cells during bioleaching of chalcopyrite with *Sulfolobus metallicus* at 70°C. Hydrometallurgy 94, 121-126.
20. Ghahremaninezhad, A., Asselin, E. and Dixon, D., 2010. Electrochemical evaluation of the surface of chalcopyrite during dissolution in sulfuric acid solution. Electrochimica Acta 55, 5041-5056.
21. Ghahremaninezhad, A., Dixon, D. and Asselin, E., 2013. Electrochemical and XPS analysis of chalcopyrite ($CuFeS_2$) dissolution in sulfuric acid solution. Electrochimica Acta 87, 97-112.
22. Ghahremaninezhad, A., Radzinski, R., Gheorghiu, T., Dixon, D.G. and Asselin, E., 2015. A model for silver ion catalysis of chalcopyrite ($CuFeS_2$) dissolution. Hydrometallurgy 155, 95-104.
23. Gomez, E., Ballester, A., Blázquez, M. and González, F., 1999. Silver-catalyzed bioleaching of a chalcopyrite concentrate with mixed cultures of moderately thermophilic microorganisms. Hydrometallurgy 51, 37-46.
24. Hallberg, K. B., Lindströmt, E. B., 1994. Characterization of *Thiobacillus caldus* sp. nov., a moderately thermophilic acidophile. Journal of Microbiology, 140, 3451-3456.
25. Hao, X., Liu, X., Zhu, P., Chen, A., Liu, H., Yin, H., Qiu, G. and Liang, Y., 2018. Carbon material with high specific surface area improves complex copper ores'

bioleaching efficiency by mixed moderate thermophiles. Minerals 8, 301.

26. Henao, J., de Delgado, G.D., Delgado, J., Castrillo, F. and Odreman, O., 1994. Single-crystal structure refinement of enargite [Cu_3AsS_4]. Materials Research Bulletin 29, 1121-1127.
27. Hippe, H., 2000. *Leptospirillum* gen. nov. (ex Markosyan 1972), nom. rev., including *Leptospirillum ferrooxidans* sp. nov. (ex Markosyan 1972), nom. rev. and *Leptospirillum thermoferrooxidans* sp. nov. (Golovacheva et al. 1992). International Journal of Systematic and Evolutionary Microbiology 50, 501-503.
28. Hiroyoshi, N., Miki, H., Hirajima, T. and Tsunekawa, M., 2000. A model for ferrous-promoted chalcopyrite leaching. Hydrometallurgy 57, 31-38.
29. Hiroyoshi, N., Miki, H., Hirajima, T. and Tsunekawa, M., 2001. Enhancement of chalcopyrite leaching by ferrous ions in acidic ferric sulfate solutions. Hydrometallurgy 60 185-197.
30. Hiroyoshi, N., Arai, M., Miki, H., Tsunekawa, M. and Hirajima, T., 2002. A new reaction model for the catalytic effect of silver ions on chalcopyrite leaching in sulfuric acid solutions. Hydrometallurgy 63, 257-267.
31. Hiroyoshi, N., Kuroiwa, S., Miki, H., Tsunekawa, M. and Hirajima, T., 2004. Synergistic effect of cupric and ferrous ions on active-passive behavior in anodic dissolution of chalcopyrite in sulfuric acid solutions. Hydrometallurgy 74, 103-116.
32. Hiroyoshi, N., Kuroiwa, S., Miki, H., Tsunekawa, M. and Hirajima, T., 2007. Effects of coexisting metal ions on the redox potential dependence of chalcopyrite leaching in sulfuric acid solutions. Hydrometallurgy 87, 1-10.
33. Hiroyoshi, N., Kitagawa, H. and Tsunekawa, M., 2008a. Effect of solution composition on the optimum redox potential for chalcopyrite leaching in sulfuric acid solutions. Hydrometallurgy 91, 144-149.
34. Hiroyoshi, N., Tsunekawa, M., Okamoto, H., Nakayama, R. and Kuroiwa, S., 2008b. Improved chalcopyrite leaching through optimization of redox potential. Canadian Metallurgical Quarterly 47, 253-258.
35. Huber, G., Stetter, K. O., 1991. *Sulfolobus metallicus*, sp. nov., a novel strictly chemolithoautotrophic thermophilic archaeal species of metal-mobilizers. Systematic and Applied Microbiology, 14, 372-378.
36. Jahromi, F. and Ghahreman, A., 2016. Activated carbon assisted atmospheric leaching of enargite in chloride media, International Copper Conference 2016 abstract, pp. 1453-1464.

37. Jahromi, F.G., Cowan, D.H. and Ghahreman, A., 2017. Lanxess Lewatit® AF 5 and activated carbon catalysis of enargite leaching in chloride media; a parameters study. Hydrometallurgy 174, 184-194.
38. Jahromi, F.G. and Ghahreman, A., 2018. In-situ oxidative arsenic precipitation as scorodite during carbon catalyzed enargite leaching process. Journal of Hazardous Materials 360, 631-638.
39. Jahromi, F.G., Alvial-Hein, G., Cowan, D.H. and Ghahreman, A., 2019. The kinetics of enargite dissolution in chloride media in the presence of activated carbon and AF 5 catalysts. Minerals Engineering 143, 106013.
40. Johnson, D.B., Okibe, N., Wakeman, K. and Yajie, L., 2008. Effect of temperature on the bioleaching of chalcopyrite concentrates containing different concentrations of silver. Hydrometallurgy 94, 42-47.
41. Lee, J., Acar, S., Doerr, D.L. and Brierley, J.A., 2011. Comparative bioleaching and mineralogy of composited sulfide ores containing enargite, covellite and chalcocite by mesophilic and thermophilic microorganisms. Hydrometallurgy 105, 213-221.
42. Leist, M., Casey, R. and Caridi, D., 2000. The management of arsenic wastes: problems and prospects. Journal of Hazardous Materials 76, 125-138.
43. Liang, C.-L., Xia, J.-L., Zhao, X.-J., Yang, Y., Gong, S.-Q., Nie, Z.-Y., Ma, C.-Y., Zheng, L., Zhao, Y.-D., and Qiu, G.-z., 2010. Effect of activated carbon on chalcopyrite bioleaching with extreme thermophile *Acidianus manzaensis*. Hydrometallurgy 105, 179-185.
44. Lièvremont, D., Bertin, P.N. and Lett, M.-C., 2009. Arsenic in contaminated waters: biogeochemical cycle, microbial metabolism and biotreatment processes. Biochimie 91, 1229-1237.
45. Ma, Y.-l., Liu, H.-c., Xia, J.-l., Nie, Z.-y., Zhu, H.-r., Zhao, Y.-d., Zheng, L., Hong, C.-h. and Wen, W., 2017. Relatedness between catalytic effect of activated carbon and passivation phenomenon during chalcopyrite bioleaching by mixed thermophilic Archaea culture at 65ºC. Transactions of Nonferrous Metals Society of China 27, 1374-1384.
46. Matschullat, J., 2000. Arsenic in the geosphere—a review. Science of the Total Environment 249, 297-312.
47. Miki, H., Iguchi, A., Hirajima, T. and Sasaki, K., 2016. Catalytic effect of silver on arsenic-containing copper sulfide dissolution in acidic solution. Hydrometallurgy 162, 1-8.

48. Morales, M., Arancibia, J., Lemus, M., Silva, J., Gentina, J. C., Aroca, G., 2011. Bio-oxidation of H_2S by *Sulfolobus metallicus*. Biotechnology Letters 33, 2141-2145.
49. Muñoz, J., Blázquez, M., González, F., Ballester, A., Acevedo, F., Gentina, J. and González, P., 2006. Electrochemical study of enargite bioleaching by mesophilic and thermophilic microorganisms. Hydrometallurgy 84, 175-186.
50. Muñoz, J., Dreisinger, D., Cooper, W. and Young, S., 2007. Silver-catalyzed bioleaching of low-grade copper ores.: Part I: Shake flasks tests. Hydrometallurgy 88, 3-18.
51. Nakazawa, H., Fujisawa, H. and Sato, H., 1998. Effect of activated carbon on the bioleaching of chalcopyrite concentrate. International Journal of Mineral Processing 55, 87-94.
52. Nasernejad, B., Kaghazchi, T., Edrisi, M. and Sohrabi, M., 1999. Bioleaching of molybdenum from low-grade copper ore. Process biochemistry 35, 437-440.
53. Nazari, G., Dixon, D. and Dreisinger, D., 2011. Enhancing the kinetics of chalcopyrite leaching in the Galvanox™ process. Hydrometallurgy 105, 251-258.
54. Nazari, G., Dixon, D. and Dreisinger, D., 2012a. The role of galena associated with silver-enhanced pyrite in the kinetics of chalcopyrite leaching during the Galvanox™ process. Hydrometallurgy 111, 35-45.
55. Nazari, G., Dixon, D. and Dreisinger, D., 2012b. The mechanism of chalcopyrite leaching in the presence of silver-enhanced pyrite in the Galvanox™ process. Hydrometallurgy 113, 122-130.
56. Nazari, G., Dixon, D. and Dreisinger, D., 2012c. The role of silver-enhanced pyrite in enhancing the electrical conductivity of sulfur product layer during chalcopyrite leaching in the Galvanox™ process. Hydrometallurgy 113, 177-184.
57. Norris, P. R., Burton, N. P., Foulis, N. A. M., 2000. Acidophiles in bioreactor mineral processing. Extremophiles 4, 71-76.
58. Ohmura, N., Sasaki, K., Matsumoto, N., Saiki, H., 2002. Anaerobic respiration using Fe^{3+}, S^0, and H_2 in the chemolithoautotrophic bacterium *Acidithiobacillus ferrooxidans*. Journal of Bacteriology, 184, 2081-2087.
59. Okibe, N., Gericke, M., Hallberg, K. B., Johnson, D. B., 2003. Enumeration and characterization of acidophilic microorganisms isolated from a pilot plant stirred-tank bioleaching operation. Applied and Environmental Microbiology, 69, 1936-1943.
60. Olson, G.J., Sakai, C.K., Parks, E. and Brinckman, F., 1990. Bioleaching of cobalt from smelter wastes by *Thiobacillus ferrooxidans*. Journal of Industrial

Microbiology & Biotechnology 6, 49-52.

61. Olvera, O., Dixon, D. and Asselin, E., 2013. Electrochemical study of the dissolution of enargite (Cu_3 AsS_4) in contact with activated carbon. Electrochimica Acta 107, 525-536.
62. Oremland, R.S. and Stolz, J.F., 2005. Arsenic, microbes and contaminated aquifers. Trends in Microbiology 13, 45-49.
63. Padilla, R., Jerez, O. and Ruiz, M., 2015. Kinetics of the pressure leaching of enargite in $FeSO_4$–H_2SO_4–O_2 media. Hydrometallurgy 158, 49-55.
64. Pina, P. S., Oliveira, V. A., Cruz, F. L. S., Leão, V. A., 2010. Kinetics of ferrous iron oxidation by *Sulfobacillus thermosulfidooxidans*. Biochemical Engineering Journal, 51, 194-197.
65. Radzinski, R., Nazari, A. and Ghahreman, A., 2016. Activated-carbon catalyzed arsenic oxidation: Formation of hydrogen peroxide in acidic solutions, Hydroprocess 2016 Conference. Santiago, Chile.
66. Riveros, P., Dutrizac, J. and Spencer, P., 2001. Arsenic disposal practices in the metallurgical industry. Canadian Metallurgical Quarterly 40, 395-420.
67. Rodriguez, Y., Ballester, A., Blazquez, M., Gonzalez, F. and Munoz, J., 2003. New information on the chalcopyrite bioleaching mechanism at low and high temperature. Hydrometallurgy 71, 47-56.
68. Ruiz, M., Vera, M. and Padilla, R., 2011. Mechanism of enargite pressure leaching in the presence of pyrite. Hydrometallurgy 105, 290-295.
69. Safarzadeh, M.S. and Miller, J.D., 2014. Reaction of enargite (Cu_3AsS_4) in hot concentrated sulfuric acid under an inert atmosphere. Part I: Enargite concentrate. International Journal of Mineral Processing 128, 68-78.
70. Sasaki, K., Nakamuta, Y., Hirajima, T. and Tuovinen, O., 2009. Raman characterization of secondary minerals formed during chalcopyrite leaching with *Acidithiobacillus ferrooxidans*. Hydrometallurgy 95, 153-158.
71. Sasaki, K., Takatsugi, K., Kaneko, K., Kozai, N., Ohnuki, T., Tuovinen, O. and Hirajima, T., 2010. Characterization of secondary arsenic-bearing precipitates formed in the bioleaching of enargite by *Acidithiobacillus ferrooxidans*. Hydrometallurgy 104, 424-431.
72. Sasaki, K., Takatsugi, K. and Hirajima, T., 2011. Effects of initial Fe^{2+} concentration and pulp density on the bioleaching of Cu from enargite by *Acidianus brierleyi*. Hydrometallurgy 109, 153-160.
73. Sato, H., Nakazawa, H. and Kudo, Y., 2000. Effect of silver chloride on the bioleaching of chalcopyrite concentrate. International Journal of Mineral Processing 59, 17-24.

74. Segerer, A., Neuner, A., Kristjansson, J. K., Stetter, K. O., 1986. *Acidianus infernus* gen. nov., sp. nov., and *Acidianus brierleyi* comb. nov.: facultatively aerobic, extremely acidophilic thermophilic sulfur-metabolizing archaebacterial. International Journal of Systematic Bacteriology, 36, 559-564.
75. Sillitoe, R.H., 2010. Porphyry copper systems. Economic Geology 105, 3-41.
76. Smedley, P. and Kinniburgh, D., 2002. A review of the source, behavior and distribution of arsenic in natural waters. Applied Geochemistry 17, 517-568.
77. Takatsugi, K., Sasaki, K. and Hirajima, T., 2011. Mechanism of the enhancement of bioleaching of copper from enargite by thermophilic iron-oxidizing archaea with the concomitant precipitation of arsenic. Hydrometallurgy 109, 90-96.
78. Vargas, T., Diaz, P. and Escobar, B., 2009. Reductive action of activated carbon on ferric iron interferes on the determination of the oxidative activity of *Acidithiobacillus ferrooxidans* on ferrous iron, Advanced Materials Research. Trans Tech Publ, pp. 291-294.
79. Waksman, S. A., Joffe, J. S., 1992. Microorganisms concerned in the oxidation of sulfur in the soil. Journal of Bacteriology, 7, 239-256
80. Xia, J., Yang, Y., He, H., Liang, C., Zhao, X., Zheng, L., Ma, C., Zhao, Y., Nie, Z., Qiu, G., 2010. Investigation of the sulfur speciation during chalcopyrite leaching by moderate thermophile *Sulfobacillus thermosulfidooxidans*. International Journal of Mineral Processing, 94, 52-57.
81. Xia, J.-l., Song, J.-j., Liu, H.-c., Nie, Z.-y., Shen, L., Yuan, P., Ma, C.-y., Zheng, L. and Zhao, Y.-d., 2018. Study on catalytic mechanism of silver ions in bioleaching of chalcopyrite by SR-XRD and XANES. Hydrometallurgy 180, 26-35.
82. Yang, T., Xu, Z., Wen, J. and Yang, L., 2009. Factors influencing bioleaching copper from waste printed circuit boards by *Acidithiobacillus ferrooxidans*. Hydrometallurgy 97, 29-32.
83. Yuehua, H., Guanzhou, Q., Jun, W. and Dianzuo, W., 2002. The effect of silver-bearing catalysts on bioleaching of chalcopyrite. Hydrometallurgy 64, 81-88.
84. Zhang, W.-M., and Gu, S.-F., 2007. Catalytic effect of activated carbon on bioleaching of low-grade primary copper sulfide ores. Transactions of Nonferrous Metals Society of China 17, 1123-1127.

Chapter 2

Methodology

2.1 Culture medium and chemical reagents

2.1.1 Culture media

2.1.1.1 Heterotrophic basal salts (HBS)

Solution composition of HBS (50×)

22.5 g/L $(NH_4)_2SO_4$

2.5 g/L KCl

2.5 g/L KH_2PO_4

25 g/L $MgSO_4 \cdot 7H_2O$

0.7 g/L $Ca(NO_3)_2 \cdot 4H_2O$

7.1 g/L Na_2SO_4

Solubilized into distilled water, stored in the sterilized bottle at ambient temperature. To make 1 L of HBS (1×) media, 20 mL of HBS stock (50×) was mixed with 980 mL of deionized water and sterilized by autoclave (120°C, 20 min).

2.1.1.2 Acidophilic basal salts (ABS)

Solution composition of ABS (50×)

22.5 g/L $(NH_4)_2SO_4$

2.5 g/L KCl

2.5 g/L KH_2PO_4

25 g/L $MgSO_4 \cdot 7H_2O$

0.7 g/L $Ca(NO_3)_2 \cdot 4H_2O$

7.5 g/L $Na_2SO_4 \cdot 10H_2O$

Solubilized into distilled water, stored in sterilized bottle at ambient temperature. To make 1 L of ABS (1×) media, 20 mL of ABS stock (50×) was mixed with 980 mL of deionized water and sterilized by autoclave (120°C, 20 min).

2.1.2 Chemical reagents

1M Ferric iron stock solution

$Fe_2(SO_4)_3 \cdot nH_2O$ (n = 5-7; Wako pure chemicals) was solubilized into acidic distilled water (pH 1.5 with H_2SO_4), and Fe^{3+} concentration was measured by *o*-phenanthroline method using ascorbic acid as reducing agent. Based on the Fe^{3+} concentration, the Fe^{3+} stock was diluted with acidic distilled water until its Fe concentration becomes 1 M. Filtrated (0.2 μm) and stored in the sterilized bottle at 4°C.

1M Ferrous iron stock solution

$FeSO_4 \cdot 7H_2O$ (Wako pure chemicals) was solubilized into acidic distilled water (pH 1.5 with H_2SO_4), filtrated (0. 2 μm), and stored in the sterilized bottle at 4°C.

10 g/l As(III) stock solutions

$NaAsO_2$ (Sigma-Aldrich) was added into distilled water and acidified to pH 1.5 with H_2SO_4. The stock solutions were filter-sterilized through 0.2 μm polyethersulfone membranes (Steritop, Millipore) and stored at 4°C.

10 g/l As(V) stock solutions

$Na_2HAsO_4 \cdot 7H_2O$ (Junsei Chemical) was added into distilled water and acidified to pH 1.5 with H_2SO_4. The stock solutions were filter-sterilized through 0.2 μm polyethersulfone membranes (Steritop, Millipore) and stored at 4°C.

10% (w/v) Yeast extract stock solution

Yeast extract (Sigma-Aldrich) was solubilized into acidic distilled water (pH 2.0 with H_2SO_4), filtered (0.2 μm), and stored in the sterilized bottle at 4°C.

Trace elements (1000×) stock solution

The following chemicals (Wako pure chemicals) were solubilized into distilled water, filtrated (0.2 μm), and stored in sterilized bottle at 4°C.

10 mg/L $ZnSO_4 \cdot 7H_2O$

1 mg/L $CuSO_4 \cdot 5H_2O$

1.09 mg/L $MnSO_4 \cdot 5H_2O$

1 mg/L $CoSO_4 \cdot 7H_2O$

0.39 mg/L $Cr_2(SO_4)_3 \cdot 7H_2O$

0.6 mg/L H_3BO_3

0.5 mg/L $Na_2MoO_4 \cdot 2H_2O$

0.1 mg/L $NaVO_3$

1 mg/L $NiSO_4 \cdot 6H_2O$

0.51 mg/L Na_2SeO_4

0.1 mg/L $Na_2WO_4 \cdot 2H_2O$

Sterilized elemental sulfur powder

Powder of elemental sulfur (Wako pure chemicals) was sterilized in the oven (100°C, overnight, thrice) and stored in the sterilized bottle at 4°C.

2.2 Microorganisms used in this study

All the cultures were maintained in 300 mL Erlenmeyer flask containing 100 mL HBS or ABS media (pH adjusted as the above) supplemented with the electron donors and yeast extract or trace elements, as is described below.

2.2.1 *Acidimicrobium ferrooxidans* strain ICP^T (DSM 10331)

Am. ferrooxidans ICP (Clark and Norris, 1996) was maintained in 300 ml Erlenmeyer flask containing 100 ml of HBS or ABS medium (pH 1.5 with H_2SO_4) with 10 mM Fe^{2+} and 0.02% (w/v) yeast extract. Flasks were incubated at 45°C, shaken at 150 rpm (G·BR-200, Taitec).

2.2.2 *Sulfobacillus sibiricus* strain N1^T (DSM 17363)

Sb. sibiricus N1 (Melamud et al., 2003) was maintained in 300 ml Erlenmeyer flask containing 100 ml of HBS or ABS medium (pH 1.5 with H_2SO_4) with 10 mM Fe^{2+} and 0.02% (w/v) yeast extract. Flasks were incubated at 45°C, shaken at 150 rpm (G·BR-200, Taitec).

2.2.3 *Acidithiobacillus caldus* strain KU^T (DSM 8584)

At. caldus KU (Hallberg and Lindström, 1994) was maintained in 300 ml Erlenmeyer flask containing 100 ml of HBS or ABS medium (pH 1.5 with H_2SO_4) with 0.01% (w/v) S^0 and trace element solution (×1). Flasks were incubated at 45°C, shaken at 150 rpm (G·BR-200, Taitec).

2.2.4 *Acidiplasma* sp. strain Fv-Ap

Acidiplasma sp. Fv-Ap (kindly provided by Prof. D.B. Johnson, Bangor University, UK) was maintained in 300 ml Erlenmeyer flask containing 100 ml of HBS or ABS medium (pH 1.5 with H_2SO_4) with 10 mM Fe^{2+} and 0.02% (w/v) yeast extract. Flasks were incubated at 45°C, shaken at 150 rpm (G·BR-200, Taitec).

2.2.5 *Leptospirillum ferriphilum* strain P_3A^T (DSM 14647)

Lp. ferriphilum P_3A (Coram and Rowlings, 2002) was maintained in 300 ml Erlenmeyer flask containing 100 ml of HBS or ABS medium (pH 1.7 with H_2SO_4) with 20 mM Fe^{2+}, 0.01% (w/v) pyrite and trace element solution (×1). Flasks were incubated at 37°C, shaken at 150 rpm (G·BR-200, Taitec).

2.2.5 *Ferroplasma acidiphilum* strain Y^T (DSM 12658)

Fp. acidiphilum Y (Golyshina et al., 2000) was maintained in 300 ml Erlenmeyer flask containing 100 ml of HBS or ABS medium (pH 1.5 with H_2SO_4) with 10 mM Fe^{2+} and 0.02% (w/v) yeast extract. Flasks were incubated at 35°C, shaken at 150 rpm (G·BR-200, Taitec).

2.3 Mineral samples used in this study

Enargite (Cu_3AsS_4)

Enargite concentrate (produced in Peru) was kindly provided by JX Nippon Mining & Metals. For all the enargite bioleaching experiments, acid-washed enargite concentrate was used.

Pyrite (FeS_2)

Pyrite concentrate (produced in Chile) was purchased by IWAMOTO mineral. Finely ground pyrite concentrate was used for the cultivation of microorganisms.

D3 concentrate

D3 concentrate (produced in Chile) was kindly by JOGMEC (Japan Oil, Gas and Metals National Corporation). D3 concentrate was directly used for the bioleaching experiment without washing.

Acid wash treatment

The concentrates were washed with 1 M HNO_3 (5 min, 25°C), deionized water (5 min, 25°C), and finally with 100% ethanol (5 min, 25°C) in order to remove residual metals and surface oxide film on the concentrate. After that, the concentrate was freeze-dried overnight.

Table 2.1 Elemental composition of enargite concentrate.

Elements	Ratio (%)
S	39
Fe	22
Cu	20
As	7.1
Zn	0.39
Sb	0.32
Al	0.22
Pb	0.18
Ca	0.08
SiO_2	2.7
SO_4^{2-}	3.2
S-0	0.89
Bi	0.04
Mg	< 100 ppm
Ti	300 ppm

Table 2.2 Mineralogical composition of enargite concentrate.

Mineral	Chemical formula	wt%*
Enargite	Cu_3AsS_4	37.4
Pyrite	FeS_2	47.3
Chalcopyrite	$CuFeS_2$	
Tennantite	$(Cu,Fe)_{12}As_4S_{13}$	
Sphalerite	ZnS	
Stibnite	Sb_2S_3	
Quartz	SiO_2	
Gibbsite	$Al(OH)_3$	
Alunite	$KAl_3(SO_4)_2(OH)_6$	

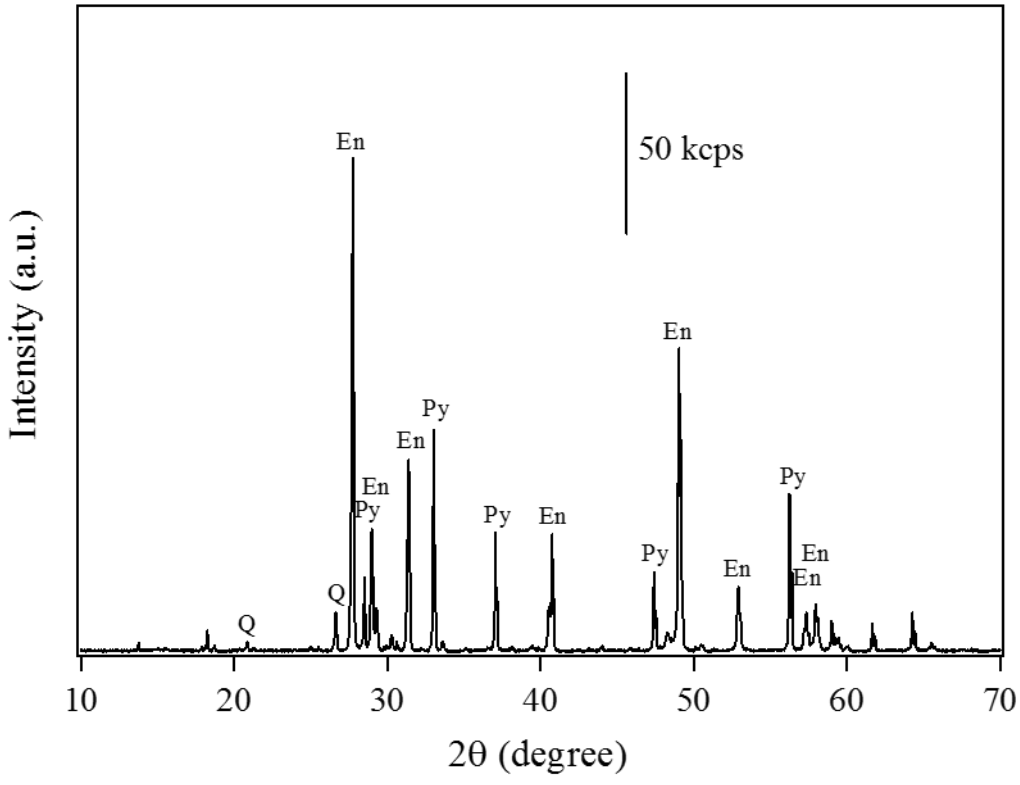

Fig. 2.1 X-ray diffraction patterns of original enargite concentrate. En: enargite (Cu_3AsS_4; PDF No. 00-035-0775), Py: pyrite (FeS_2; PDF No. 00-042-1340), Q: quartz (SiO_2: PDF No. 01-070-3755).

Table 2.3 Elemental composition of D3 concentrate.

Elements	Ratio (%)
As	4.16
Cu	29.6
Fe	17.65
Zn	4.08
Sb	0.31
S	31.7
Ag	0.04
Al	0.09
Ca	0.13
Mg	0.03
Na	0.02
K	0.1
Cd	268 ppm
Cr	10 ppm
Hg	4 ppm
Mo	309 ppm
Pb	4290 ppm

Table 2.4 Mineralogical composition of D3 concentrate.

Mineral	Chemical formula	wt%*
Enargite	Cu_3AsS_4	21
Pyrite	FeS_2	30
Chalcopyrite	$CuFeS_2$	12
Tennantite	$(Cu,Fe)_{12}As_4S_{13}$	1.8
Bornite	Cu_5FeS_4	6.7
Chalcocite	Cu_2S	14
Geerite	Cu_8S_5	3.8
Tetrahedrite	$(Cu,Fe,Zn,Ag)_{12}Sb_3S_4$	1.0
Other Cu suflde		1.3
Other sulfide		5.2
Gangue		3.1

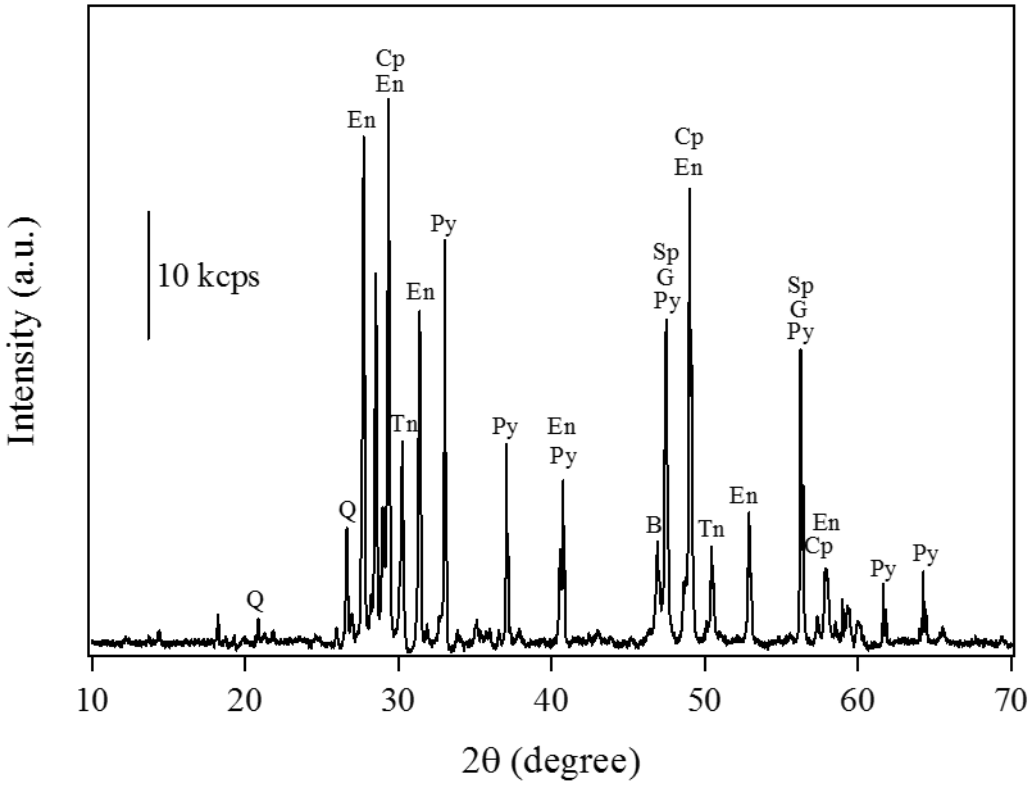

Fig. 2.2 X-ray diffraction patterns of original D3 concentrate. En: enargite (PDF No. 03-065-1097), Cp: chalcopyrite (PDF No. 01-075-6866), Py: pyrite (PDF No. 00-042-1340), Q: Quartz (PDF No. 01-086-1560), B: bornite (PDF No. 01-073-1667), Tn: tennantite (PDF No. 01-074-1027), Sp: sphalerite (PDF No. 01-077-8756), G: geerite (PDF No. 00-033-0491).

2.4 Sampling procedures

2.4.1 Liquid samples

Liquid samples were regularly taken from the experimental cultures after compensation of water evaporation with pure water, and then used for cell counting using a microscope, filtered using 0.2 μm cartridge filters, and used for the determination of metal concentrations, pH values, and solution redox potential (E_h) values.

2.4.2 Solid residues

At the end of the experiments, solid residues were collected by filtration using the vacuum pump, and freeze-dried overnight.

2.5 pH and solution redox potential (E_h) measurements

Solution pH and redox potential values (E_h; Ag/AgCl reference electrode) were measured using pH-E_h meter (MM-60R, TOADKK). The measured E_h values were automatically converted to values vs. SHE as follows;

$$E_h \text{ (mV vs. SHE)} = E_h \text{ (mV vs. Ag/AgCl)} + 206 - 0.7 \text{ (“Solution Temp.” - 25)} \quad \text{(Eq. 2-1)}$$

2.6 Spectrophotometry

2.6.1 *o*-phenanthroline method

o-phenanthroline method was used in this study as a Fe^{2+} assay. The procedures are described below (Caldwell and Adams, 1946).

1. Add 30 μL of 1 M HCl to some wells of 96-well measuring plate.
2. Add 3 μL of liquid samples to the wells. Note that all samples were filtered to remove all particles, and subsequently diluted (e.g., ×10) using 1 M HCl if needed.
3. Add 30 μL of ascorbic acid solution to the wells for the determination of total soluble Fe. Note that ascorbic acid solution was made right before the measurement since the chemical is unstable in solution (one spoon of ascorbic acid powder (Wako pure chemicals) solubilized into 5 mL of distilled water).
4. Give 5 min to react to Fe^{3+} ions with ascorbic acid.
5. Add 30 μL of 5 mM *o*-phenanthroline solution (solubilized in deionized water; Wako pure chemical) to the wells in order to form $[Fe(phenanthoroline)_3]^{2+}$ complex.
6. Add 30 μL of 2 M sodium acetate solution (solubilized in deionized water; Wako pure chemical) to the wells.
7. Add distilled water to make the volume up to 300 μL.
8. Give 10 min for reaction time.
9. Measure the absorbance at 510 nm using spectrophotometer (Multiskan Go, Thermo Scientific).

A standard curve used is shown in Fig. 2.3. Note that the calibration curve was re-drawn every time new chemical reagents were made.

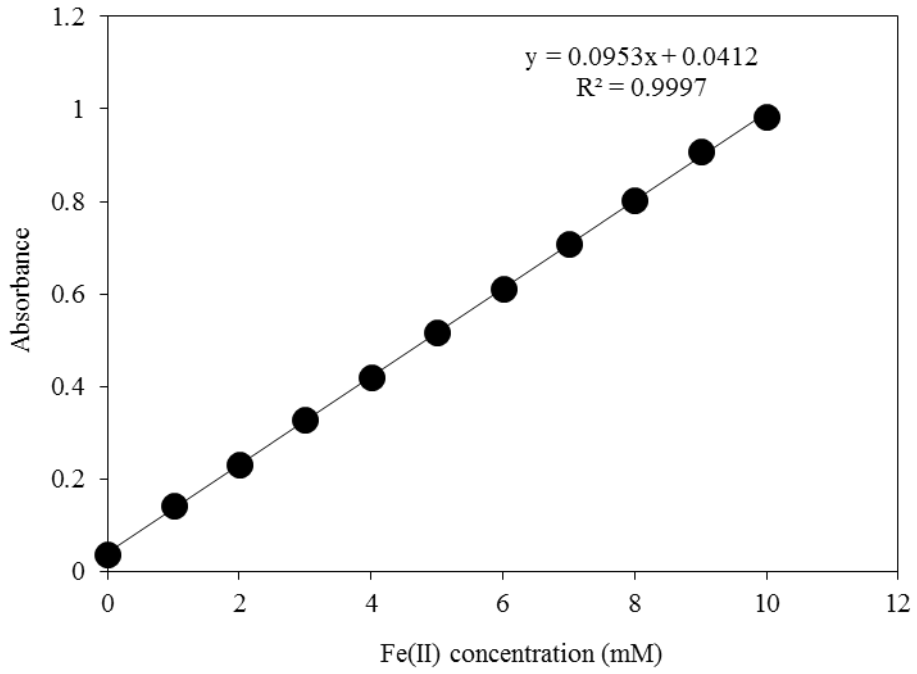

Fig. 2.3 Standard curve of Fe^{2+} concentration determined by *o*-phenanthroline method.

2.6.2 Ferrozine method

For the determination of Fe^{2+} concentration during bioleaching As-bearing copper sulfide, Ferrozine method was used instead of *o*-phenanthroline method. The procedures are described below (Lovely and Phillips, 1987).

Ferrozine solution

1. Dissolve 0.59575 g HEPES in 40 mL deionized water and adjust pH to 7.0 with 1 M KOH.
2. Add 0.05 g ferrozine (3-(2-pyridyl)-5,6-bis(4-phenyl-sulfonic acid)-1,2,4-triazine; Wako pure chemical).
3. Make up to 50 mL with deionized water.

This ferrozine solution must be kept in a dark place for up to 1 month.

Procedure

1. Add 10 μL of liquid samples to the wells of 96-well measuring plate. Note that all samples were filtered to remove all particles, and subsequently diluted (e.g., ×10) using 1 M H_2SO_4 if needed.
2. Add 290 μL of the mixed reagent of ferrozine solution to the wells.
3. Give 10 min to get stable.
4. Measure absorbance at 562 nm using spectrophotometer (Multiskan Go, Thermo Scientific).

A standard curve used is shown in Fig. 2.4. Note that calibration curve was re-drawn every time new chemical reagents were made.

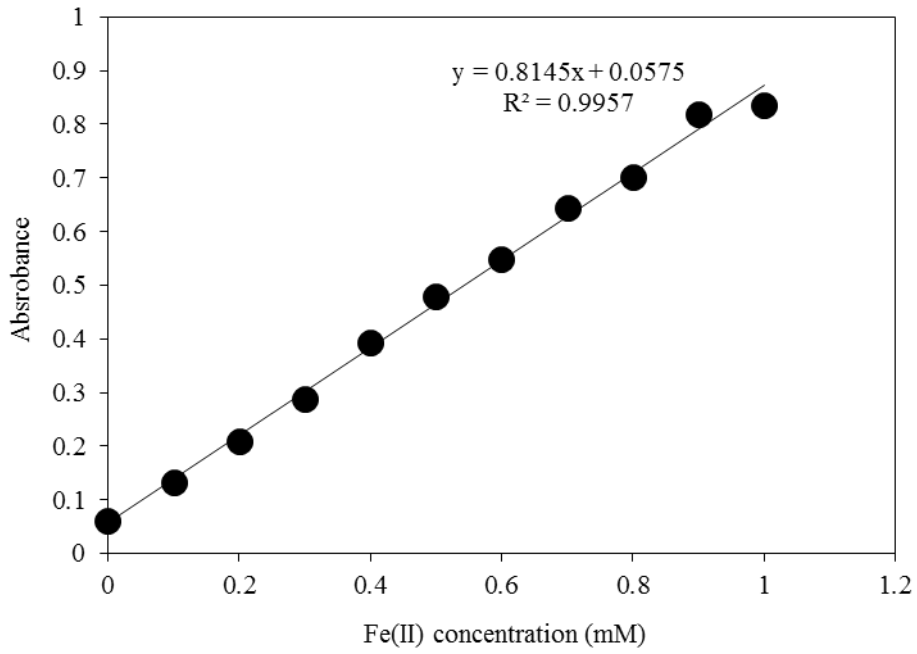

Fig. 2.4 Standard curve of Fe^{2+} concentration determined by ferrozine method.

2.6.3 Molybdenum blue method

Molybdenum blue method was used for the determination of As(III) concentration. The details are described in chapter 3.

2.6.4 Turbidimetric method

Turbidimetic method was used in this study as a sulfate assay. The procedures are described below.

Conditioning reagent

1. Add 50 mL glycerol (Wako pure chemical), 30 mL concentrated HCl, 10 mL 95% ethanol (Wako pure chemical), and 75 g sodium chloride (Wako pure chemical) into 250 mL of deionized water.
2. Make up to 500 mL with deionized water.

Procedure

1. Add 100 μL of liquid samples to the 1.5 mL tube. Note that all samples were filtered to remove all particles, and subsequently diluted (e.g., ×10) using 1 M HCl if needed.
2. Add 900 μL of conditioning reagent and mix thoroughly.
3. Add fine-grain barium chloride (ca. 60 mg; Wako pure chemical) and mix the solution with vortex for 1 min.
4. Transfer the solution into the wells of 96-well measuring plate and measure absorbance at 420 nm using spectrophotometer (Multiskan Go, Thermo Scientific).

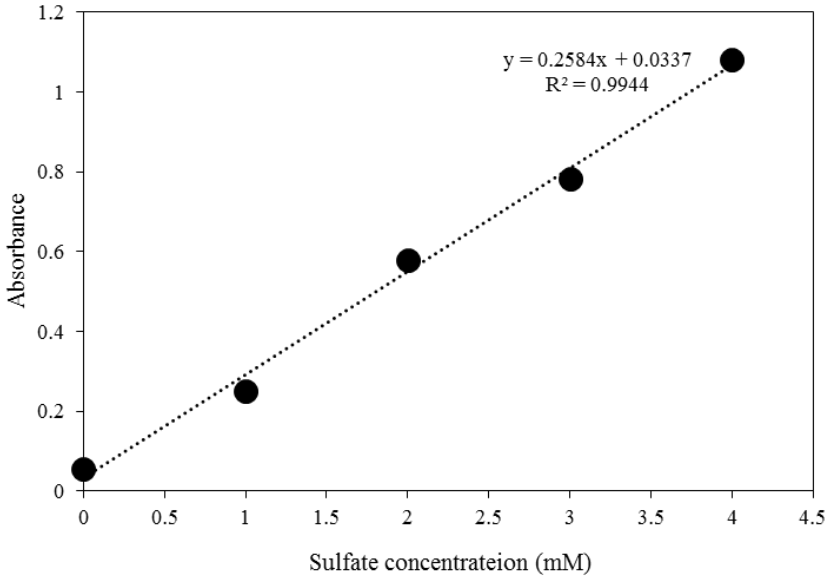

Fig. 2.5 Standard curve of sulfate concentration determined by turbidimetric method.

2.7 Inductively coupled plasma-optical emission spectrometry (ICP-OES)

Concentrations of total soluble metal ions (e.g., Fe, Cu, As) in acid solution samples were measured using ICP-OES (Optima 8300DV, PerkinElmer Japan Co., Ltd). After original liquid samples were taken from Erlenmeyer flasks, falcon tubes or serum bottles, they were filtered (0.20 μm) or centrifuged (12,000 rpm, 8 min) using Minispin (Eppendolf) in order to separate solution and solid phases, and subsequently diluted depending on estimated concentrations of target metal ions in them (e.g., ×25, 100, 250) using 0.1 M HNO_3. All the measurements using ICP-OES were carried out in duplicates: The average values were used for the results. Wavelengths measured for each metal are described as follows:

Fe: 238.204, 239.562, 259.939 nm

Cu: 327.393, 324.752, 224.700 nm

As: 188.979, 193.696, 197.197 nm

2.8 X-ray diffraction (XRD)

XRD measurement (Ultima IV, Rigaku) was performed with Cu-Kα radiation as an X-ray source. The accelerating voltage and current were 40 kV and 40 mA, with a scanning speed of 2°/min and scanning step of 0.02°.

2.9 Electron probe micro analyzer (EPMA)

For the preparation of EPMA specimens, the freeze-dried samples were embedded in resin and polished to determine the chemical composition of constituent minerals by Electron Probe Micro Analyzer (EPMA; JEOL JXA-8530F; 6 nA, 20 kV). The incident electron beam was focused to 1 mm in diameter, and counting time was set to 20 seconds for each element. The acquired X-ray intensities were corrected by ZAF method to obtain element concentrations for quantitative analysis. (Boekestein et al., 1983).

2.10 Attenuated total reflection Fourier transform infrared spectroscopy (ATR-FT-IR)

For the analysis of surface functional groups of AC, attenuated total reflection Fourier transform infrared spectroscopy (ATR-FT-IR) was employed using FT/IR-670

(JASCO) with ZnSe crystal in the range of 360–4000 cm^{-1} (resolution: 16 cm^{-1}).

2.11 Raman spectroscopy

For the analysis of the structure of AC, Raman spectroscopy was employed using DXR Smart Raman (Thermo Scientific) with 532 nm laser (10 mW).

2.12 Microwave treatment

Hydrothermal pre-treatment was carried out as follows: Teflon vessels containing a known amount of solid samples and 60% HNO_3 solution or aqua regia (12M HCL and 60% HNO_3 are mixed in a volume ratio 3:1) were placed in the microwave digestion system (Ethos Plus, Milestone) and heated to 230°C with 7°C /min increments, kept for 15 min at 230°C, and finally allowed to cool to room temperature.

References

1. Anwar, M. A., Iqbal, M., Qamar, M. A., Rehman, M. and Khalid, A. M., 2000. Technical communication: Determination of cuprous ions in bacterial leachates and for environmental monitoring. World Journal of Microbiology and Biotechnology 16, 135-138.
2. Boekestein, A., Stadhouders, A. M., Stols, A. L. H. and Roomans, G. M., 1983. A comparison of ZAF-correction methods in quantitative X-ray microanalysis of light-element specimens. Ultramicroscopy 12, 65-68.
3. Caldwell, D. H. and Adams, R. B., 1946. Colorimetric determination of iron in water with *o*-phenanthroline. Journal of American Water Works Association 38, 727-730.
4. Clark, D.A. and Norris, P.R., 1996. *Acidimicrobium ferrooxidans* gen. nov., sp. Nov.: mixed-culture ferrous iron oxidation with *Slufobacillus* species. Microbiology 142, 785-790.
5. Coram, N. J. and Rowlings, D. E., 2002. Molecular relationship between two groups of the genus *Leptospirillum* and the finding that *Leptospirillum ferriphilu*m sp. nov. dominates South African commercial biooxidation tanks that operate at 40°C. Applied and Environmental Microbiology 68, 838-845 .
6. Golyshina, O.V., Pivovarova, T.A., Karavaiko, G.I., Kondrat'eva, T.F., Moore, E.R.B., Abraham, W.R., Lunsdorf, H., Timmis, K.N., Yakimov M.M. and Golyshin, P.N., 2000. *Ferroplasma acidiphilum* gen. nov., sp. nov., an acidophilic, autotrophic, ferrous-iron-oxidizing, cell-wall-lacking, mesophilic member of the *Ferroplasmaceae* fam. nov., comprising a distinct lineage of the Archaea, International Journal of Systematic and Evolutionary Microbiology 50, 997–1006.
7. Hallberg, K.B. and Lindström, E.B., 1994. Characterization of *Thiobacillus caldus* sp. nov., a moderately thermophilic acidophile. Microbiology 140, 3451-3456.
8. Lovely, D. R. and Phillips, E. J. P., 1987. Rapid assay for microbially reduced ferric iron in aquatic sediments. Applied and Environmental Microbiology 53, 1536-1540.
9. Melamud, V.S., Pivovarova, T.A., Tourova, T.P., Kolganova, T.V., Osipov, G.A., Lysenko, A.M., Kondrat'eva, T.F. and Karavaiko, G.I., 2003. *Sulfobacillus sibiricus* sp. nov., a New Moderately Thermophilic Bacterium. Microbiology 72,

605-612.

Chapter 3

Effect of co-existing metals on modified molybdenum blue method for the determination of As concentration in the copper sulfide leachate

Abstract

The effect of co-existing metal ions such as copper (Cu) and iron (Fe) was studied for the application of modified molybdenum blue method (arsenic-antimony-molybdenum ternary chelation) to Cu sulfide leachate. While solo metal contamination (20 mM Fe^{2+}, 20 mM Fe^{3+}, or 25 mM Cu^{2+}) showed no inhibitory effect on arsenic (As) determination, large amount of metal ions composed of 25 mM Fe^{2+}, 25 mM Fe^{2+}, and 50 mM Cu^{2+} (100 mM in total) led to slight oxidation of As(III) to As(V) (4% in 15 min), resulting in the overestimation of As(V) (the underestimation of As(III)). Phosphate, which also chelates with molybdic acid, was also tested as a minor inhibitor of As(III) quantification usually contained in Cu sulfide leachate. While < 2.5 mM of phosphate was capable of chelating at the same ratio with As, more existence would completely consume molybdic acid, resulting in the unsuccessful standard curve. Applicability of this method to Cu sulfide leachate was indeed confirmed through the test using real Cu leachate obtained by bioleaching of enargite (Cu_3AsS_4) concentrate. Recommended procedure for As determination was finally summarized, which is specially modified for Cu sulfide leachate.

3.1 Introduction

Along with the recent depletion of high-grade copper ore, the contamination of As-bearing minerals such as enargite (Cu_3AsS_4) and tennantite ($Cu_{13}AsS_{14}$) become increasingly serious problems. Since these minerals are also expected as one of the potential future copper resources, the novel approach for extraction of Cu from them has been therefore desperately required. For the exploitation of these minerals, the hydrometallurgical process has been thought appropriate since toxic As leached from the minerals remains in the solution phase in this process, while As in the minerals are volatilized to the air with unmanageable form in the pyrometallurgical process, resulting in the cause of air pollution. However, even after the hydrometallurgical process, dissolved As must be strictly managed not to leak them into the environment by using a physic-chemical treatment such as the adsorption and co-precipitation.

Dissolved As in the solution such as Cu sulfide leachate is predominantly present in the form of inorganic trivalent arsenic, As(III) (arsenite; $H_2AsO_3^-$), and pentavalent arsenic, As(V) (arsenate; $H_2AsO_4^{2-}$), with the former being more toxic and mobile than the latter, especially at acidic pH (Matschullat, 2000; Hung et al., 2004). Since As(V) is more effectively immobilized than As(III), a pre-treatment is required to oxidize As(III) to As(V) by using strong oxidizing reagents before the immobilization step. Prior to pre-treatment, As(III) concentration needs to be determined to know the desired amount of the oxidant to accomplish As(III) oxidation for the economic process.

To determine the As(III) concentration, the various measurement techniques have been developed in the past several decades, such as Anodic Stripping Voltammetry (ASV) (Kopanica and Novotný, 1998), Hydride Generation–Atomic Absorption Spectrometry (HG-AAS) (Shraim et al., 1999), High Performance Liquid Chromatography (HPLC) (Raessler et al., 2000), and Inductively Coupled Plasma–Optical Emission Spectrometry (ICP-OES) (Amran et al., 1997). However, some of these measurements have following disadvantages: (i) necessity of expensive facilities and a large amount of chemicals, (ii) not applicable to in-situ measurement (Dasgupta et al., 2002), (iii) high dilution rate (around 10000 times), leading to the large dilution error. In terms of the last one, these measurement techniques are, in other words, susceptible to the tiny amount of As, which are assumed to be applied for the analysis of the drinking or ground water. In the case of the leachate containing a high concentration of As, however,

the sample needs to be diluted many times for the application to the above techniques, resulting in the seriously large dilution error. Therefore, an alternative method is desirable, which is capable of *in-situ* quick measurement with less dilution.

To overcome this problem, colorimetric molybdenum blue method is considered as one of the promising techniques, which has been proposed by Osmond (1887) and improved by a number of researchers (Bogdanova, 1984; Carvalho et al., 1998; Johnson and Pilson, 1972). Molybdenum blue method is based on the formation of the molybdic heteropoly-acid complex: Molybdenum blue is formed via the reduction of the complex composed of As and molybdic acid under acidic condition. However, color development has been known as a slow-step in this conventional method, requiring the heating for the time-reduction. To shorten this time-consuming process, the modified molybdenum blue method was developed by Murphy and Riley (1962), where ascorbic acid was used as a reducing reagent in the presence of trivalent antimony to form the arsenic-antimony-molybdenum ternary complex. Owing to this modification, reaction time was shortened to less than 15 minutes even at room temperature (Blomqvist et al., 1993).

Common contaminants in ground water, such as phosphate, fluoride, and silicate, have been recognized as the inhibitory elements of molybdenum blue method, which is also able to form the heteropoly-acid complex with molybdic acid (Blomqvist et al., 1993; Kitazume and Yagi, 1981). In order to eliminate their inhibitory effects, oxidation and/or reduction of As species have been tested (Lenoble et al., 2003; Tsang et al., 2007); only As(V) but not As(III) is detectable by molybdenum blue method, the oxidation and reduction of As species in samples enable to observe different As species separated from major inhibitory elements as mentioned above. However, the number of studies investigating the inhibitory effect of Fe and Cu on molybdenum blue method is limited. When Cu sulfide leachate is assumed the sample, the major contaminant is not phosphate, fluoride, and silicate but metal ions such as Cu and Fe, suggesting that the effect of these metal ions must be investigated. Therefore, the objective of this study was set to evaluate the inhibitory effect of metal ions on modified molybdenum blue method for application to Cu sulfide leachate.

3.2 Materials and methods

3.2.1. Solution reagents for analysis

All solution reagents were prepared with deionized water. Ascorbic acid solution was prepared right before the measurement by dissolving 0.03 g L-ascorbic acid ($C_6H_8O_6$; Wako pure chemical) in 5 mL deionized water to be 0.6% (w/v) in final concentration. The stock solution of 1 mM potassium permanganate ($KMnO_4$; Wako pure chemical) was made as an oxidizing reagent for As(III) and stored in a dark plastic bottle. The stock solution of molybdenum-antimony reagent containing 1% (w/v) ammonium molybdate tetrahydrate ($(NH_4)_6Mo_7O_{14}•4H_2O$; Wako pure chemical) and 0.02% (w/v) potassium antimonyl tartrate ($K_2(SbO)_2C_8H_4O_{10}•3H_2O$; Sigma Aldrich) was also prepared. For acidification, 1M sulfuric acid (H_2SO_4) was used.

3.2.2. Arsenic and phosphate standard solution

Each solution of 50 mM As(III) (arsenite) and As(V) (arsenate) were prepared by dissolving sodium meta-arsenite ($NaAsO_2$; Wako pure chemical) and sodium arsenate heptahydrate ($Na_2HAsO_4·7H_2O$; Junsei Chemical), which were diluted to 0.5, 1.0, 2.5, 5.0 with 0.1 mM H_2SO_4 to draw the standard curve. The As standard solutions containing 20 mM Fe^{2+} (as $FeSO_4·7H_2O$; Wako pure chemical), 20 mM Fe^{3+} (as $Fe_2(SO_4)_3·nH_2O$; Wako pure chemical), 25 mM Cu^{2+} (as $CuSO_4·5H_2O$; Wako pure chemical), or mixture of 25 mM Fe^{2+}, 25 mM Fe^{3+}, and 50 mM Cu^{2+} were also tested to evaluate the effect of co-existing metals. Separately, phosphate standard solution was prepared by dissolving potassium dihydrogen phosphate (KH_2PO_4; Wako pure chemical) with the same variety of concentration as As standard solution.

3.2.3. Analytical procedure

All absorbance measurements were carried out in 96-well plastic plate by Multiscan GO (Thermo Fisher Scientific). Three μL of sample solution was mixed with 30 μL H_2SO_4, 30 μL ascorbic acid, 30 μL molybdenum-antimony stock solution, and 207 μL deionized water to make the mixture up to 300 μL for As(V) detection. In order to measure the total As concentration, 30 μL potassium permanganate was further added prior to adding ascorbic acid and reduce the deionized water to 177 μL; note that the order of the addition must not be changed. These mixtures were prepared in

quadruplicate. The time dependence of color development was investigated by changing the reaction time before the absorbance measurement from 15 min to 30 min with 5 min interval. Absorbance of the solution was read at 880 nm (Blomqvist et al., 1993).

3.2.4. Application to real copper sulfide leachate

In order to evaluate the applicability of modified molybdenum blue method to copper sulfide leachate, bioleaching of enargite concentrate was carried out to obtain the real copper leachate used for the determination of As concentration. The detail of the bioleaching experiment was mentioned by Oyama et al. (2018). Enargite concentrate, mainly containing 7.1% As, 20% (w/w) Cu, 22% Fe, and 39% S, was added into the HBS media.(initial pH adjusted to 2.0; 200 mL in 500 mL Erlenmeyer flask), followed by the sterilization by autoclaving. Mixed culture of moderately thermophilic bacteria was inoculated. This flask was incubated and shaken at 45ºC and 150 rpm. Solution sample was regularly withdrawn to monitor As concentration by molybdenum blue method. As concentration was also determined by ICP-OES to compare with the value obtained by molybdenum blue method.

3.3 Results and discussion

3.3.1 Check for the pure arsenic standard solution

At first, pure As standard solutions were tested for the absorbance measurements to obtain the ideal standard curve for the determination of As concentration. In the absence of any contaminants, standard curves were successfully drawn in the range from 0 to 5 mM (Fig. 3.1, Table 3.1; Eqs. 3-1 to 3-16). In addition to the complete As(III) oxidation by $KMnO_4$ (Fig. 3.1a,b, Table 3.1; Eqs. 3.1 to 3.8), the difference in the standard curve equation using As(V) standard solution between in the presence and absence of $KMnO_4$ was negligible (Fig. 3.1c,d, Table 3.1; Eqs. 3-9 to 3-16). This confirmed that $KMnO_4$ is appropriately applicable to this method as an oxidant for As(III). Since color-development was apparently visible until 15 min of reaction time, time-course color-development after 15 min was monitored by absorbance measurement with 5 min interval. The slope changes with time course were also negligibly small (< 0.05) in every case (Table 3.1; Eqs. 3.1 to 3.16). Based on these results, the optimal reaction time of this method was decided to be 15 min.

Table 3.1 List of the standard curve equations and R^2 values.

Standard solution	$KMnO_4$	Reaction time (min)	Stadard curve	R^2	Equation number	Reference
As(III)	-	15	y = -0.0003x + 0.0633	0.3958	3-1	Fig. 3.1a
		20	y = -0.0004x + 0.0627	0.5521	3-2	
		25	y = -0.0003x + 0.0628	0.3260	3-3	
		30	y = -0.0003x + 0.0627	0.4330	3-4	
	+	15	y = 0.1865x + 0.0648	0.9999	3-5	Fig. 3.1b
		20	y = 0.1854x + 0.0646	0.9999	3-6	
		25	y = 0.1845x + 0.0654	0.9998	3-7	
		30	y = 0.1839x + 0.0657	0.9998	3-8	
As(V)	-	15	y = 0.1711x + 0.0636	1.0000	3-9	Fig. 3.1c
		20	y = 0.1697x + 0.0636	0.9999	3-10	
		25	y = 0.1692x + 0.0643	0.9999	3-11	
		30	y = 0.1688x + 0.0646	0.9999	3-12	
	+	15	y = 0.1712x + 0.0631	1.0000	3-13	Fig. 3.1d
		20	y = 0.1701x + 0.0628	1.0000	3-14	
		25	y = 0.1696x + 0.0633	1.0000	3-15	
		30	y = 0.1689x + 0.0638	1.0000	3-16	
PO_4	-	15	y = 0.197x + 0.0722	0.9976	3-17	Fig. 3.2a
		20	y = 0.1973x + 0.0743	0.9967	3-18	
		25	y = 0.1978x + 0.0758	0.9960	3-19	
		30	y = 0.1989x + 0.0778	0.9949	3-20	
	+	15	y = 0.1909x + 0.0721	0.9985	3-21	Fig. 3.2b
		20	y = 0.1908x + 0.0736	0.9979	3-22	
		25	y = 0.1916x + 0.0747	0.9977	3-23	
		30	y = 0.1915x + 0.0755	0.9974	3-24	
As(III) + 20 mM Fe^{2+}	-	15	y = 0.0006x + 0.0614	0.7322	3-25	Fig. 3.3a
		20	y = 0.0005x + 0.0614	0.7040	3-26	
		25	y = 0.0007x + 0.0608	0.8169	3-27	
		30	y = 0.0009x + 0.0611	0.8727	3-28	
	+	15	y = 0.1895x + 0.0654	1.0000	3-29	Fig. 3.3b
		20	y = 0.1883x + 0.0663	0.9999	3-30	
		25	y = 0.1872x + 0.0672	0.9999	3-31	
		30	y = 0.1864x + 0.0688	0.9999	3-32	
As(III) + 20 mM Fe^{3+}	-	15	y = 0.0008x + 0.0627	0.8200	3-33	Fig. 3.3c
		20	y = 0.0009x + 0.0625	0.8971	3-34	
		25	y = 0.0011x + 0.0619	0.9396	3-35	
		30	y = 0.0012x + 0.0625	0.9546	3-36	
	+	15	y = 0.1907x + 0.0689	0.9992	3-37	Fig. 3.3d
		20	y = 0.1895x + 0.0703	0.9991	3-38	
		25	y = 0.188x + 0.0709	0.9990	3-39	
		30	y = 0.1878x + 0.072	0.9991	3-40	
As(III) + 25 mM Cu^{2+}	-	15	y = 0.0003x + 0.0691	0.7174	3-41	Fig. 3.3e
		20	y = 0.0005x + 0.0693	0.7768	3-42	
		25	y = 0.0004x + 0.0698	0.6891	3-43	
		30	y = 0.0005x + 0.0702	0.7824	3-44	
	+	15	y = 0.1856x + 0.0756	0.9997	3-45	Fig. 3.3f
		20	y = 0.1837x + 0.0777	0.9996	3-46	
		25	y = 0.1826x + 0.0796	0.9995	3-47	
		30	y = 0.1817x + 0.0808	0.9995	3-48	
As(III) + 25 mM Fe^{2+} + 25 mM Fe^{3+} + 50 mM Cu^{2+}	-	15	y = 0.0081x + 0.0681	0.9988	3-49	Fig. 3.4a
		20	y = 0.0098x + 0.068	0.9991	3-50	
		25	y = 0.0114x + 0.0676	0.9994	3-51	
		30	y = 0.0132x + 0.0677	0.9991	3-52	
	+	15	y = 0.1852x + 0.0742	0.9999	3-53	Fig. 3.4b
		20	y = 0.1834x + 0.0752	0.9999	3-54	
		25	y = 0.1828x + 0.0753	0.9999	3-55	
		30	y = 0.1823x + 0.0758	0.9999	3-56	
As(V) + 25 mM Fe^{2+} + 25 mM Fe^{3+} + 50 mM Cu^{2+}	-	15	y = 0.1725x + 0.0714	0.9992	3-57	Fig. 3.4c
		20	y = 0.1708x + 0.0715	0.9993	3-58	
		25	y = 0.1696x + 0.0719	0.9992	3-59	
		30	y = 0.1696x + 0.0723	0.9993	3-60	
	+	15	y = 0.1733x + 0.0715	0.9994	3-61	Fig. 3.4d
		20	y = 0.1718x + 0.0714	0.9995	3-62	
		25	y = 0.171x + 0.0716	0.9994	3-63	
		30	y = 0.1706x + 0.072	0.9994	3-64	

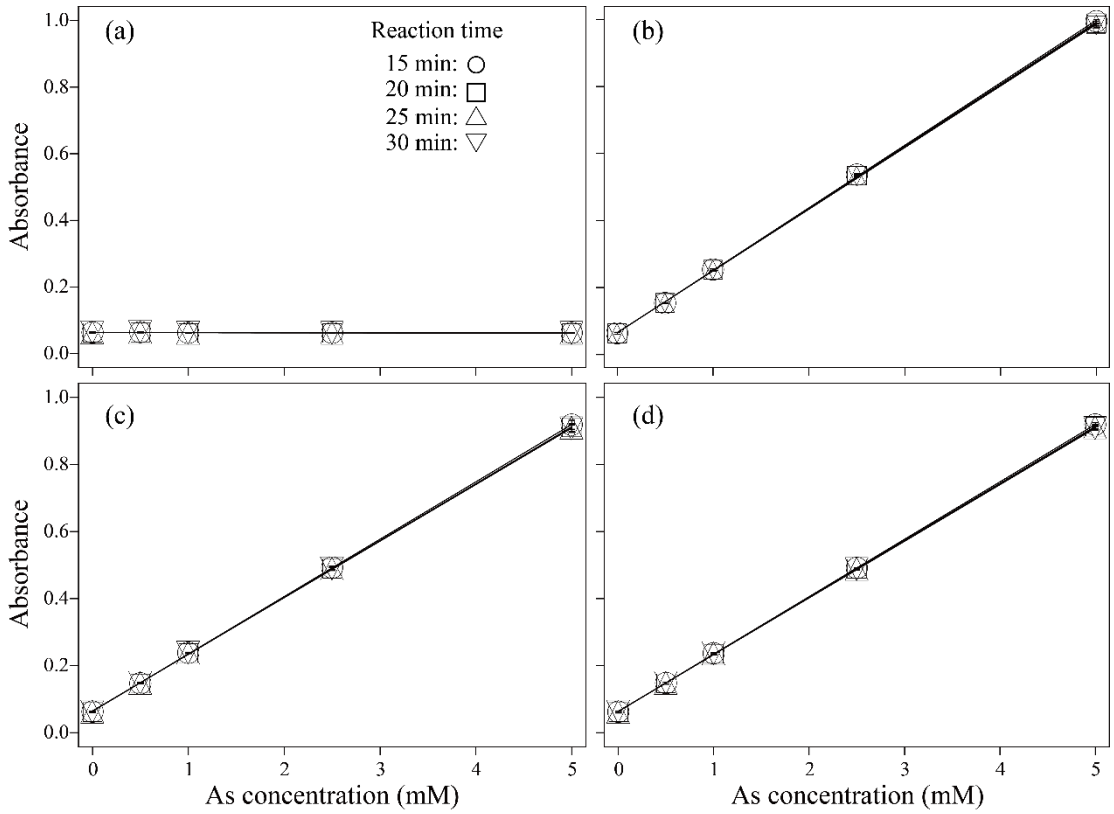

Fig. 3.1 Relationship between absorbance and As concentration with the reaction time of 15 min (○), 20 min (□), 25 min (△), and 30 min (▽). As(III) (a,b) and As(V) (c, d) standard solution without (a, c) and with $KMnO_4$ (b, d) were used for the analysis. Markers, error bars, and standard curves were overlapped due to the high reproducibility.

3.3.2 Test of phosphate as a major inhibitor of As detection

Even though its concentration is low, phosphate might be dissolved from some gangues or clay minerals during the leaching process. Moreover, if the biological technique is employed to enhance the dissolution of Cu sulfides, acid basal salts medium must be used as a lixiviant for the microbial growth during the leaching process, which contains phosphate compounds as a component. Since this phosphate is also capable of chelating with molybdic acid and possibly inhibiting the detection of As, the effect of phosphate must be evaluated in the molybdenum blue method.

In the range of phosphate concentration from 0 to 2.5 mM, standard curve was successfully drawn, and time-course color-development was negligible even after 30 min of reaction time (Fig. 3.2, Table 3.1; Eqs. 3-17 to 3-24). While Blomqvist et al. (1993) reported that the reaction rate of phosphate differed from that of arsenate, similar reaction-rate (slope of the standard curve equation) was obtained in this study (see Eqs. 3-5 to 3-8 and Eqs. 3-21 to 3-24 in Table 3.1). However, with increase of phosphate concentration to 5.0 mM, slope and R^2 values suddenly dropped to around 0.15 and 0.98, respectively. This could attribute to the difference in the mechanism of chelating with molybdic acid; phosphate could require a larger amount of molybdic acid to form the complex than arsenate, possibly resulting in the complete consumption of molybdic acid and the unsuccessful standard curve. These observations suggest that phosphate concentration in samples must be, or diluted to be, less than 2.5 mM. Since phosphate concentration in the basal salt medium is basically around 0.2 mM (10 times lower than the above limit), Cu sulfide leachate would be directly applicable to this As detection method.

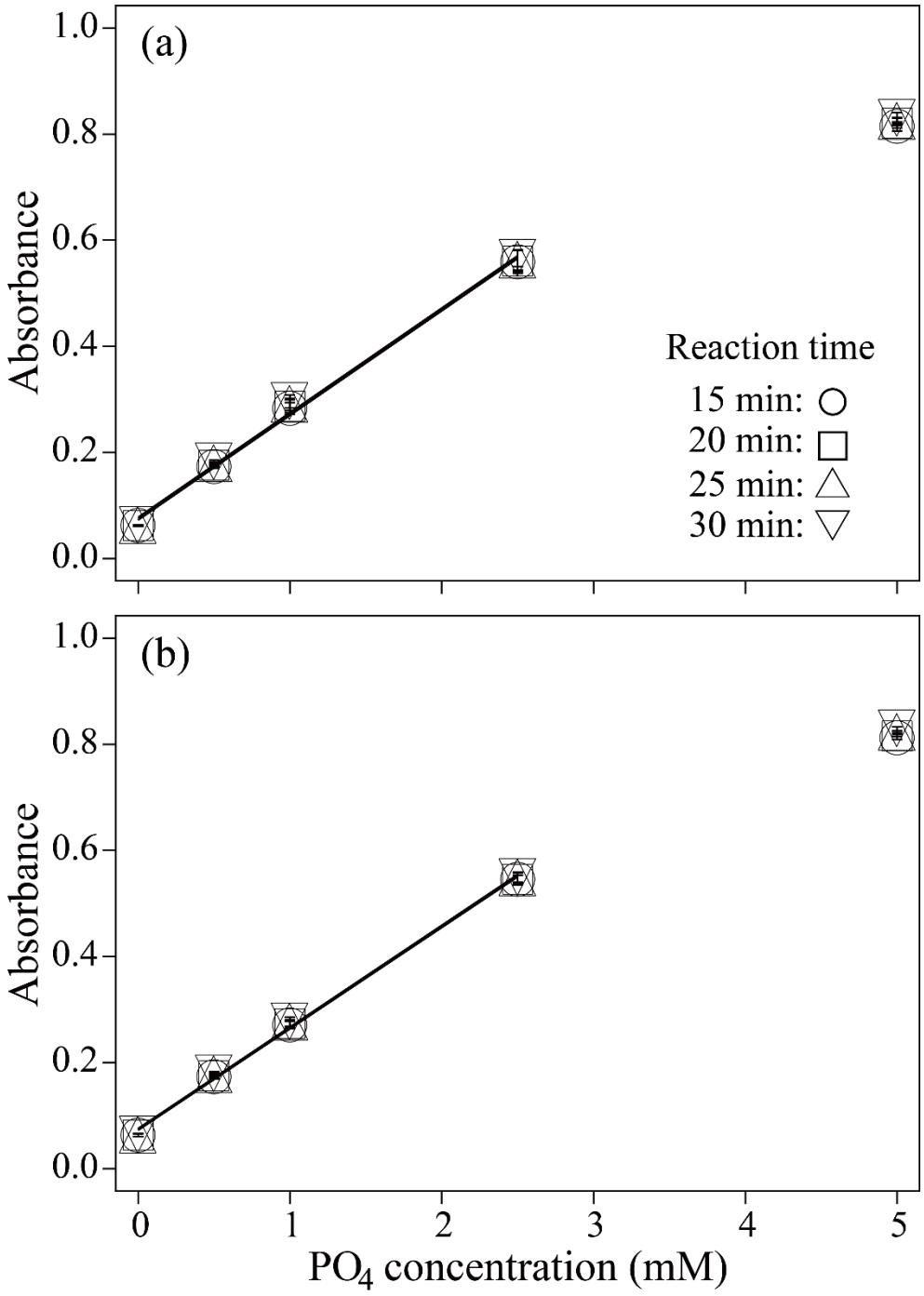

Fig. 3.2 Relationship between absorbance and PO_4 concentration with the reaction time of 15 min (○), 20 min (□), 25 min (△), and 30 min (▽). PO_4 standard solution without (a) and with $KMnO_4$ (b) were used for the analysis. Markers, error bars, and standard curves were overlapped due to the high reproducibility.

3.3.3. Evaluation of Fe^{2+}, Fe^{3+}, and/or Cu^{2+} as the inhibitors for As detection

In order to evaluate the effect of possible inhibitory metals contained in Cu sulfide leachate, the As standard solutions mixed with Fe and/or Cu ware also tested. Solo metal contamination showed no inhibitory effect on the As detection by molybdenum blue method (Fig. 3.3). The standard curves hardly changed even in the presence of either 20 mM Fe^{2+}, 20 mM Fe^{3+}, or 25 mM Cu^{2+} with high R^2 value (> 0.999; Table 3.1; Eqs. 3-25 to 3-48). These results indicate that the presence of Fe^{2+}, Fe^{3+}, or Cu^{2+} solely did not affect on the chelating reaction between As and molybdic acid.

However, in the presence of all metal ions (25 mM Fe^{2+}, 25 mM Fe^{3+}, and 50 mM Cu^{2+}) at the same time (100 mM in total), slight increase in absorbance with time was observed in the case using As(III) standard solution without $KMnO_4$ (Fig. 3.4a, Table 3.1; Eqs. 3-49 to 3-52). Additionally, obtained slopes of the standard equation (Eqs. 3-49 to 3-52) were 10 times higher than the others (e.g. Eqs. 3-1 to 3-4). Considering the time-course difference of As(V) standard curve was not observed (Fig. 3.4c,d, Table 3.1), it was assumed that small amount of As(III) was gradually oxidized, leading to the increase in the absorbance with time. Large amount of metal ions could change the ionic activity in the solution, possibly accelerating As(III) oxidation coupled with Fe^{3+} reduction to Fe^{2+} (undetectable with the change in Fe^{2+} concentration due to its small difference). Even though this absorbance increase somewhat overestimate the As(V) concentration (in other words, As(III) is underestimated), the oxidized As(III) concentration was only 4% (roughly calculated by Eqs. 3-1, 3-5, and 3-49). Although it is desirable to remove Fe and Cu from the sample as much as possible, the Cu leaching solution, containing larger amount of Cu and Fe than that of As, is directly applicable to this method if slight oxidation of As(III) is acceptable.

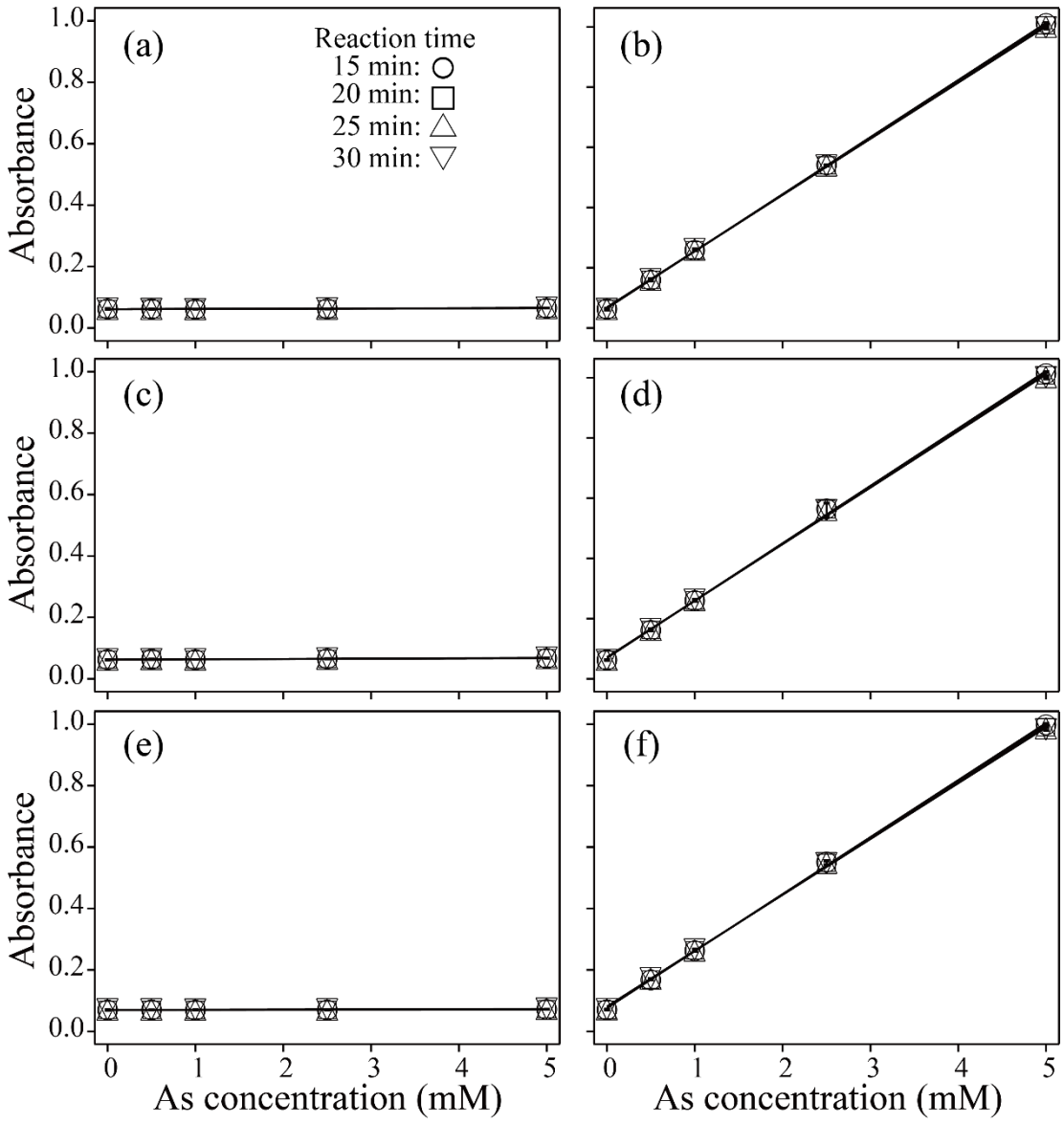

Fig. 3.3 Relationship between absorbance and As concentration with the reaction time of 15 min (○), 20 min (□), 25 min (△), and 30 min (▽). As(III) standard solution containing 20 mM Fe^{2+} (a,b), 20 mM Fe^{3+} (c,d), or 25 mM Cu^{2+} (e,f) without (a,c,e) and with $KMnO_4$ (b,d,f) were used for the analysis. Markers, error bars, and standard curves were overlapped due to the high reproducibility.

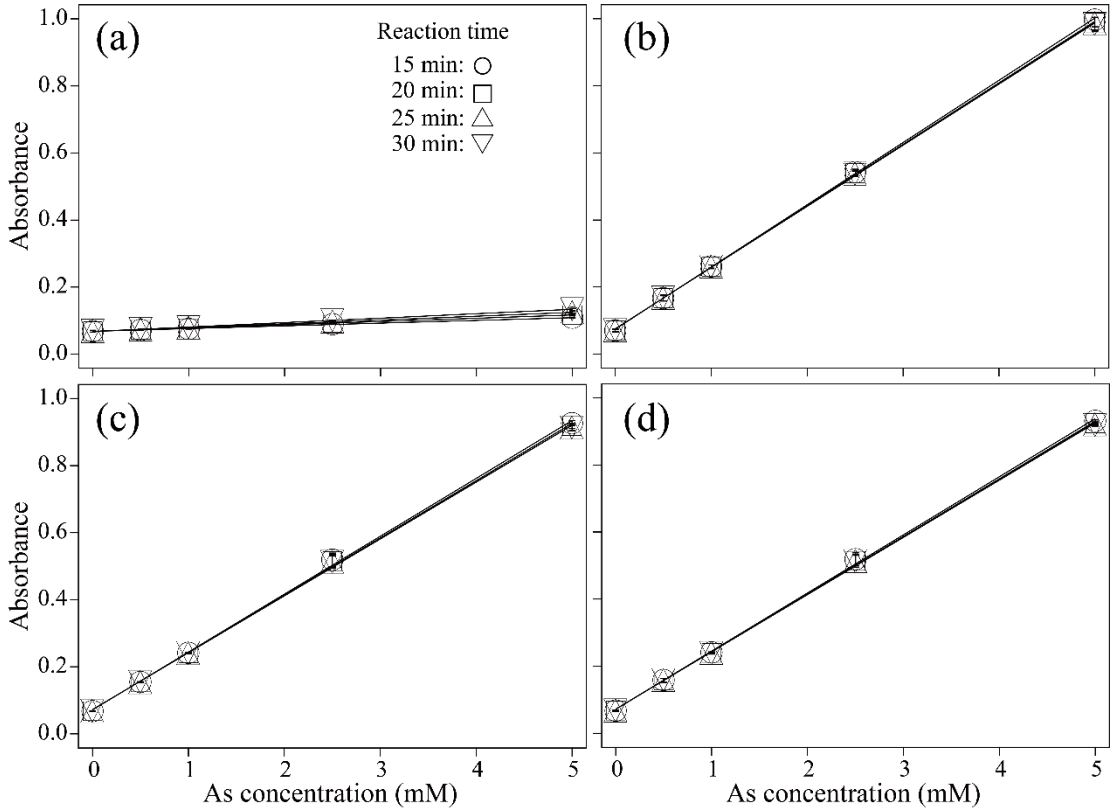

Fig. 3.4 Relationship between absorbance and As concentration with the reaction time of 15 min (○), 20 min (□), 25 min (△), and 30 min (▽). As(III) (a,b) and As(V) (c,d) standard solution containing 25 mM Fe^{2+}, 25 mM Fe^{3+}, and 50 mM Cu^{2+} without (a,c) and with $KMnO_4$ (b,d) were used for the analysis. Markers, error bars, and standard curves were overlapped due to the high reproducibility.

3.3.4 As detection in real copper leachate by molybdenum blue method compared with ICP-OES

Arsenic-containing Cu leachate was obtained by bioleaching of enargite concentration to ensure the accuracy of As qualification by modified molybdenum blue method via the comparison with ICP-OES. Fig. 3.5 shows the trends of As concentration leached from enargite during the bioleaching test. The total As concentration determined by modified molybdenum blue method showed a similar trend with that determined by ICP-OES, indicating that the accuracy of the former method is as competitively high as that of the latter. The maximum error in As concentration between two methods was only 0.4 mM, including 0.2 mM of phosphate derived from the ingredient of HBS media (actual error was only 0.2 mM) even though 23 mM of Cu and 80 mM of Fe ions were co-existed. This indicates that the molybdenum blue method is indeed applicable to Cu sulfide leachate with high performance as well as ICP-OES.

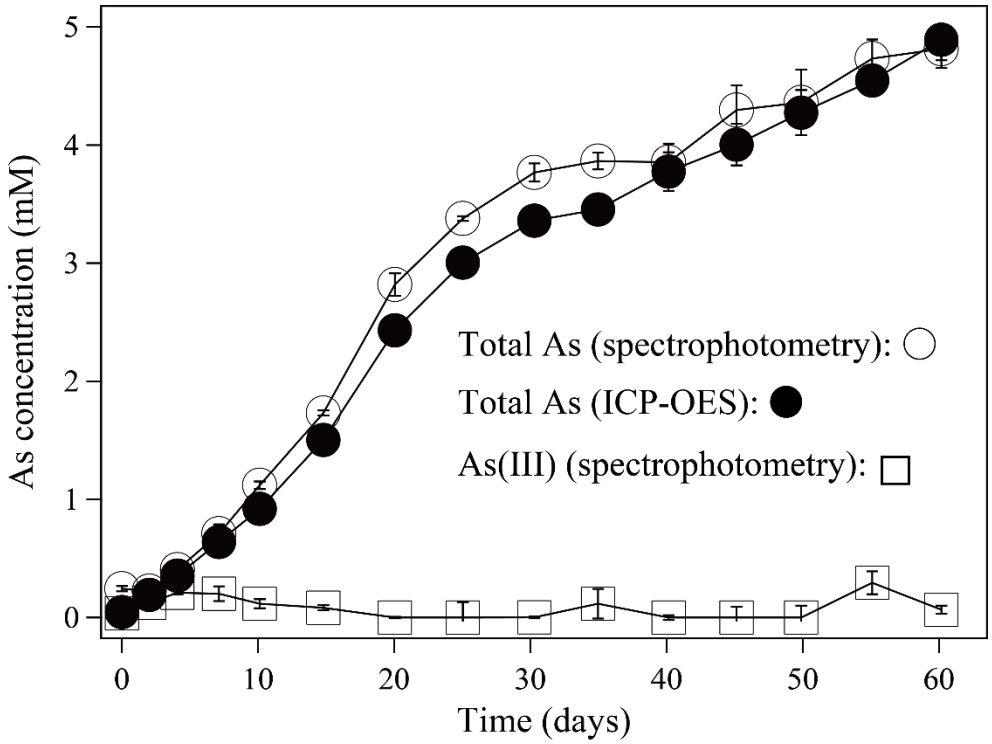

Fig. 3.5 Changes in As(III) (□) and total As (○) during bioleaching of enargite concentrate. The concentration was determined by modified molybdenum blue method (open symbol) and ICP-OES (solid symbol).

3.3.5 Summary of the procedure to determine As concentration in Cu sulfide leachate by modified molybdenum blue method

Sample containing negligibly small amount of phosphate should be applied to modified molybdenum blue method with the following procedure;

(i) For As(V) determination, 3 μL of the sample solution is mixed with 30 μL H_2SO_4, 30 μL ascorbic acid, 30 μL molybdenum-antimony stock solution, and 207 μL deionized water to make the mixture up to 300 μL.

(ii) For total As determination, 30 μL potassium permanganate is further added prior to adding ascorbic acid and the deionized water decreased to 177 μL.

(iii) After 15 min of reaction time, absorbance of the solution is read at 880 nm.

Since the difference between (i) and (ii) corresponded to the concentration of As(III), all As species (As(III), As(V) and total As) can be determined in this procedure. If the large amount of Cu and Fe are co-existed, metal-ion removal or sample dilution is recommended to prevent the As(III) oxidation.

It should be noted that if the sample is contaminated with phosphate, step (i) and (ii) determined the concentration of As(V) + PO_4 and total As + PO_4, respectively. Therefore, the only As(III) concentration is able to be determined by subtracting the value obtained in step (i) from that obtained in step (ii). If the contamination of phosphate is higher than 2.5 mM, the sample must be diluted to be less than 2.5 mM of phosphate concentration.

3.4 Conclusions

The effect of contamination such as Cu, Fe, and phosphate was investigated in the As(III) detection by modified molybdenum blue method. While solo metal contamination (20 mM Fe^{2+}, 20 mM Fe^{3+}, or 25 mM Cu^{2+}) showed no inhibitory effect on As quantification, mixture of Fe^{2+}, Fe^{3+}, and Cu^{2+} (100 mM metals ions in total) led to slight oxidation of As(III) with time, resulting in overestimation of As(V) (underestimation of As(III)). Since the amount of oxidized As(III) was correspond to 4% in 15 min, the sample containing large amount of Fe and Cu ions is directly applicable to this molybdenum blue method if the slight oxidation is acceptable; if not, Cu and Fe must be removed from the sample as much as possible. While phosphate could be inhibitory contamination, <2.5 mM of phosphate is capable of chelating with molybdic acid at the same ratio with arsenate. More phosphate contamination could lead to the lack of molybdic acid for the reaction, thus phosphate concentration must be, or diluted to be, less than 2.5 mM.

References

1. Amran, M.B., Lagarde, F. and Leroy, M.J., 1997. Determination of arsenic species in marine organisms by HPLC-ICP-OES and HPLC-HG-QFAAS. Microchimica Acta 127, 195-202.
2. Blomqvist, S., Hjellström, K. and Sjösten, A., 1993. Interference from arsenate, fluoride and silicate when determining phosphate in water by the phosphoantimonyl molybdenum blue method. International Journal of Environmental Analytical Chemistry 54, 31-43.
3. Bogdanova, V., 1984. The choice of optimal conditions for the determination of arsenic in form of molybdenum blue. Microchimica Acta 83, 317-330.
4. Carvalho, L., De Koe, T. and Tavares, P., 1998. An improved molybdenum blue method for simultaneous determination of inorganic phosphate and arsenate. Restoration 1.
5. Dasgupta, P.K., Huang, H., Zhang, G. and Cobb, G.P., 2002. Photometric measurement of trace As (III) and As (V) in drinking water. Talanta 58, 153-164.
6. Hung, D.Q., Nekrassova, O. and Compton, R.G., 2004. Analytical methods for inorganic arsenic in water: a review. Talanta 64, 269-277.
7. Johnson, D.L. and Pilson, M.E., 1972. Spectrophotometric determination of arsenite, arsenate, and phosphate in natural waters. Analytica Chimica Acta 58, 289-299.
8. Kitazume, E. and Yagi, K., 1981. Spectrophotometric determination of arsenic in semiconductor silicon dioxide film through formation of an arsenic-antimony-molybdenum ternary complex, Analytical Chemistry 30, 608-612.
9. Kopanica, M. and Novotný, L., 1998. Determination of traces of arsenic (III) by anodic stripping voltammetry in solutions, natural waters and biological material. Analytica Chimica Acta 368, 211-218.
10. Lenoble, V., Deluchat, V., Serpaud, B. and Bollinger, J.-C., 2003. Arsenite oxidation and arsenate determination by the molybdene blue method. Talanta 61, 267-276.
11. Matschullat, J., 2000. Arsenic in the geosphere—a review. Science of the Total Environment 249, 297-312.
12. Murphy, J. and Riley, J.P., 1962. A modified single solution method for the

determination of phosphate in natural waters. Analytica Chimica Acta 27, 31-36.

13. Osmond, M., 1887. Sur une reaction pouvant servir on dosage coloimetrique du phospore dans le fontes, les aciers, etc. Bull Soc Chim 47, 745-749.
14. Oyama, K., Shimada, K., Ishibashi, J.-i., Miki, H. and Okibe, N., 2018. Silver-catalyzed bioleaching of enargite concentrate using moderately thermophilic microorganisms. Hydrometallurgy 177, 197-204.
15. Raessler, M., Michalke, B., Schulte-Hostede, S. and Kettrup, A., 2000. Long-term monitoring of arsenic and selenium species in contaminated groundwaters by HPLC and HG-AAS. Science of the Total Environment 258, 171-181.
16. Shraim, A., Chiswell, B. and Olszowy, H., 1999. Speciation of arsenic by hydride generation–atomic absorption spectrometry (HG–AAS) in hydrochloric acid reaction medium. Talanta 50, 1109-1127.
17. Tsang, S., Phu, F., Baum, M.M. and Poskrebyshev, G.A., 2007. Determination of phosphate/arsenate by a modified molybdenum blue method and reduction of arsenate by $S_2O_4^{2-}$. Talanta 71, 1560-1568.

Chapter 4

Evaluating catalytic ability of silver in bioleaching of enargite concentrate and elucidating its catalytic mechanism

Abstract

Effect of silver (Ag) catalyst in bioleaching of enargite (Cu_3AsS_4) concentrate was studied using mixed cultures of moderately thermophilic acidophilic microorganisms at 45°C. Addition of Ag_2S enabled selective Cu dissolution from enargite while suppressing pyrite oxidation: At the highest Ag_2S concentration of 0.04%, Cu recovery reached 96%while Fe dissolution was suppressed to reach only 29% by day 72. Overall results from thermodynamic calculation, liquid/solid analyses and kinetic study suggested that Ag-catalyzed bioleaching of enargite concentrate proceeds via formation of at least two types of secondary products (chalcocite, Cu_2S; trisilver arsenic sulfide, Ag_3AsS_4): Addition of Ag_2S as Ag catalyst thermodynamically and microbiologically contributed to lowering E_h during bioleaching, consequently satisfying E_{ox} (Cu_2S) < E_h < E_c (Ag^+) to enhance enargite dissolution via formation of chalcocite intermediate. Formation of trisilver arsenic sulfide and its intermediate layer $(Cu,Ag)_3AsS_4$ indicated that Cu ion in the enargite lattice is gradually substituted with Ag. Such secondary products did not impose a rate-limiting step, since the Ag-catalyzed bioleaching was shown to be controlled by a chemical surface reaction, rather than diffusion through product film which was the case in the absence of Ag_2S.

4.1 Introduction

Recent depletion of high-grade copper ores has been directing researchers' attention towards the utilization of low-grade and refractory copper sulfides such as chalcopyrite ($CuFeS_2$) and enargite (Cu_3AsS_4). In order to improve dissolution efficiency of such minerals, different approaches have been investigated including pressure leaching (Ruiz et al., 2011; Padilla et al., 2015), chemical acid leaching (Safarzadeh and Miller, 2014) and biological leaching (Acevedo et al., 1998; Sasaki et al., 2009). Bioleaching is expected to be one of the most promising approaches in targeting such refractory ores/concentrates, and in fact, high-temperature bioleaching (60-70°C) generally resulted in high copper recoveries (52-91%; Escobar et al., 2000; Muñoz et al., 2006; Lee et al., 2011; Takatsugi et al., 2011; Sasaki et al., 2011). Whilst at low-temperatures (25-30°C), bioleaching still remains to be improved (< 30%; Escobar et al., 1997; Canales et al., 2002; Corkhill et al., 2008; Sasaki et al., 2010). These results suggest that the addition of reaction catalysts would be useful in low-temperature bioleaching to realize better copper recovery.

In the case of chalcopyrite bioleaching, the catalytic effect of different metal ions has been studied so far: Among those metals tested, silver ion was found to be effective in catalyzing chalcopyrite dissolution, whereas cobalt, manganese, antimony, bismuth, nickel and tin ions showed weak or no catalytic ability (Ballesster et al., 1990; Muñoz et al., 2007).

The mechanism of silver-catalyzed chalcopyrite leaching has been explained by different research groups based on abiotic leaching studies, such as via (i) improvement of electrical conductivity by formation of Ag_2S inside S^0 layer on the chalcopyrite surface (Nazari et al., 2012), (ii) Ag atom diffusion into the metal-deficient sulfur-rich passive layer formed on the chalcopyrite surface (Ghahremaninezhad et al., 2015) and (iii) Ag_2S formation which rapidly consumes H_2S produced via intermediate chalcocite (Cu_2S) formation from chalcopyrite, indirectly accelerating chalcopyrite dissolution (Hiroyoshi et al., 2000, 2001, 2002, 2007, 2008). The third theory was proposed by detailed electrochemical/chemical studies and thermodynamic calculations, revealing the correlation between the silver-catalyzed chalcopyrite dissolution behavior and solution redox potential (E_h). Formation of intermediate Cu_2S (Eq. 4-3; the sum of Eqs. 4-1 and 4-2) and its oxidation to yield Cu^{2+} (Eq. 4-4) proceed simultaneously, when E_h

satisfies the optimal range of $E_{ox} < E_h < E_c$,

where,

E_{ox} ("oxidation potential"); the equilibrium redox potential for the subsequent oxidation of chalcocite to Cu^{2+}

E_c ("critical potential"); the equilibrium redox potential for the intermediate chalcocite formation from chalcopyrite.

$$2CuFeS_2 + 6H^+ + 2e^- \rightarrow Cu_2S + 2Fe^{2+} + 3H_2S \quad \text{(Eq. 4-1)}$$

$$2Ag^+ + H_2S \rightarrow Ag_2S + 2H^+ \quad \text{(Eq. 4-2)}$$

$$2CuFeS_2 + 6Ag^+ + 2e^- \rightarrow Cu_2S + 2Fe^{2+} + 3Ag_2S \quad \text{(Eq. 4-3)}$$

$$Cu_2S \rightarrow 2Cu^{2+} + S^0 + 4e^- \quad \text{(Eq. 4-4)}$$

As for enargite leaching, studies on the mechanism of silver catalyst is still very limited. An electrochemical study by Miki et al. (2016) suggested that the addition of silver expands the optimal E_h range, which allows enhanced enargite dissolution. However, the detailed mechanism is yet unclear, and its effect in bioleaching is largely unknown. Although the use of silver catalyst is considered unpractical for copper extraction, clarifying its catalytic mechanism would be beneficial in understanding how enargite leaching can be facilitated.

The objectives of this study were therefore set to evaluate the catalytic effect of silver on bioleaching of enargite concentrate and to elucidate its mechanism.

4.2 Materials and methods

4.2.1 Silver-catalyzed bioleaching of enargite concentrate using moderately thermophilic microorganisms

The cell of the three bacterial strains, *Am. ferrooxidans* ICP, *Sb. sibiricus* N1, *At. caldus* KU, and one archaeal strain, *Fp. acidiphilum* Y were pre-grown, as was described in chapter 2. Pre-grown cells were collected by centrifugation (9000 rpm, 10 min at 4°C) and washed twice with acidified water (pH 1.7), prior to inoculation into 200 mL HBS medium (pH 2.0; in 500 mL Erlenmeyer flasks) containing 2% (w/v) enargite concentrate and 5 mM Fe^{2+} (so as to set the initial cell density of each strain at 1.0×10^7 cells/mL; i.e. 4.0×10^7 cells/mL in total). Silver sulfide (Ag_2S) was added as silver catalyst into the medium at different concentrations: 0, 0.005, 0.01, 0.02, 0.03 and 0.04% (w/v). Flasks were incubated shaken at 45˚C and 150 rpm for 72 days. Samples were regularly withdrawn to monitor pH, Eh, cell density and concentrations of Fe^{2+} by the *o*-phenanthroline method, total Fe, As and Cu by inductively coupled plasma optical emission spectrometry (ICP-OES; Optima 8300DV; PerkinElmer). Leaching residues were collected after bioleaching and freeze-dried overnight for X-ray diffraction (XRD; Rigaku Ultima IV; CuKα 40 mA, 40 kV) analysis. For quantitative elemental composition analysis by electron probe micro analyzer (EPMA; JOEL JXA-8530F; 6 nA, 20 kV), the leaching residues were embedded into resin and polished. The incident electron beam was focused to 1 μm in diameter, and counting time was set to 20 sec for each element. The acquired results were collected by ZAF method (Boekestein et al., 1983).

4.2.2 Analysis of microbial population structure in silver-catalyzed bioleaching of enargite concentrate

In order to investigate the microbial population structure in bioleaching cultures, real-time PCR (MiniOpticon, Bio-Rad) was conducted according to the methods described by Tanaka et al. (2015) with some modifications as follows: The purified genomic DNA from each strain was used as the template to PCR amplify the 16S rRNA gene fragment (~1473 bp) using the universal primer set (27f and 1492r for bacteria or Arch 21f and 1492r for archaea: Table 4.1). The resultant PCR products derived from each strain were purified using ISOSPIN PCR Product (NIPPON GENE), quantified, and finally

diluted to give a final concentration of 1.0×10^3 to 1.0×10^9 copies/μL, to be used as template DNA for real-time PCR. Once linearity in the standard curve was obtained within the range from 1.0×10^3 to 1.0×10^9 copies/μL for all species, synthetic DNA mixtures (composed of template DNA from each one of the four species at 1.0×10^3 to 1.0×10^9 copies/μL) was tested against each one of the four species-specific primer sets (Table 4.1) to ensure the accuracy in order to display the results as percentages in whole number. Genomic DNA extracted from the actual bioleaching mixed cultures were tested against the corresponding species-specific primer sets.

Table 4.1 PCR and Real-Time PCR primer sets used in this study.

Purpose	Primer set	Primer sequence (5'-3')	Target species	PCR product size (bp)
PCR	27f Universal	AGAGTTTGATCMTGGCTCAG	Bacteria	~1473
	1492r Universal	TACGGYTACCTTGTTACGACTT		
	Arch 21f	TTCCGGTTGATCCYGCCGGA	Archaea	1451
	1492r Universal	-		
Real-Time PCR	Amferro-F1	TCATTCGACGGGCTCCGTG	Species-specific: *Am. ferrooxidans*	232
	Buniv-R1	GAGCTGACGACARCCATGCA		
	Sbsib-F1	TAGGTGTCGCCCGGGTCCAC	Species-specific: *Sb. sibiricus*	241
	Buniv-R1	-		
	Acaldus-F3	TAGGTGCTGAGTGTCGTAGCTAACG	Species-specific: *At. caldus*	231
	Buniv-R1	-		
	Fpacidi-F2	GAAGCTTAACTCCAGAAAGTCTGAAGAGA	Species-specific: *Fp. acidiphilum*	193
	Fpacidi-R1	GGACTACCCGGGTATCTAATCCGGT		

4.3 Results and discussion

4.3.1 Dissolution behavior of Cu, Fe, and As during bioleaching with and without Ag_2S

In the absence of Ag_2S, Cu recovery was 43% on day 72 (Fig. 4.1a), while Fe started to dissolve mainly from pyrite on day 10 to a rapid completion (100%) by day 40 (Fig. 4.1c), accompanied by the stably high E_h at around 770 mV (Fig. 4.1e). This high redox condition supported pyrite dissolution, whereas enargite oxidation was hindered due to the formation of the passivation layer such as jarosite (Muñoz et al., 2006; Takatsugi et al., 2011). Increasing addition of Ag_2S (0.005–0.04%) led to consecutively greater Cu recoveries (Fig. 4.1a) and lower Fe dissolutions (Fig. 4.1c), with Fe^{2+} oxidation seemingly being increasingly delayed (Fig. 4.1d) and thus E_h values being increasingly suppressed (Fig. 4.1e). The results thus indicate that Ag_2S addition improves Cu recovery by enabling selective Cu dissolution from enargite concentrate. Selective suppression of pyrite dissolution has also been reported in Ag-catalyzed chalcopyrite bioleaching studies (Ahonen and Tuovinen, 1990; Ballester et al., 1990). As for cell growth, active cell growth was seen despite the presence of the antibacterial effect of Ag^+ (Marambio-Jones and Hoek, 2010). Rather, the addition of Ag_2S was found effective in maintaining high cell densities, which otherwise decreased towards the end of the stationary phase (Fig. 4.1f). At the highest Ag_2S concentration of 0.04%, Cu recovery reached 96% (Fig. 4.1a), while Fe dissolution was suppressed to reach only 29% by day 72 (Fig. 4.1c). Under this condition, 56% of dissolved As was calculated to be re-immobilized during bioleaching by day 72, compared with 36% As re-immobilization observed in the absence of Ag_2S (Fig. 4.1b, h) (calculated based on the theoretical amount of As solubilized from enargite at the ratio of Cu:As=3:1).

XRD analysis of the original enargite concentrate (Fig. 4.2a) and bioleached residues (Fig. 4.2b–g) indeed showed the trend that enargite peaks selectively and progressively diminished, while leaving pyrite peaks increasingly unchanged at higher Ag_2S concentrations. Jarosite ($KFe_3(SO_4)_2(OH)_6$) peaks were found after bioleaching only in the absence of Ag_2S (Fig. 4.2b), where pyrite was selectively and completely dissolved by day 40 (Fig. 4.1c). During bioleaching, fine red precipitates floating on the bioleaching liquors became increasingly visible at higher Ag_2S concentrations. Although no XRD peaks attributing As secondary minerals were detected when bulk

bioleached residue samples were analyzed (Fig. 4.2), selective recovery of the red precipitates enabled their identification by XRD as trisilver arsenic sulfide (Ag_3AsS_4) (Fig. 4.3).

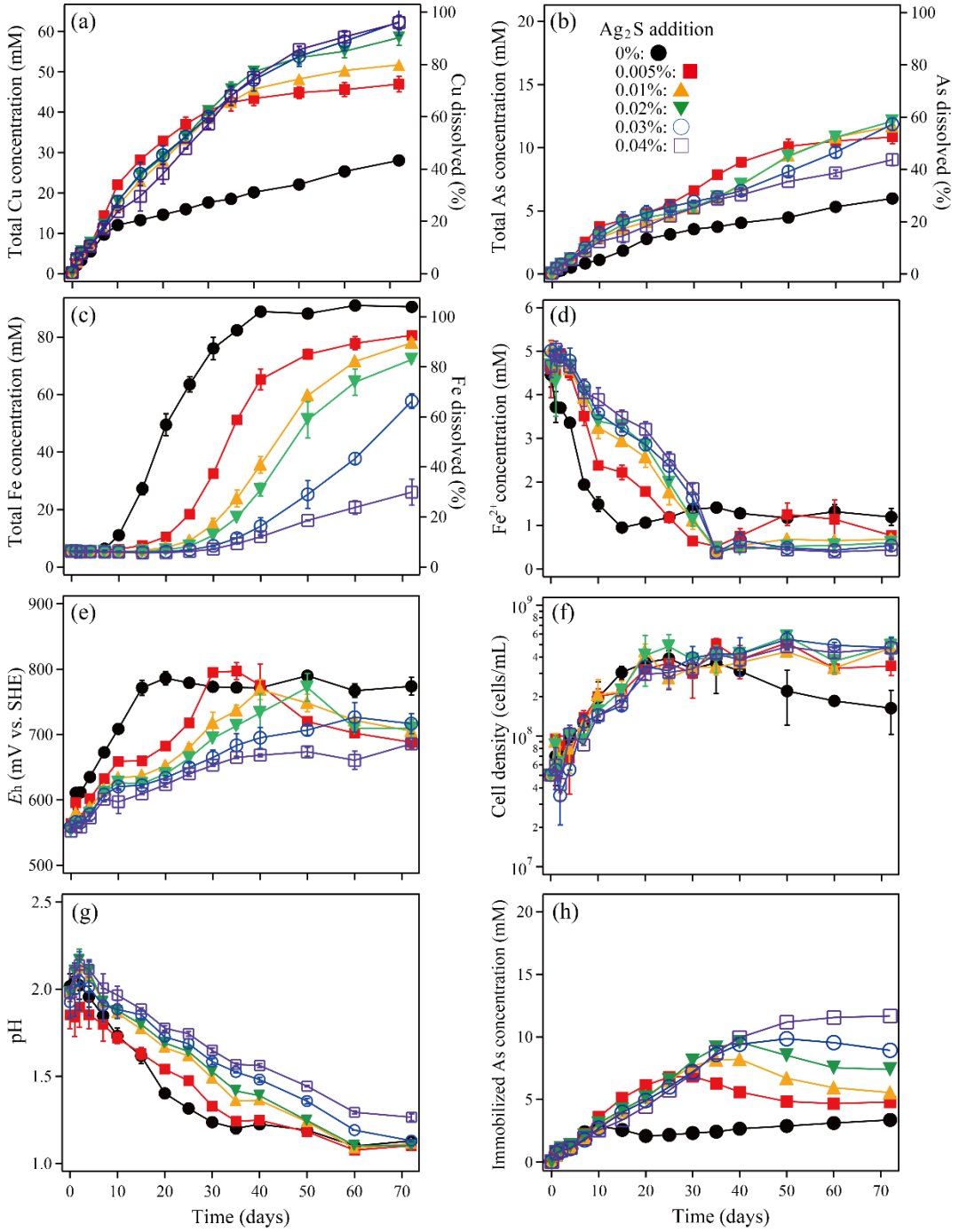

Fig. 4.1 Changes in the total soluble Cu concentration (a), total soluble As concentration (b), total soluble Fe concentration (c), Fe^{2+} concentration (d), E_h (e), cell density (f), pH (g), and immobilized As concentration (h) during bioleaching of enargite concentrate at 0% (●), 0.005% (■), 0.01% (▲), 0.02% (▼), 0.03% (○) or 0.04% (□) of Ag_2S. Data points are mean values from duplicate cultures. Error bars depicting averages are not visible in some cases as they are smaller than the data point symbols.

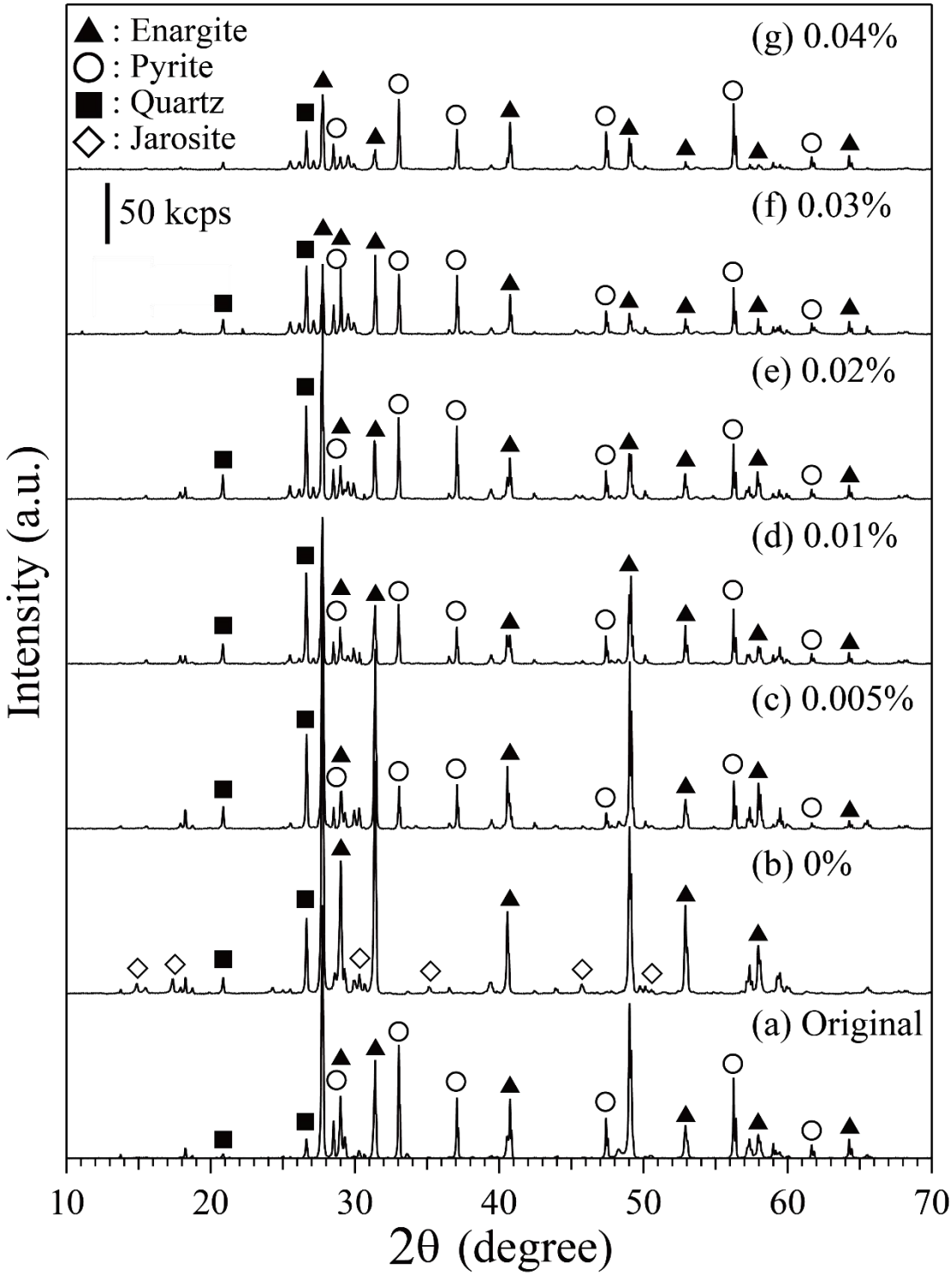

Fig. 4.2 X-ray diffraction patterns of original enargite concentrate (a) and bioleached residues (b-g) recovered on day 72 from cultures containing 0% (b), 0.005% (c), 0.01% (d), 0.02% (e), 0.03% (f) or 0.04% (g) of Ag_2S.▲: enargite (Cu_3AsS_4; PDF No. 00-035-0775), ○: pyrite (FeS_2; PDF No. 00-042-1340), ■: quartz (SiO_2; PDF No. 01-070-3755), ◇: jarosite ($K(Fe_3(SO_4)_2(OH)_6$); PDF No. 01-076-0629).

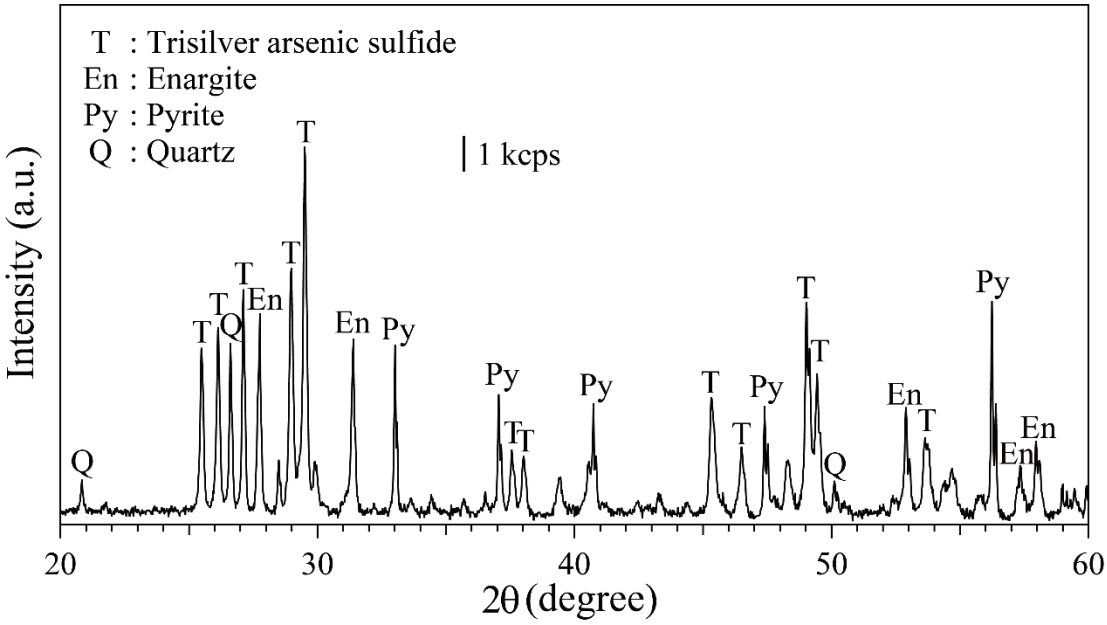

Fig. 4.3 X-ray diffraction patterns of red precipitates selectively collected from the bioleaching culture containing 0.04% Ag_2S. T: trisilver arsenic sulfide (Ag_3AsS_4; PDF No. 01-089-1370), En: enargite (Cu_3AsS_4; PDF No. 00-035-0775), Py: pyrite (FeS_2; PDF No. 00-042-1340), Q: quartz (SiO_2; PDF No. 01-070-3755).

4.3.2 Suppression of pyrite dissolution by Ag_2S

The effect of Ag_2S in selective suppression of pyrite dissolution can be attributed to the following reasons; (i) the change in microbial population structure due to inhibitory effect of Cu^{2+} and/or antibacterial Ag^+ ions, causing the low solution redox condition, (ii) the difference in rest potentials of co-existing minerals (enargite, pyrite and Ag_2S) displaying different subjectivity to the oxidation. As for (i), the real-time PCR analysis found that Fe-oxidizing *Am. ferrooxidans* ICP was the dominant species in the absence of Ag_2S (97–75% on day 15–30, Fig. 4.4). However, the addition of 0.04% Ag_2S decreased its abundance to 57–31% whereas S-oxidizing *At. caldus* KU became the dominant species by increasing its ratio from 1–5% (0% Ag_2S) to 42–53% (0.04% Ag_2S) (on day 15–30; Fig. 4.4). The lower tolerance of *Am. ferrooxidans* ICP (9 mM) than *At. caldus* KU (24 mM) to Cu^{2+} (Watkin et al., 2009) may be responsible for this observation, as Cu dissolution advanced steadily to reach 19–37mM on day 15–30 when 0.04% Ag_2S was added (in contrast to 13–18mM at 0% Ag_2S; Fig. 4.1a). The abundance of *Sb. sibiricus* N1 became noticeable at the later stage of bioleaching both at 0% and 0.04% Ag_2S (Fig. 4.4), probably resulting from its extremely high tolerance

to Cu^{2+} (299 mM) and As (V) (100 mM) (Watling et al., 2008). The population of *Fp. acidiphilum* Y did not emerge throughout the experiment in both cases, probably due to its sensitivity to the temperature condition used here (Golyshina et al., 2000). There may also have been an antibacterial effect of Ag^{+} to the microbes used, but their individual sensitivity to Ag^{+} is unclear. This difference in microbial population structure resulted in deterioration of microbial Fe^{2+} oxidation in the presence of Ag_2S, which may have partly caused the apparent delay of pyrite oxidation (Fig. 4.1c) and the suppression of E_h values (Fig. 4.1e). As for (ii), rest potentials of the minerals were reported to be as follows: 164 mV vs. SCE (408 mV vs. SHE) for enargite, 398 mV vs. SCE (642 mV vs. SHE) for pyrite (Rivera-Vasquez and Dixon, 2015) and 280 mV (vs. SHE) for Ag_2S (Majima, 1969). Therefore, consumption of the oxidant, Fe^{3+}, may have been more readily directed towards oxidation of Ag_2S to release Ag^{+} ions, rather than to oxidation of pyrite. Due to the low solubility product of Ag_2S (Goates et al., 1951; Hseu and Rechnitz, 1968), solubilized Ag^{+} ions would have been immediately transformed back to Ag_2S, which is then re-oxidized by Fe^{3+}. This continuous Ag_2S-oxidation coupled with Fe^{3+}-reduction may have caused the apparent lag-time of Fe^{2+} oxidation (Fig. 4.1d) and the suppression of E_h values (Fig. 4.1e). Since pyrite bioleaching favors high E_h conditions, the above effects would likely have contributed to the suppression of pyrite bioleaching.

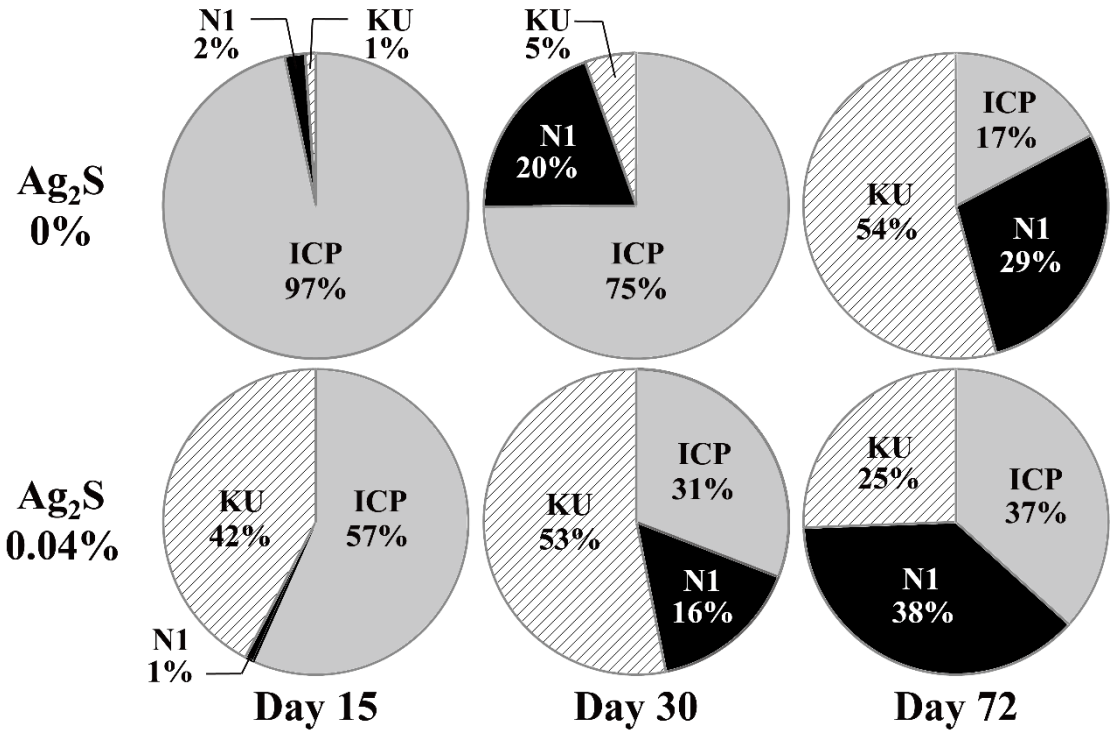

Fig. 4.4 Microbial population structure on day 15, 30, and 72 in bioleaching cultures of enargite concentrate at 0% and 0.04% of Ag_2S. N1, ICP, and KU indicate *Am. ferrooxidans* ICP, *Sb. sibiricus* N1, and *At. caldus* KU, respectively.

4.3.3 Promotion of enargite dissolution by Ag_2S

The theory of Ag-catalyzed chalcopyrite leaching (Hiroyoshi et al., 2002) was applied to that of Ag-catalyzed electrochemical enargite leaching by Miki et al. (2016), suggesting the existence of the optimal E_h range for enhanced enargite dissolution as follows: In the absence of Ag, when E_h is within the optimal range, enargite dissolution proceeds via formation of intermediate Cu_2S (Eq. 4-5) and H_2S generated by Eq. 4-5 is consumed by Cu^{2+} to form Cu_2S (Eq. 4-6). The overall reaction of Eqs. 4-5 and 4-6 can be summarized as Eq. 4-7, and the resultant Cu_2S is amenable to oxidation to produce Cu^{2+} (Eq. 4-8). However, this optimal range is narrow and exists at the relatively lower redox potential level (0.501–0.503 V; Miki et al., 2016), implying that Eqs. 4-7 and 4-8 hardly occur simultaneously in general bioleaching cultures. If Ag is present, however, H_2S generated by Eq. 4-5 is immediately removed by Ag^+ to form Ag_2S (Eq. 4-9) to result in Eq. 4-10 (the sum of Eq. 4-5 and Eq. 4-9), leading to the expansion of the optimal E_h range (0.501–1.020V in the presence of 10^{-5} M Ag^+, Miki et al., 2016).

$$2Cu_3AsS_4 + 6H_2O + 4H^+ + 4e^- \rightarrow 3Cu_2S + 5H_2S + 2H_3AsO_3 \quad \text{(Eq. 4-5)}$$

$$2Cu^{2+} + H_2S + 2e^- \rightarrow Cu_2S + 2H^+ \quad \text{(Eq. 4-6)}$$

$$2Cu_3AsS_4 + 6H_2O + 10Cu^{2+} + 14e^- \rightarrow 8Cu_2S + 2H_3AsO_3 + 6H^+ \quad \text{(Eq. 4-7)}$$

$$Cu_2S \rightarrow 2Cu^{2+} + S^0 + 4e^- \quad \text{(Eq. 4-8)}$$

$$2Ag^+ + H_2S \rightarrow Ag_2S + 2H^+ \quad \text{(Eq. 4-9)}$$

$$2Cu_3AsS_4 + 6H_2O + 10Ag^+ + 4e^- \rightarrow 3Cu_2S + 5Ag_2S + 2H_3AsO_3 + 6H^+ \quad \text{(Eq. 4-10)}$$

The optimal E_h ranges in the absence and presence of Ag are expressed as Eqs. 4-11 and 4-12, respectively.

$$E_{ox}(Cu_2S) < E_h < E_c(Cu^{2+}) \quad \text{(Eq. 4-11)}$$

$$E_{ox}(Cu_2S) < E_h < E_c(Ag^+) \quad \text{(Eq. 4-12)}$$

$E_c(Cu^{2+})$ and $E_c(Ag^+)$ ("critical potential"): the equilibrium redox potential for the intermediate Cu_2S formation from enargite in the absence (Eq. 4-7) and presence (Eq. 4-10) of Ag, respectively.

$E_{ox}(Cu_2S)$ ("oxidation potential"): the equilibrium redox potential for the subsequent oxidation of Cu_2S to Cu^{2+} (Eq. 4-8).

$E_c(Cu^{2+})$, $E_c(Ag^+)$ and $E_{ox}(Cu_2S)$ were calculated by using Eq. 4-13, 4-14 and 4-15, respectively:

$$E_c(Cu^{2+}) = E_c^0(Cu^{2+}) + \frac{RT}{14F} \ln \frac{(\alpha_{Cu^{2+}})^{10}}{(\alpha_{H_3AsO_3})^2(\alpha_{H^+})^6} \quad \text{(Eq. 4-13)}$$

$$E_c(Ag^+) = E_c^0(Ag^+) + \frac{RT}{4F} \ln \frac{\left(\alpha_{Ag^+}\right)^{10}}{\left(\alpha_{H_3AsO_3}\right)^2\left(\alpha_{H^+}\right)^6} \quad \text{(Eq. 4-14)}$$

$$E_{ox}(Cu_2S) = E_{ox}^0(Cu_2S) + \frac{RT}{4F} \ln \left(\alpha_{Cu^{2+}}\right)^2 \quad \text{(Eq. 4-15)}$$

R, T, F, and α_i are gas constant (J/Kmol), temperature (K), Faraday constant (C/mol), and activities of species i, respectively.

Here, $E_c^0(Cu^{2+})$, $E_c^0(Ag^+)$ and $E_{ox}^0(Cu_2S)$ indicate the standard redox potentials (V) of Eq. 4-7, 4-10 and 4-8 calculated by Eq. 4-16, 4-17 and 4-18, respectively:

$$E_c^0(Cu^{2+}) = -\frac{1}{14F}(8\Delta G_{Cu_2S}^0 + 2\Delta G_{H_3AsO_3}^0 + 6\Delta G_{H^+}^0 - 2\Delta G_{Cu_3AsS_4}^0 - 6\Delta G_{H_2O}^0 - 10\Delta G_{Cu^{2+}}^0) \quad \text{(Eq. 4-16)}$$

$$E_c^0(Ag^+) = -\frac{1}{4F}(3\Delta G_{Cu_2S}^0 + 5\Delta G_{Ag_2S}^0 + 2\Delta G_{H_3AsO_3}^0 + 6\Delta G_{H^+}^0 - 2\Delta G_{Cu_3AsS_4}^0 - 6\Delta G_{H_2O}^0 - 10\Delta G_{Ag^+}^0) \quad \text{(Eq. 4-17)}$$

$$E_{ox}^0(Cu_2S) = -\frac{1}{4F}(\Delta G_{Cu_2S}^0 - 2\Delta G_{Cu^{2+}}^0 - \Delta G_{S^0}^0) \quad \text{(Eq. 4-18)}$$

ΔG_i^0 indicates the standard Gibbs free energy of species i and those used for calculation are listed in Table 4.2. The values of $E_c^0(Cu^{2+})$, $E_c^0(Ag^+)$, and $E_{ox}^0(Cu_2S)$ were thus calculated to be 0.628, 1.867, and 0.561 V, respectively.

Since Ag concentrations in leachates were below the detection limit of ICP-OES, they were thermodynamically calculated as follows and listed in Tables 4.3 and 4.4. Dissolution of Ag_2S in bioleaching culture (Eq. 4-19) and the equilibrium potential of Eq. 4-19 (Eq. 4-20) are expressed as below (Miki et al., 2016):

$$Ag_2S \rightarrow 2Ag^+ + S^0 + 2e^- \quad \text{(Eq. 4-19)}$$

$$E_{ox}(Ag_2S) = E^0_{ox}(Ag_2S) + \frac{RT}{F}\ln(\alpha_{Ag^+}) \quad \text{(Eq. 4-20)}$$

$E_{ox}(Ag_2S)$ ("oxidation potential") indicates the equilibrium redox potential for oxidation of Ag_2S to Ag^+ (Eq. 4-19).

$E^0_{ox}(Ag_2S)$ indicates the standard redox potential of Eq. 4-19, as calculated by Eq. 4-21.

$$E^0_{ox}(Ag_2S) = -\frac{1}{2F}(\Delta G^0_{Ag_2S} - 2\Delta G^0_{Ag^+} - \Delta G^0_{S^0}) \quad \text{(Eq. 4-21)}$$

Based on Eq. 4-20, when the activity coefficient is defined as 1, the Ag concentration was calculated by the function of $E_{ox}(Ag_2S)$ as shown in Fig. 4.5.

In order to estimate whether or not the above Cu_2S intermediate reaction contributed to enargite bioleaching in this study, actual measured values were evaluated if they satisfy Eq. 4-11 and/or Eq. 4-12. Actual As(III) concentrations were not measured in this study. Therefore, calculations for $E_c(Cu^{2+})$, $E_c(Ag^+)$ and $E_{ox}(Cu_2S)$ values were conducted based on both assumptions that (i) total As concentrations equal to As(III) concentrations (Table 4.3) and (ii) As(III) concentrations are negligible (10^{-5} M) (Table 4.4), in order to ensure that the results are similar in both cases. Copper extraction rates and E_{have} values were calculated using Eqs. 4-13 and 4-14, respectively, and listed in Tables 4.3 and 4.4.

$$\text{Cu extraction rate} = (X_n - X_{n-1}) / (t_n - t_{n-1}) \quad \text{(Fig. 4-13)}$$

$$E_{have} = (E_{hn} + E_{hn-1}) / 2 \quad \text{(Fig. 4-14)}$$

t_n: the sampling time (day)

X_n: total dissolved Cu concentration on day t_n (M)

E_{hn}: E_h value on day t_n (V vs. SHE)

The calculated $E_c(Cu^{2+})$ values in all cultures were 0.588–0.607 V and 0.607–0.633 V as shown in Tables 4.3 and 4.4, respectively. These values were only about maximum of 0.1 V higher than the $E_{ox}(Cu_2S)$ values (0.501–0.524 V; Tables 4.3 and 4.4).

Measured E_{have} values could hardly locate within this < 0.1 V-wide optimal range, indicating that enargite dissolution was hardly contributed by the Cu_2S intermediate reaction in the absence of Ag.

In the presence of Ag, this optimal range was greatly expanded due to the higher redox potential of $E_c(Ag^+)$: 1.044–1.500 V and 1.120–1.590 V (Tables 4.3 and 4.4, respectively). The correlation between E_{have} values and Cu extraction rates was plotted in Fig. 4.6, by employing the maximum $E_{ox}(Cu_2S)$ value of 0.524 V and the minimum value of $E_c(Ag^+)$ (1.044 V) as the strictest evaluation (Tables 4.3 and 4.4). All plots were within the optimal range satisfying $E_{ox}(Cu_2S) < E_h < E_c(Ag^+)$ (Eq. 4-12), with generally higher Cu extraction rates at elevated Ag_2S concentrations (Fig. 4.6). The results suggest that the Cu_2S intermediate reaction was involved in enargite bioleaching in the presence of Ag_2S.

Table 4.2 Standard Gibbs free energy of each species used for thermodynamic calculation in Tables 4.3 and 4.4 (Padilla et al. (2013); Outokumpu (HSC Chemistry 5 software)).

species	Cu_3AsS_4	Cu_2S	Cu^{2+}	H_3AsO_3	Ag_2S	Ag^+	H_2S	H_2O	H^+
ΔG_i^0	-178.9	-86.7	65.1	-632.6	-40.9	75.2	-34.2	-233.9	0.0

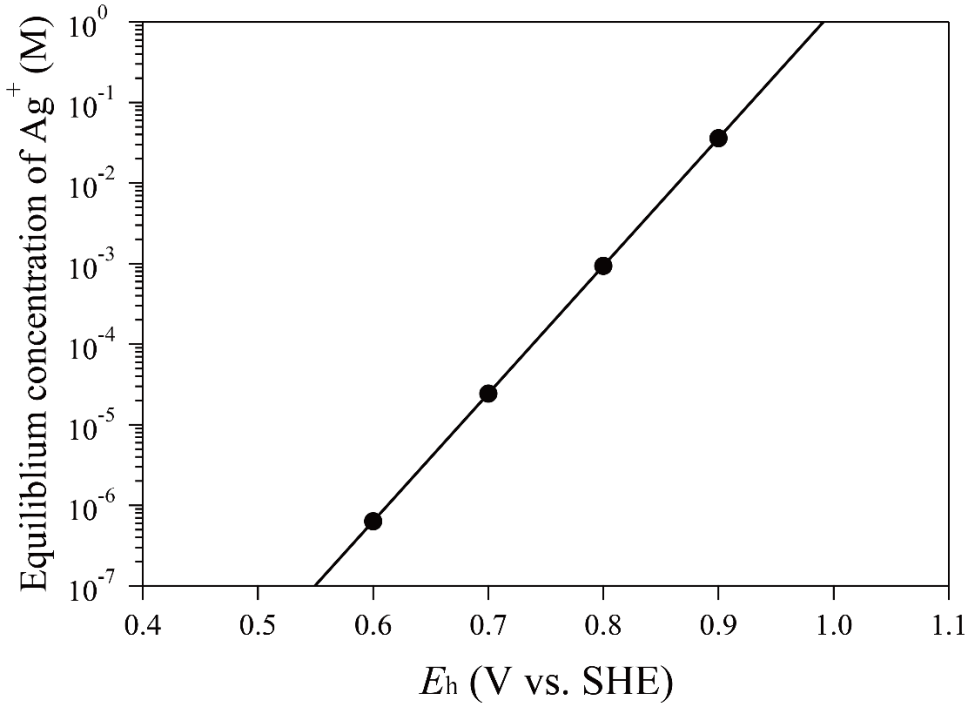

Fig. 4.5 Relationship between solution redox potential (E_h) and thermodynamically calculated equilibrium concentration of Ag^+.

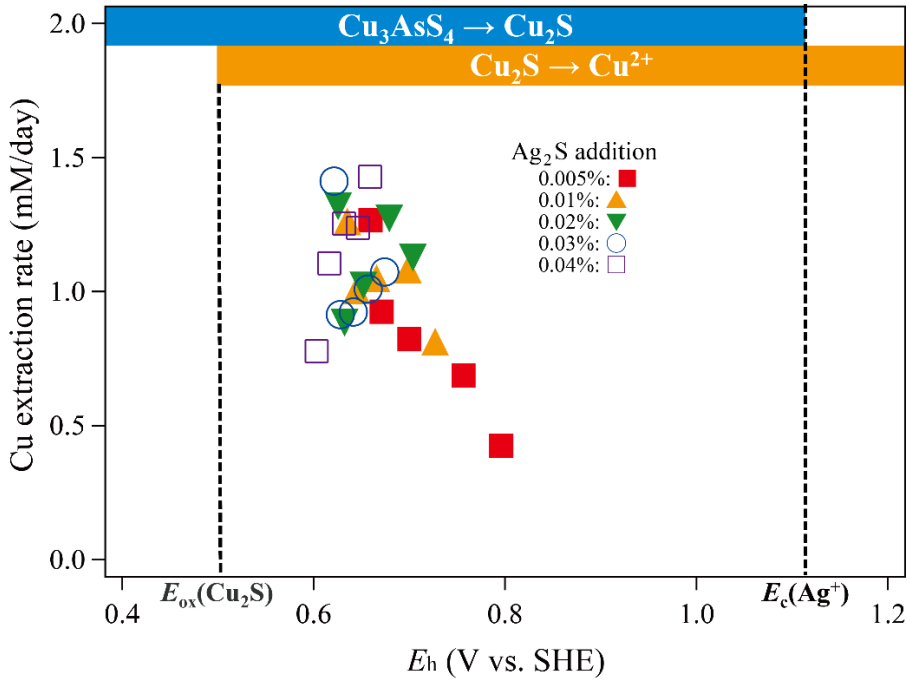

Fig. 4.6 Relationship between the Cu leaching rate and E_h value in bioleaching of enargite concentrate at 0.005% (■), 0.01% (▲), 0.02% (▼), 0.03% (○), and 0.04% (□) of Ag_2S. Data sets obtained from day 15 to 35 were employed.

Table 4.3 Values used for thermodynamic calculations to obtain $E_c(Cu^{2+})$, $E_c(Ag^+)$, and $E_{ox}(Cu_2S)$, assuming that the total soluble As concentration equals to the As(III) concentration.

Ag_2S	Day	pH	$[H^+]$ (M)	$[H_3AsO_3]$ (M)	$[Ag^+]$ (M)	$[Cu^{2+}]$ (M)	Cu extraction rate (M/day)	Eh (V)	Eh_{ave} (V)	$E_c(Cu^{2+})$ (V)	$E_c(Ag^+)$ (V)	$E_{ox}(Cu_2S)$ (V)
0%	10	1.733	0.177	1.123×10^{-3}	-	12.02×10^{-3}	0.733×10^{-3}	0.709	0.691	0.588	-	0.501
	15	1.618	0.198	1.850×10^{-3}	-	13.27×10^{-3}	0.257×10^{-3}	0.772	0.740	0.587	-	0.502
	20	1.403	0.246	2.781×10^{-3}	-	14.62×10^{-3}	0.267×10^{-3}	0.786	0.779	0.585	-	0.504
	25	1.316	0.268	3.144×10^{-3}	-	15.97×10^{-3}	0.270×10^{-3}	0.779	0.783	0.585	-	0.505
	30	1.238	0.290	3.552×10^{-3}	-	17.65×10^{-3}	0.345×10^{-3}	0.773	0.776	0.585	-	0.506
	35	1.202	0.301	3.738×10^{-3}	-	18.52×10^{-3}	0.179×10^{-3}	0.772	0.772	0.586	-	0.507
	40	1.226	0.294	4.055×10^{-3}	-	20.17×10^{-3}	0.331×10^{-3}	0.771	0.772	0.587	-	0.508
	50	1.192	0.304	4.476×10^{-3}	-	22.10×10^{-3}	0.189×10^{-3}	0.790	0.781	0.588	-	0.509
	60	1.101	0.333	5.319×10^{-3}	-	25.34×10^{-3}	0.330×10^{-3}	0.767	0.778	0.589	-	0.511
	72	1.130	0.323	5.983×10^{-3}	-	28.07×10^{-3}	0.227×10^{-3}	0.774	0.770	0.591	-	0.513
0.005%	10	1.721	0.179	3.771×10^{-3}	0.545×10^{-5}	22.09×10^{-3}	2.409×10^{-3}	0.659	0.646	0.595	1.183	0.509
	15	1.631	0.196	4.288×10^{-3}	0.563×10^{-5}	28.23×10^{-3}	1.265×10^{-3}	0.660	0.659	0.598	1.180	0.513
	20	1.541	0.214	4.820×10^{-3}	1.285×10^{-5}	32.89×10^{-3}	0.925×10^{-3}	0.682	0.671	0.600	1.231	0.515
	25	1.475	0.229	5.560×10^{-3}	4.668×10^{-5}	37.02×10^{-3}	0.823×10^{-3}	0.718	0.700	0.601	1.315	0.517
	30	1.329	0.265	6.609×10^{-3}	78.67×10^{-5}	40.36×10^{-3}	0.688×10^{-3}	0.795	0.757	0.600	1.500	0.518
	35	1.243	0.289	7.858×10^{-3}	84.32×10^{-5}	42.44×10^{-3}	0.425×10^{-3}	0.797	0.796	0.600	1.499	0.518
	40	1.249	0.287	8.867×10^{-3}	38.13×10^{-5}	43.40×10^{-3}	0.193×10^{-3}	0.775	0.786	0.600	1.443	0.519
	50	1.183	0.307	10.10×10^{-3}	5.040×10^{-5}	44.84×10^{-3}	0.142×10^{-3}	0.720	0.748	0.599	1.300	0.519
	60	1.077	0.341	10.52×10^{-3}	2.632×10^{-5}	45.59×10^{-3}	0.076×10^{-3}	0.702	0.711	0.598	1.251	0.519
	72	1.103	0.332	10.85×10^{-3}	1.585×10^{-5}	46.95×10^{-3}	0.113×10^{-3}	0.688	0.695	0.599	1.217	0.520
0.01%	10	1.863	0.155	2.820×10^{-3}	0.214×10^{-5}	16.90×10^{-3}	1.767×10^{-3}	0.633	0.624	0.593	1.129	0.506
	15	1.771	0.170	3.590×10^{-3}	0.246×10^{-5}	23.02×10^{-3}	1.261×10^{-3}	0.637	0.635	0.597	1.132	0.510
	20	1.664	0.189	4.137×10^{-3}	0.424×10^{-5}	28.09×10^{-3}	1.005×10^{-3}	0.652	0.645	0.599	1.163	0.513
	25	1.618	0.198	4.578×10^{-3}	1.154×10^{-5}	33.36×10^{-3}	1.049×10^{-3}	0.680	0.666	0.601	1.228	0.515
	30	1.490	0.225	5.182×10^{-3}	4.584×10^{-5}	38.61×10^{-3}	1.082×10^{-3}	0.717	0.698	0.602	1.315	0.517
	35	1.360	0.257	6.025×10^{-3}	9.287×10^{-5}	42.57×10^{-3}	0.812×10^{-3}	0.737	0.727	0.602	1.356	0.518
	40	1.363	0.256	7.024×10^{-3}	29.64×10^{-5}	45.73×10^{-3}	0.634×10^{-3}	0.768	0.753	0.603	1.434	0.519
	50	1.239	0.290	9.379×10^{-3}	14.18×10^{-5}	48.23×10^{-3}	0.246×10^{-3}	0.748	0.758	0.601	1.374	0.520
	60	1.087	0.337	10.832×10^{-3}	5.392×10^{-5}	50.33×10^{-3}	0.214×10^{-3}	0.722	0.735	0.600	1.300	0.521
	72	1.114	0.328	11.696×10^{-3}	2.931×10^{-5}	51.76×10^{-3}	0.119×10^{-3}	0.705	0.713	0.600	1.258	0.521

Ag_2S	Day	pH	$[H^+]$ (M)	$[H_3AsO_3]$ (M)	$[Ag^+]$ (M)	$[Cu^{2+}]$ (M)	Cu extraction rate (M/day)	Eh (V)	Eh_{ave} (V)	$E_c(Cu^{2+})$ (V)	$E_c(Ag^+)$ (V)	$E_{ox}(Cu_2S)$ (V)
0.02%	10	1.877	0.153	2.908×10^{-3}	0.166×10^{-5}	18.00×10^{-3}	1.877×10^{-3}	0.626	0.619	0.594	1.112	0.507
	15	1.799	0.166	3.933×10^{-3}	0.156×10^{-5}	24.40×10^{-3}	1.318×10^{-3}	0.625	0.626	0.598	1.100	0.511
	20	1.692	0.184	4.477×10^{-3}	0.271×10^{-5}	28.85×10^{-3}	0.883×10^{-3}	0.640	0.632	0.599	1.132	0.513
	25	1.642	0.194	4.809×10^{-3}	0.653×10^{-5}	33.99×10^{-3}	1.023×10^{-3}	0.664	0.652	0.602	1.189	0.515
	30	1.528	0.217	5.287×10^{-3}	1.966×10^{-5}	40.17×10^{-3}	1.273×10^{-3}	0.694	0.679	0.603	1.259	0.518
	35	1.417	0.243	6.083×10^{-3}	3.976×10^{-5}	45.66×10^{-3}	1.127×10^{-3}	0.713	0.704	0.604	1.301	0.519
	40	1.390	0.249	7.092×10^{-3}	8.129×10^{-5}	50.01×10^{-3}	0.874×10^{-3}	0.733	0.723	0.605	1.346	0.521
	50	1.247	0.287	9.317×10^{-3}	33.56×10^{-5}	53.52×10^{-3}	0.344×10^{-3}	0.772	0.752	0.603	1.434	0.522
	60	1.104	0.332	10.82×10^{-3}	3.448×10^{-5}	55.10×10^{-3}	0.161×10^{-3}	0.710	0.741	0.602	1.270	0.522
	72	1.105	0.331	12.10×10^{-3}	3.436×10^{-5}	58.49×10^{-3}	0.282×10^{-3}	0.709	0.709	0.602	1.268	0.523
0.03%	10	1.885	0.152	3.241×10^{-3}	0.134×10^{-5}	17.88×10^{-3}	1.973×10^{-3}	0.620	0.614	0.594	1.096	0.507
	15	1.854	0.157	4.278×10^{-3}	0.143×10^{-5}	24.73×10^{-3}	1.412×10^{-3}	0.622	0.621	0.598	1.095	0.511
	20	1.726	0.178	4.861×10^{-3}	0.217×10^{-5}	29.34×10^{-3}	0.914×10^{-3}	0.634	0.628	0.600	1.117	0.513
	25	1.687	0.185	5.318×10^{-3}	0.385×10^{-5}	33.97×10^{-3}	0.923×10^{-3}	0.649	0.642	0.602	1.154	0.515
	30	1.585	0.205	5.738×10^{-3}	0.677×10^{-5}	38.87×10^{-3}	1.009×10^{-3}	0.665	0.657	0.603	1.187	0.517
	35	1.525	0.218	6.106×10^{-3}	1.333×10^{-5}	44.10×10^{-3}	1.073×10^{-3}	0.683	0.674	0.605	1.230	0.519
	40	1.482	0.227	6.594×10^{-3}	2.039×10^{-5}	48.02×10^{-3}	0.788×10^{-3}	0.695	0.689	0.605	1.256	0.520
	50	1.358	0.257	8.100×10^{-3}	3.119×10^{-5}	53.86×10^{-3}	0.573×10^{-3}	0.707	0.701	0.605	1.278	0.522
	60	1.192	0.304	9.642×10^{-3}	6.389×10^{-5}	57.55×10^{-3}	0.376×10^{-3}	0.726	0.717	0.604	1.317	0.523
	72	1.131	0.323	11.86×10^{-3}	4.460×10^{-5}	62.37×10^{-3}	0.402×10^{-3}	0.717	0.721	0.604	1.288	0.524
0.04%	10	1.967	0.140	2.571×10^{-3}	0.057×10^{-5}	15.39×10^{-3}	1.336×10^{-3}	0.597	0.599	0.593	1.044	0.504
	15	1.887	0.152	3.024×10^{-3}	0.089×10^{-5}	19.16×10^{-3}	0.777×10^{-3}	0.609	0.603	0.595	1.069	0.507
	20	1.777	0.169	3.799×10^{-3}	0.148×10^{-5}	24.74×10^{-3}	1.106×10^{-3}	0.623	0.616	0.598	1.096	0.511
	25	1.745	0.175	4.602×10^{-3}	0.271×10^{-5}	31.03×10^{-3}	1.254×10^{-3}	0.640	0.631	0.601	1.134	0.514
	30	1.650	0.192	5.260×10^{-3}	0.437×10^{-5}	37.04×10^{-3}	1.238×10^{-3}	0.653	0.646	0.603	1.161	0.517
	35	1.569	0.208	5.915×10^{-3}	0.676×10^{-5}	44.01×10^{-3}	1.429×10^{-3}	0.665	0.659	0.605	1.186	0.519
	40	1.563	0.210	6.271×10^{-3}	0.767×10^{-5}	48.64×10^{-3}	0.931×10^{-3}	0.668	0.667	0.607	1.193	0.520
	50	1.444	0.236	7.319×10^{-3}	0.934×10^{-5}	55.50×10^{-3}	0.674×10^{-3}	0.674	0.671	0.607	1.200	0.522
	60	1.294	0.274	7.997×10^{-3}	0.581×10^{-5}	58.66×10^{-3}	0.321×10^{-3}	0.661	0.667	0.606	1.160	0.523
	72	1.266	0.282	9.051×10^{-3}	1.452×10^{-5}	62.18×10^{-3}	0.293×10^{-3}	0.686	0.673	0.607	1.220	0.524

Table 4.4 Values used for thermodynamic calculations to obtain $E_c(Cu^{2+})$, $E_c(Ag^+)$, and $E_{ox}(Cu_2S)$, assuming that the As(III) concentrations are negligible (10^{-5} M).

Ag_2S	Day	pH	$[H^+]$ (M)	$[H_3AsO_3]$ (M)	$[Ag^+]$ (M)	$[Cu^{2+}]$ (M)	Cu extraction rate (M/day)	Eh (V)	Eh_{ave} (V)	$E_c(Cu^{2+})$ (V)	$E_c(Ag^+)$ (V)	$E_{ox}(Cu_2S)$ (V)
0%	10	1.733	0.177	10^{-5}	-	12.02×10^{-3}	0.733×10^{-3}	0.709	0.691	0.607	-	0.501
	15	1.618	0.198	10^{-5}	-	13.27×10^{-3}	0.257×10^{-3}	0.772	0.740	0.607	-	0.502
	20	1.403	0.246	10^{-5}	-	14.62×10^{-3}	0.267×10^{-3}	0.786	0.779	0.607	-	0.504
	25	1.316	0.268	10^{-5}	-	15.97×10^{-3}	0.270×10^{-3}	0.779	0.783	0.607	-	0.505
	30	1.238	0.290	10^{-5}	-	17.65×10^{-3}	0.345×10^{-3}	0.773	0.776	0.608	-	0.506
	35	1.202	0.301	10^{-5}	-	18.52×10^{-3}	0.179×10^{-3}	0.772	0.772	0.609	-	0.507
	40	1.226	0.294	10^{-5}	-	20.17×10^{-3}	0.331×10^{-3}	0.771	0.772	0.611	-	0.508
	50	1.192	0.304	10^{-5}	-	22.10×10^{-3}	0.189×10^{-3}	0.790	0.781	0.612	-	0.509
	60	1.101	0.333	10^{-5}	-	25.34×10^{-3}	0.330×10^{-3}	0.767	0.778	0.614	-	0.511
	72	1.130	0.323	10^{-5}	-	28.07×10^{-3}	0.227×10^{-3}	0.774	0.770	0.616	-	0.513
0.005%	10	1.721	0.179	10^{-5}	0.545×10^{-5}	22.09×10^{-3}	2.409×10^{-3}	0.659	0.646	0.618	1.265	0.509
	15	1.631	0.196	10^{-5}	0.563×10^{-5}	28.23×10^{-3}	1.265×10^{-3}	0.660	0.659	0.622	1.263	0.513
	20	1.541	0.214	10^{-5}	1.285×10^{-5}	32.89×10^{-3}	0.925×10^{-3}	0.682	0.671	0.624	1.316	0.515
	25	1.475	0.229	10^{-5}	4.668×10^{-5}	37.02×10^{-3}	0.823×10^{-3}	0.718	0.700	0.626	1.402	0.517
	30	1.329	0.265	10^{-5}	78.67×10^{-5}	40.36×10^{-3}	0.688×10^{-3}	0.795	0.757	0.626	1.589	0.518
	35	1.243	0.289	10^{-5}	84.32×10^{-5}	42.44×10^{-3}	0.425×10^{-3}	0.797	0.796	0.626	1.590	0.518
	40	1.249	0.287	10^{-5}	38.13×10^{-5}	43.40×10^{-3}	0.193×10^{-3}	0.775	0.786	0.626	1.536	0.519
	50	1.183	0.307	10^{-5}	5.040×10^{-5}	44.84×10^{-3}	0.142×10^{-3}	0.720	0.748	0.626	1.395	0.519
	60	1.077	0.341	10^{-5}	2.632×10^{-5}	45.59×10^{-3}	0.076×10^{-3}	0.702	0.711	0.625	1.346	0.519
	72	1.103	0.332	10^{-5}	1.585×10^{-5}	46.95×10^{-3}	0.113×10^{-3}	0.688	0.695	0.626	1.312	0.520
0.01%	10	1.863	0.155	10^{-5}	0.214×10^{-5}	16.90×10^{-3}	1.767×10^{-3}	0.633	0.624	0.615	1.206	0.506
	15	1.771	0.170	10^{-5}	0.246×10^{-5}	23.02×10^{-3}	1.261×10^{-3}	0.637	0.635	0.620	1.212	0.510
	20	1.664	0.189	10^{-5}	0.424×10^{-5}	28.09×10^{-3}	1.005×10^{-3}	0.652	0.645	0.622	1.245	0.513
	25	1.618	0.198	10^{-5}	1.154×10^{-5}	33.36×10^{-3}	1.049×10^{-3}	0.680	0.666	0.625	1.312	0.515
	30	1.490	0.225	10^{-5}	4.584×10^{-5}	38.61×10^{-3}	1.082×10^{-3}	0.717	0.698	0.627	1.401	0.517
	35	1.360	0.257	10^{-5}	9.287×10^{-5}	42.57×10^{-3}	0.812×10^{-3}	0.737	0.727	0.627	1.444	0.518
	40	1.363	0.256	10^{-5}	29.64×10^{-5}	45.73×10^{-3}	0.634×10^{-3}	0.768	0.753	0.628	1.524	0.519
	50	1.239	0.290	10^{-5}	14.18×10^{-5}	48.23×10^{-3}	0.246×10^{-3}	0.748	0.758	0.628	1.468	0.520
	60	1.087	0.337	10^{-5}	5.392×10^{-5}	50.33×10^{-3}	0.214×10^{-3}	0.722	0.735	0.627	1.396	0.521
	72	1.114	0.328	10^{-5}	2.931×10^{-5}	51.76×10^{-3}	0.119×10^{-3}	0.705	0.713	0.628	1.355	0.521

Ag_2S	Day	pH	$[H^+]$ (M)	$[H_3AsO_3]$ (M)	$[Ag^+]$ (M)	$[Cu^{2+}]$ (M)	Cu extraction rate (M/day)	Eh (V)	Eh_{we} (V)	$E_c(Cu^{2+})$ (V)	$E_c(Ag^+)$ (V)	$E_{ox}(Cu_2S)$ (V)
0.02%	10	1.877	0.153	10^{-5}	0.166×10^{-5}	18.00×10^{-3}	1.877×10^{-3}	0.626	0.619	0.616	1.190	0.507
	15	1.799	0.166	10^{-5}	0.156×10^{-5}	24.40×10^{-3}	1.318×10^{-3}	0.625	0.626	0.621	1.182	0.511
	20	1.692	0.184	10^{-5}	0.271×10^{-5}	28.85×10^{-3}	0.883×10^{-3}	0.640	0.632	0.623	1.216	0.513
	25	1.642	0.194	10^{-5}	0.653×10^{-5}	33.99×10^{-3}	1.023×10^{-3}	0.664	0.652	0.626	1.274	0.515
	30	1.528	0.217	10^{-5}	1.966×10^{-5}	40.17×10^{-3}	1.273×10^{-3}	0.694	0.679	0.628	1.345	0.518
	35	1.417	0.243	10^{-5}	3.976×10^{-5}	45.66×10^{-3}	1.127×10^{-3}	0.713	0.704	0.629	1.388	0.519
	40	1.390	0.249	10^{-5}	8.129×10^{-5}	50.01×10^{-3}	0.874×10^{-3}	0.733	0.723	0.631	1.436	0.521
	50	1.247	0.287	10^{-5}	33.56×10^{-5}	53.52×10^{-3}	0.344×10^{-3}	0.772	0.752	0.630	1.528	0.522
	60	1.104	0.332	10^{-5}	3.448×10^{-5}	55.10×10^{-3}	0.161×10^{-3}	0.710	0.741	0.629	1.366	0.522
	72	1.105	0.331	10^{-5}	3.436×10^{-5}	58.49×10^{-3}	0.282×10^{-3}	0.709	0.709	0.630	1.366	0.523
0.03%	10	1.885	0.152	10^{-5}	0.134×10^{-5}	17.88×10^{-3}	1.973×10^{-3}	0.620	0.614	0.616	1.175	0.507
	15	1.854	0.157	10^{-5}	0.143×10^{-5}	24.73×10^{-3}	1.412×10^{-3}	0.622	0.621	0.622	1.178	0.511
	20	1.726	0.178	10^{-5}	0.217×10^{-5}	29.34×10^{-3}	0.914×10^{-3}	0.634	0.628	0.624	1.202	0.513
	25	1.687	0.185	10^{-5}	0.385×10^{-5}	33.97×10^{-3}	0.923×10^{-3}	0.649	0.642	0.626	1.240	0.515
	30	1.585	0.205	10^{-5}	0.677×10^{-5}	38.87×10^{-3}	1.009×10^{-3}	0.665	0.657	0.628	1.274	0.517
	35	1.525	0.218	10^{-5}	1.333×10^{-5}	44.10×10^{-3}	1.073×10^{-3}	0.683	0.674	0.630	1.318	0.519
	40	1.482	0.227	10^{-5}	2.039×10^{-5}	48.02×10^{-3}	0.788×10^{-3}	0.695	0.689	0.631	1.345	0.520
	50	1.358	0.257	10^{-5}	3.119×10^{-5}	53.86×10^{-3}	0.573×10^{-3}	0.707	0.701	0.632	1.369	0.522
	60	1.192	0.304	10^{-5}	6.389×10^{-5}	57.55×10^{-3}	0.376×10^{-3}	0.726	0.717	0.631	1.412	0.523
	72	1.131	0.323	10^{-5}	4.460×10^{-5}	62.37×10^{-3}	0.402×10^{-3}	0.717	0.721	0.632	1.384	0.524
0.04%	10	1.967	0.140	10^{-5}	0.057×10^{-5}	15.39×10^{-3}	1.336×10^{-3}	0.597	0.599	0.614	1.120	0.504
	15	1.887	0.152	10^{-5}	0.089×10^{-5}	19.16×10^{-3}	0.777×10^{-3}	0.609	0.603	0.618	1.148	0.507
	20	1.777	0.169	10^{-5}	0.148×10^{-5}	24.74×10^{-3}	1.106×10^{-3}	0.623	0.616	0.621	1.178	0.511
	25	1.745	0.175	10^{-5}	0.271×10^{-5}	31.03×10^{-3}	1.254×10^{-3}	0.640	0.631	0.625	1.218	0.514
	30	1.650	0.192	10^{-5}	0.437×10^{-5}	37.04×10^{-3}	1.238×10^{-3}	0.653	0.646	0.628	1.247	0.517
	35	1.569	0.208	10^{-5}	0.676×10^{-5}	44.01×10^{-3}	1.429×10^{-3}	0.665	0.659	0.630	1.273	0.519
	40	1.563	0.210	10^{-5}	0.767×10^{-5}	48.64×10^{-3}	0.931×10^{-3}	0.668	0.667	0.632	1.282	0.520
	50	1.444	0.236	10^{-5}	0.934×10^{-5}	55.50×10^{-3}	0.674×10^{-3}	0.674	0.671	0.633	1.290	0.522
	60	1.294	0.274	10^{-5}	0.581×10^{-5}	58.66×10^{-3}	0.321×10^{-3}	0.661	0.667	0.633	1.252	0.523
	72	1.266	0.282	10^{-5}	1.452×10^{-5}	62.18×10^{-3}	0.293×10^{-3}	0.686	0.673	0.633	1.313	0.524

4.3.4 Copper substitution on enargite surface with silver

Following identification of trisilver arsenic sulfide by XRD (Fig. 4.3), EPMA elemental mapping was performed in order to confirm the formation of Ag-containing passivation layers around the enargite surface after bioleaching with 0.04% Ag_2S (Fig. 4.7). Emergence of bright white areas on the enargite surface indicated the formation of secondary minerals consisting of heavier metals than Cu, such as Ag (Fig. 4.7a). The enargite grain was indeed covered with a thick but porous secondary layer (Fig. 4.7a; solid arrow), consisting of Ag, As, and S (Fig. 4.7b, d, e), onto which another partial layer (Fig. 4.7a; broken arrow) of ferric arsenate (Fig. 4.7d, f) was observed. To further analyze the formation of Ag-containing passivation layers, EPMA quantitative analysis was conducted on different locations of the particle (Fig. 4.8): Spot 1, the core of enargite grain (grey); Spot 4, the passivation layer around the enargite surface (white); Spots 2 and 3, the interface between Spots 1 and 4 (light grey). Spots 1–4 shared the approximate atomic ratio of (Cu+Ag):As:S=3:1:4, with different Ag:Cu ratios (Table 4.5). An increasing dominance of Ag relative to Cu, from the core to surface of the enargite particle indicated that Cu was dissolved from enargite (Cu_3AsS_4; Spot 1) possibly by substitution with Ag ($(Cu,Ag)_3AsS_4$; Spots 2 and 3), eventually leaving the passivation layer of trisilver arsenic sulfide (Ag_3AsS_4; Spot 4) (Fig. 4.8).

In chemical/electrochemical studies for chalcopyrite, metal-deficient sulfur-rich layers ($Cu_{1-x}Fe_{1-y}S_2$ or $Cu_{1-x}Fe_{1-y}S_{2-z}$) were reported to passivate the mineral surface (Warren et al., 1982; Hackl et al., 1995; Ghahremaninezhad et al., 2010, 2013). Ghahremaninezhad et al. (2015) explained the mechanism of Ag-catalyzed chalcopyrite dissolution by Ag diffusion into such metal-deficient sulfur-rich layers, eventually producing Ag_2S passivation. Likewise, trisilver arsenic sulfide detected in this study might have been formed via Ag ion diffusion into enargite-type metal-deficient sulfur-rich layers ($Cu_{3-x}AsS_4$; Córdova et al., 1997; Fantauzzi et al., 2007, 2009).

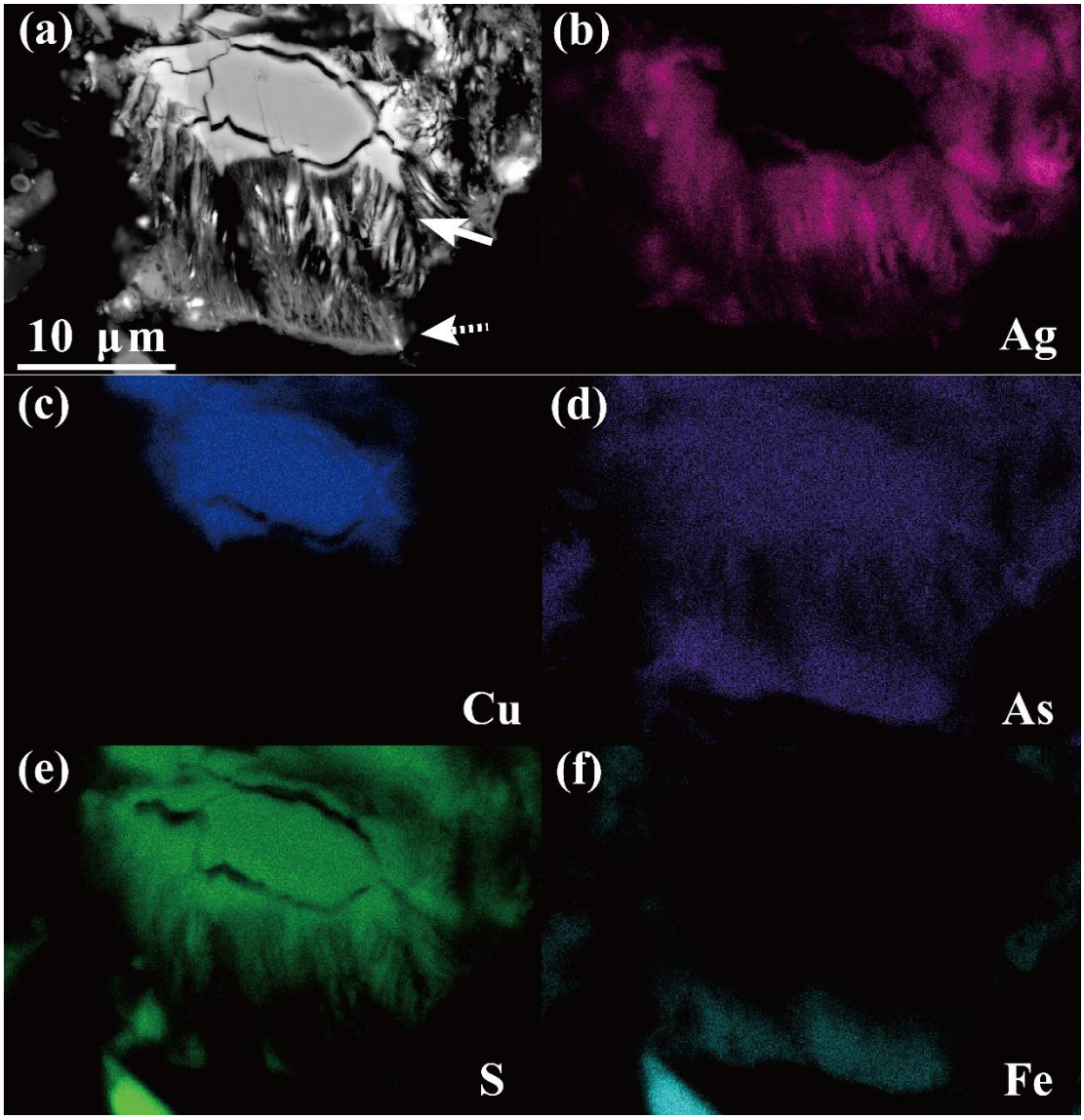

Fig. 4.7 EPMA elemental mapping of enargite concentrate residue bioleached for 72 days with 0.04% Ag_2S: The backscattered electron image at 2000-fold magnification (a) was mapped for Ag (b), Cu (c), As (d), S (e) and Fe (f). The surface of an enargite grain is covered with Ag-containing secondary mineral (solid arrow), on which deposition of ferric arsenate is observed (broken arrow).

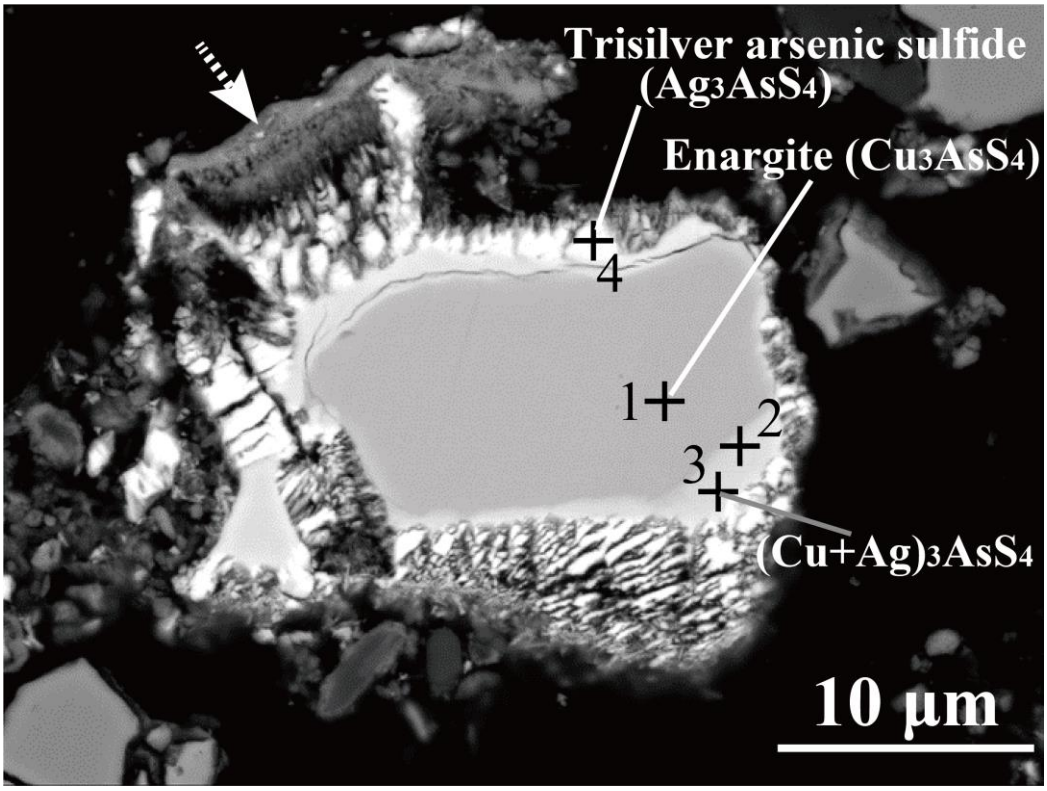

Fig. 4.8 Backscattered electron image of an enargite grain bioleached for 72 days with 0.04% Ag_2S at the 2000-fold magnification. Cross points 1–4 indicate the beam spot positions for quantitative analysis (results summarized in Table 4.5).

Table 4.5 EPMA quantitative analysis of secondary minerals formed on the enargite surface after bioleaching: Numbers 1-4 indicate the cross points 1-5 in Fig. 4.8, respectively.

No.	Atomic content (%)					Atomic ratio
	S	Ag	As	Fe	Cu	
1	49.66	1.26	11.42	0.91	36.76	Cu : Ag = 40.4 : 1.0 (Cu+Ag) : As : S = 3.3 : 1.0 : 4.3
2	49.15	12.02	11.63	0.91	26.29	Cu : Ag = 2.2 : 1.0 (Cu+Ag) : As : S = 3.3 : 1.0 : 4.2
3	45.56	27.77	12.08	0.87	13.73	Cu : Ag = 1.0 : 2.0 (Cu+Ag) : As : S = 3.4 : 1.0 : 3.8
4	48.00	33.16	13.65	0.84	4.35	Cu : Ag = 1.0 : 7.6 (Cu+Ag) : As : S = 2.7 : 1.0 : 3.5
5	0.78	0.04	6.20	6.05	0.09	Fe : As : O = 1.0 : 1.0 : 3.9

4.3.5 Kinetic study on Ag-catalyzed bioleaching of enargite concentrate

The shrinking core model is frequently utilized to model the mineral dissolution process. Based on this model, the dissolution reaction proceeds either via diffusion through the liquid film (Eq. 4-22), diffusion through product film (Eq. 4-23) or surface chemical reaction (Eq. 4-24), one of which may become the rate-limiting step under certain conditions (Wadsworth and Sohn, 1979).

$$X = k_l t \quad \text{(Eq. 4-22)}$$

$$1 - 3(1-X)^{2/3} + 2(1-X) = k_d t \quad \text{(Eq. 4-23)}$$

$$1 - (1-X)^{1/3} = k_r t \quad \text{(Eq. 4-24)}$$

X: the fraction of dissolved Cu

t: the reaction time

k: the rate constant

In order to investigate which process rate-limits Cu dissolution during bioleaching of enargite concentrate with and without Ag_2S, measured values from Fig. 4.1a were fitted to Eqs. 4-23 and 4-24 (Fig. 4.9). The fluid film resistance was considered negligible relative to other effects, and in fact no linear relationships between X against t were found. The *k* and R^2 values were calculated from the fitting results and listed in Table 4.6. Linear lines were drawn where R^2 values of regression analyses were > 0.99 (Table. 4.6).

In the absence of Ag_2S, rapid Fe dissolution (Fig. 4.1c) caused precipitation of jarosite (as confirmed by XRD; Fig. 4.2), resulting in the reaction being fitted to diffusion through product film throughout the bioleaching period (Fig. 4.9a; Table 4.6). At higher Ag_2S concentration of 0.03 and 0.04%, on the other hand, surface chemical reaction was likely the rate-limiting step until the end (Fig. 4.9e, f; Table 4.6), suggesting that formation of trisilver arsenic sulfide layer (as well as ferric arsenate "outer" layer) around the enargite surface did not rate-limit the enargite dissolution. Rather, the formation of trisilver arsenic sulfide was likely involved in the mechanism of facilitated enargite dissolution. At 0.005–0.02% Ag_2S concentrations, enargite dissolution was

controlled by surface chemical reaction but only at the early stage (0–20 days at 0.005% and 0–40 days at 0.01–0.02%; Fig. 4.9b–d; Table 4.6) due to depletion of Ag.

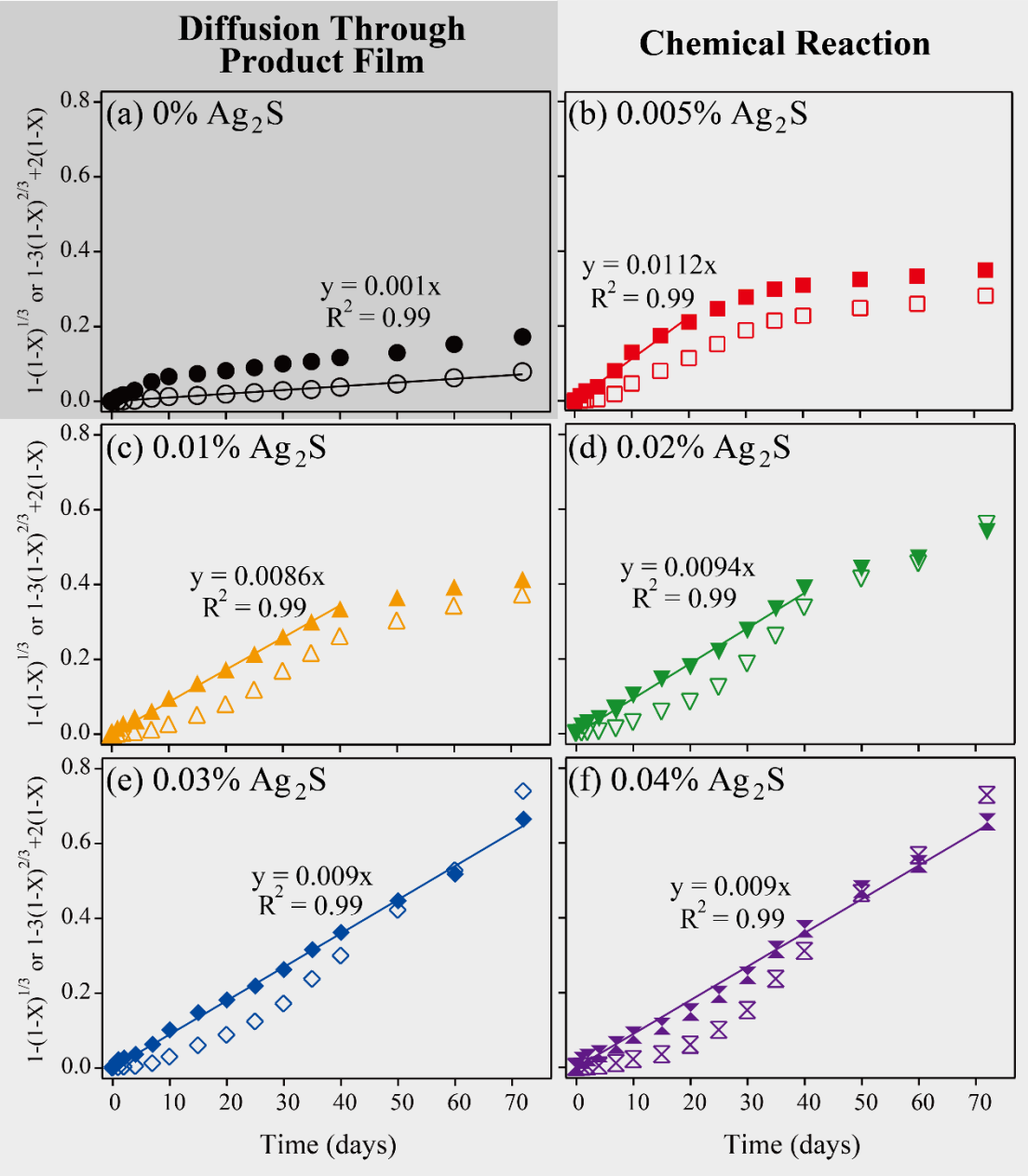

Fig. 4.9 Kinetic modeling on bioleaching of enargite concentrate at different Ag_2S concentrations: (a) 0%, (b) 0.005%, (c) 0.01%, (d) 0.02%, (e) 0.03% and (f) 0.04%. Solid and open symbols indicate the fitting data to surface chemical reaction ($1-(1-X)^{1/3}=k_rt$) and diffusion through product film ($1-3(1-X)^{2/3}+2(1-X)=k_dt$), respectively. Linear lines were drawn where R^2 values were calculated to be > 0.99.

Table 4.6 R^2 and *k* values calculated using the kinetic model of surface chemical reaction and diffusion through product film. Shadowed cells ($R^2 > 0.99$) indicate which one of the two models fits the experimental data.

Ag_2S addition (%)	Leaching period (day)	Reaction model			
		Surface chemical reaction		Diffusion through product film	
		k_r	R^2	k_d	R^2
0	0 - 72	0.0028	0.82	0.0010	0.99
0.005	0 - 20	0.0112	0.99	0.0051	0.94
	25 - 72	0.0019	0.88	0.0025	0.90
0.01	0 - 40	0.0086	0.99	0.0056	0.93
	50 - 72	0.0022	0.98	0.0031	0.98
0.02	0 - 40	0.0094	0.99	0.0066	0.89
	50 - 72	0.0045	0.96	0.0068	0.96
0.03	0 - 72	0.0090	0.99	0.0084	0.92
0.04	0 - 72	0.0090	0.99	0.0085	0.90

4.4 Conclusions

Based on the overall results obtained in this study, a proposed mechanism for Ag-catalyzed bioleaching of enargite concentrate was summarized in Fig. 4.10. The mechanism includes the formation of at least two types of secondary products (chalcocite and trisilver arsenic sulfide).

Chalcocite intermediate: Due to the low rest potential of Ag_2S (compared to those of enargite and pyrite), consumption of Fe^{3+} is more likely directed towards oxidation of Ag_2S to produce Fe^{2+} and Ag^+. Instead, oxidation of pyrite by Fe^{3+} is suppressed (I). Addition of Ag_2S may also partially inhibit the activity of Fe-oxidizing microorganisms (II). Due to (I) and (II), Fe^{2+} becomes more abundant than Fe^{3+} to maintain lower E_h to satisfy E_{ox} (Cu_2S) < E_h < Ec (Ag^+). Consequently, enargite dissolution was enhanced via the formation of Cu_2S intermediate, accompanied by the production of H_2S which is rapidly removed by Ag^+ to re-form Ag_2S (III). The resultant Cu_2S is amenable to oxidation by Fe^{3+} to solubilize Cu^{2+} (IV).

Trisilver arsenic sulfide: Cu ion in the enargite structure is gradually substituted with Ag^+ solubilized from Ag_2S to form an intermediate layer of $(Cu,Ag)_3AsS_4$. Eventually, trisilver arsenic sulfide (Ag_3AsS_4) covers the surface of enargite (V). The formation of this product film, however, does not impose a rate-limiting step.

The combination of the above reactions contributes to enhanced enargite bioleaching in the presence of Ag_2S as an effective Ag catalyst.

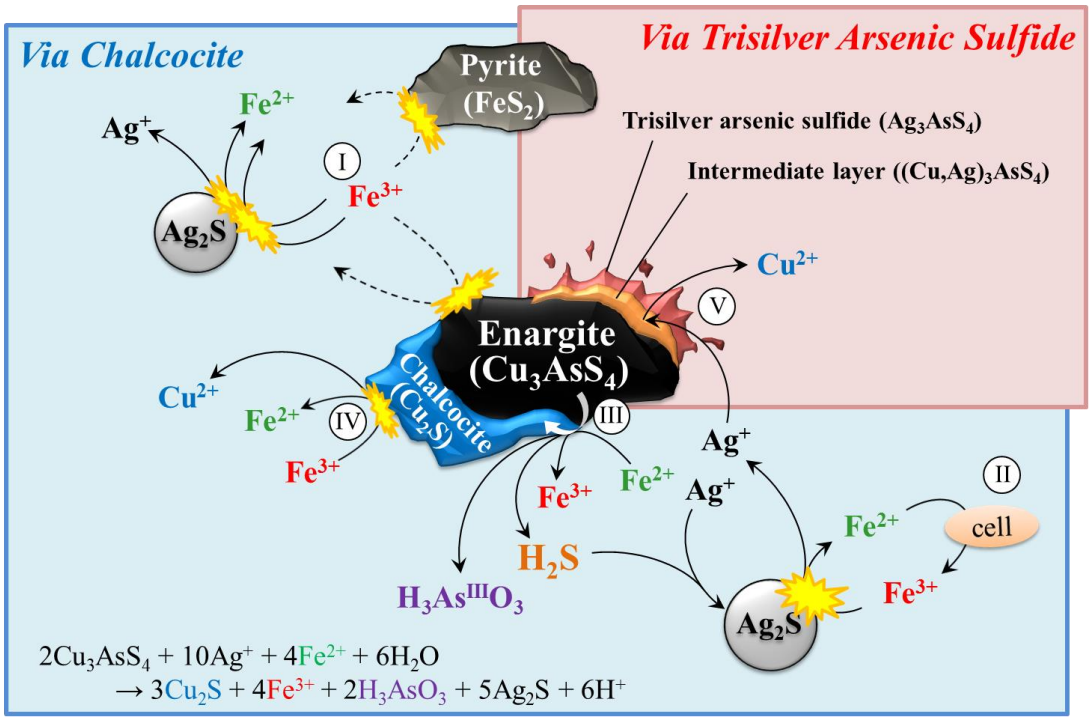

Fig. 4.10 Schematic image illustrating the proposed mechanism of Ag-catalyzed bioleaching of enargite concentrate.

References

1. Acevedo, F., Gentina, J.C. and García, N., 1998. CO_2 supply in the biooxidation of an enargite-pyrite gold concentrate. Biotechnology Letters 20, 257-259.
2. Ahonen, L. and Tuovinen, O.H., 1990. Catalytic effects of silver in the microbiological leaching of finely ground chalcopyrite-containing ore materials in shake flasks. Hydrometallurgy 24, 219-236.
3. Ballester, A., González, F., Blázquez, M.L. and Mier, J.L., 1990. The influence of various ions in the bioleaching of metal sulphides. Hydrometallurgy 23, 221-235.
4. Boekestein, A., Stadhouders, A.M., Stols, A.L.H. and Roomans, G.M., 1983. A comparison of ZAF-correction methods in quantitative X-ray microanalysis of light-element specimens. Ultramicroscopy 12, 65-68.
5. Córdova, R., Gómez, H., Real, S.G., Schrebler, R. and Vilche, J.R., 1997. Characterization of natural enargite/aqueous solution systems by electrochemical techniques. Journal of the Electrochemical Society 144, 2628-2636.
6. Escobar, B., Huenupi, E. and Wiertz, J.V., 1997. Chemical and biological leaching of enargite. Biotechnology Letters 19, 719-722.
7. Escobar, B., Huenupi, E., Godoy, I. and Wiertz, J.V., 2000. Arsenic precipitation in the bioleaching of enargite by *Sulfolobus* BC at 70˚C. Biotechnology Letters 22, 205-209.
8. Fantauzzi, M., Elsener, B., Atzei, D., Lattanzi, P. and Rossi, A., 2007. The surface of enargite after exposure to acidic ferric solutions: an XPS/XAES study. Surface and Interface Analysis 39, 908-915.
9. Fantauzzi, M., Rossi, G., Elsener, B., Loi, G., Atzei, D. and Rossi, A., 2009. An XPS analytical approach for elucidating the microbially mediated enargite oxidative dissolution. Analytical and Bioanalytical Chemistry 393, 1931-1941.
10. Ghahremaninezhad, A., Asselin, E. and Dixon, D.G., 2010. Electrochemical evaluation of the surface of chalcopyrite during dissolution in sulfuric acid solution. Electrochimica Acta 55, 5041-5056.
11. Ghahremaninezhad, A., Dixon, D.G. and Asselin, E., 2013. Electrochemical and XPS analysis of chalcopyrite ($CuFeS_2$) dissolution in sulfuric acid solution. Electrochimica Acta 87, 97-112.
12. Ghahremaninezhad, A., Radzinski, R., Gheorghiu, T., Dixon, D.G. and Asselin, E.,

2015. A model for silver ion catalysis of chalcopyrite ($CuFeS_2$) dissolution. Hydrometallurgy 155, 95-104.

13. Goates, J.R., Cole, A.G., Gray, E.L. and Faux, N.D., 1951. Thermodynamic properties of silver sulfide. Journal of the American Chemical Society 73, 707-708.
14. Golyshina, O.V., Pivovarova, T.A., Karavaiko, G.I., Kondratéva, T.F., Moore, E.R.B., Abraham, W.-R., Lünsdorf, H., Timmis, K.N., Yakimov, M.M. and Golyshin, P.N., 2000. *Ferroplasma acidiphilum* gen. nov., sp. nov., an acidophilic, autotrophic, ferrous-iron-oxidizing, cell-wall-lacking, mesophilic member of the *Ferroplasmaceae* fam. nov., comprising a distinct lineage of the Archaea. International Journal of Systematic and Evolutionary Microbiology 50, 997-1006.
15. Hackl, R.P., Dreisinger, D.B., Peters, E. and King, J.A., 1995. Passivation of chalcopyrite during oxidative leaching in sulfate media. Hydrometallurgy 39, 25-48.
16. Hiroyoshi, N., Miki, H., Hirajima, T. and Tsunekawa, M., 2000. A model for ferrous-promoted chalcopyrite leaching. Hydrometallurgy 57, 31-38.
17. Hiroyoshi, N., Miki, H., Hirajima, T. and Tsunekawa, M., 2001. Enhancement of chalcopyrite leaching by ferrous ions in acidic ferric sulfate solutions. Hydrometallurgy 60, 185-197.
18. Hiroyoshi, N., Arai, M., Miki, H., Tsunekawa, M. and Hirajima, T., 2002. A new reaction model for the catalytic effect of silver ions on chalcopyrite leaching in sulfuric acid solutions. Hydrometallurgy 63, 257-267.
19. Hiroyoshi, N., Kuroiwa, S., Miki, H., Tsunekawa, M. and Hirajima, T., 2007. Effects of coexisting metal ions on the redox potential dependence of chalcopyrite leaching in sulfuric acid solutions. Hydrometallurgy 87, 1-10.
20. Hiroyoshi, N., Kitagawa, H. and Tsunekawa, M., 2008. Effect of solution composition on the optimum redox potential for chalcopyrite leaching in sulfuric acid solutions. Hydrometallurgy 91, 144-149.
21. Hseu, T.M. and Rechnitz, G.A., 1968. Analytical study of a sulfide ion-selective membrane electrode in alkaline solution. Analytical Chemistry 40, 1054-1060.
22. Lee, J., Acar, S., Doerr, D.L. and Brierley, J.A., 2011. Comparative bioleaching and mineralogy of composited sulfide ores containing enargite, covellite and chalcocite by mesophilic and thermophilic microorganisms. Hydrometallurgy 105,

213-221.

23. Majima, H., 1969. How oxidation affects selective flotation of complex sulphide ores. Canadian Metallurgical Quarterly 8, 269-273.
24. Marambio-Jones, C. and Hoek, E.M., 2010. A review of the antibacterial effects of silver nanomaterials and potential implications for human health and the environment. Journal of Nanoparticle Research 12, 1531-1551.
25. Miki, H., Iguchi, A., Hirajima, T. and Sasaki, K., 2016. Catalytic effect of silver on arsenic-containing copper sulfide dissolution in acidic solution. Hydrometallurgy 162, 1-8.
26. Muñoz, J.A., Blázquez, M.L., González, F., Ballester, A., Acevedo, F., Gentina, J.C. and González, P., 2006. Electrochemical study of enargite bioleaching by mesophilic and thermophilic microorganisms. Hydrometallurgy 84, 175-186.
27. Muñoz, J.A., Dreisinger, D.B., Cooper, W.C. and Young, S.K., 2007. Silver-catalyzed bioleaching of low-grade copper ores. Part I: Shake flasks tests. Hydrometallurgy 88, 3-18.
28. Nazari, G., Dixon, D.G. and Dreisinger, D.B., 2012. The role of silver-enhanced pyrite in enhancing the electrical conductivity of sulfur product layer during chalcopyrite leaching in the Galvanox™ process. Hydrometallurgy 113-114, 177-184.
29. Padilla, R., Fan, Y. and Wilkomirsky, I., 2001. Decomposition of enargite in nitrogen atmosphere. Canadian Metallurgical Quarterly 40, 335-342.
30. Padilla, R., Jerez, O. and Ruiz, M.C., 2015. Kinetics of the pressure leaching of enargite in $FeSO_4$–H_2SO_4–O_2 media. Hydrometallurgy 158, 49-55.
31. Rivera-Vasquez, B.F. and Dixon, D., 2015. Rapid atmospheric leaching of enargite in acidic ferric sulfate media. Hydrometallurgy 152, 149-158.
32. Ruiz, M.C., Vera, M.V. and Padilla, R., 2011. Mechanism of enargite pressure leaching in the presence of pyrite. Hydrometallurgy 105, 290-295.
33. Safarzadeh, M.S. and Miller, J.D., 2014. Reaction of enargite (Cu_3AsS_4) in hot concentrated sulfuric acid under an inert atmosphere. Part I: Enargite concentrate. International Journal of Mineral Processing 128, 68-78.
34. Sasaki, K., Nakamuta, Y., Hirajima, T. and Tuovinen, O.H., 2009. Raman characterization of secondary minerals formed during chalcopyrite leaching with

Acidithiobacillus ferrooxidans. Hydrometallurgy 95, 153-158.

35. Sasaki, K., Takatsugi, K., Kaneko, K., Kozai, N., Ohnuki, T., Tuovinen, O.H. and Hirajima, T., 2010. Characterization of secondary arsenic-bearing precipitates formed in the bioleaching of enargite by *Acidithiobacillus ferrooxidans*. Hydrometallurgy 104, 424-431.
36. Sasaki, K., Takatsugi, K. and Hirajima, T., 2011. Effects of initial Fe^{2+} concentration and pulp density on the bioleaching of Cu from enargite by *Acidianus brierleyi*. Hydrometallurgy 109, 153-160.
37. Takatsugi, K., Sasaki, K. and Hirajima, T., 2011. Mechanism of the enhancement of bioleaching of copper from enargite by thermophilic iron-oxidizing archaea with the concomitant precipitation of arsenic. Hydrometallurgy 109, 90-96.
38. Tanaka, M., Yamaji, Y., Fukano, Y., Shimada, K., Ishibashi, J.-I., Hirajima, T., Sasaki, K., Sawada, M. and Okibe, N., 2015. Biooxidation of gold-, silver, and antimony-bearing highly refractory polymetallic sulfide concentrates, and its comparison with abiotic pretreatment techniques. Geomicrobiology Journal 32, 538-548.
39. Wadsworth, M.E. and Sohn, H.Y., 1979. Rate processes of extractive metallurgy. Plenum Press.
40. Warren, G.W., Wadsworth, M.E. and El-Raghy, S.M., 1982. Passive and transpassive anodic behavior of chalcopyrite in acid solutions. Metallurgical Transactions B 13, 571-579.
41. Watkin, E.L.J., Keeling, S.E., Perrot, F.A., Shiers, D.W., Palmer, M.-L. and Watling, H.R., 2009. Metals tolerance in moderately thermophilic isolates from a spent copper sulfide heap, closely related to *Acidithiobacillus caldus*, *Acidimicrobium ferrooxidans* and *Sulfobacillus thermosulfidooxidans*. Journal of Industrial Microbiology & Biotechnology 36, 461-465.
42. Watling, H.R., Perrot, F.A. and Shiers, D.W., 2008. Comparison of selected characteristics of *Sulfobacillus* species and review of their occurrence in acidic and bioleaching environments. Hydrometallurgy 93, 57-65.

Data shown in this chapter are partially included in the paper submitted to Hydrometallurgy (2018, 177, 197-204) entitled “Silver-catalyzed bioleaching of enargite concentrate using moderately thermophilic microorganisms”.

Chapter 5

Evaluating catalytic ability of activated carbon in bioleaching of enargite concentrate and elucidating its catalytic mechanism

Abstract

The catalytic effect of activated carbon (AC) on bioleaching of enargite (Cu_3AsS_4) concentrate was studied to evaluate its catalytic capability in copper (Cu) and iron (Fe) solubilization, arsenic (As) immobilization, and solution redox potential, E_h control. In the absence of AC, co-existing pyrite (FeS_2) in the concentrate began to rapidly solubilize at day 7, which was increasingly delayed by the addition of 0.1% and 0.2% AC to day 25 and 35, respectively. Suppression of pyrite dissolution was the result of the lowered E_h level via Fe^{3+}-reduction coupled with reduced inorganic sulfur compounds (RISCs)-oxidation on the AC surface acting as an electron-mediator. Real-time PCR analysis found that the abundance of S-oxidizing bacteria dropped in the presence of AC, proving that RISCs as an energy source for S-oxidizing bacteria were indeed consumed via the coupling reaction. While final Cu recovery was improved from 36% (0% AC) to 46% (0.1%) and 53% (0.2%), electrochemical study suggested that this was not much contributed by the galvanic interaction between enargite and AC. A kinetic study using the shrinking core model revealed that AC addition let Cu solubilize slowly but steadily and continuously at lower E_h under the suppression of pyrite dissolution, consequently improving the final Cu recovery. Addition of AC also facilitated the As immobilization from 3.1 mM (0% AC at day 10) to 5.2 mM (0.1% AC at day 30), 7.0 mM (0.2% AC at day 40), and 6.9 mM (0.3% AC at day 60). EPMA analysis found that As was immobilized as ferric arsenate selectively on the enargite surface, while its re-solubilization was observed coincided with rapid pyrite dissolution. This observation implied that high dissolved sulfate concentration from pyrite might have the effect of triggering re-solubilization of As-precipitates. Based on the results obtained above, the overall mechanism of AC-catalyzed bioleaching of enargite concentrate was proposed.

5.1 Introduction

Arsenic contamination in copper mine has been increasingly recognized as a serious problem in the copper mining industry in decades. Although enargite (Cu_3AsS_4) is well-known as one of the As-bearing sulfides, it also has a potential for future Cu resource. Hence, the installation of environmental-friendly and economical technique, by which Cu is selectively extracted rather than As from enargite, has been desperately awaited. Conventional pyrometallurgical process is inapplicable to these As-bearing copper sulfides from the environmental point of view (Takatsugi et al., 2011); the smelting let As volatilize into the air in the unmanageable gaseous form. Hydrometallurgical process has been therefore thought appropriate for the exploitation of As-bearing sulfides such as pressure leaching (Ruiz et al., 2011; Padilla et al., 2015), acid leaching (Safarzadeh et al., 2014), and alkaline leaching (Li et al., 2018). Bioleaching is also considered as one of the most promising hydrometallurgical processes due to its environmental and economic advantages, and high-temperature bioleaching of enargite have indeed succeeded to exclusively extract Cu rather than As; > 90% Cu solubilized into the solution while < 90% As remained in the solid phase (Sasaki et al., 2011). Likewise, other tests of high-temperature (65-70ºC) bioleaching have achieved high Cu recovery (52-91%; Escobar et al., 2000; Muñoz et al., 2006; Lee et al., 2011; Takatsugi et al., 2011; Sasaki et al., 2011), whereas those of low-temperature (25-30ºC) bioleaching still need to be improved (< 15%; Escobar et al., 1997; Sasaki et al., 2010). These investigations suggest the necessity of the additive such as a catalyst to further promote the Cu dissolution under lower-temperature condition.

Although the number is limited, some studies have investigated the effect of the catalysts on enargite dissolution: silver (Ag; Miki et al., 2016; Oyama et al., 2018) and carbon materials (Olvera et al., 2013; Jahromi et al., 2016, 2017, 2018, 2019). The former has long been recognized as the most effective catalyst on the dissolution of refractory copper sulfides, especially for chalcopyrite ($CuFeS_2$; Ahonen and Tuovinen et al., 1990; Ballester et al., 1990; Hiroyoshi et al., 2002; Muñoz et al., 2007; Nazari et al., 2012a and 2012b; Ghahremaninezhad et al., 2015). Miki et al. (2016) reported that even enargite dissolution was dramatically enhanced in the presence of Ag by promoting the transformation from enargite into more amenable intermediate, chalcocite, at the specific E_h range. Moreover, Oyama et al. (2018) concluded that

bioleaching of enargite concentrate was also catalyzed by the addition of Ag_2S based on the collaborative two different mechanisms: (i) Miki's theory and (ii) Ag atom diffusion into enargite structure via the replacement with Cu atom. Although its catalytic capability is outstanding among possible catalysts, there are some drawbacks to its difficulty in recycling use. Nazari et al. (2011) employed silver-doped pyrite for enabling the easier silver-recycling system, while the loss of silver was inevitable, resulting in the prolonged leaching period in the recycled experiment. It indicates that an alternative catalyst, which is much cheaper and certainly consumable, needs to be sought for the more practical process.

The latter has recently attracted researchers' attention due to its electrochemically catalytic effect on the dissolution of refractory copper sulfides. Originally, the utility of AC as one of the carbon materials has been reported in the chalcopyrite bioleaching experiment (Nakazawa et al., 1998; Zhang et al., 2007; Liang et al., 2010). In these studies, chalcopyrite dissolution was thought to be enhanced basically through galvanic interaction between electrically nobler AC and electrically poorer chalcopyrite. Olvera et al. (2013) tested its catalytic effect in enargite leaching by electrochemical study, suggesting its potential for the enhancement of enargite dissolution by causing galvanic effect as well as modifying semi-conductive surface property of enargite. Jahromi et al. (2016) indeed confirmed the effectiveness of AC in enargite leaching, where enargite dissolution was promoted based on (i) the oxidation of Fe^{2+} to Fe^{3+} (oxidant regeneration) and (ii) direct enargite oxidation by in-situ hydrogen peroxide production. These mechanisms were proposed by Ahumada et al. (2002), where the oxidation reactions occur on the surface of AC as follows;

$$2C_{red}^{*} + O_2 + 2H_2O = 2H_2O_2 + 2C_{ox}^{*} \quad \text{(Eq. 7-1)}$$

$$2Fe^{2+} + H_2O_2 + 2H^{+} = 2Fe^{3+} + 2H_2O \quad \text{(Eq. 7-2)}$$

C_{red} and C_{ox} indicate that surface functional groups on the surface of AC. Eq. 7-1 shows the generation of hydrogen peroxide occurring on the surface of AC through the reaction of quinone or other oxidative functional groups such as carboxylic acid, anhydrides, hydroxyls, lactol groups, lactone groups, and phenol groups. This

hydrogen peroxide is subsequently (i) consumed to directly oxidize enargite or (ii) used for the oxidation of Fe^{2+} to Fe^{3+} (Eq. 7-2), followed by enargite oxidation by produced Fe^{3+}. Modification of functional groups on the surface of AC with sulfuric acid, hydrochloric acid, or nitric acid was tested, confirming that the oxidation ability of AC was indeed varied with different acid treatments even in the leaching process (Jahromi et al., 2019).

On the other hand, it has been reported that the presence of AC suppress E_h rise during bioleaching process, implying that AC would also catalyze the Fe^{3+}-reduction (Nakazawa et al., 1998; Zhang et al., 2007; Ma et al., 2017; Hao et al., 2018). This adverse catalytic effect of AC was confirmed in the chemical experiment conducted by Vargas et al. (2009), where Fe^{3+}-reduction to Fe^{2+} was able to be catalyzed by the AC. Liang et al. (2010) observed the decrease in Fe^{3+}/Fe^{2+} ratio with the addition of AC during chalcopyrite bioleaching, ensuring that Fe^{3+} was indeed catalytically reduced to Fe^{2+} by AC even in the presence of microorganisms. Although the reduction mechanism has yet been well-described, not only Fe^{2+}-oxidation but also Fe^{3+}-reduction have to be considered as the catalytic reaction caused by AC during the bioleaching process.

The addition of AC also shows a positive effect on the formation of scorodite ($FeAsO_4 \cdot 2H_2O$) as an immobilized form of once-dissolved As from enargite (Jahromi et al., 2018). This would attribute to the catalytic reaction on the surface of AC; As-oxidation was greatly enhanced in the presence of AC, possibly by hydrogen peroxide generated (Radzinski et al., 2016). The enhanced As-oxidation on the AC surface led to the As(V) supply for the in-situ formation of scorodite during enargite leaching, consequently promoting the immobilization of As in the solid phase (Jahromi et al., 2018).

Although the catalytic mechanism of AC in the leaching process is roughly summarized as (i) electrochemical reaction to accelerate the electron transfer (e.g. galvanic interaction and other redox reaction) and (ii) chemical reaction by surface functional groups to produce the oxidant (e.g. Fe^{3+} and hydrogen peroxide), further discussion is still necessary to reach a consensus among researchers. Moreover, the number of studies investigating the effect of AC on enargite bioleaching is still limited, while the addition of AC in chemical enargite leaching is shown effective in enhanced Cu

dissolution and As immobilization. This study, therefore, aimed to evaluate the catalytic capability of AC in Cu and Fe solubilization, As immobilization, and E_h control during enargite bioleaching. The electrochemical study, kinetic model fitting, microbiological population structure analysis were also carried out to clarify the underlying catalytic mechanism in the presence of AC.

5.2 Materials and methods

5.2.1 Activated carbon (AC)

AC (Wako) used in this study was granular shape with an average particle size of around 5 mm. The BET specific surface area and average pore diameter of AC were determined as was described by Konadu et al. (2017). The sample was pre-treated in two steps: vacuum degassing for 90 min at 150ºC and finally vacuum pre-treatment for 15 h at 150ºC. The measurement was conducted by N_2 (99.99%) adsorption using BELSORP-max porosimeter (JAPAN BELL). The obtained data were analyzed by BEL master software in version 6.3.0.0 (JAPAN BELL) based on the non-local density functional theory (Lastoskie et al., 1993). The obtained specific surface area and average pore diameter were 1212 m^2/g and 1.77 nm, respectively.

5.2.2 Bioleaching experiments

Pre-grown culture of each of three strains (*Am. ferrooxidans* ICP, *Sb. sibiricus* N1, and *At. caldus* KU) was centrifuged (9000 rpm, 10 min at 4°C) to collect cells and washed twice with acidified water (pH 1.7), prior to inoculation into 200 mL HBS medium (pH 2.0; in 500 mL Erlenmeyer flasks) containing 2% (w/v) enargite concentrate and 5 mM Fe^{2+} (to set the initial cell density of each strain at 1.0×10^7 cells/mL; i.e. 3.0×10^7 cells/mL in total). AC was added into the medium at different concentrations; 0, 0.1, 0.2, 0.3% (w/v). Flasks were incubated shaken at 45˚C and 150 rpm for 60 days. Samples were regularly withdrawn to monitor pH, E_h, cell density, and concentrations of Fe^{2+} (*o*-phenanthroline method), As(III) (molybdenum blue method), and total Fe, As and Cu (ICP-OES). Solid residue was collected and freeze-dried overnight for the analysis by EPMA.

5.2.3 Abiotic evaluation of catalytic ability of AC

As for the abiotic experiment, AC (0.1% (w/v)) was added with 100 mL of ABS medium (pH adjusted to 2.0 with 1 M H_2SO_4) into the 300 mL of Erlenmeyer flask. For the series of experiments, 10 mM Fe^{2+} or Fe^{3+}, 5 mM of sodium tetrathionate and/or 0.02% yeast extract were solely or simultaneously added into the medium. As for the biotic experiment, heterotrophic basal salts media (200 ml in 500 ml Erlenmeyer flasks; pH adjusted to 2.0 with 1 M H_2SO_4) containing 5 mM of sodium tetrathionate or 5 mM

of As(III) as $NaAsO_2$ were prepared and sterilized by autoclaving. Fe-oxidizing bacterium without S- and As-oxidizing ability, *Am. ferrooxidans* ICP, was inoculated into the sterilized medium to set the initial cell density to 1.0×10^7 cells/mL. Five mM Fe^{2+} and 0.02% (w/v) yeast extract were also supplemented for bacterial growth at the initial stage of the bioleaching experiments. Inoculated cultures with and without the addition of 0.2% (w/v) AC were prepared in duplicate. These flasks were incubated and shaken at 45ºC and 150 rpm. Solution samples were regularly withdrawn to monitor pH, E_h, Fe^{2+} and total Fe concentration (*o*-phenanthroline method), As(III) concentration (molybdenum blue method), and sulfate concentration (turbidimetric method).

5.2.4 Real-time PCR

In order to investigate the microbial population structure in bioleaching cultures, Real-Time PCR (MiniOpticon, Bio-Rad) was conducted according to the methods described by Oyama et al. (2018) as follows. The purified genomic DNA from each strain was used as the template to PCR amplify the 16S rRNA gene fragment (~1473 bp) using the universal primer set (27f and 1492r: Table 5.1). The resultant PCR products derived from each strain were purified using ISOSPIN PCR Product (NIPPON GENE), quantified, and finally diluted to give a final concentration of 1.0×10^3 to 1.0×10^9 copies/μL, to be used as template DNA for Real-Time PCR. Once linearity in the standard curve was obtained within the range from 1.0×10^3 to 1.0×10^9 copies/μL for all species, synthetic DNA mixtures (composed of template DNA from each one of the four species at 1.0×10^3 to 1.0×10^9 copies/μL) was tested against each one of the four species-specific primer sets (Table 5.1) to ensure the accuracy in order to display the results as percentages in whole number. Genomic DNA extracted from the actual bioleaching mixed cultures were tested against the corresponding species-specific primer sets.

Table 5.1 PCR and Real-Time PCR primers used in this study.

	Primer set	Primer sequence (5'-3')	Target species	PCR product size (bp)
PCR	27f Universal	AGAGTTTGATCMTGGCTCAG	Bacteria	~1473
	1492r Universal	TACGGYTACCTTGTTACGACTT		
Real-Time PCR	Amferro-F1	TCATTCGACGGGCTCCGTG	Species-specific: *Am. ferrooxidans*	232
	Buniv-R1	GAGCTGACGACARCCATGCA		
	Sbsib-F1	TAGGTGTCGCCCGGGTCCAC	Species-specific: *Sb. sibiricus*	241
	Buniv-R1	-		
	Acaldus-F3	TAGGTGCTGAGTGTCGTAGCTAACG	Species-specific: *At. caldus*	231
	Buniv-R1	-		

5.2.5 Electrochemical analysis for the detection of galvanic reaction

In order to obtain the evidence of galvanic reaction occurring thought the contact between enargite and AC, electrochemical analysis was carried out. The mineral electrodes were prepared from the pure massive enargite, pyrite, and AC samples by cutting them into cubes (around 1 cm^3). One side of the massive samples was used as the electrode surface, and the other side was connected to a copper wire using silver conductive paste. This was embedded into the resin for the fixation. The surface of each mineral electrode was polished by emery-paper to provide a flat surface and rinsed with pure water. Before each measurement, the polishing was conducted again to ensure that the pure mineral surface is properly exposed.

To obtain the solutions with varied E_h, 0.1 M H_2SO_4 solution was prepared containing 0.1 M Fe with varied Fe^{2+}/Fe^{3+} ratio to adjust the E_h to 0.5, 0.53, 0.6, 0.68, 0.74, 0.8, 0.86, 0.9 V (vs. SHE).

Electrochemical analysis was carried out with the three-electrode method by using the electrochemical instrument (Solartron Analytical 1280 C, TOYO Corporation). Firstly, the E_h were measured by Ag/AgCl reference electrode and platinum working electrode. After that, mineral electrode potential at certain E_h was measured by replacing from platinum electrode to each one of the mineral electrode (enargite, pyrite, AC). Measurement time of solution E_h and electrode potential was set to 300 sec to reach the stationary phase. After the measurement, copper wire of two of mineral electrodes (enargite-pyrite or enargite-AC) were contacted together, which was further connected to the working electrode to measure the "minerals-contacted electrode potential". This electrode potential is assumed to be the actual potential when two minerals are contacted and the galvanic reaction occurs. Measurement time for this step was set to 60 sec.

For the galvanic current measurement, both reference and counter electrode were connected to one of AC or pyrite electrode, while the working electrode was connected to enargite electrode. In this condition, each mineral electrode was indirectly connected through electrochemical instrument; each electrode potential is independent but not the potential when two mineral electrodes were directly connected. In order to shift this mineral electrode potential to galvanic potential for artificially causing galvanic interaction, the difference between electrode potential and "minerals-contacted

electrode potential" was intentionally applied to enargite electrode. The current value observed here was postulated as the galvanic current. The measurement time was set to 300 sec to reach the stationary phase.

5.3 Results and discussion

5.3.1 Dissolution behavior of Cu and Fe during bioleaching with and without AC addition

In the absence of AC without inoculation, Cu recovery at day 60 was only 11%, which increased to 23% by the addition of 0.3% AC (Fig. 5.1a). Meanwhile, Fe solubilization was also enhanced from 9% (0% AC) to 16% (0.3% AC) (Fig. 5.1b). This slightly facilitated Cu and Fe solubilization in AC-catalyzed abiotic leaching would result from the slight increase in E_h; The E_h in the presence of AC was slightly higher (20-30 mV) throughout the experiment than that in the absence of AC (Fig. 5.1c). The oxidant generation (i.e. Fe^{3+}), by AC-catalyzed Fe^{2+}-oxidation could be the reason of this difference in E_h, suggesting that AC shows the Fe^{2+}-oxidizing ability as was observed by the previous study (Jahromi et al., 2019).

Bioleaching without AC addition achieved higher Cu recovery than AC-catalyzed abiotic leaching, reaching 36% of final Cu recovery at day 60 (Fig. 5.1a). Similarly with sterile cultures, the addition of 0.1% and 0.2% AC further improved the Cu recovery to 46% and 53%, respectively (Fig. 5.1a), which show stronger catalyzing effect with less amount of AC addition (0.1% and 0.2%) than sterile cultures with 0.3% AC addition, implying the existence of synergistic effect between microbiologically catalyzing and AC-catalyzing effects on the enhanced Cu dissolution. However, excess amount of AC addition (0.3%) adversely affected on the Cu dissolution (35% of final Cu recovery at day 60; Fig. 5.1a), thus necessitating the strict optimization of the AC addition. It was reported that there is no specific E_h range where enargite dissolution is dramatically enhanced, and strongly oxidative condition (e.g. higher E_h) is favorable for the faster enargite dissolution (Lattanzi et al., 2008). Excessively lowered E_h by the addition of 0.3% AC less than 700 mV throughout the experiment could be the reason of suppressed enargite dissolution (Fig. 5.1c).

Contrary to the enhancement of Cu dissolution, the addition of AC in the bioleaching cultures showed a suppressive effect on Fe solubilization. In the absence of AC, the rapid dissolution of Fe from pyrite began at day 7, readily reaching >80% Fe solubilization by day 40 (Fig. 5.1b). Addition of 0.1 and 0.2% AC increasingly delayed Fe dissolution to day 25 and 35, respectively, and at 0.3% AC, Fe dissolution was suppressed almost completely until day 60 (Fig. 5.1b). Pyrite is the only Fe source in

this concentrate, suppressed Fe dissolution was thus derived from selective suppression of pyrite dissolution. This trend was accompanied by lowered E_h levels during bioleaching; it took 7 (0% AC), 25 (0.1% AC), and 35 days (0.2% AC) to reach 700 mV, and < 700 mV was kept throughout the experiment in the presence of 0.3% AC (Fig. 5.1c). Lowered E_h level by the addition of AC was likely the result of Fe^{3+} reduction to Fe^{2+}, which is confirmed by the behavior of Fe^{2+} concentration; the decrease in Fe^{2+} concentration was deteriorated with the addition of AC (Fig. 5.1d). Since it has been reported that E_h rise to around 700 mV led to the initiation of the rapid pyrite dissolution in bioleaching cultures (Gu et al., 2012), AC likely played a key role to maintain the lower E_h level by reducing Fe^{3+} to Fe^{2+} to delay unwanted pyrite solubilization. Based on the above results, it was assumed that enargite dissolution could be indirectly catalyzed by the addition of AC via lowering E_h level to < 700 mV, followed by suppressing pyrite dissolution to prevent passivation of enargite surface with Fe precipitates.

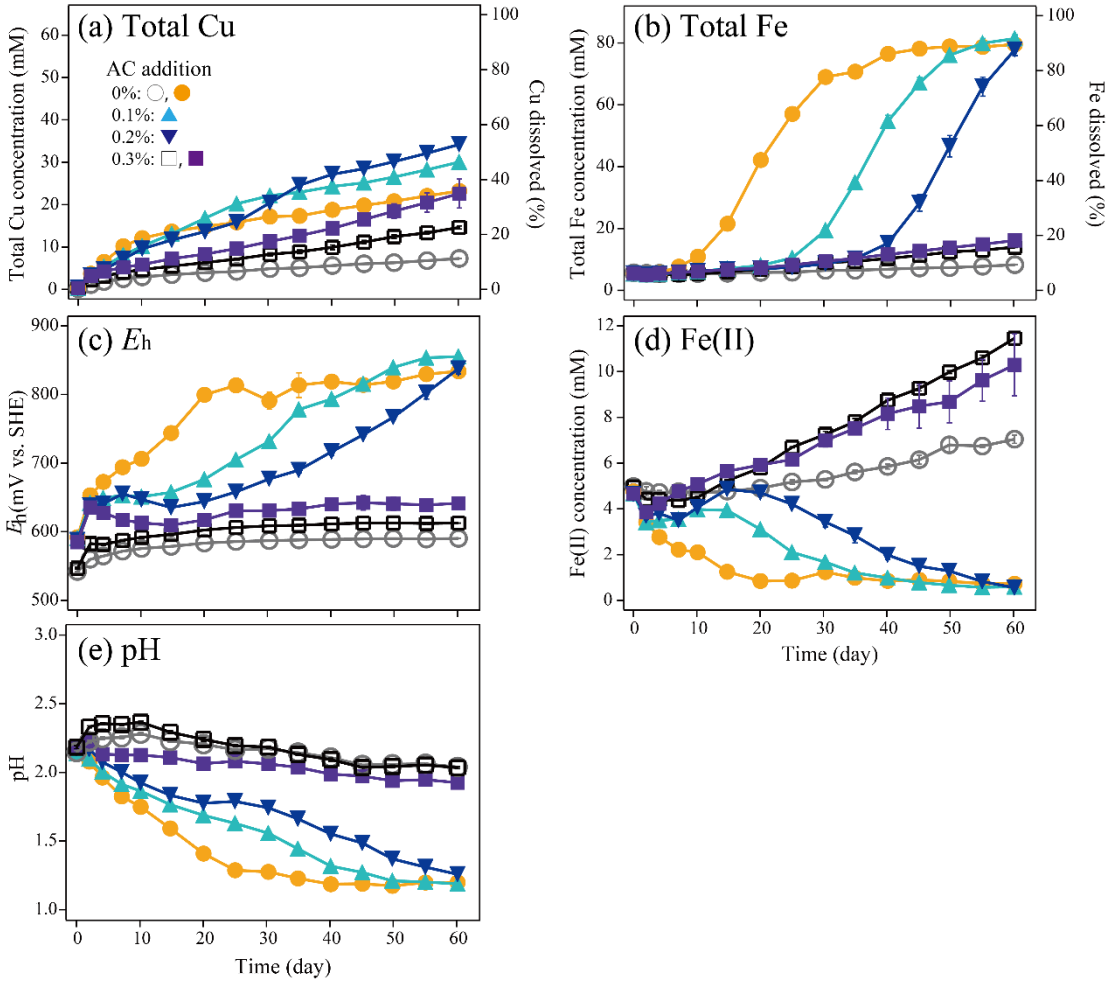

Fig. 5.1 Changes in the total soluble Cu concentration (a), total soluble Fe concentration (b), E_h (c), Fe^{2+} concentration (d), and pH (e) during abiotic leaching (open symbol) or bioleaching (closed symbol) of enargite concentrate at 0% (○, ●), 0.1% (▲), 0.2% (▼), or 0.3% (w/v) (□, ■) of AC. Data points are mean values from duplicate cultures. Error bars depicting averages are not visible in some cases as they are smaller than the data point symbols.

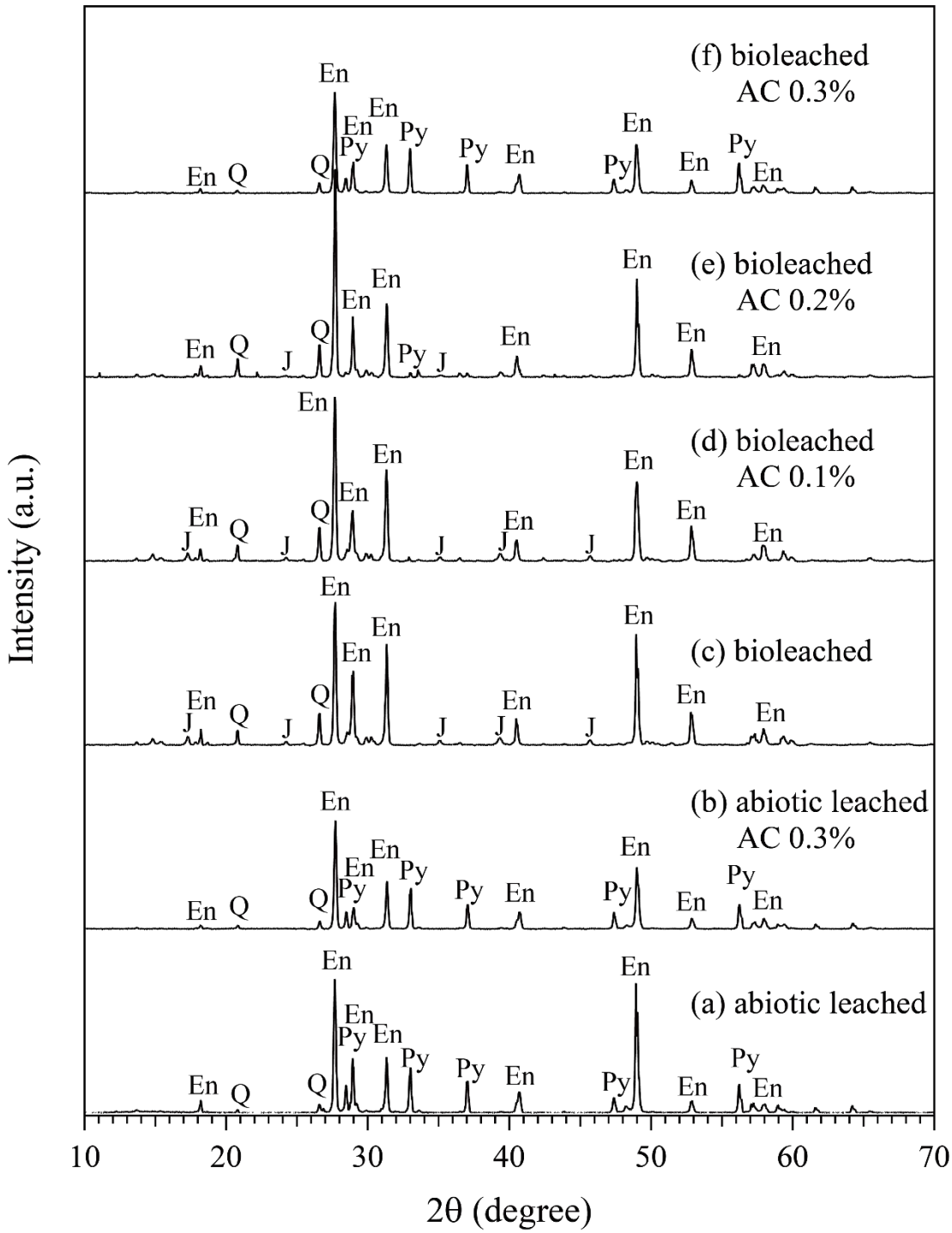

Fig. 5.2 X-ray diffraction patterns of abiotic leached (a, b) and bioleached residues (c-f) recovered on day 60 from cultures containing 0% (a, c), 0.1% (d), 0.2% (e), or 0.3% (b, f) of AC. En: enargite (Cu_3AsS_4; PDF No. 00‑035-0775), Py: pyrite (FeS_2; PDF No. 00-042-1340), Q: quartz (SiO_2; PDF No. 01 ‑ 070-3755), J: jarosite ($K(Fe_3(SO_4)_2(OH)_6)$; PDF No. 01-076-0629).

5.3.2 Catalytic mechanism of AC in the E_h control

Above results indicate that Fe^{3+} could be reduced by the catalytic effect of AC, possibly via (i) the reaction with surface functional groups of AC and/or (ii) the electrochemical redox reaction on the surface of AC. To clearly understand this catalytic mechanism of AC in the E_h control, the separate abiotic experiment was performed with the conditions as follows;

(a) 10 mM Fe^{3+} + 0.1% AC
(b) 10 mM Fe^{2+} + 0.1% AC
(c) 5 mM tetrathionate + 0.1% AC
(d) 10 mM Fe^{3+} + 5 mM tetrathionate
(e) 10 mM Fe^{3+} + 5 mM tetrathionate + 0.1% AC
(f) 10 mM Fe^{3+} + 0.02% yeast extract + 0.1% AC

Condition (a), (b), and (c) aimed to evaluate the oxidative/reductive ability of AC against solely present Fe^{3+}, Fe^{2+}, tetrathionate. Condition (d), (e), and (f) were set to investigate the redox reaction electrochemically catalyzed by AC and find the suitable electron donor for strongly promoting Fe^{3+} reduction. Tetrathionate and yeast extract were employed as the model material of reduced inorganic sulfur compounds (RISCs) generated via the dissolution of sulfide minerals and organic metabolites produced by microorganisms, respectively. These materials were thought sufficiently present in the bioleaching culture throughout the experiment to act as the electron donor for Fe^{3+} reduction.

In the presence of AC with Fe^{3+} (Fig. 5.3), a slight reduction of Fe^{3+} to Fe^{2+} (0.6 mM; Fig. 5.3a) was observed and thus E_h dropped from 829 mV to 741 mV in 4 h right after the experiment began (Fig. 5.3b; condition (a)). Subsequently, Fe^{2+} concentration and E_h kept constant until the end of the experiment, suggesting that slight and rapid reduction of Fe^{3+} to Fe^{2+} at the beginning of the experiment was likely derived from the interaction with surface functional groups of AC. This result also indicates that functional groups on the AC surface would be insufficient to keep lowering the E_h throughout the leaching experiment. In the presence of AC with Fe^{2+} or tetrathionate solely (conditions (b) and (c)), Fe^{2+} and tetrathionate were constantly oxidized (Fig.

5.3); Fe^{2+} concentration decreased from 9.4 mM (day 0) to 6.0 mM (day 6; Fig. 5.3a) and sulfate production increased from 0 (day 0) to 2.3 mM (day 6; Fig. 5.3c). These oxidations were catalyzed by AC, possibly via either (i) the oxidation by hydrogen peroxide produced by oxidative functional groups on the AC surface as was described by Ahumada et al. (2002) or (ii) the direct oxidation by O_2 supplied from the air. In summary, AC was shown effective in (i) continuously oxidizing Fe^{2+} to increase E_h and (ii) weakly reducing Fe^{3+} to decrease E_h, which is contradictory to the E_h trend observed in bioleaching experiment. It, therefore, indicates that the suppressed E_h increase during the bioleaching experiment could be the result of Fe^{3+}-reduction probably via some redox reaction electrochemically catalyzed by AC, but not the interaction with surface functional groups of AC.

While Fe^{3+} and tetrathionate did not react each other (only 0.37 mM Fe^{3+} reduction; condition (d); Fig. 5.3a), addition of AC strongly enhanced both the reduction of Fe^{3+} (9.2 mM in 6 days; Fig. 5.3a) and oxidation of tetrathionate (10.5 mM sulfate production; in Fig. 5.3c); thus E_h continuously decreased from 826 mV (day 0) to 621 mV (day 6) (condition (e); Fig. 5.3b). Considering the weak Fe^{3+}-reduction capability of AC, the presence of tetrathionate played the key role to reduce Fe^{3+} to Fe^{2+}, proving that electrochemical redox reaction catalyzed by AC resulted in the suppressed E_h increase. Additionally, Fe^{3+} was not greatly reduced in the presence of yeast extract as an electron donor (condition (f); Fig. 5.3a), suggesting that RISCs must be the major electron donor for the coupling reaction.

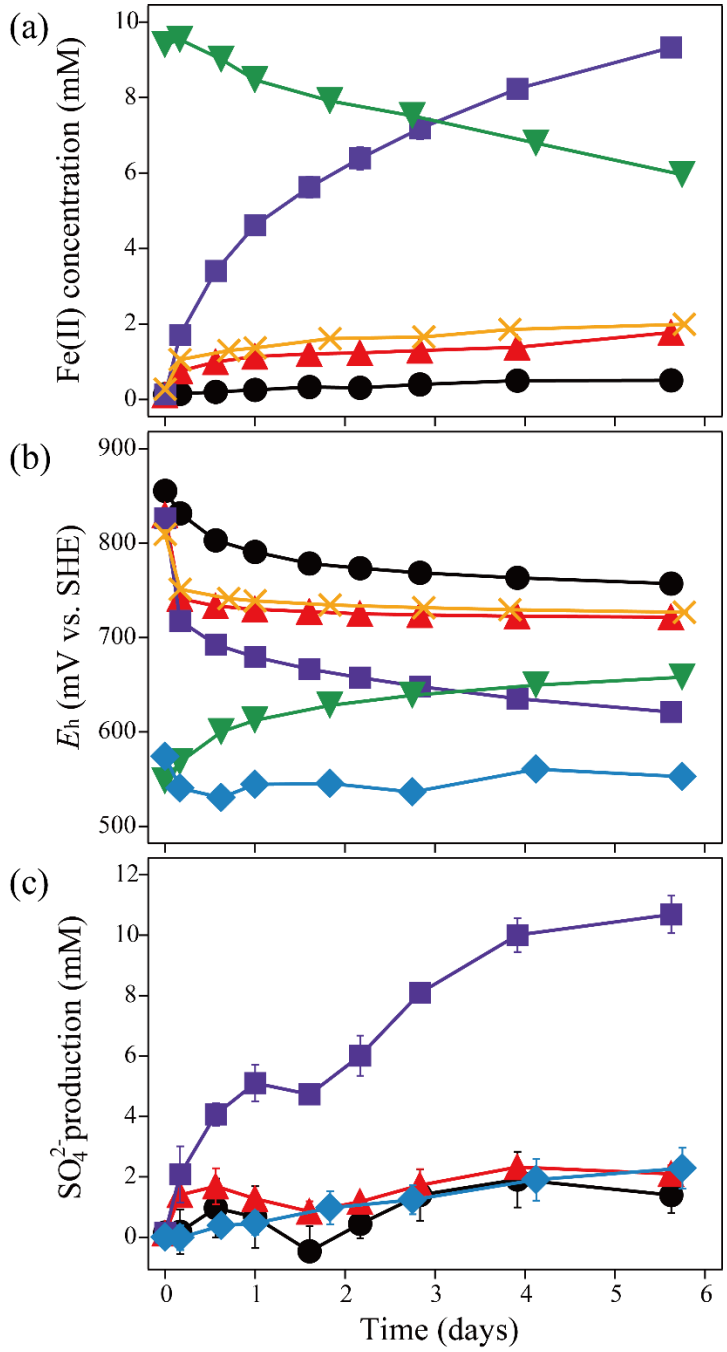

Fig. 5.3 Changes in the Fe^{2+} concentration (a), E_h (b), and sulfate production (c) during abiotic experiment for evaluation of catalytic capability of AC. Cultures containing 0.1% (w/v) AC + Fe^{3+} (▲; condition (a)), 0.1% AC + Fe^{2+} (▼; condition (b)), 0.1% AC + tetrathionate (◆; condition (c)), Fe^{3+} + tetrathionate (●; condition (d)), 0.1% AC + Fe^{3+} + tetrathionate (■; condition (e)), or 0.1% AC + Fe^{3+} + yeast extract (×; condition (f)) were tested. Data points are mean values from duplicate cultures. Error bars depicting averages are not visible in some cases as they are smaller than the data point symbols.

This hypothesis was also checked in the biotic experiment using Fe-oxidizing microorganism without As-oxidizing and S-oxidizing capability, *Am. ferrooxidans* ICP. Although the concentration is thought insufficient to keep lowering E_h during bioleaching, As(III) was also tested as an electron donor to evaluate the possibility of AC-catalyzed As(III)-oxidation for the enhancement of As immobilization. In the absence of AC, both tetrathionate and As(III) were little oxidized by Fe^{3+} (less than 5% of oxidation ratio in both cases), whereas the presence of 0.2% AC greatly facilitate their oxidations, achieving 78% (tetrathionate) and 24% (As(III)) at day 4 (Fig. 5.4). Even though suppressed E_h increase was hardly visible due to the robust and continuous Fe^{2+}-oxidation by *Am. ferrooxidans* ICP (data not shown), the facilitated oxidations proved that the coupling reaction on the AC surface indeed occurs even in the presence of microorganisms. Moreover, it was confirmed that As-oxidation could be the counterpart of the coupling reaction on the AC surface, likely contributing to As immobilization during bioleaching. Consequently, the catalytic mechanism of AC in the E_h control was summarized as follows; (i) the short-term oxidation by surface functional groups (E_h rising), (ii) continuous oxidation of Fe^{2+}, RISCs, As(III) by hydrogen peroxide or O_2 (E_h rising), and (iii) Fe^{3+} reduction coupled with As(III) and, especially, RISCs oxidation (E_h lowering). It was thus concluded that Fe^{3+}-reduction coupled with tetrathionate oxidation is much favorable than Fe^{2+}-oxidation by above reactions (i) and (ii), thus E_h increase was suppressed in the presence of AC during bioleaching.

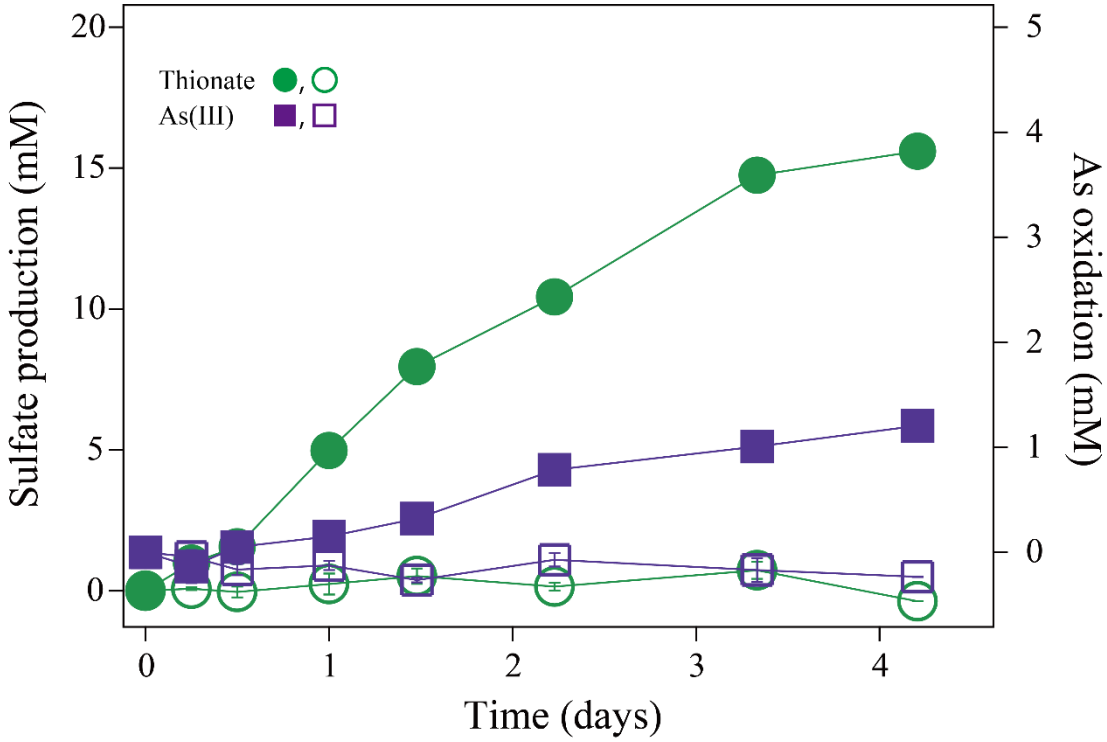

Fig. 5.4 Changes in oxidation ratio of tetrathionate (○, ●) and As(III) (□, ■) during the biotic experiment for evaluation of catalytic ability of AC in the absence (open symbol) or presence (closed symbol) of 0.2% AC (closed symbol). Data points are mean values from duplicate cultures. Error bars depicting averages are not visible in some cases as they are smaller than the data point symbols.

5.3.3 Modification of microbiological population structure by AC addition

It was found that planktonic cell density gradually decreased with the addition of AC (Fig. 5.5), implying that the presence of AC could show some inhibitory effect on cell growth. In order to clarify its effect, Real-Time PCR analysis was carried out to trace the chronological change in the microbiological population structure in the absence and presence of AC. In the absence of AC, the abundance of S-oxidizing *At caldus* KU and Fe-oxidizing *Am. ferrooxidans* ICP were competitive at day 30 (56.1% and 43.5%, respectively), which changed into 71.4% (KU) and 17.2% (ICP) at day 60 (Fig. 5.5). At the same time, the abundance of Fe- and S-oxidizing Sb. sibiricus N1 became noticeable by increasing its ratio from 0.4% (day 30) to 11.4% (day 60; Fig. 5.5), implying that S-oxidizing bacteria actively grew in the middle to end stage of the experiment. However, the addition of AC suppressed the growth of S-oxidizer; 0.1% and 0.2% AC dropped the abundance of *At caldus* KU into 36.9% and 37.7%, respectively (day 30). Especially at 0.2% AC, *At caldus* KU was not the dominant species even at day 60 (only 29.9%), whereas Fe-oxidizing *Am. ferrooxidans* ICP possessed the largest population (67.2%). RISCs-consumption by coupling reaction (Fe^{3+}-reduction coupled with RISCs-oxidation) on the AC surface attributed to the lack of energy source for the growth of S-oxidizer, which might be the reason of decrease in the abundance of *At caldus* KU. This modification of the microbial population structure also proved that the coupling reaction certainly occurred during bioleaching of enargite.

Since cell growth was strictly inhibited in the presence of 0.3% AC (Fig. 5.5), the result of Real-Time PCR analysis was not consistence with that obtained in the other cultures.

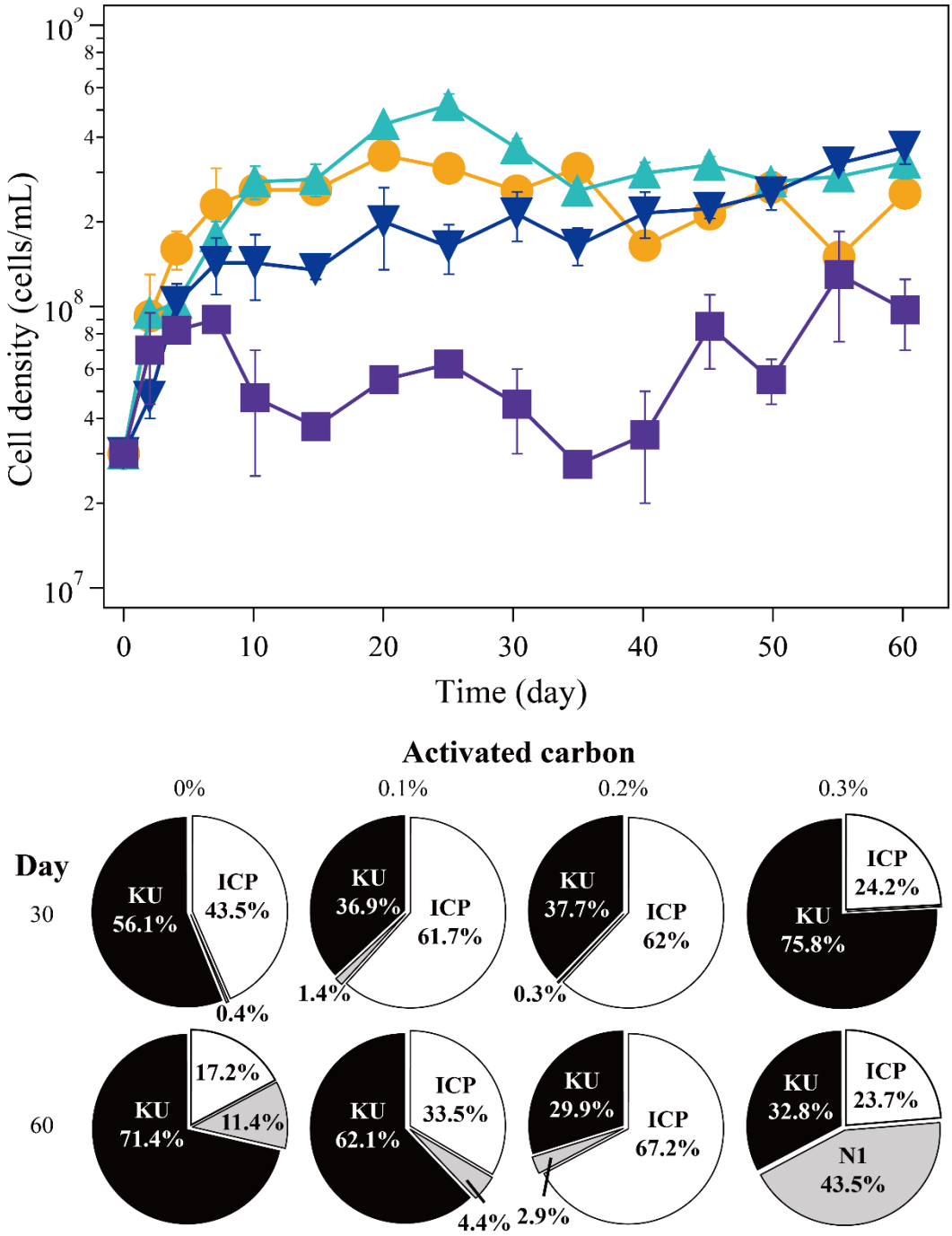

Fig. 5.5 Changes in planktonic cell density during bioleaching of enargite concentrate in the presence of 0% (●), 0.1% (▲), 0.2% (▼), and 0.3% (w/v) AC (■). Data points are mean values from duplicate cultures. Error bars depicting averages are not visible in some cases as they are smaller than the data point symbols. Microbial population structure on day 30 and 60 in bioleaching cultures of enargite concentrate at 0%, 0.1%, 0.2%, and 0.3% (w/v) of AC are also depicted.

5.3.4 Contribution of galvanic interaction to enargite dissolution

Galvanic interaction is well-known as the electrochemically catalytic effect of carbon material on the dissolution of refractory copper sulfides. While its catalytic capability has been recognized, especially in the AC-catalyzed chalcopyrite bioleaching (Nakazawa et al., 1998; Zhang et al., 2007; Liang et al., 2010), no study has indeed confirmed the existence of catalytic galvanic current. In this study, electrochemical analysis was therefore carried out with the aim to indirectly observe the galvanic current and evaluate its catalytic capability.

Fig. 5.6a shows the electrode potential of each mineral electrode in various potential solutions. Every electrode potential constantly increases accompanied with the E_h increase in the range from 0.5 V to 0.7 V. However, once E_h becomes higher than 0.75 V, electrode potentials of enargite and AC were not able to keep up with the increase in E_h, while pyrite electrode still shows the same potential with E_h. At around 0.8 V, each electrode potential finally reached almost stationary value of 0.72 V (enargite), 0.74 V (AC), and 0.81 V (pyrite), followed by slight increase in electrode potential at further higher E_h (> 0.8 V). Since the difference in electrode potential of each mineral corresponds to the galvanic electromotive force, it is expected that the higher E_h range (> 0.75 V) is favorable to facilitate the galvanic reaction. Furthermore, pyrite showed the highest electrode potential, followed by AC and enargite, in the range of E_h being achievable during bioleaching, suggesting that pyrite-enargite system would cause a stronger galvanic effect than AC-enargite system.

Galvanic current measurement confirmed that the pyrite-enargite system indeed showed higher current value than AC-enargite system in the bioleaching E_h range (0.6 – 0.85 V; Fig. 5.6b). Moreover, the galvanic current of AC-enargite system was negligibly small (< 1mA) at the lower E_h range (< 0.7 V) than the higher E_h range (> 0.7 V), where enargite dissolution was promoted during bioleaching. Conclusively, enargite dissolution is unlikely catalyzed by galvanic interaction between enargite and AC at which Cu steadily solubilized during the bioleaching experiment.

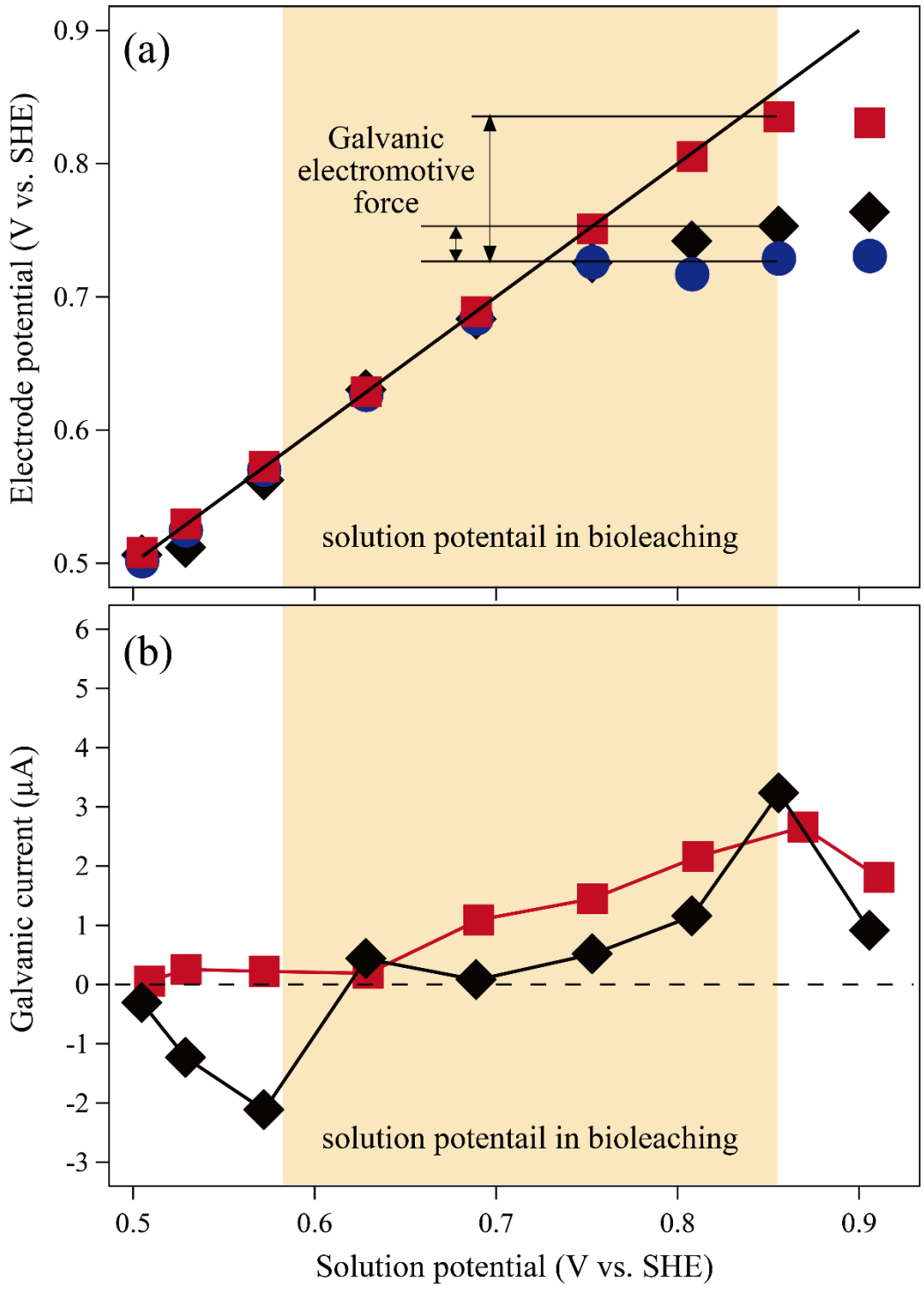

Fig. 5.6 Relationship between solution potential (E_h) and electrode potential (a) of enargite (●), pyrite (■), and AC (◆), or galvanic current (b) in enargite-pyrite (■) or enargite-AC (◆) system. Difference in the electrode potential between minerals corresponds to the galvanic electromotive force.

5.3.5 Kinetic study in AC-catalyzed bioleaching of enargite concentrate

The shrinking core model is frequently utilized to model the mineral dissolution process. This has been indeed used in the chalcopyrite and enargite bioleaching by Masaki et al. (2018) and Oyama et al. (2018), confirming its applicability even to bioleaching. Since it was found that enargite dissolution was negligibly enhanced by the galvanic interaction between AC and enargite, shrinking core model was employed in this study for modeling the dissolution behavior to disclose the factors affecting on the improved final Cu recovery.

In the abiotic cultures, Cu dissolution behavior in the absence of AC was well-fit to diffusion through production film model, while that in the presence of 0.3% AC showed slightly better fitting to the surface chemical reaction model, known as faster dissolution model than the other, throughout the experiment (Fig. 5.7). Kinetic constant, k, greatly increased from 0.00007 (without AC) to 0.0014 (0.3% AC; Table 5.2), indicating that AC addition indeed accelerated the enargite dissolution by modifying the dissolution mechanism; facilitated oxidation by Fe^{3+} produced via AC-catalyzing Fe^{2+} oxidation to Fe^{3+} as was described in section 5.3.1.

On the other hand, all biotic cultures were rate-limited by surface chemical reaction model but not diffusion through product film model, implying that the fundamental reaction mechanism would be scarcely changed by the addition of AC (Fig. 5.7a). Contrary to abiotic cultures, kinetic constant became gradually smaller with the addition of AC from 0.0081 (0% AC) to 0.049 (0.1%), 0.04% (0.2% AC), and 0.0021 (0.3% AC) (Table 5.2); enargite dissolution was not, in fact, accelerated by the addition of AC. This could be due to the lowered E_h with the addition of AC, while higher E_h is favorable for faster enargite dissolution (Lattanzi et al., 2008 37). However, the fitting durations were prolonged with the addition of AC from 7 days (0% AC) to 25 days (0.1%), 35 days (0.2%), and 60 days (0.3%; Fig. 5.7a); the fitting was halted at which the correlation factor, R^2, start to decrease. Since these timings are almost consistent with the initiation of rapid Fe solubilization, deteriorated pyrite solubilization by AC addition would enable to prolong the duration being fit with faster reaction model, surface chemical reaction model. Consequently, improved Cu recovery was resulted from the slower but long and stable Cu solubilization from enargite via the E_h modification by AC.

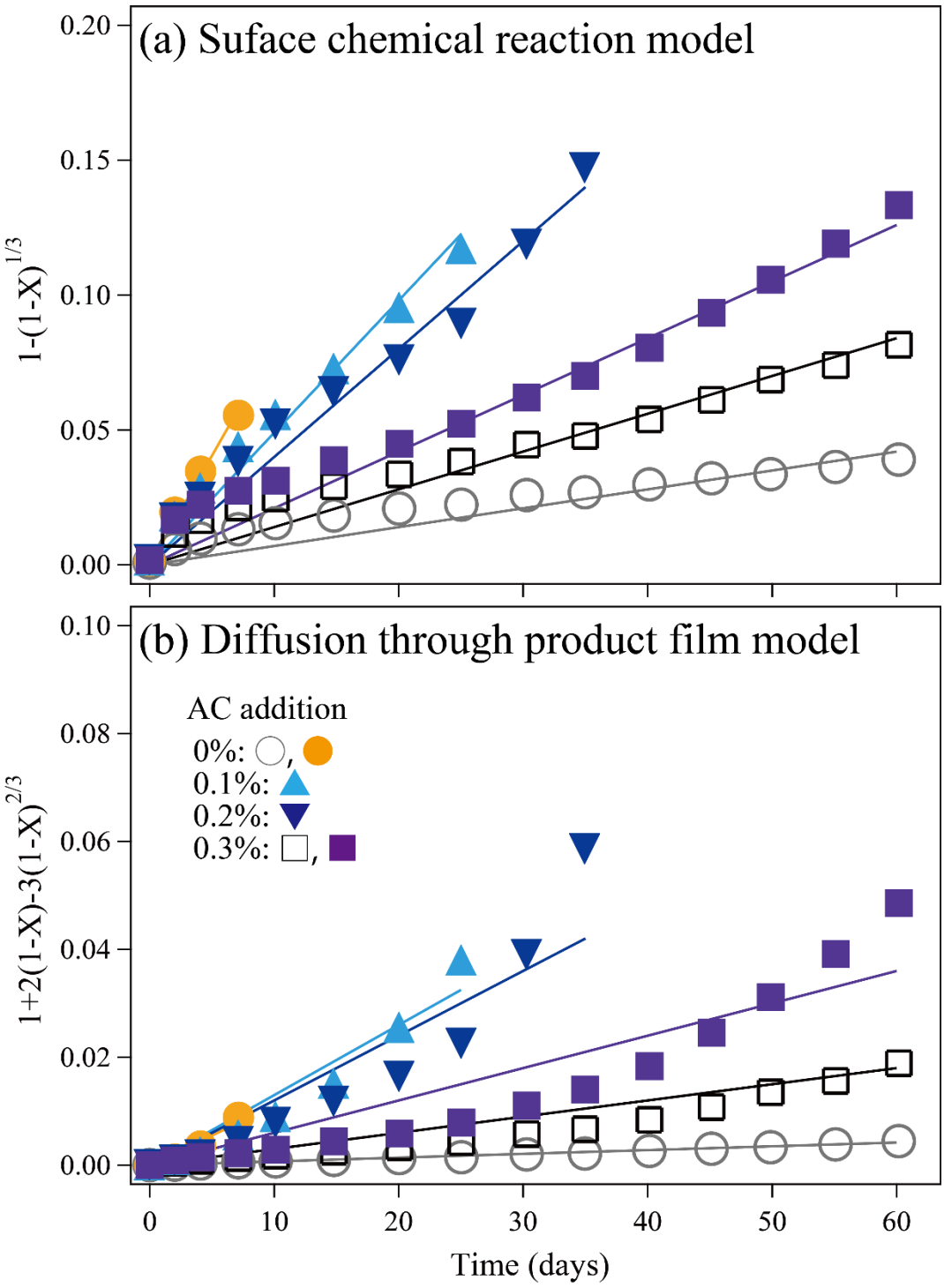

Fig. 5.7 Kinetic modeling on abiotic leaching (open symbol) or bioleaching (closed symbol) of enargite concentrate in the presence of 0% (○, ●), 0.1% (▲), 0.2% (▼), and 0.3% (w/v) (□, ■) AC; (a) surface chemical reaction ($1 - (1-X)^{1/3} = k_r t$) and (b) diffusion through product film ($1 + 2(1-X) - 3(1-X)^{2/3} = k_d t$). Linear lines were drawn until where R^2 values increase.

Table 5.2 Correlation factor R^2 and kinetic constant k values calculated using the kinetic model of surface chemical reaction and diffusion through product film.

	AC addition (%)	Fitting duration (day)	Reaction model			
			Surface chemical reaction		Diffusion through product film	
			k_r	R^2	k_d	R^2
abiotic leaching	0	0 - 60	0.0007	0.800	0.00007	0.990
	0.3	0 - 60	0.0014	0.928	0.0003	0.923
bioleaching	0	0 - 7	0.0081	0.987	0.0011	0.932
	0.1	0 - 25	0.0049	0.974	0.0013	0.930
	0.2	0 - 35	0.0040	0.969	0.0012	0.855
	0.3	0 - 60	0.0021	0.967	0.0006	0.860

5.3.6 Arsenic solubilization and immobilization during bioleaching with and without AC

The behavior of As (dissolution and immobilization) is also one of the most important factors in enargite leaching. In the abiotic cultures, As solubilization was negligible (< 3% in the absence and presence of AC; Fig. 5.8a) and the majority of once-dissolved As was immediately immobilized throughout the experiment (75% and 94% As immobilized in the absence and presence of AC, respectively; Fig. 5.8a and 5.8b). Slow dissolution of enargite resulted in the small amount of As supplied into the solution, which could be successively immobilized via the co-precipitation with Fe. On the other hand, As solubilization was visible in the biotic cultures (except for the culture in the presence of 0.3% AC) due to the faster dissolution of enargite than abiotic cultures, reaching 24%, 29%, 35%, 3% As dissolution at day 60 in the a presence of 0, 0.1, 0.2, and 0.3% AC, respectively (Fig. 5.8a). However, the addition of AC enables to delay the initiation of As dissolution from day 10 (0% AC) to 30 (0.1%) and 40 (0.2%), and almost no As solubilization was observed until the end of the experiment at 0.3% AC (Fig. 5.8a).

Fig. 5.8b shows the immobilized As concentration in each culture calculated by the following equation;

$$\text{As immobilized (mM)} = \text{Total Cu dissolved (mM)} / 3 - \text{Total As dissolved (mM)} \quad \text{(Eq. 7-3)}$$

Regardless of the absence or presence of AC, the amount of As immobilized once increased with time to reach the highest amount of 3.1 mM (0% AC at day 10), 5.2 mM (0.1% at day 30), 7.0 mM (0.2% at day 40), and 6.9 mM (0.3% at day 60), corresponding to 77%, 70%, 77%, and 92% of immobilization ratio, respectively (Fig. 5.8b). However, it later started to decrease at day 10 (0%), 30 (0.1%), and 40 (0.2%), resulting in < 40% As immobilization at day 60 in each case; in the presence of 0.3% AC, As immobilization constantly increased throughout the experiment. The initiation of the decrease in As immobilization was consistent with that of the As solubilization into the solution (Fig 5.8a and 5.8b), suggesting that the once-immobilized As was likely re-solubilized.

EPMA analysis was carried out to understand the As immobilization form and its re-solubilization mechanism. Bioleaching residues of 0.2% AC culture at day 30 and day 60 were collected to obtain the "before As re-solubilization" and "after As re-solubilization" samples (indicated in Fig. 5.8b), respectively. In the former sample, enargite grains covered with some thin layer (1-3 μm) were uniformly found (Fig. 5.8b), which completely disappeared in the latter sample (Fig. 5.8c), alternatively forming jarosite ($KFe_3(OH)_6(SO_4)_2$) as a major secondary mineral. Elemental mapping analysis revealed that the thin layer was composed of Fe, As, and O, corresponding to ferric arsenate ($FeAsO_4$; Fig. 5.9). This observation suggests that dissolved As successively co-precipitates with Fe on the surface of enargite to form amorphous ferric arsenate layer, which was later re-solubilized to release As and Fe into the solution again, thus resulting in the decrease in As immobilization. It was expected that some As would be still immobilized by co-precipitating with jarosite, which was observed as the majority of secondary mineral in "after As re-solubilization" sample. The re-solubilization could be triggered by the dissolution of pyrite, since the initiation of As re-solubilization was almost accompanied by that of rapid Fe dissolution (Fig. 5.1b). It has been reported that sulfate ion is likely involved in the dissolution-recrystallization process of As-bearing precursor to finally form highly crystalline scorodite ($FeAsO_4 \cdot 2H_2O$; Tanaka et al., 2018). Large amount of sulfate ion supplied by rapid pyrite dissolution would thus hinder the stabilization of once-immobilized ferric arsenate by transferring the chemical equilibrium toward the formation of ferric sulfate such as jarosite. Stabilization of ferric arsenate and its transformation into highly crystalline scorodite might be achievable by the optimization of AC addition to maintain the E_h level to < 700 mV throughout the experiment for completely suppressing the sulfate solubilization from pyrite.

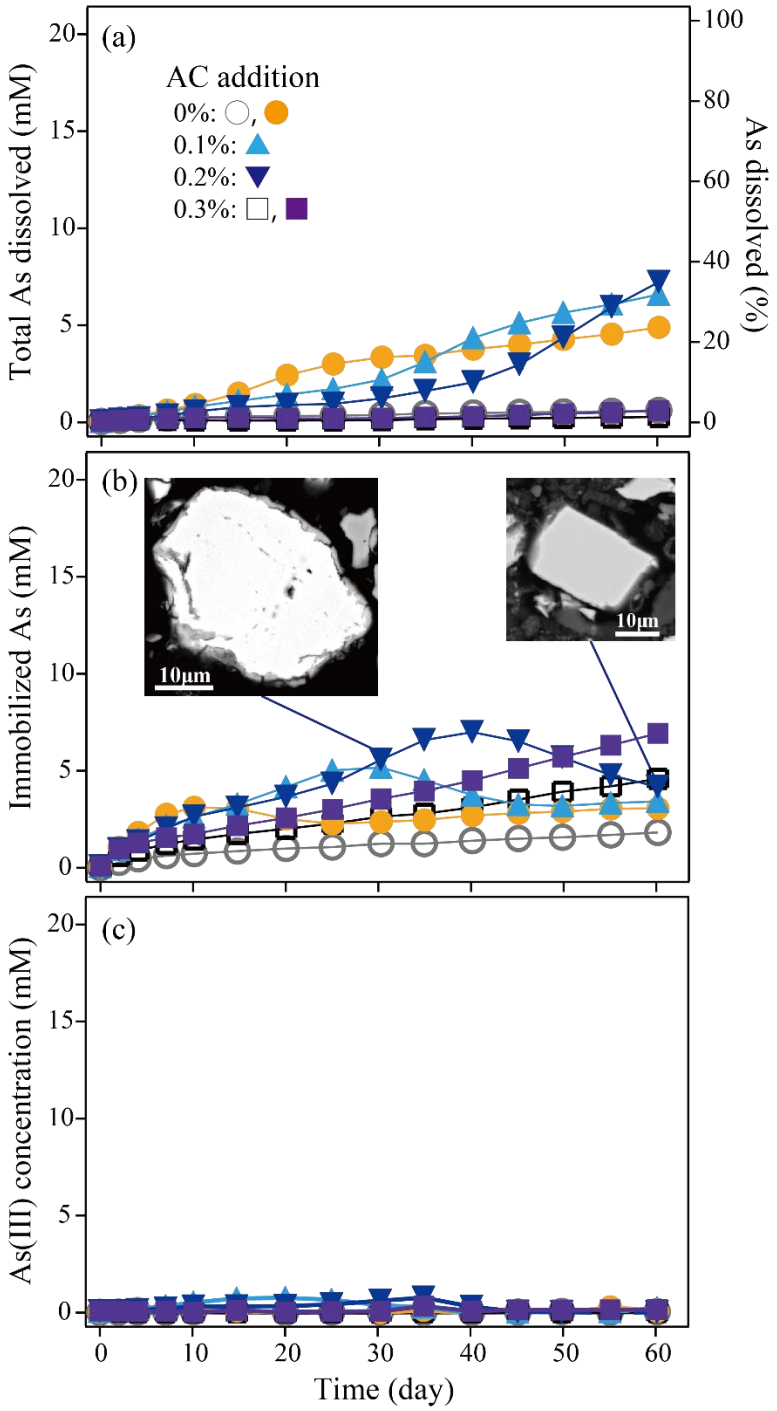

Fig. 5.8 Changes in the concentration of total soluble As (a), immobilized As (b), and soluble As (III) (c) during abiotic leaching (open symbol) or bioleaching (closed symbol) of enargite concentrate at 0% (○, ●), 0.1% (▲), 0.2% (▼), or 0.3% (w/v) (□, ■) of AC. Backscattered electron image of an enargite grain bioleached for 30 or 60 days with 0.2% (w/v) AC at the 2700-fold or 1000-fold magnification was also depicted, respectively. White brighter grain (enargite) was covered with gray layer at day 30, which disappeared at day 60.

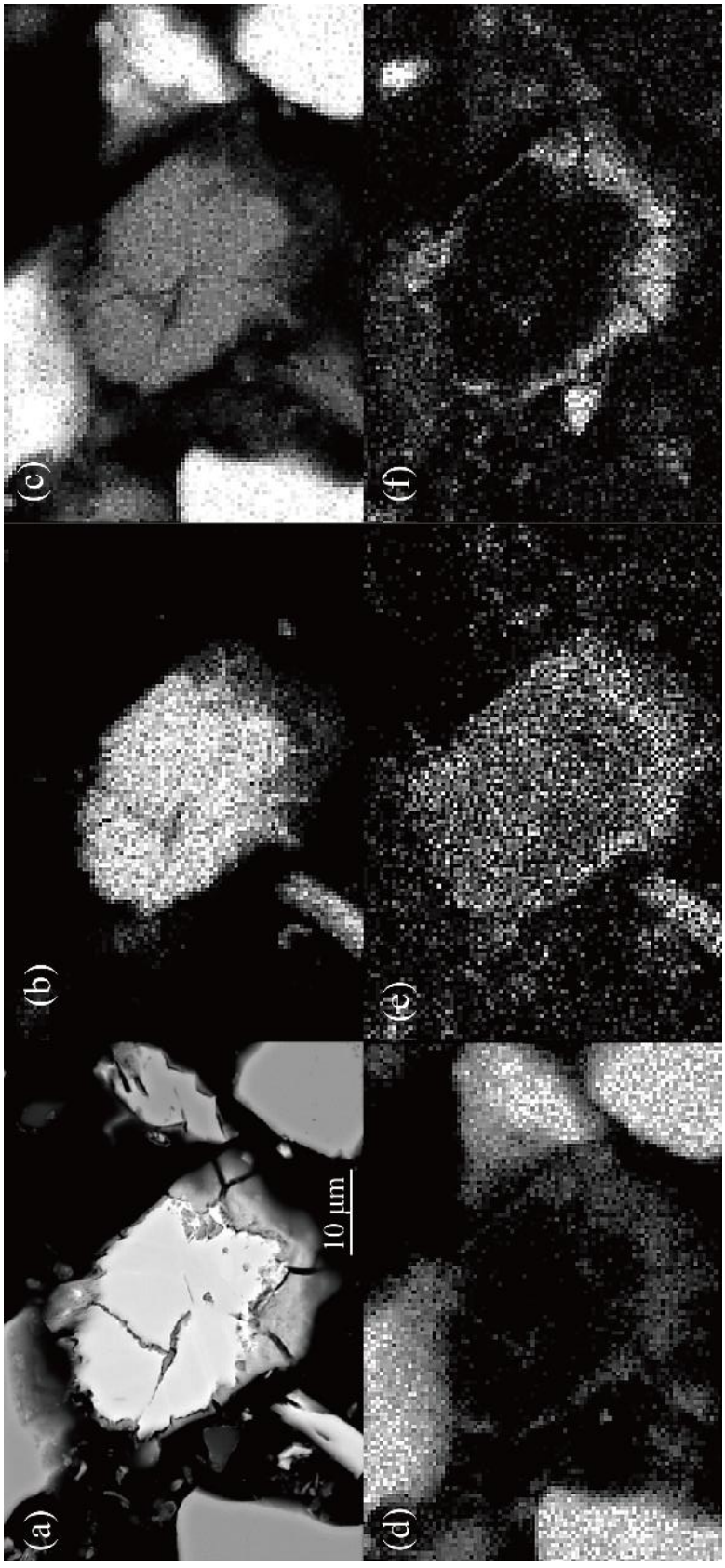

Fig. 5.9 EPMA elemental mapping of enargite concentrate residue bioleached for 30 days with 0.2% AC: The backscattered electron image at 3000-fold magnification (a) was mapped for Cu (b), S (c), Fe (d), As (e) and O (f). The surface of an enargite grain is covered with Fe-, As-, O-containing secondary mineral, ferric arsenate.

5.4 Conclusions

Based on the overall findings, the mechanism of AC-catalyzed bioleaching of enargite concentrates is proposed in Fig. 5.10.

The presence of AC suppresses the E_h increase via the coupling reaction (Fe^{3+}-reduction and RISCs-oxidation) on the AC surface acting as an electron mediator (i). This E_h lowering effect by AC deteriorates the initiation of pyrite dissolution (ii), which starts to dissolve when E_h reaches to 700 mV. At the same time, enargite dissolution is also slightly slowed down according to the addition of AC, since high E_h is favorable for the faster dissolution. The galvanic interaction between enargite and AC negligibly contributes to Cu solubilization at the lower E_h level. However, suppressed pyrite dissolution results in the less passivation of enargite with Fe precipitates such as jarosite, consequently leading to the steady and long Cu solubilization (iii).

Once dissolved As from enargite is successively and immediately immobilized as ferric arsenate selectively on the enargite surface (iv). However, large amount of sulfate supplied from rapid pyrite dissolution would destabilize the ferric arsenate by shifting the chemical equilibrium toward the formation of ferric sulfate such as jarosite. As a result, As re-solubilization occurs to release As into the solution again, and some of them co-precipitates with jarosite (v).

This proposed mechanism suggests that completely suppressed pyrite dissolution is a key point to realize much longer Cu solubilization and the stabilized As immobilization. Therefore, further investigation on the catalytic ability of AC will be beneficial to completely prevent pyrite dissolution by maintaining the E_h less than 700 mV.

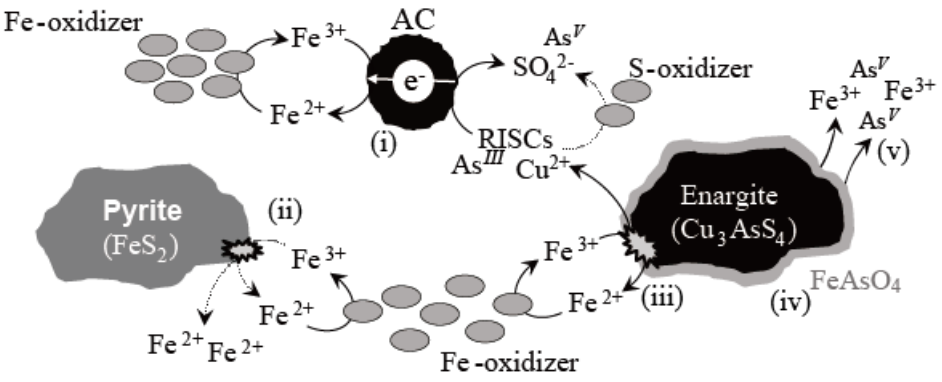

Fig. 5.10 The schematic image of overall mechanism of AC-catalyzed bioleaching of enargite concentrate.

References

1. Ahonen, L. and Tuovinen, O.H., 1990. Catalytic effects of silver in the microbiological leaching of finely ground chalcopyrite-containing ore materials in shake flasks. Hydrometallurgy 24, 219-236.
2. Ahumada, E., Lizama, H., Orellana, F., Suárez, C., Huidobro, A., Sepúlveda-Escribano, A. and Rodrıguez-Reinoso, F., 2002. Catalytic oxidation of Fe(II) by activated carbon in the presence of oxygen: Effect of the surface oxidation degree on the catalytic activity. Carbon 40, 2827-2834.
3. Ballester, A., Gonzalez, F., Blázquez, M. and Mier, J., 1990. The influence of various ions in the bioleaching of metal sulphides. Hydrometallurgy 23, 221-235.
4. Escobar, B., Huenupi, E. and Wiertz, J.V., 1997. Chemical and biological leaching of enargite. Biotechnology Letters 19, 719-722.
5. Escobar, B., Huenupi, E., Godoy, I. and Wiertz, J.V., 2000. Arsenic precipitation in the bioleaching of enargite by *Sulfolobus* BC at 70 C. Biotechnology Letters 22, 205-209.
6. Ghahremaninezhad, A., Radzinski, R., Gheorghiu, T., Dixon, D.G. and Asselin, E., 2015. A model for silver ion catalysis of chalcopyrite ($CuFeS_2$) dissolution. Hydrometallurgy 155, 95-104.
7. Gu, G.-h., Sun, X.-j., Hu, K.-t., Li, J.-h. and Qiu, G.-z., 2012. Electrochemical oxidation behavior of pyrite bioleaching by *Acidthiobacillus ferrooxidans*. Transactions of Nonferrous Metals Society of China 22, 1250-1254.
8. Hao, X., Liu, X., Zhu, P., Chen, A., Liu, H., Yin, H., Qiu, G. and Liang, Y., 2018. Carbon material with high specific surface area improves complex copper ores' bioleaching efficiency by mixed moderate thermophiles. Minerals 8, 301.
9. Hiroyoshi, N., Arai, M., Miki, H., Tsunekawa, M. and Hirajima, T., 2002. A new reaction model for the catalytic effect of silver ions on chalcopyrite leaching in sulfuric acid solutions. Hydrometallurgy 63, 257-267.
10. Jahromi, F. and Ghahreman, A., 2016. Activated carbon assisted atmospheric leaching of enargite in chloride media, International Copper Conference 2016 abstract, pp. 1453-1464.
11. Jahromi, F.G., Cowan, D.H. and Ghahreman, A., 2017. Lanxess Lewatit® AF 5 and activated carbon catalysis of enargite leaching in chloride media; a parameters

study. Hydrometallurgy 174, 184-194.

12. Jahromi, F.G. and Ghahreman, A., 2018. In-situ oxidative arsenic precipitation as scorodite during carbon catalyzed enargite leaching process. Journal of Hazardous Materials 360, 631-638.
13. Jahromi, F.G., Alvial-Hein, G., Cowan, D.H. and Ghahreman, A., 2019. The kinetics of enargite dissolution in chloride media in the presence of activated carbon and AF 5 catalysts. Minerals Engineering 143, 106013.
14. Konadu, K.T., Sasaki, K., Kaneta, T., Ofori-Sarpong, G. and Osseo-Asare, K., 2017. Bio-modification of carbonaceous matter in gold ores: Model experiments using powdered activated carbon and cell-free spent medium of *Phanerochaete chrysosporium*. Hydrometallurgy 168, 76-83.
15. Lastoskie, C., Gubbins, K.E. and Quirke, N., 1993. Pore size distribution analysis of microporous carbons: a density functional theory approach. The Journal of Physical Chemistry 97, 4786-4796.
16. Lattanzi, P., Da Pelo, S., Musu, E., Atzei, D., Elsener, B., Fantauzzi, M. and Rossi, A., 2008. Enargite oxidation: A review. Earth-Science Reviews 86, 62-88.
17. Lee, J., Acar, S., Doerr, D.L. and Brierley, J.A., 2011. Comparative bioleaching and mineralogy of composited sulfide ores containing enargite, covellite and chalcocite by mesophilic and thermophilic microorganisms. Hydrometallurgy 105, 213-221.
18. Li, T., Zhang, Y., Zhang, B., Zhang, J. and Qin, W., 2018. Selective leaching of arsenic from enargite concentrate using alkaline leaching in the presence of pyrite. Hydrometallurgy 181, 143-147.
19. Liang, C.-L., Xia, J.-L., Zhao, X.-J., Yang, Y., Gong, S.-Q., Nie, Z.-Y., Ma, C.-Y., Zheng, L., Zhao, Y.-D. and Qiu, G.-z., 2010. Effect of activated carbon on chalcopyrite bioleaching with extreme thermophile *Acidianus manzaensis*. Hydrometallurgy 105, 179-185.
20. Ma, Y.-l., Liu, H.-c., Xia, J.-l., Nie, Z.-y., Zhu, H.-r., Zhao, Y.-d., Zheng, L., Hong, C.-h. and Wen, W., 2017. Relatedness between catalytic effect of activated carbon and passivation phenomenon during chalcopyrite bioleaching by mixed thermophilic Archaea culture at 65ºC. Transactions of Nonferrous Metals Society of China 27, 1374-1384.

21. Masaki, Y., Hirajima, T., Sasaki, K., Miki, H. and Okibe, N., 2018. Microbiological redox potential control to improve the efficiency of chalcopyrite bioleaching. Geomicrobiology Journal 35, 648-656.
22. Miki, H., Iguchi, A., Hirajima, T. and Sasaki, K., 2016. Catalytic effect of silver on arsenic-containing copper sulfide dissolution in acidic solution. Hydrometallurgy 162, 1-8.
23. Muñoz, J., Blázquez, M., González, F., Ballester, A., Acevedo, F., Gentina, J. and González, P., 2006. Electrochemical study of enargite bioleaching by mesophilic and thermophilic microorganisms. Hydrometallurgy 84, 175-186.
24. Muñoz, J., Dreisinger, D., Cooper, W. and Young, S., 2007. Silver-catalyzed bioleaching of low-grade copper ores: Part I: Shake flasks tests. Hydrometallurgy 88, 3-18.
25. Nakazawa, H., Fujisawa, H. and Sato, H., 1998. Effect of activated carbon on the bioleaching of chalcopyrite concentrate. International Journal of Mineral Processing 55, 87-94.
26. Nazari, G., Dixon, D. and Dreisinger, D., 2011. Enhancing the kinetics of chalcopyrite leaching in the Galvanox™ process. Hydrometallurgy 105, 251-258.
27. Nazari, G., Dixon, D. and Dreisinger, D., 2012a. The role of silver-enhanced pyrite in enhancing the electrical conductivity of sulfur product layer during chalcopyrite leaching in the Galvanox™ process. Hydrometallurgy 113, 177-184.
28. Nazari, G., Dixon, D. and Dreisinger, D., 2012b. The mechanism of chalcopyrite leaching in the presence of silver-enhanced pyrite in the Galvanox™ process. Hydrometallurgy 113, 122-130.
29. Olvera, O., Dixon, D. and Asselin, E., 2013. Electrochemical study of the dissolution of enargite (Cu_3AsS_4) in contact with activated carbon. Electrochimica Acta 107, 525-536.
30. Oyama, K., Shimada, K., Ishibashi, J.-i., Miki, H. and Okibe, N., 2018. Silver-catalyzed bioleaching of enargite concentrate using moderately thermophilic microorganisms. Hydrometallurgy 177, 197-204.
31. Padilla, R., Jerez, O. and Ruiz, M., 2015. Kinetics of the pressure leaching of enargite in $FeSO_4$–H_2SO_4–O_2 media. Hydrometallurgy 158, 49-55.
32. Radzinski, R., Nazari, A. and Ghahreman, A., 2016. Activated-carbon catalyzed

arsenic oxidation: Formation of hydrogen peroxide in acidic solutions, Hydroprocess 2016 Conference. Santiago, Chile.

33. Ruiz, M., Vera, M. and Padilla, R., 2011. Mechanism of enargite pressure leaching in the presence of pyrite. Hydrometallurgy 105, 290-295.
34. Safarzadeh, M.S. and Miller, J.D., 2014. Reaction of enargite (Cu_3AsS_4) in hot concentrated sulfuric acid under an inert atmosphere. Part I: Enargite concentrate. International Journal of Mineral Processing 128, 68-78.
35. Sasaki, K., Takatsugi, K., Kaneko, K., Kozai, N., Ohnuki, T., Tuovinen, O. and Hirajima, T., 2010. Characterization of secondary arsenic-bearing precipitates formed in the bioleaching of enargite by *Acidithiobacillus ferrooxidans*. Hydrometallurgy 104, 424-431.
36. Sasaki, K., Takatsugi, K. and Hirajima, T., 2011. Effects of initial Fe^{2+} concentration and pulp density on the bioleaching of Cu from enargite by *Acidianus brierleyi*. Hydrometallurgy 109, 153-160.
37. Takatsugi, K., Sasaki, K. and Hirajima, T., 2011. Mechanism of the enhancement of bioleaching of copper from enargite by thermophilic iron-oxidizing archaea with the concomitant precipitation of arsenic. Hydrometallurgy 109, 90-96.
38. Tanaka, M., Sasaki, K. and Okibe, N., 2018. Behavior of sulfate ions during biogenic scorodite crystallization from dilute As(III)-bearing acidic waters. Hydrometallurgy 180, 144-152.
39. Vargas, T., Diaz, P. and Escobar, B., 2009. Reductive action of activated carbon on ferric iron interferes on the determination of the oxidative activity of *Acidithiobacillus ferrooxidans* on ferrous iron, Advanced Materials Research. Trans Tech Publ, pp. 291-294.
40. Zhang, W.-M. and Gu, S.-F., 2007. Catalytic effect of activated carbon on bioleaching of low-grade primary copper sulfide ores. Transactions of Nonferrous Metals Society of China 17, 1123-1127.

Chapter 6

Physicochemical properties determining the catalytic ability of activated carbon

Abstract

To clarify the property determining the E_h-control ability of AC, 8 types of AC (A-powder, B-granular, B-powder, C-powder, D-powder, E-powder, F-powder, and G-powder) with the variety of surface property were compared in the abiotic experiment. Three AC (A-powder, B-granular, and B-powder) were also used in the bioleaching experiment for further understanding of AC-catalyzing mechanism. Series of the test revealed that Fe^{3+}-reduction coupled with the oxidation of tetrathionate was greatly facilitated by using chemical-activated carbon (A-powder and G-powder), rather than steam-activated carbon. Raman spectroscopy analysis revealed that the well-developed graphene structure in the former type of AC was likely the reason of its superiority as an electron mediator, leading to the strongest E_h-reducing ability. Other parameters such as specific surface area, total pore volume, size, activation degree, and raw material were found negligibly influential in E_h-control ability. Even in the bioleaching experiment, the utility of chemical-activated carbon (A-powder) was confirmed as an E_h-controlling catalyst. Moreover, faster dissolution behavior of enargite was retained by using powder AC, while it was slowed down when granular AC was used. High contact frequency of the former AC would facilitate enargite dissolution, likely canceling out the slowed enargite dissolution due to the AC-catalyzed E_h-reduction. In summary, powder AC produced by chemical activation was found the most suitable for AC-catalyzing bioleaching of enargite concentrate.

6.1 Introduction

In order to accelerate the dissolution of refractory copper sulfides such as chalcopyrite ($CuFeS_2$) and enargite (Cu_3AsS_4), a promising catalyst which is applicable to the bioleaching process has been sought in decades. Silver is one of the candidates, actively studied by a number of researcher's so far especially in the chalcopyrite bioleaching system (Ahonen et al., 1990; Ballester et al., 1990; Gómez et al., 1999; Sato et al., 2000; Yuehua et al., 2002; Muñoz et al., 2007; Johnson et al., 2008; Feng et al., 2013; Abdollahi et al., 2015; Xia et al., 2018). Regardless of its strong catalytic ability, however, other possibilities must be found due to the economic infeasibility of silver-utilization in real operation.

As an alternative, carbon materials such as graphite or AC are considered useful (Hao et al., 2018). Possible utility of AC was indeed confirmed in previous chapter 5 in this thesis, where the final Cu recovery was improved with AC addition during bioleaching of enargite concentrate based on the indirect catalysis mechanism; AC act as an E_h-controlling catalyst to prevent unwanted pyrite dissolution, enabling slower but steady dissolution of enargite without Fe passivation. Although Fe^{3+} reduction coupled with RISCs oxidation on the AC surface was found the key reaction of AC-catalyzed E_h-control, the property determining the E_h-controlling ability of AC is still unclear.

The effected of specific surface area have been tested by comparing graphite and AC with various specific surface area (Hao et al., 2018). Even though electrical conductivity of graphite (0.6 S/m) is rather higher than that of the others (0.1 S/m), AC with the highest specific surface (1200 m^2/g) performed the strongest E_h-reduction in bioleaching of complex copper ores, proving the importance of the specific surface area. Jahromi et al. (2018) modified the surface functional groups on the AC surface with sulfuric acid, hydrochloric acid, and nitric acid to investigate the effect of varied surface functional groups on abiotic enargite leaching. It clarified that the modification with different acid changed the abundance of oxidative functional groups on the AC surface such as quinone and carboxyl groups. These oxidative functional groups are catalytically capable of producing H_2O_2 via the following equations, proposed by Ahumada et al., (2002);

$$2C_{red} + O_2 + 2H_2O = 2H_2O_2 + 2C_{ox} \quad \text{(Eq. 6-1)}$$

$$2Fe^{2+} + H_2O_2 + 2H^+ = 2Fe^{3+} + 2H_2O \quad \text{(Eq. 6-2)}$$

C_{red} and C_{ox} indicate that surface functional groups on the surface of AC. This H_2O_2 formed in Eq. 6-1 could be consumed to oxidize the Fe^{2+} to Fe^{3+} (Eq. 6-2), possibly shifting E_h to the higher level. Therefore, surface functional groups must also be considered as one of the properties determining the E_h-controlling ability of AC.

Moreover, the properties of AC significantly affected on the dissolution kinetics of minerals during the leaching process. Nakazawa et al. (1998) found the necessity of contact with AC to enhance the chalcopyrite dissolution; almost no catalytic ability was noticeable without contact between AC and chalcopyrite. This suggests that the particle size (or shape) of AC must be finer to maximize the catalytic ability of AC by increasing the contact frequency. Besides this, other parameters such as pore size, pore volume, raw material, and activation method would determine the catalytic ability of AC.

This chapter, therefore, aimed to find the most crucial property determining the catalytic ability of activated carbon. Series of abiotic and biotic tests were carried out to compare the various AC with varied surface and structural properties. The obtained information would be summarized for a further comprehensive understanding of AC-catalyzed bioleaching of enargite concentrate.

6.2 Materials and methods

6.2.1 Comparison of granular and powder AC

In order to evaluate the effect of AC-shape (granular or powder) on redox reactions occurring on the surface of AC, three AC, powder AC, granular AC (used in chapter 5), and crushed granular AC (hereinafter, referred to as A-powder, B-granular, B-powder, respectively; purchased from Wako) were employed; B-powder was prepared by crushing the B-granular so as to set its particle size to be similar with A-powder. Material property and pore size distribution of each AC were summarized in Table 6.1 and Fig. 6.1. A-powder and B-powder were also used for the analyses by Raman spectroscopy and ATR-FT-IR.

ABS medium (100 mL; pH adjusted to 2.0 by using 1 M H_2SO_4) was added into the 300 mL of Erlenmeyer flask. Each type of AC at the pulp density of 0.1% (w/v), 10 mM Fe^{2+} or Fe^{3+}, and/or 5 mM of tetrathionate were respectively added into the medium to prepare the experimental cultures listed below. These flasks were incubated and shaken at 45ºC and 150 rpm, respectively. Solution samples were regularly withdrawn to monitor pH, E_h, Fe^{2+} and total Fe concentration (*o*-phenanthroline method), and SO_4^{2-} concentration (turbidimetric method).

1	10 mM Fe^{3+} + 5 mM tetrathionate	+ 0.1% A-powder
		+ 0.1% B-granular
		+ 0.1% B-powder
2	10 mM Fe^{3+}	+ 0.1% A-powder
		+ 0.1% B-granular
		+ 0.1% B-powder
3	10 mM Fe^{2+}	+ 0.1% A-powder
		+ 0.1% B-granular
		+ 0.1% B-powder
4	5 mM tetrathionate	+ 0.1% A-powder
		+ 0.1% B-granular
		+ 0.1% B-powder

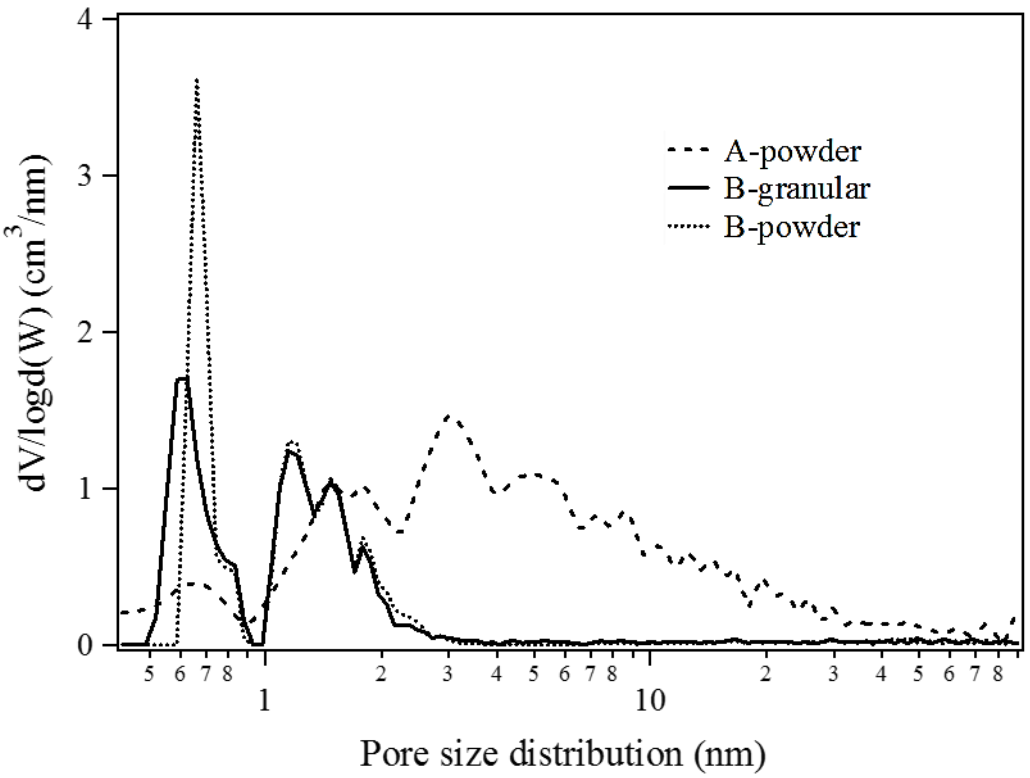

Fig. 6.1 Pore size distribution of A-powder, B-granular, and B-powder.

Table 6.1. Material properties of A-powder, B-granular, and B-powder.

	A-powder	B-granular	B-powder
Specific surface Area (m^2/g)	1429	1212	1261
Total pore volume (cm^3/g)	1.33	0.54	0.57
Average pore diameter (nm)	3.71	1.77	1.81
Average particle size (μm)	42.2	5000	237.8
Raw material	Woody chip	Coconut shell	Coconut shell
Activation	Chemical-activated	Steam-activated	Steam-activated

6.2.2 Comparison of other AC with various properties

For further discussion, other types of powder AC (C-powder, D-powder, E-powder, F-powder, and G-powder) were also tested in the abiotic condition. Material properties of each AC were summarized in Table 6.2. These were also used for the analyses by Raman spectroscopy and ATR-FT-IR.

ABS medium (100 mL; pH adjusted to 2.0 by using 1 M H_2SO_4) was added into the 300 mL of Erlenmeyer flask. Each type of AC at the pulp density of 0.1% (w/v), 10 mM Fe^{3+}, and 5 mM of tetrathionate were also added into the medium. These flasks were incubated and shaken at 45ºC and 150 rpm, respectively. Solution sample were regularly withdrawn to monitor pH, E_h, Fe^{2+} and total Fe concentration (*o*-phenanthroline method), SO_4^{2-} concentration (turbidimetric method).

Table 6.2. Material properties of other types of AC (C-powder, D-powder, E-powder, F-powder, and G-powder).

AC	Raw material	Activation	Specific surface area (m^2/g)	Total pore volume (mL/g)	Average pore diameter (nm)
C-powder	Coconut shell	Steam-activated	1683	0.807	1.9
D-powder	Coconut shell	Steam-activated	1075	0.483	1.8
E-powder	Woody chip	Steam-activated	959	0.554	2.3
F-powder	Coal	Steam-activated	916	0.454	2.0
G-powder	Woody chip	Chemical-activated	1395	1.243	3.6

6.2.3 Comparison of AC in enargite bioleaching system

Bioleaching of enargite concentrate using A-powder or B-powder were carried out to compare their catalytic ability in biotic condition. HBS media (200 ml in 500 ml flasks; pH adjusted to 2.0 with 1 M H_2SO_4) containing 2.0% (4.0 g) enargite concentrate (average particle size: 46.5 μm) and 0, 0.02, 0.04, 0.06 and 0.08% (w/v) A-powder or B-powder were prepared and sterilized by autoclaving. Pre-grown culture of each of three strains (*Am. ferrooxidans* ICP, *Sb. sibiricus* N1, and *At. caldus* KU) was centrifuged (9000 rpm, 10 min at 4°C) to collect cells and washed twice with acidified

water (pH 1.7), prior to inoculation. Initial cell density in total was set to 3.0×10^7 cells /mL (1.0×10^7 cells /mL for each strain) and 5 mM $FeSO_4 \cdot 7H_2O$ was supplemented for initial cell growth. These flasks were incubated and shaken at 45˚C and 150 rpm. Samples were regularly withdrawn to monitor pH, E_h, cell density, and concentrations of Fe^{2+} (*o*-phenanthroline method), As(III) (molybdenum blue method), and total Fe, As, and Cu (ICP-OES). Finally, the obtained data in this bioleaching experiment was compared with that obtained in chapter 5, bioleaching of enargite concentrate using B-granular as an AC catalyst.

6.3 Results and discussion

6.3.1 Catalytic reaction affected by the shape of AC

In this abiotic experiment, three different AC were employed to compare the difference in physical property: (i) A-powder is a powder AC (average size: 42 μm) made from woody chip by chemical-activation, (ii) B-granular is a granular AC (average size: around 5000 μm) made from coconut shell by steam-activation, (iii) B-powder is a powder AC (average size: 238 μm) obtained by crushing the B-granular. Even though the raw material of each AC are different, the comparison among these AC would enable to evaluate the effect of shape (granular or powder) on AC-catalyzed redox reaction, especially for E_h-controlling effect.

In the presence of Fe^{3+} and tetrathionate with any AC, rapid decrease in E_h occurred at the beginning of the experiment (Fig. 6.2b). This must be due to the coupling reaction confirmed in chapter 5; Fe^{3+}-reduction coupled with tetrathionate-oxidation on the AC surface acting as an electron mediator. The other trends, decrease in pH, increase in SO_4 production, and increase in acid production, also proved that tetrathionate indeed plays a role as an electron donor for Fe^{3+}-reduction (Fig. 6.2a,e,f) regardless of AC type. In the culture with B-granular, relatively slower kinetics was observed compared to the other two powder AC (Fig. 6.2a,b,c,e,f), suggesting that granular AC inferior to powder AC, possibly in terms of ion-capturing capability; in other words, granular AC is more susceptible to the diffusion of ionic species than the others. However, E_h in the presence of B-granular was consequently lowered to 620 mV at the end of the experiment, which is as low as that in the presence of B-powder, indicating that long-term E_h-reduction ability of AC could not be determined by the shape(granular and powder).

Interestingly, the stronger E_h-reduction ability of A-powder became noticeable in the later stage of the experiment after day 3 (Fig. 6.2b). E_h reached to significantly low level (557 mV) at the end of the experiment (day 6), accompanied with complete Fe^{3+} reduction to Fe^{2+} (Fig. 6.2c,d). Based on this fact, A-powder was found the most effective in E_h-reduction among these three AC. This different E_h trend between A-powder and B-powder is also evidence that the shape of AC is not the predominant property determining its E_h-controlling ability.

On the other hand, larger amount of SO_4 was continuously produced in the presence of B-powder throughout the experiment than other cultures, even though smaller amount

of tetrathionate was assumed to be used for the Fe^{3+}-reduction in this culture. This implies that the surface property of B-powder would be suitable for the oxidative reaction rather than that of A-powder.

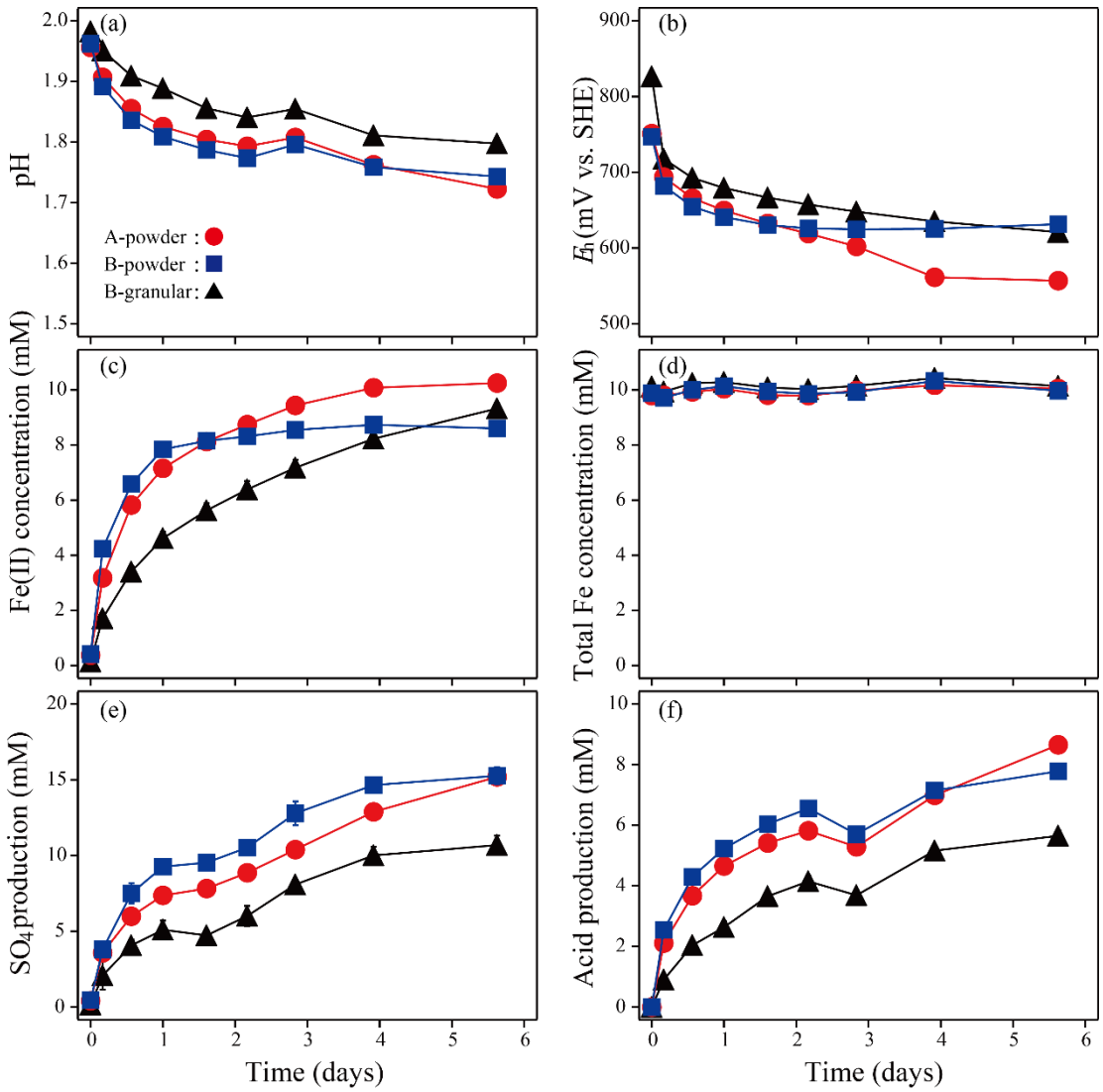

Fig. 6.2 Changes in pH (a), E_h (b), Fe^{2+} concentration (c), total Fe concentration (d), sulfate production (e), and acid production (f) during the abiotic experiment in the presence of 10 mM Fe^{3+} and 5 mM sodium tetrathionate for the evaluation of catalytic capability of three AC: A-powder (●), B-granular (▲), and B-powder (■). Data points are mean values from duplicate cultures. Error bars depicting averages are not visible in some cases as they are smaller than the data point symbols.

In order to evaluate the oxidative ability of AC itself, cultures containing each one of three AC and either 10 mM Fe^{2+} (Fig. 6.3) or 5 mM sodium tetrathionate (Fig. 6.4) were prepared. The results obviously showed that the oxidation of Fe^{2+} and tetrathionate were rather promoted in the presence of B-powder (Fig. 6.3c, Fig. 6.4c), confirming that its stronger oxidative ability than A-powder. This might be due to the difference in the surface functional groups on the AC surface. As Eq. 6-1, oxidative type surface functional group such as quinone and carboxyl catalyzes the H_2O_2 production, which can be consumed for the oxidation of Fe^{2+} (Eq. 6-2). Likewise, Fe^{2+} and tetrathionate might be oxidized by H_2O_2 generated on the surface of B-powder. This hypothesis implies that B-powder would possess the larger amount of oxidative type surface functional group such as quinone and carboxyl on its surface than A-powder. The details will be further discussed in the following section based on the analysis of the surface functional group by ATR-FT-IR.

Cultures containing each one of three AC and 10 mM Fe^{3+} were also prepared to evaluate the reductive ability of AC itself (Fig. 6.5). Contrary to the culture evaluating the oxidative ability of AC (Fig. 6.3, 6.4), the difference in Fe^{3+}-reducing ability among three AC was not explicit; E_h reached to the stable phase (around 720 mV) at the beginning of the experiment in any cases (Fig. 6.5b). Since rapid E_h drop until day 1 is likely the result of the reaction between Fe^{3+} and the surface functional group (Fig. 6.5b,c), it was expected that each AC possesses the similar reductive type surface functional group on their surface.

In summary, the difference in the shape of AC (granular or powder) was found less influential in E_h-controlling ability of AC. Based on the experimental results, although A-powder showed the best E_h-reducing ability among three AC, the key factor determining the E_h-controlling ability of AC is still unclear, thus requiring a further discussion about the properties of AC.

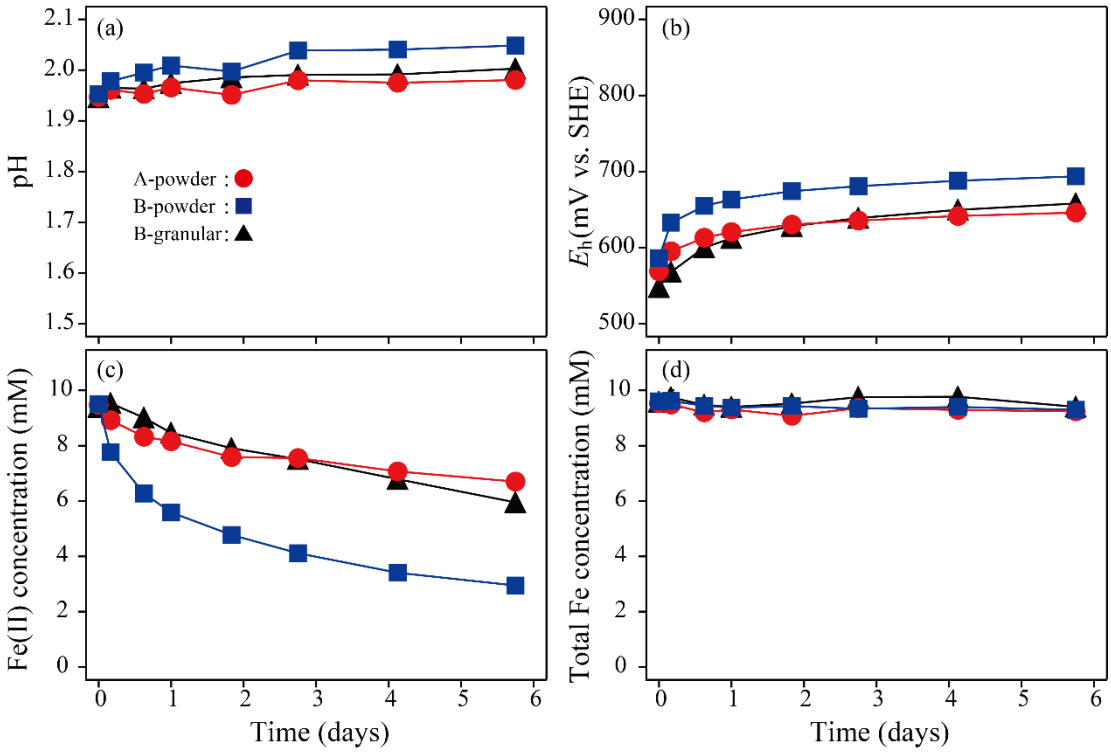

Fig. 6.3 Changes in pH (a), E_h (b), Fe^{2+} concentration (c), and total Fe concentration (d), during the abiotic experiment in the presence of 10 mM Fe^{2+} for the evaluation of catalytic capability of three AC: A-powder (●), B-granular (▲), and B-powder (■). Data points are mean values from duplicate cultures. Error bars depicting averages are not visible in some cases as they are smaller than the data point symbols.

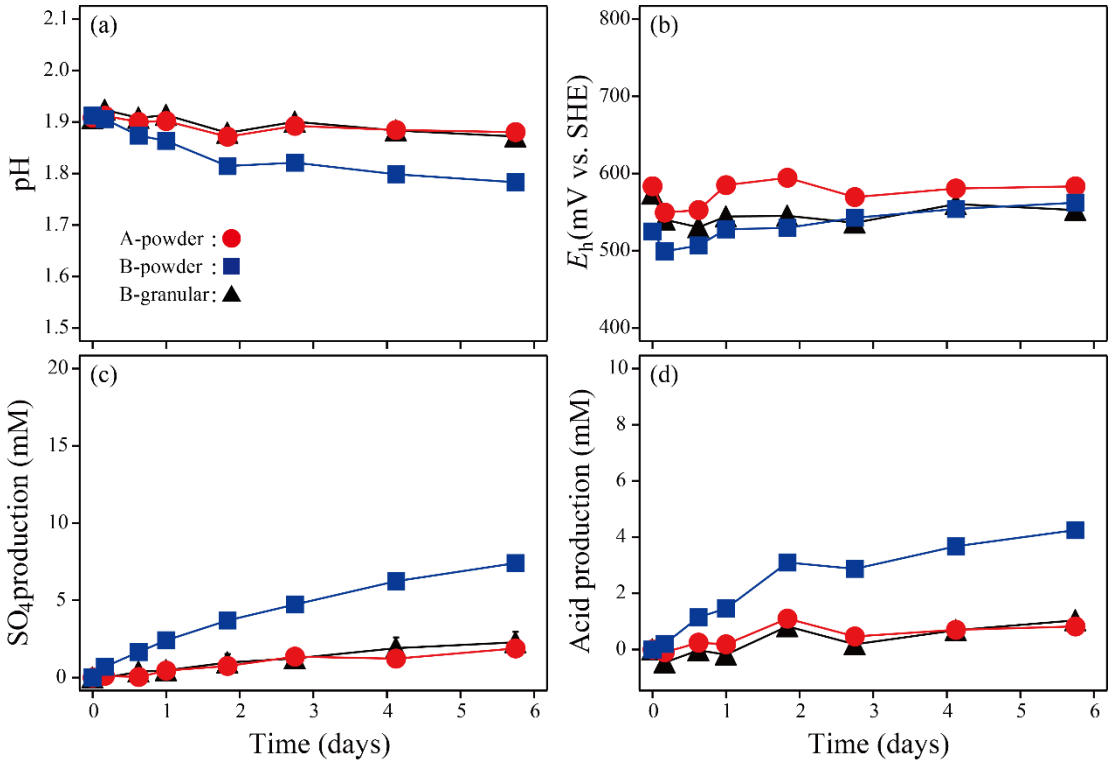

Fig. 6.4 Changes in pH (a), E_h (b), sulfate production (c), and acid production (d), during the abiotic experiment in the presence of 5 mM sodium tetrathionate for the evaluation of catalytic capability of three AC: A-powder (●), B-granular (▲), and B-powder (■). Data points are mean values from duplicate cultures. Error bars depicting averages are not visible in some cases as they are smaller than the data point symbols.

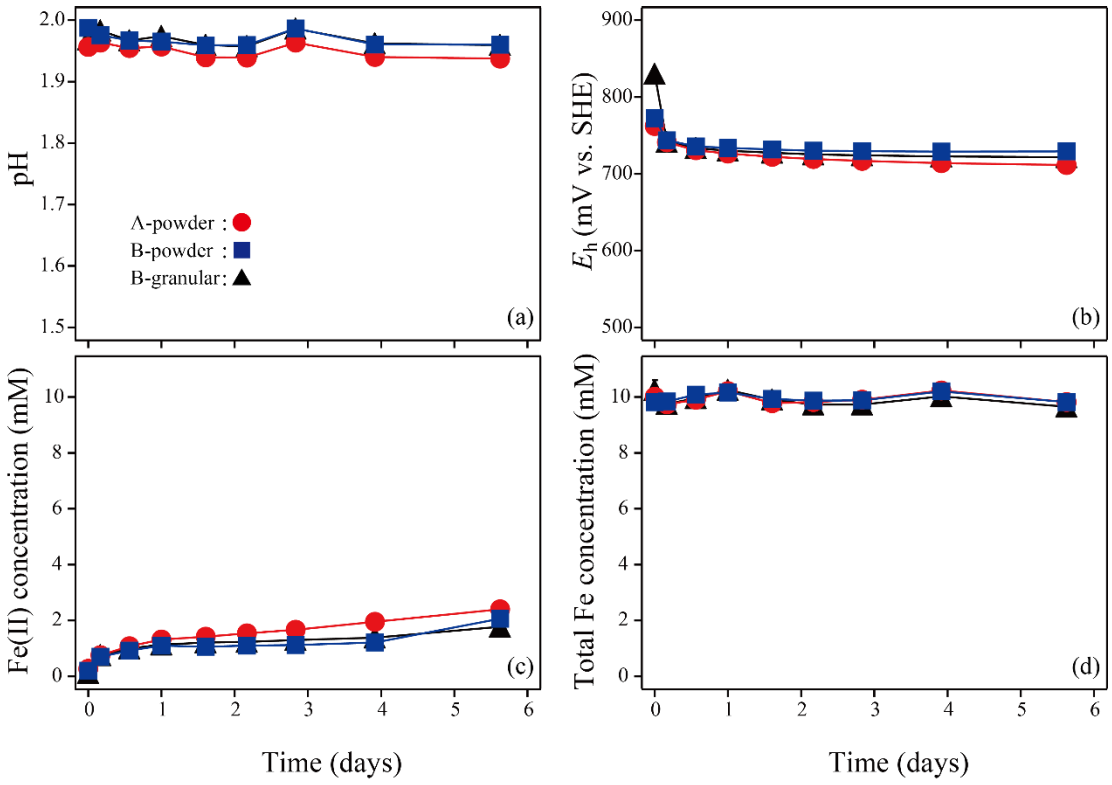

Fig. 6.5 Changes in pH (a), E_h (b), Fe^{2+} concentration (c), and total Fe concentration (d), during abiotic experiment in the presence of 10 mM Fe^{3+} for the evaluation of catalytic capability of three AC: A-powder (●), B-granular (▲), and B-powder (■). Data points are mean values from duplicate cultures. Error bars depicting averages are not visible in some cases as they are smaller than the data point symbols.

6.3.2 Further comparison of AC properties (specific surface area, pore volume, raw material, and activation method)

Based on the comparison of A-powder, B-granular, and B-powder in the previous section, it was found that E_h-reduction ability of AC was not affected by the shape of AC (granular or powder). In order to specify the property determining the E_h-controlling ability of AC, further investigation was carried out by comparing five different powder AC as listed in Table 6.2. Since C-powder possesses larger specific surface area (1683 m^2/g) and total pore volume (0.807 mL/g) than D-powder (1075 m^2/g of specific surface area and 0.483 mL/g of total pore volume), the effect of activation degree is able to be clarified through the comparison of them; the former was activated with higher temperature than the latter. The difference of raw material was also studied using D-powder, E-powder, and F-powder made of coconut shell, woody chip, and coal, respectively. Although both E-powder and G-powder were made of the same raw material, woody chip, activation methods are different (E-powder; steam-activated carbon, G-powder; chemical-activated carbon). This comparison also could provide useful information to clarify the property determining the E_h-controlling ability of AC.

Fig. 6.6 shows the results of the abiotic test adding each AC into the solution containing 10 mM Fe^{3+} and 5 mM tetrathionate. Obvious difference was observed in the presence of G-powder, where E_h rapidly reduced to the 537 mV in the early stage of the experiment, whereas the other type of AC showed less E_h-reducing capability. Common property between G-powder and A-powder (the best E_h-reducing AC in the previous section) is the activation method, indicating that chemical-activated carbon is the most suitable for the E_h-controlling AC catalyst.

Raman spectrum of each AC showed two main peaks at 1350 cm^{-1} and 1600 cm^{-1} (Fig. 6.7). The former is known as the D-band, which is derived from the defect and/or edge (= surface functional group) structure of AC, while the latter peak is known as G-band, which is derived from the graphene structure of AC (Fig. 6.8). The A_D/A_G ratio of chemical-activated carbon (A-powder and G-powder) was much smaller (2.3-2.6; Table 6.3) than that of steam-activated carbon (B-powder, C-powder, D-powder, E-powder, and F-powder; 3.1-4.2; Table 6.3), indicating that graphene structure is well-developed in the chemical-activated carbon. This might be due to the difference in the

activation process between steam- and chemical-activated carbons.

In the steam-activation process, carbon is removed from the structure via its transformation into CO or CO_2 to form fine pores as following equations;

$$C + H_2O \rightarrow CO + H_2O \quad \text{(Eq. 6-3)}$$

$$C + 2H_2O \rightarrow CO_2 + 2H_2 \quad \text{(Eq. 6-4)}$$

Therefore, graphene structure is selectively decomposed, followed by the formation of finer pores with a large amount of defects (Fig. 6.9), resulting in a relatively bigger A_D/A_G ratio (Table 6.3).

On the other hand, in the chemical-activation process, fine pore is formed via the dehydration from water-containing organic compounds, but leaving the carbon in the AC structure.

$$n(C_6H_{10}O_5) + ZnCl \rightarrow n(6C + 5H_2O) + ZnCl_2 \quad \text{(Eq. 6-5)}$$

Since the decomposition of graphene structure hardly occurs, relatively coarser defects are formed, resulting in the formation of coarser pores (Fig. 6.10). Remained graphene structure with less defect in the chemical-activated carbon will be the reason of its smaller A_D/A_G ratio (Table 6.3).

Considering the extremely high electric conductivity of graphene, well-developed graphene structure in the chemical-activated carbon would realize the faster electron transfer mediated by AC. In conclusion, the activated method was found key properties determining the E_h-reducing ability of AC, and chemical-activated carbon (in this experiment, A-powder or G-powder) is considered suitable AC for E_h-controlling catalyst.

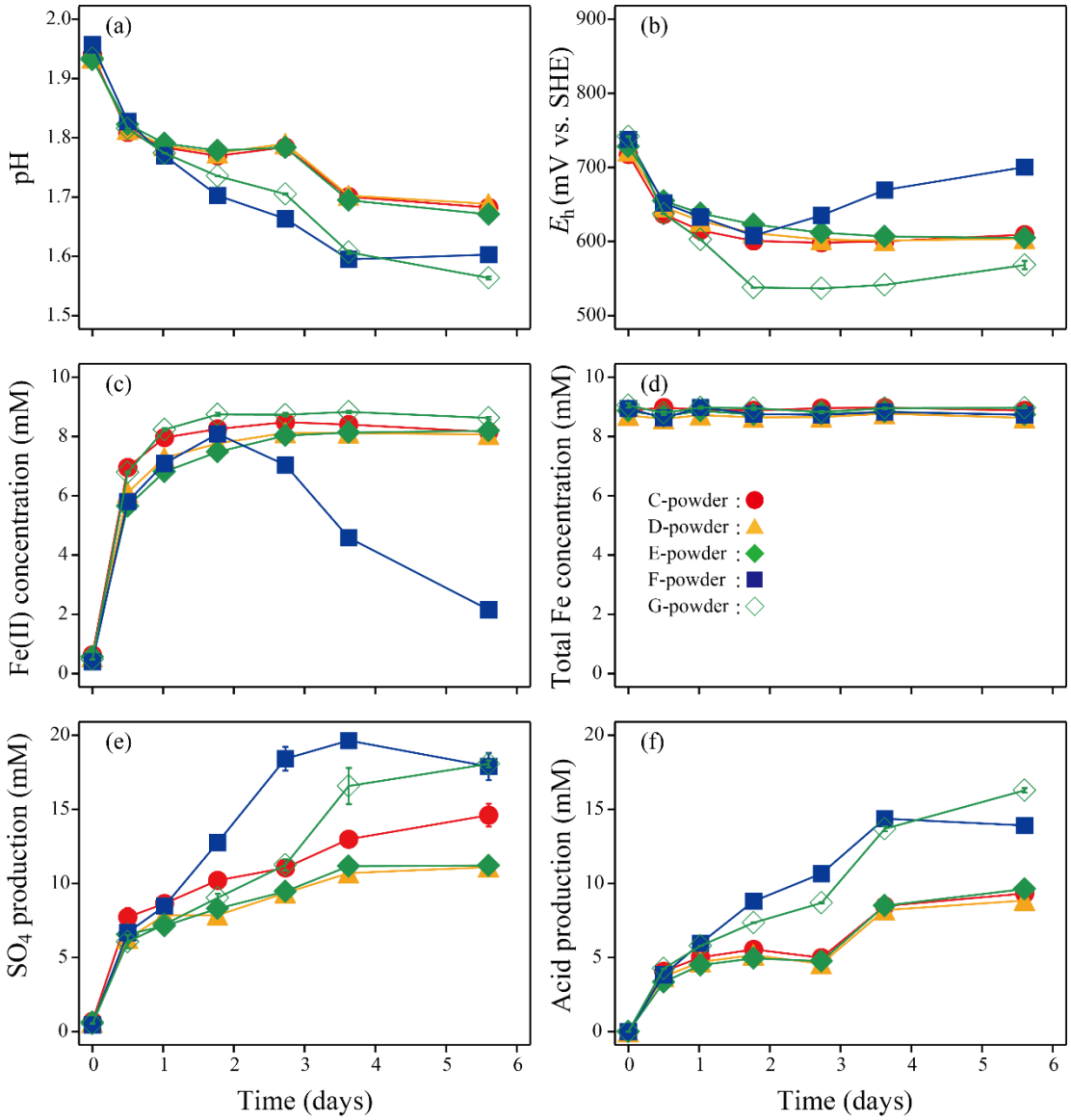

Fig. 6.6 Changes in pH (a), E_h (b), Fe^{2+} concentration (c), total Fe concentration (d), sulfate production (e), and acid production (f) during abiotic experiment in the presence of 10 mM Fe^{3+} and 5 mM sodium tetrathionate for the evaluation of catalytic capability of various AC: C-powder (●), D-powder (▲), E-powder (◆), F-powder (■), and G-powder (◇). Data points are mean values from duplicate cultures. Error bars depicting averages are not visible in some cases as they are smaller than the data point symbols.

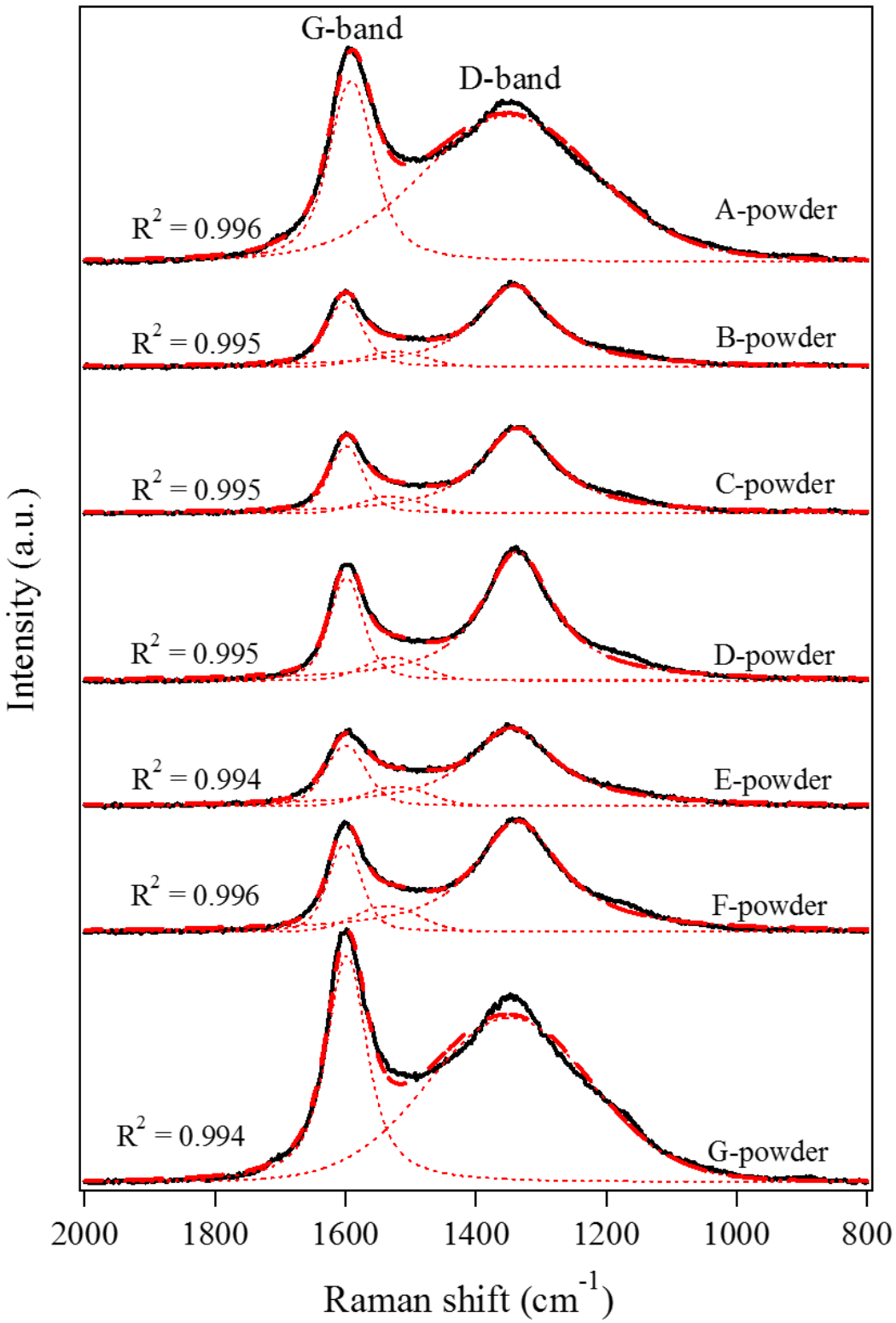

Fig. 6.7 Raman spectra of various AC (A-powder, B-powder, C-powder, D-powder, E-powder, F-powder, and G-powder). Black solid line and red broken line indicate the original Raman spectra and peak fitting result, respectively.

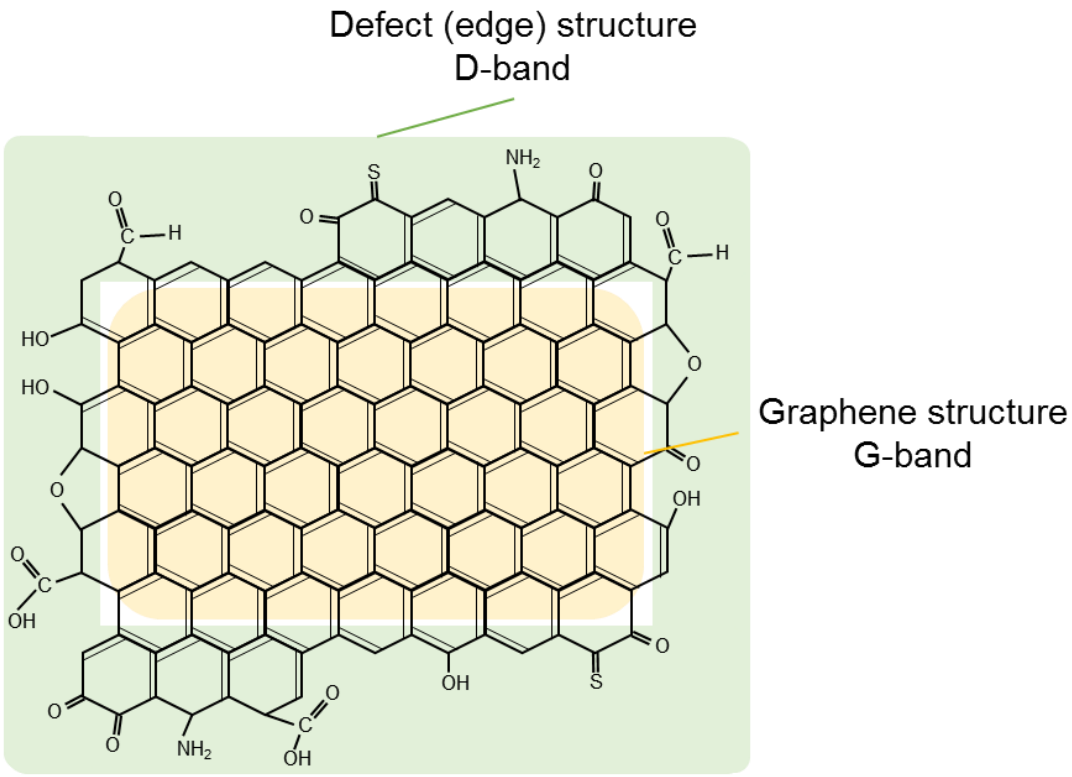

Fig. 6.8 Schematic image of G-band and D-band structure.

Table 6.3 D-band/G-band ratio of each AC. I_i, A_i indicates that fitting peak intensity and area, respectively.

	original	fitting	
	I_D/I_G	I_D/I_G	A_D/A_G
A-powder	0.753	0.805	2.627
B-powder	1.127	1.252	3.119
C-powder	1.151	1.253	3.212
D-powder	1.081	1.269	3.449
E-powder	1.032	1.270	4.075
F-powder	1.071	1.287	3.426
G-powder	0.743	0.727	2.263

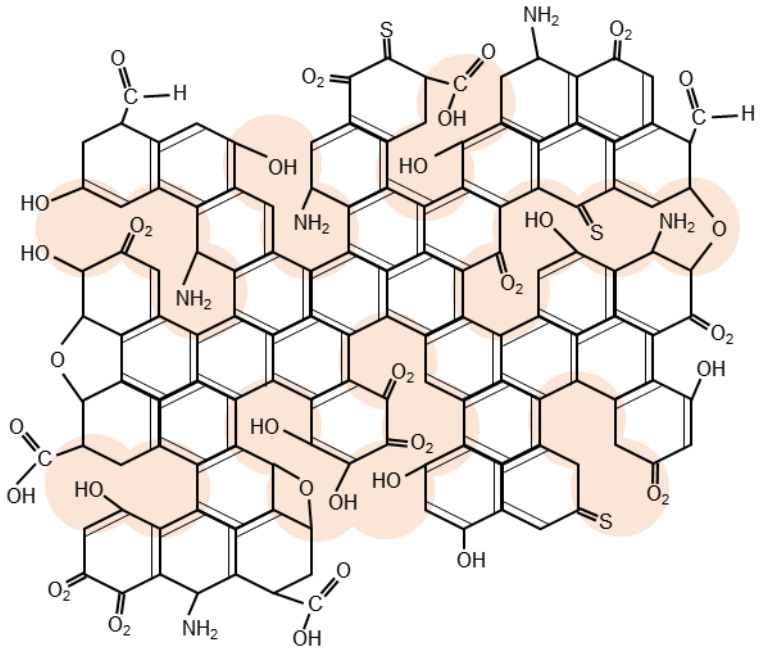

Fig. 6.9 Schematic image of steam-activated carbon. Highlighted area with orange color indicates the finer defects formed in the activation process.

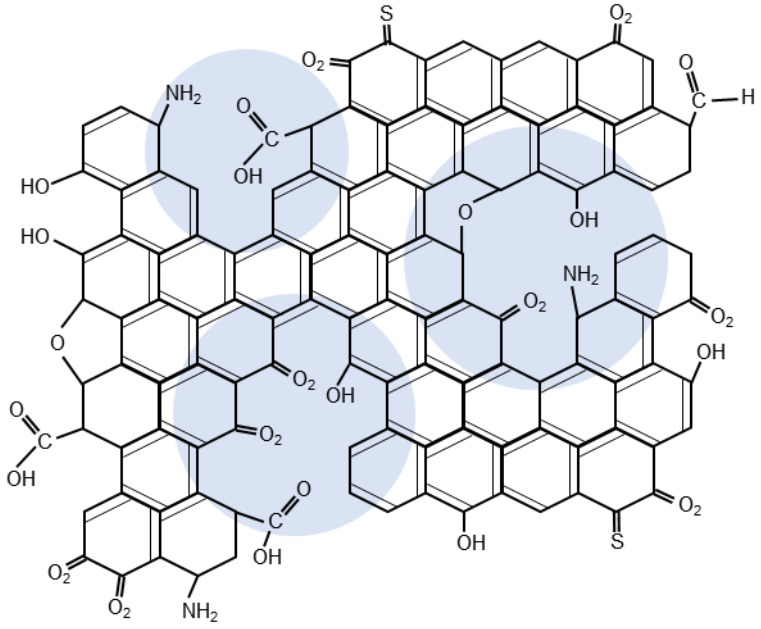

Fig. 6.10 Schematic image of chemical-activated carbon. Highlighted area with blue color indicates the coarser defects formed in the activation process.

Regarding the C-powder and D-powder, even though the specific surface area of the former (1683 m^2/g) was rather higher than that of the latter (1075 m^2/g), almost similar trend of E_h was observed (Fig. 6.6b). Since the difference between two of them is the only activation degree (same activation method and raw material), it was confirmed that E_h-reducing ability was not determined by activation degree; in other words, specific surface area and total pore volume. Likewise, the difference of raw material (D-powder: coconut shell, E-powder: woody chip) hardly affected on the E_h-reduction trend. On the other hand, in the culture containing F-powder (made of coal), E_h started to rapidly increase at day 2 (Fig. 6.6b), accompanied by the continuous oxidation of Fe^{2+} to Fe^{3+} until the end of the experiment (Fig. 6.6c). Considering the almost complete consumption of tetrathionate in this case (20 mM of sulfate is theoretically produced when 5 mM of tetrathionate is completely oxidized), it was assumed that tetrathionate-oxidation by H_2O_2 produced on the AC surface would be the predominant reaction rather than Fe^{3+}-reduction coupled with tetrathionate-oxidation. Hence, tetrathoinate would be lacked for continuous Fe^{3+}-reduction, resulting in the initiation of E_h rise via the oxidation of once reduced Fe^{2+} to Fe^{3+}.

Based on the Eq. 6-1, the presence of large amount of oxidative type surface functional group on the AC surface is thought favorable for H_2O_2 production and following oxidation reaction. In order to clarify the difference of surface functional groups among 7 AC, ATR-FT-IR analysis was conducted (Fig. 6.11); note that FT-IR analysis is often carried out as a qualitative analysis method rather than a quantitative method (Biniak et al., 1997). The bands at around 1700 cm^{-1} (1682, 1704, 1752, and 1793 cm^{-1}; Fig. 6.11), which were observed in all AC analyses, were likely due to the stretching vibrations of C=O in ketone (derived from carbonyl, quinone, and aldehydes), carboxyl, and anhydride. The other broad peak at 1061 cm^{-1} might be assigned to C-O-C bonding in ester (derived from lactone) or ether (Fig. 6.11). Even though slight difference in the peak intensity of these oxidative type surface functional group was observed, notable changes, which is assumed significantly influential on H_2O_2 production ability of AC, was not detected. This resulted in the unclear understanding of the relationship between the oxidative ability of AC and surface functional group on its surface, suggesting the necessity of further investigation of surface functional group on AC.

Unfortunately, the clear difference in surface functional group was not detected by

ATR-FT-IR (Fig. 6.11), though A_D/A_G ratio of F-powder is indeed the highest among 7 AC tested in this study (Table 6-3), possibly implying that plentiful surface functional groups on the surface of F-powder could be the reason of its stronger oxidative ability. In summary, following reactions are catalyzed by AC with different priority depending on the type of AC;

(i) Fe^{3+}-reduction coupled with tetrathionate-oxidation (E_h-reducing reaction)

(ii) Fe^{2+}-oxidation (E_h-rising reaction)

(iii) tetrathionate-oxidation (consequently leading to E_h-rise)

Although each reaction could occur in parallel, reaction (i) is basically predominant reaction in the presence of both Fe^{3+} and tetrathionate regardless of AC-type. This trend would be more noticeable when chemical-activated carbon is used due to its high performance as an electron mediator based on the high electric conductivity of massive graphene structure. On the other hand, reaction (ii) and (iii) would be strongly promoted by AC made of coal, likely resulting from its plentiful surface functional groups. Overall, it was concluded that chemical-activated carbon is the most desirable E_h-controlling catalyst for the bioleaching process.

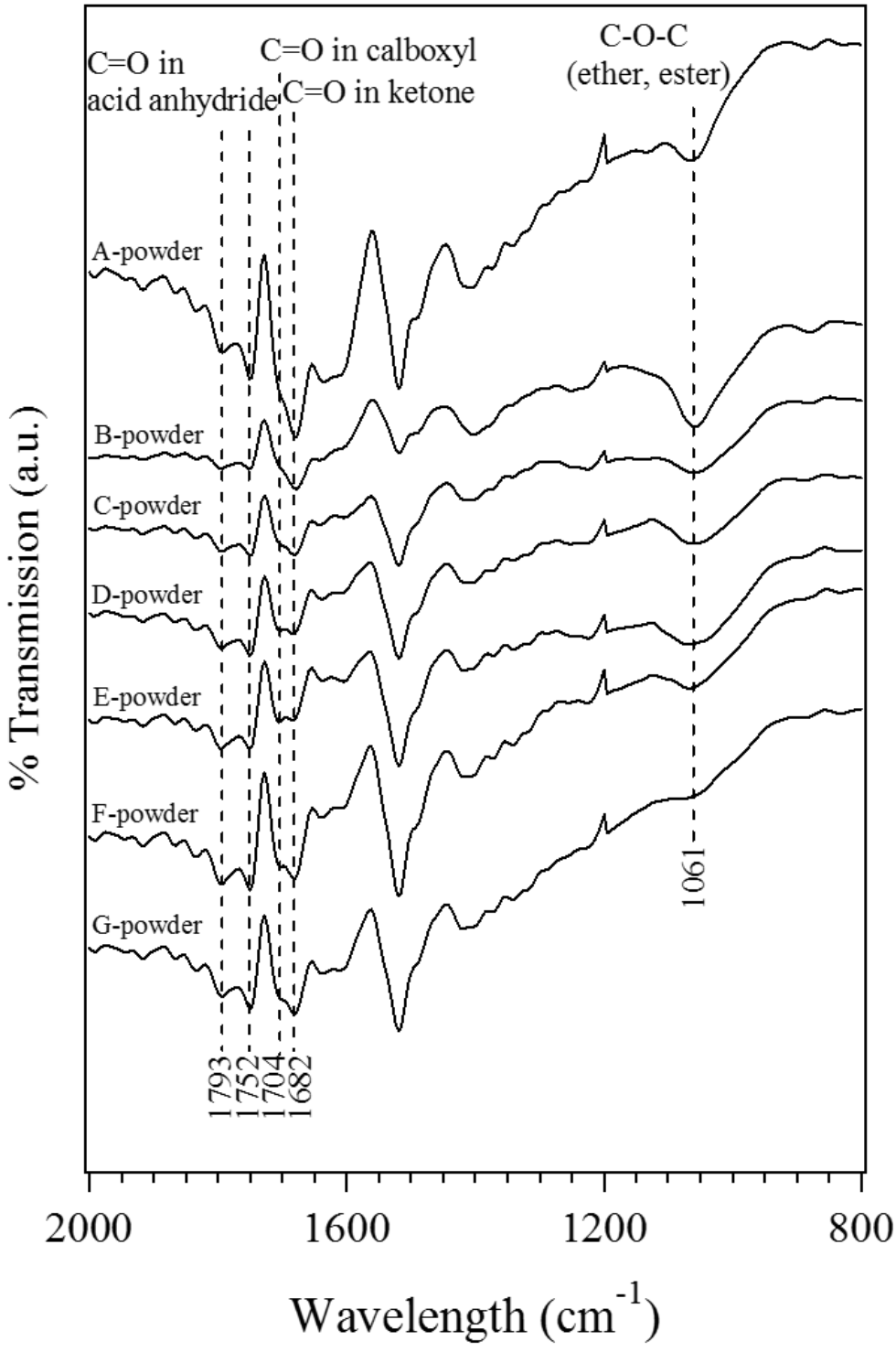

Fig. 6.11 The transmission ATR-FT-IR spectra of various AC (A-powder, B-powder, C-powder, D-powder, E-powder, F-powder, and G-powder) in the 2000-800 cm^{-1} range.

6.3.3 Varied catalytic effect of A-powder, B-granular, and B-powder on Cu solubilization and E_h-control during bioleaching of enargite concentrate

Based on the knowledge obtained by the abiotic test in section 6.3.1 and 6.3.2, the catalytic effect of different AC was evaluated in bioleaching of enargite concentrate. In this study, the AC used in section 6.3.1 (A-powder, B-granular, and B-powder) were also employed, since the contact between enargite and AC, which could contribute to Cu solubilization via the galvanic interaction, must be dominated by the AC size, while E_h-controlling ability was negligibly affected by the shape of AC (granular or powder) in section 6.3.1.

Bioleaching results using A-powder, B-granular, and B-powder as the AC catalyst were summarized in Fig. 6.12, 6.13, 6.14, respectively. In any cases, fundamental phenomena in the presence of each AC were basically same; (i) suppressed E_h-rise (Fig. 6.12b, 6.13b, 6.14b), (ii) deteriorated Fe dissolution (= pyrite dissolution; Fig. 6.12f, 6.13f, 6.14f), (iii) prolonged Cu solubilization (= enargite dissolution; Fig. 6.12e, 6.13e, 6.14e), and (iv) improved As immobilization and its re-solubilization (Fig. 6.12h, 6.13h, 6.14h). Cell density was the only parameter obviously affected by the shape of AC. The sharp decrease in planktonic cell density at the beginning of the experiment was visible in the presence of powder AC (A-powder and B-powder; Fig. 6.12c and 6.14c), which was not confirmed with B-granular (Fig. 6.13c); note that the lowest value of y-axis in Fig. 6.12c and 6.14c was 10^6 cells/mL, while that in Fig. 6.13c was 10^7 cells/mL. This was likely the result of the difference in contact frequency between microorganisms and AC. Since the number of powder AC particles in solution was extremely higher than that of granular AC, more frequent contacts with the microorganisms occurred, possibly leading to immobilization of cells by attaching on the AC surface.

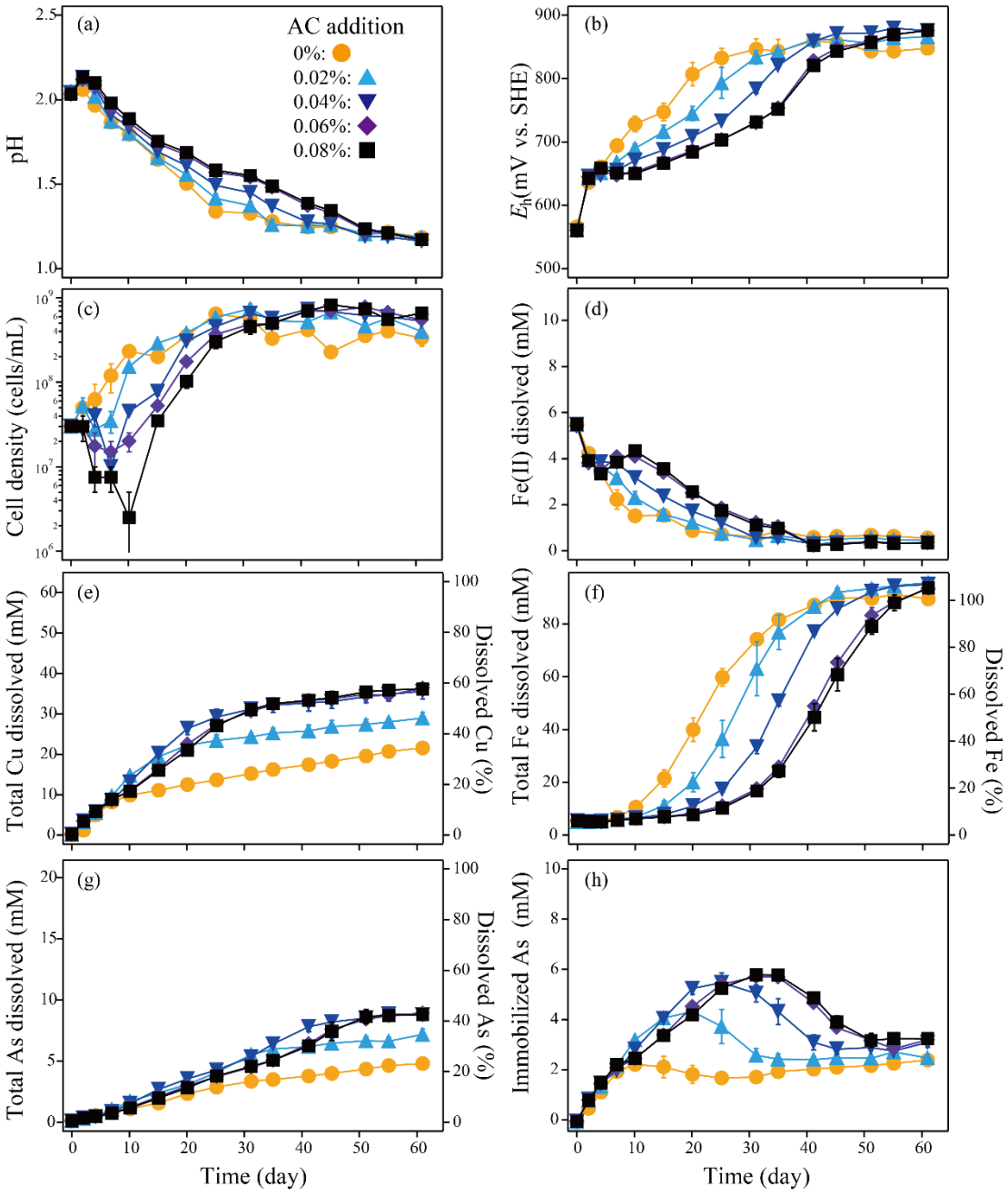

Fig. 6.12 Summary of results in bioleaching of enargite concentrate in the absence (●) or presence of 0.02 (▲), 0.04 (▼), 0.06 (◆), and 0.08% (w/v) (■) A-powder as the AC catalyst; (a) pH, (b) E_h, (c) cell density , (d) Fe^{2+} concentration, (e) total Cu concentration, (f) total Fe concentration, (g) total As concentration, and (f) immobilized As concentration. Data points are mean values from duplicate cultures. Error bars depicting averages are not visible in some cases as they are smaller than the data point symbols.

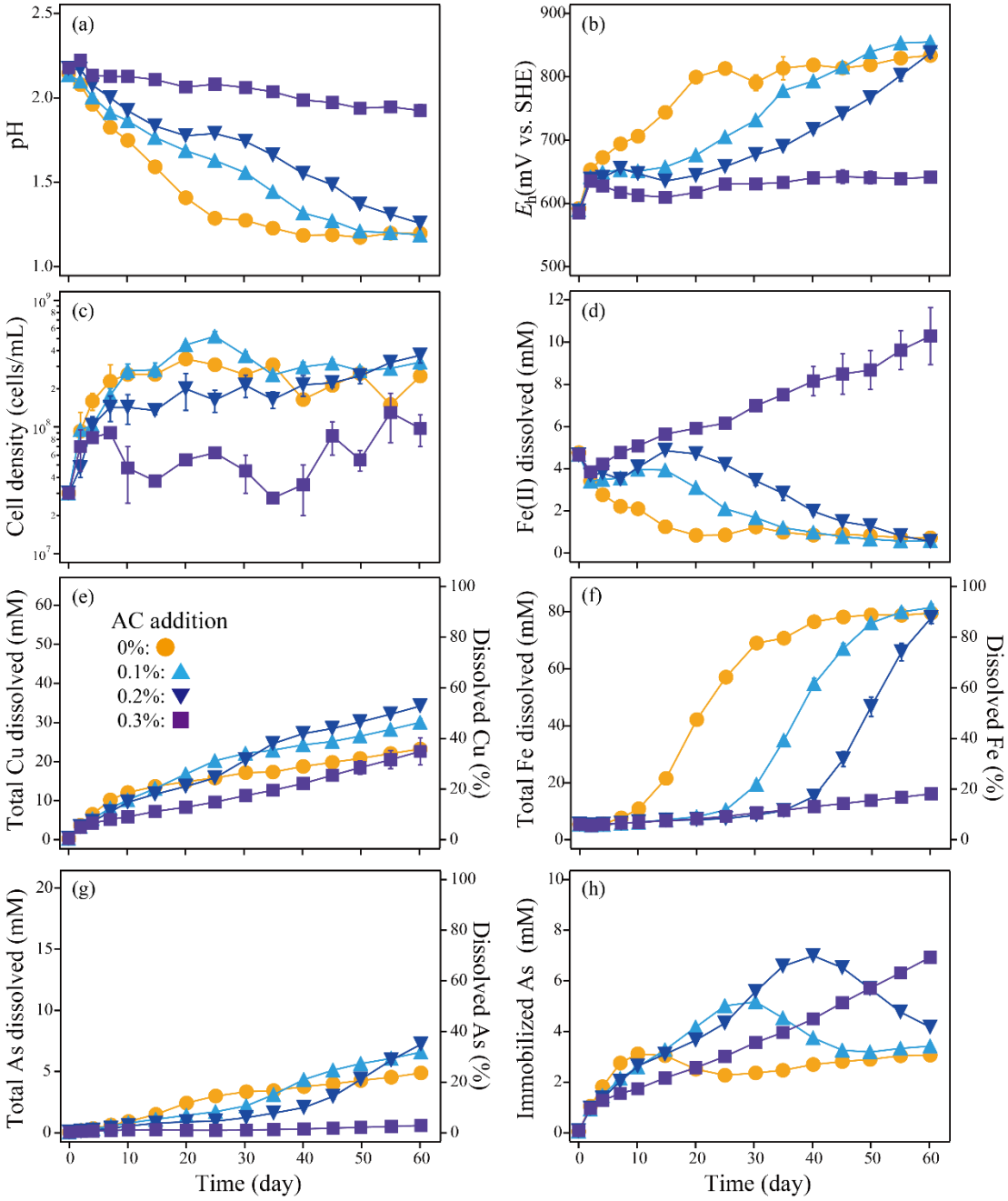

Fig. 6.13 Summary of results in bioleaching of enargite concentrate in the absence (●) or presence of 0.1 (▲), 0.2 (▼), and 0.3% (w/v) (■) B-granular as the AC catalyst; (a) pH, (b) E_h, (c) cell density , (d) Fe^{2+} concentration, (e) total Cu concentration, (f) total Fe concentration, (g) total As concentration, and (f) immobilized As concentration. Data points are mean values from duplicate cultures. Error bars depicting averages are not visible in some cases as they are smaller than the data point symbols.

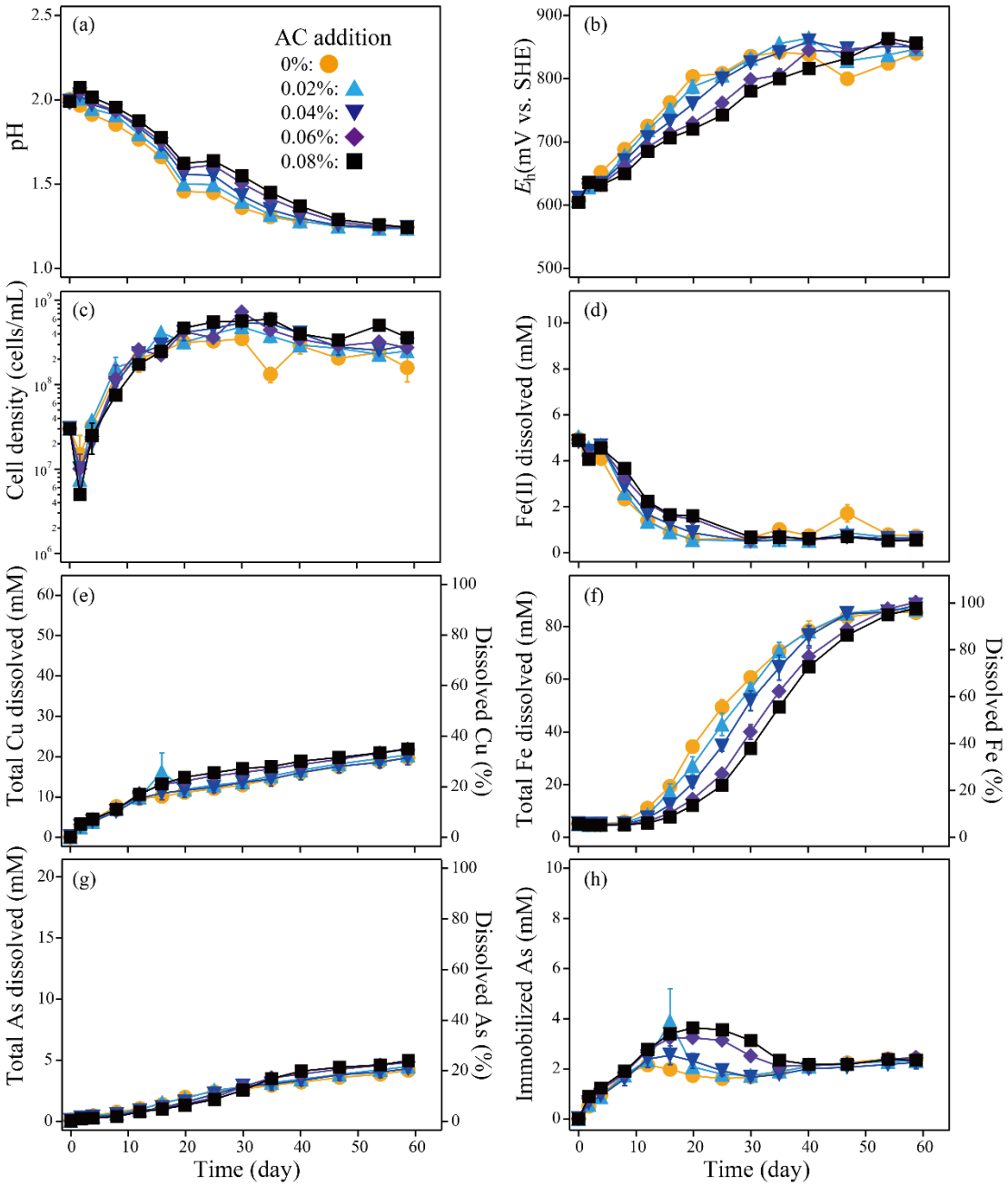

Fig. 6.14 Summary of results in bioleaching of enargite concentrate in the absence (●) or presence of 0.02 (▲), 0.04 (▼), 0.06 (◆), and 0.08% (w/v) (■) B-powder as the AC catalyst; (a) pH, (b) E_h, (c) cell density , (d) Fe^{2+} concentration, (e) total Cu concentration, (f) total Fe concentration, (g) total As concentration, and (f) immobilized As concentration. Data points are mean values from duplicate cultures. Error bars depicting averages are not visible in some cases as they are smaller than the data point symbols.

For the clear comparison, changes in E_h, total Cu, Fe, and As concentration in each culture were summarized in Fig. 6.15, respectively. The bioleaching result obtained under similar conditions, in the presence of 0.08% A-powder, 0.08% B-powder, and 0.1% B-granular, were selected for the fair comparison.

Seemingly, E_h trend was hardly affected by AC-type (Fig. 6.15a), though the difference was more noticeable on the AC-catalyzed E_h-reduction (Fig. 6.16). Strong E_h-reduction was maintained by A-powder in the long-term period, proving the superiority of chemical-activated carbon in the E_h-controlling ability as was found in section 6.3.1 and 6.3.2. As a result of lowered E_h by AC, Fe dissolution (= pyrite dissolution) was deteriorated (Fig. 6.15c), which enabled the prolonged enargite dissolution without Fe passivation (Fig. 6.15b).

Interestingly, the highest Cu recovery (58% at day 61) was achieved by the addition of A-powder (Fig. 6.15b), even though the successive AC-catalyzed E_h-reduction was realized in this culture (Fig. 6.16); higher E_h is theoretically favorable for the faster enargite dissolution (Lattanzi et al., 2008). In order to understand the reason of this contradiction, kinetic fitting using shrinking core model was conducted for each culture (Fig. 6.17 and 6.18). All results were obviously well-fit to surface chemical reaction model (Fig. 6.17) rather than diffusion through product film model (Fig. 6.18), indicating that the fundamental reaction mechanism was unlikely changed by AC-type. However, it was found that the increasing addition of powder AC (A-powder, B-powder) enabled to retain the relatively faster dissolution kinetics of enargite (around 0.006-0.008), while that of granular AC (B-granular) significantly reduced the kinetic constant from 0.0081 (without B-granular) to 0.0021 (with 0.3% B-granular). This suggests that the former AC-type might slightly enhance the enargite dissolution, possibly based on the galvanic reaction, leading to the cancelling out of the slowed enargite dissolution derived from AC-catalyzed lowered E_h. Even though the effect of galvanic interaction in the individual contact was found negligibly small (see chapter 5), the numerous particle number of powder AC would repeatedly cause the reaction due to its high contact frequency, likely resulting in the noticeable contribution of galvanic effect to enargite dissolution. In conclusion, the utilization of powder AC during bioleaching process was found effective in retaining faster enargite dissolution, but not in AC-catalyzed E_h-controlling.

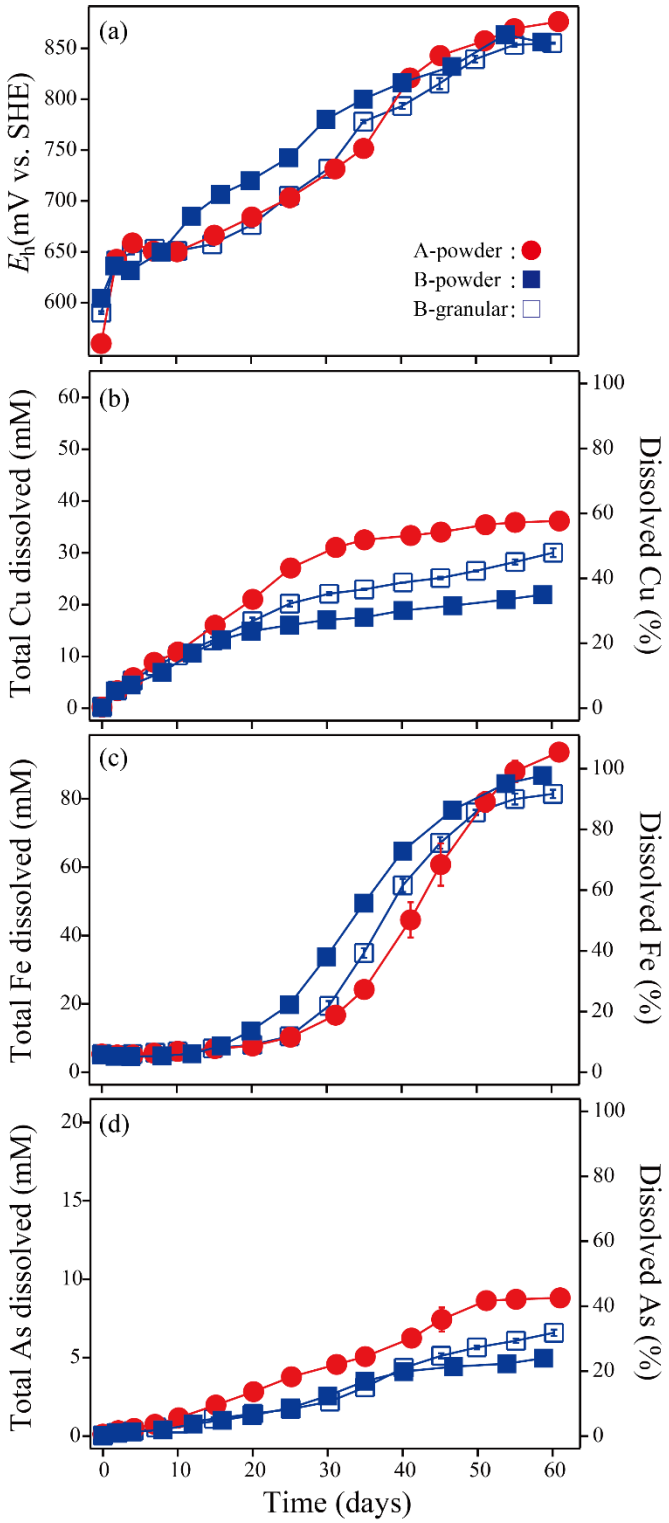

Fig. 6.15 Comparison of the results obtained from bioleaching of enargite concentrate in the presence of 0.08% A-powder (●), 0.08% B-powder (■), or 0.1% B-granular (□); (a) E_h, (b) total Cu concentration, (c) total Fe concentration, and (d) total As concentration.

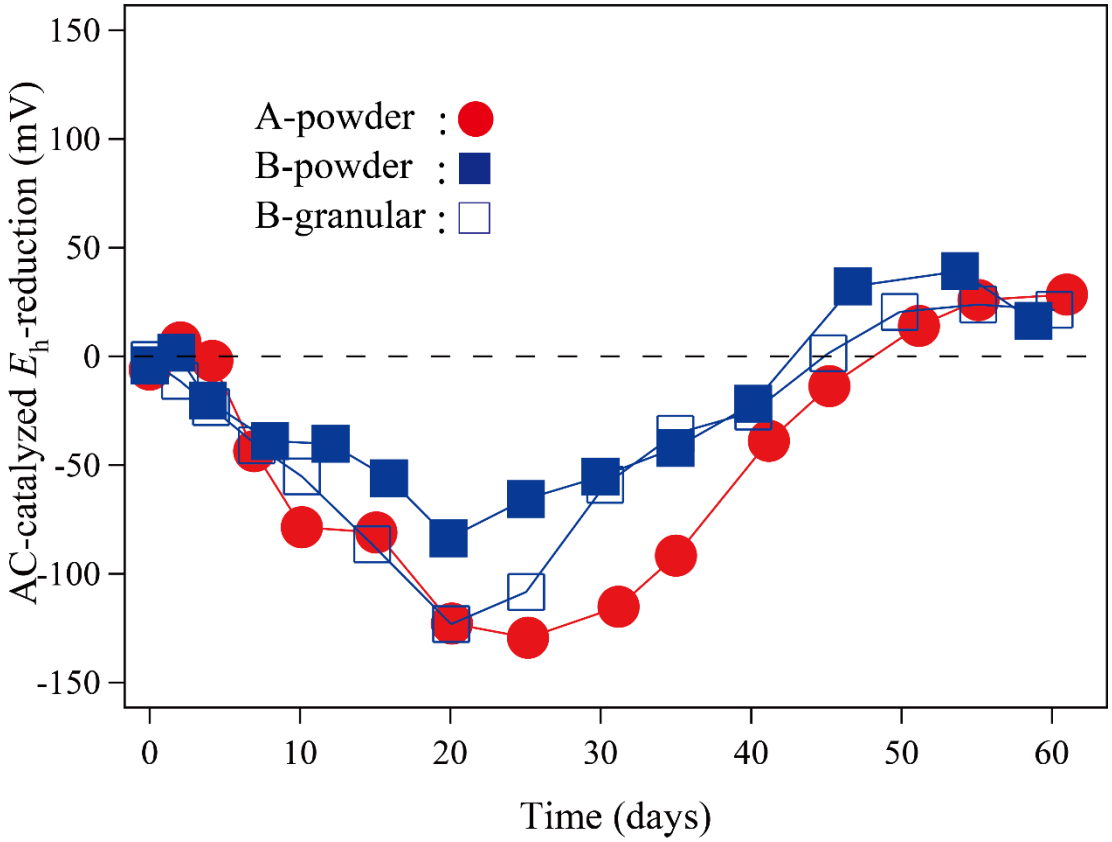

Fig. 6.16 AC-catalyzed E_h-reduction during bioleaching of enargite concentrate in the presence of 0.08% A-powder (●), 0.08% B-powder (■), or 0.1% (w/v) B-granular (□). E_h value in each bioleaching culture without AC was normalized to 0 (broken line). The plots depict the difference in E_h between culture without AC and with AC: E_h [bioleaching without AC] – E_h [bioleaching with AC].

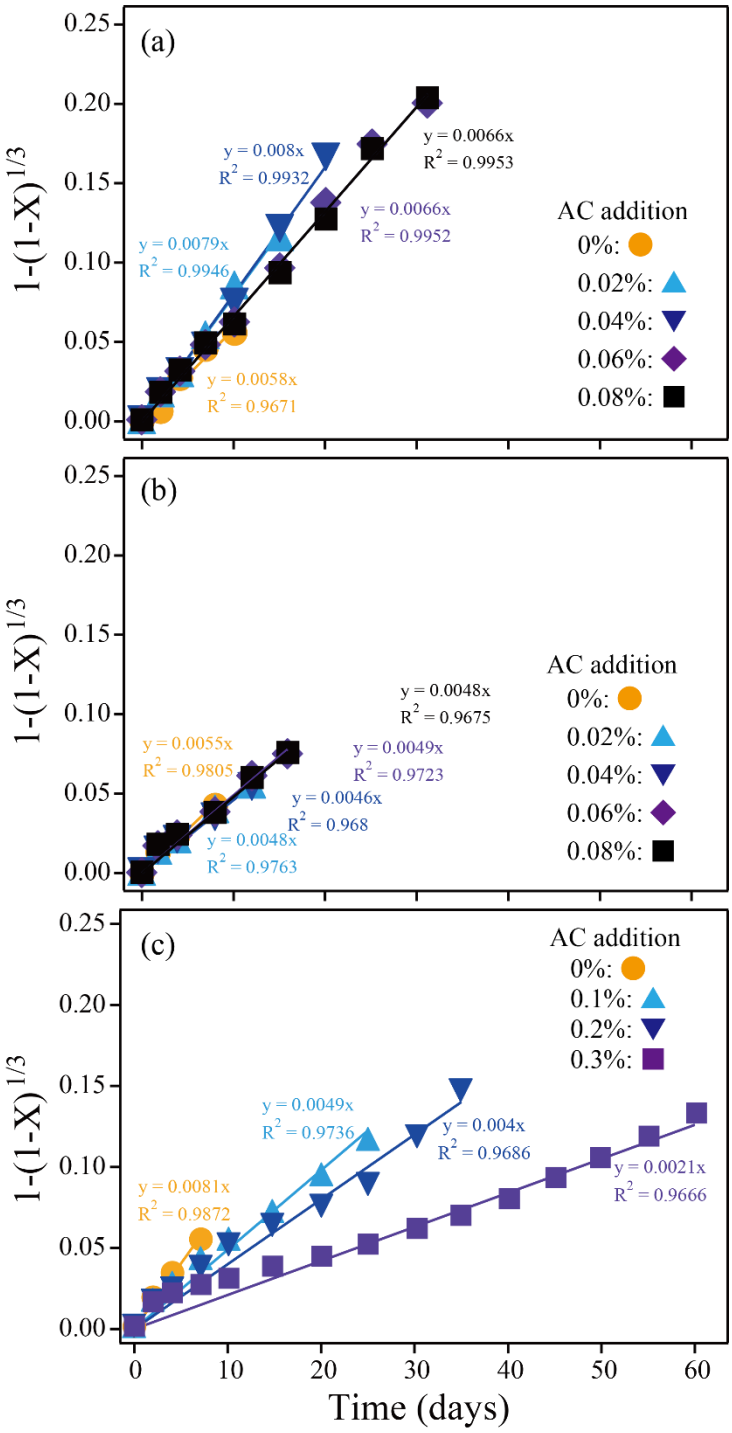

Fig. 6.17 Kinetic fitting with surface chemical reaction model on bioleaching of enargite concentrate in the presence of 0 (●), 0.02 (▲), 0.04 (▼), 0.06 (◆) and 0.08% (■) A-powder (a) or B-powder (b), or 0 (●), 0.1 (▲), 0.2 (▼), and 0.3% (■) B-granular (c). Fitting duration was restricted until when rapid Fe dissolution was initiated during bioleaching.

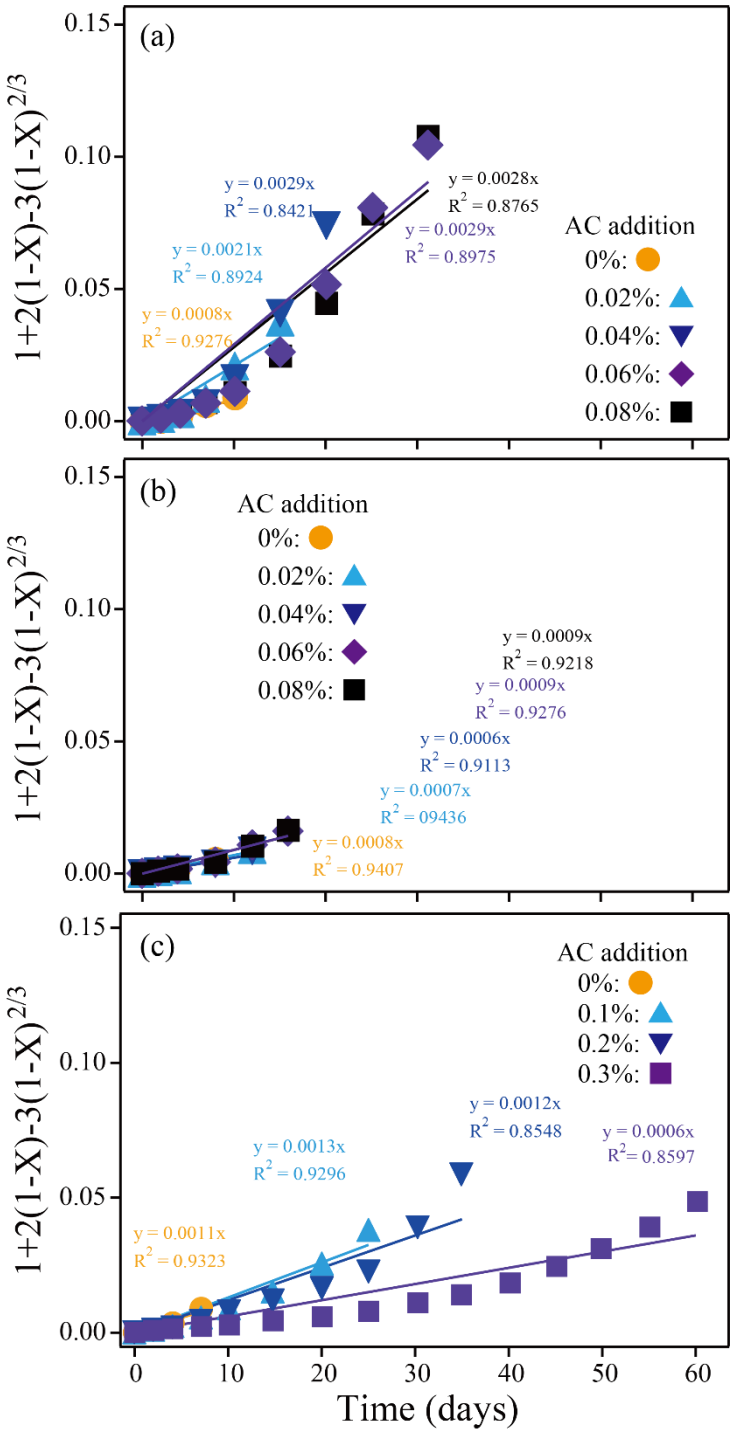

Fig. 6.18 Kinetic fitting with diffusion through product film model on bioleaching of enargite concentrate in the presence of 0 (●), 0.02 (▲), 0.04 (▼), 0.06 (◆) and 0.08% (■) A-powder (a) or B-powder (b), or 0 (●), 0.1 (▲), 0.2 (▼), and 0.3% (■) B-granular (c). Fitting duration was restricted until when rapid Fe dissolution was initiated during bioleaching.

6.4 Conclusions

Based on the series of abiotic tests evaluating the catalytic effect of various AC and their application into bioleaching culture, catalytic mechanism, especially in terms of E_h-control and Cu solubilization, were summarized as below.

1. E_h-controlling ability of AC

It was found that E_h-controlling ability of AC is determined by the structural property such as graphene and defect (edge) structure formed during the activation process, but not shape (powder or granular), specific surface area, and total pore volume. Due to the extremely high electric conductivity of graphene, AC with massive graphene structure would enable faster electron transfer for the coupling reaction that occurred on the AC surface. On the other hand, AC with plentiful defect structure is more advantageous in the oxidation reaction (e.g. Fe^{2+}- and tetrathionate-oxidation), since the abundant surface functional group in the defect structure might catalyze the H_2O_2 production on the AC surface, followed by its consumption for the oxidation reaction. Only AC made of coal, possessing the largest amount of defect structure among AC tested in this study, shows stronger oxidation ability than that made of coconut shell and woody chip, while no difference was confirmed in E_h-reducing ability among three of them. Chemical-activated carbon is thought the best E_h-controlling AC due to its well-developed graphene structure, whilst the abundant defect structure in steam-activated carbon is undesirable for E_h-controlling catalyst.

2. Enhancement of Cu solubilization from enargite

Even though the contribution of the galvanic effect is negligibly small in the individual contact, extremely increased contact frequency by employing the powder AC could maximize the effect of galvanic interaction. As a result, slowed enargite dissolution by AC-catalyzed E_h-reduction was likely canceled out, resulting in retained faster enargite dissolution even in the presence of AC. This observation suggests that, therefore, finer AC must be used for the improvement of Cu solubilization from enargite.

Overall, powder AC made by the chemical-activation process is the best AC catalyst for bioleaching of enargite concentrate in terms of E_h-controlling ability and improved Cu solubilization.

References

1. Abdollahi, H., Noaparast, M., Shafaei, S.Z., Manafi, Z., Muñoz, J.A. and Tuovinen, O.H., 2015. Silver-catalyzed bioleaching of copper, molybdenum and rhenium from a chalcopyrite–molybdenite concentrate. International Biodeterioration & Biodegradation 104, 194-200.
2. Ahonen, L. and Tuovinen, O.H., 1990. Catalytic effects of silver in the microbiological leaching of finely ground chalcopyrite-containing ore materials in shake flasks. Hydrometallurgy 24, 219-236.
3. Ahumada, E., Lizama, H., Orellana, F., Suárez, C., Huidobro, A., Sepúlveda-Escribano, A. and Rodrıguez-Reinoso, F., 2002. Catalytic oxidation of Fe(II) by activated carbon in the presence of oxygen: Effect of the surface oxidation degree on the catalytic activity. Carbon 40, 2827-2834.
4. Ballester, A., Gonzalez, F., Blázquez, M. and Mier, J., 1990. The influence of various ions in the bioleaching of metal sulphides. Hydrometallurgy 23, 221-235.
5. Biniak, S., Szymański, G., Siedlewski, J. and Świątkowski, A., 1997. The characterization of activated carbons with oxygen and nitrogen surface groups. Carbon 35, 1799-1810.
6. Feng, S., Yang, H., Xin, Y., Gao, K., Yang, J., Liu, T., Zhang, L. and Wang, W., 2013. A novel and highly efficient system for chalcopyrite bioleaching by mixed strains of *Acidithiobacillus*. Bioresource Technology 129, 456-462.
7. Gomez, E., Ballester, A., Blázquez, M. and González, F., 1999. Silver-catalysed bioleaching of a chalcopyrite concentrate with mixed cultures of moderately thermophilic microorganisms. Hydrometallurgy 51, 37-46.
8. Hao, X., Liu, X., Zhu, P., Chen, A., Liu, H., Yin, H., Qiu, G. and Liang, Y., 2018. Carbon material with high specific surface area improves complex copper ores' bioleaching efficiency by mixed moderate thermophiles. Minerals 8, 301.
9. Jahromi, F.G. and Ghahreman, A., 2018. In-situ oxidative arsenic precipitation as scorodite during carbon catalyzed enargite leaching process. Journal of Hazardous Materials 360, 631-638.
10. Johnson, D.B., Okibe, N., Wakeman, K. and Yajie, L., 2008. Effect of temperature on the bioleaching of chalcopyrite concentrates containing different concentrations of silver. Hydrometallurgy 94, 42-47.
11. Lattanzi, P., Da Pelo, S., Musu, E., Atzei, D., Elsener, B., Fantauzzi, M. and Rossi, A., 2008. Enargite oxidation: A review. Earth-Science Reviews 86, 62-88.
12. Muñoz, J., Dreisinger, D., Cooper, W. and Young, S., 2007. Silver-catalyzed bioleaching of low-grade copper ores.: Part I: Shake flasks tests. Hydrometallurgy

88, 3-18.

13. Nakazawa, H., Fujisawa, H. and Sato, H., 1998. Effect of activated carbon on the bioleaching of chalcopyrite concentrate. International Journal of Mineral Processing 55, 87-94.
14. Sato, H., Nakazawa, H. and Kudo, Y., 2000. Effect of silver chloride on the bioleaching of chalcopyrite concentrate. International Journal of Mineral Processing 59, 17-24.
15. Xia, J.-l., Song, J.-j., Liu, H.-c., Nie, Z.-y., Shen, L., Yuan, P., Ma, C.-y., Zheng, L. and Zhao, Y.-d., 2018. Study on catalytic mechanism of silver ions in bioleaching of chalcopyrite by SR-XRD and XANES. Hydrometallurgy 180, 26-35.
16. Yuehua, H., Guanzhou, Q., Jun, W. and Dianzuo, W., 2002. The effect of silver-bearing catalysts on bioleaching of chalcopyrite. Hydrometallurgy 64, 81-88.

Chapter 7

Application study;
AC-catalyzed bioleaching of As-bearing copper concentrate at high pulp density in the stirred tank reactor

Abstract

For the application of AC-catalyzed bioleaching to practical process, catalytic ability of AC was evaluated in bioleaching of As-bearing copper concentrate, composed of refractory (e.g. chalcopyrite, enargite) and easily soluble copper sulfide (chalcocite, geerite, bornite) at the high pulp density in the stirred tank reactor level. The consortia of moderate thermophiles was successfully adapted to As-bearing copper concentrate at high pulp density, by subsequently transferring the culture grown at lower pulp density to that at high pulp density; sterpwisely, increased from 2, 3, 5, 8, finally, to 10% (w/v). Two different amounts of AC (0.05% and 0.5% (w/v)) were indeed added into the 10% pulp density condition to investigate the catalytic ability of AC on high pulp density bioleaching in stirred tank reactor. The difference in final Cu recovery corrected by solution volume was hardly seen (38%, 38%, and 41% with 0, 0.05, and 0.5% AC, respectively), which became noticeable with the correction by both solution volume and the amount of unreacted residue (80%, 100%, and 98% with 0, 0.05, and 0.5% AC, respectively). The drops in abundance of chalcopyrite and enargite by the addition of AC were detected by MLA, likely resulting from their enhanced dissolution based on (i) AC-catalyzed E_h-control to the optimal potential, and (ii) high frequency of contact with AC accelerating the electron transfer (galvanic interaction). AC was also found effective in promoting As immobilization as the Fe-As precipitates revealed by MLA; the abundance of Fe-As precipitates dramatically improved from 11% (0% AC) to 53% (0.05%) and 61% (0.5%). Overall, AC-catalyzed bioleaching was successively found applicable to practical situation (high pulp density, complex mineralogy, stirred tank reactor).

7.1 Introduction

For the development of technique targeting the exploitation of refractory copper sulfides such as chalcopyrite and enargite, a number of bioleaching studies employing the reaction catalyst (e.g. Ag and AC) have been carried out (see Table 1.4). Nevertheless, most of these studies have been basically conducted as the fundamental research, especially in AC-catalyzed bioleaching: low-pulp density, concentrate with high purity, and flask level (Nakazawa et al., 1998; Liang et al., 2010; Ma et al., 2017)., Application study employing high-pulp density, complex mineralogy, and scale-up system must be thus investigated for the future implementation of AC-catalyzed bioleaching system into real mining operation.

There are the limited number of AC-catalyzed bioleaching study targeting complex copper sulfide ores under high pulp density condition (Zhang et al., 2007; Hao et al., 2018); the pulp density of each study was 25% and 10%, respectively. However, the used ores in both studies were low-grade copper sulfide ores containing only 1.1% and 0.38% of primary copper sulfide. The majority of these ores were quartz (SiO_2) or other kinds of silicate mineral such as feldspar and mica, indicating that physical contact between copper sulfides and AC was expected less occurred. For more appropriate evaluation of catalytic effect by AC, complex copper concentrate with less gangue minerals should be utilized instead of low-grade ores.

Arsenic accumulation in the leachate must be also serious issue during bioleaching of As-bearing mineral (e.g. enargite) at the high pulp density. Gradual increase in pulp density from 5% to 30% was tested in bioleaching of flotation gold concentrate containing As-bearing mineral such as enargite and tennantite ($Cu_{12}As_4S_{13}$), where obvious depression of metal extraction with increase of pulp density was indeed observed; almost 100% Cu at the pulp density of 5% was dropped to 30% at the pulp density of 30% (Astudillo and Acevedo, 2008). In this study, adapted culture to As-bearing gold concentrate was also prepared, which showed better metal extraction ability than non-adapted culture. These might be the indication that the condensed As during high pulp density bioleaching of As bearing concentrate could toxically inhibit the microbial activity, and it would become worse at the high pulp density condition.

Moreover, based on our knowledge, all AC-catalyzed bioleaching have been carried out in the flask shaking experiment (see Table 1.4). When this process would be scaled

up to stirred tank reactor, in addition to the factors ascribed above, the effects of physical collision between microorganisms and minerals, oxygen transfer, stirring efficiency, and mechanochemical damage to microbes by agitating propeller have to be taken into account. This could lead to different bioleaching behavior from flask level AC-catalyzed bioleaching, suggesting the necessity of test in stirred tank reactor level. In this section, based on the knowledge obtained in chapter 5 and 6, AC-catalyzed bioleaching system was therefore up-graded form flask to stirred tank reactor. At the same time, the catalytic effect of AC on the dissolution of As-bearing copper sulfide at the high pulp density was evaluated.

7.2 Materials and Methods

7.2.1 Adaptation of moderate thermophiles consortia to high pulp density bioreactor

The pulp density of bioreactor experiment was stepwisely increased from 2% to 10% in order to gradually adapt the consortia of moderate thermophiles to higher pulp density condition.

HBS media (1 L; pH adjusted to 2.0 with 1 M H_2SO_4) containing 0.02% (w/v) yeast extract was sterilized by autoclaving, which was added into the tank reactor vessel with 30 g of unwashed As-bearing copper sulfide concentrate, D3 concentrate (2% pulp density). These media were stirred and mixed at 45ºC for 1 day prior to inoculation, in order to solubilize the acid-soluble minerals and stabilize the solution condition. Pre-grown culture of four bacteria (*Am. ferrooxidans* ICP, *Sb. sibiricus* N1, *At. caldus* KU, and *Lp. ferriphilum* P_3A) and one archaeon (*Acidiplasma* sp. Fv-Ap) were collected (100 mL for each; 500 mL in total) and directly inoculated into the reactor so as to set the final culture volume to be 1.5 L. In this leaching experiment, pH was automatically kept at 2.0 by adding 0.5 M H_2SO_4 and 0.5 M NaOH throughout the experiment. Temperature was held constant at 45˚C. The bioreactor were aerated with 0.5 L/min and stirred at 150 rpm. Samples were regularly withdrawn to monitor pH, E_h, cell density, and concentrations of total Fe, As, and Cu.

For the bioreactor experiment at the pulp density of 3%, 300 mL of bioreactor culture at the 2% pulp density was used as the inoculum and 1.2 L of HBS media containing 0.02% yeast extract was also added (final volume: 1.5 L) with 45 g of D3 concentrate. At the beginning, the pH was set to be 1.8 to prevent excess Fe precipitation, while it was re-set to 2.0 at day 7 since no cell growth was observed. To enhance the microbiological activity, aeration rate was increased to 1.0 L/min. Other experimental conditions were same with that at 2% pulp density.

For the further improvement of pulp density (5, 8, 10%), pH setting was kept at 2.0 throughout the experiment. Desired amount of D3 concentrate (75 g, 120 g, and 150 g for 5, 8, and 10% pulp density, respectively) was added into the tank reactor vessel with 1.2 L HBS media and 300 mL of previous bioreactor culture (3→5%, 5→8%, 8→10%).

7.2.2 AC-catalyzed bioleaching of D3 concentrate at the pulp density of 10% in the stirred tank reactor

HBS media (1.2 L; pH adjusted to 2.0 with 1 M H_2SO_4) containing 0.02% (w/v) yeast extract was sterilized by autoclaving, which was added into the tank reactor vessel with 150 g of unwashed D3 concentrate (10% pulp density). Two different amount of AC (0.05% and 0.5% (w/v) of A-powder) were also added as the catalyst. These media were stirred and mixed at 45ºC for 1 day prior to inoculation, in order to solubilize the acid-soluble minerals and stabilize the solution condition. Pre-grown bioreactor culture at the pulp density of 10% (300 mL) was added as the inoculum so as to set the final volume to be 1.5 L. Solution pH was automatically kept at 2.0 by adding 0.5 M H_2SO_4 and 0.5 M NaOH throughout the experiment. Temperature was held constant at 45˚C. The bioreactor were aerated with 1.0 L/min and stirred at 150 rpm. Samples were regularly withdrawn to monitor pH, E_h, cell density, and concentrations of Fe^{2+} (*o*-phenanthroline method), As(III) (molybdenum blue method), and total Fe, As, and Cu (ICP-OES).

7.3 Results and Discussion

7.3.1 Stepwise adaptation of moderate thermophiles to high pulp density of D3 concentrate

The adaptation of moderate thermophiles to high pulp density of D3 concentrate were successfully achieved by subsequently transferring the culture pre-grown at lower pulp density to new culture at higher pulp density. At the beginning of the experiment, high pH varied from 2.4 to5.4 were observed in any cultures, whereas the pH of medium was set to 2.0 (Fig. 7.1a). This would be due to the dissolution of easily soluble copper sulfide and small fraction of chalcopyrite, which consume the proton during their dissolution process as follows;

$$CuFeS_2 + O_2 + 4H^+ \rightarrow Cu^{2+} + Fe^{2+} + 2S^0 + 2H_2O \quad \text{(Eq. 7.1)}$$

$$2CuS_2 + O_2 + 4H^+ \rightarrow 2Cu^{2+} + 4S^0 + 2H_2O \quad \text{(Eq. 7.2)}$$

$$2CuS + O_2 + 4H^+ \rightarrow 2Cu^{2+} + 2S^0 + 2H_2O \quad \text{(Eq. 7.3)}$$

After day 1, pH were lowered and perfectly controlled to 2.0 in all cultures (or 1.8 in 3% pulp density culture) to prepare the suitable condition for active cell growth (Fig. 7.1a). Rapid increase of cell density up to around 6×10^8 cells/mL with short lag phase were thus observed in almost all cultures, while the lag phase was longer in the culture at the pulp density of 3% (Fig. 7.1c). Lower initial pH (1.8) compared to other cultures (2.0) might cause less Fe precipitation, likely allowing the toxic elements contained in D3 concentrate (e.g. As, Cd, Pb) to be mobile in solution phase. This was prevented by re-setting the pH to 2.0 at day 7, followed by rapid increase in cell number (Fig. 7.1c). The faster cell growth with increase in pulp density were apparently seen, which might be attributed to (i) microbial adaptation to this concentrate or (ii) miss-counting of mineral particles. Although the microbiological analyses have been insufficient, it was assumed the possibility that (i) each microorganism has acquired the tolerance against the D3 concentrate (or toxic metal in the concentrate), or (ii) population structure has been optimized for bioleaching of the concentrate by modifying the abundance of each microbes.

With increase in the pulp density, E_h-rise was deteriorated, which consequently reached a plateau at around 750 mV in any cases (Fig. 7.1b). This delayed E_h increase was caused by the presence of larger amount of easily soluble copper sulfide at higher pulp density; Cu solubilization was indeed dramatically improved with increase in pulp density (Fig. 7.1d), from 49 mM (2%) to 89 mM (3%), 156 mM (5%), 228 mM (8%), and 233 mM (10%). Relatively similar final Cu recovery confirmed that easily soluble copper sulfide was mainly subjected to Fe(III) oxidation, but not refractory copper sulfide: 54, 59, 61, 60 at the pulp density of 2, 3, 5, 8%, respectively (Fig. 7.2a). Only the 10% pulp density culture resulted in the lower Cu recovery (41%), suggesting the possibility of inefficient stirring. Likewise, final Fe and As recovery showed similar value regardless of the pulp density, even though the dissolved concentration were obviously increased with increase in the pulp density. In any cultures, only around 10% of Fe was stable as the ionic form in the solution, since once-dissolved Fe was easily immobilized by forming ferric sulfate precipitates such as jarosite ($KFe_3(SO_4)_2(OH)_6$) at pH 2. Accompanying with this Fe precipitates, it was expected that As would be also immobilized as ferric arsenate or co-precipitated with jarosite, resulting in only around 7% of final recovery. Final recovery of Cu, As, Fe at the variety of pulp density were summarized in Table 7.1.

Table 7.1 Final recovery of Cu, As, and Fe in the bioreactor experiment at different pulp density.

Pulp density (%)	Recovery (%)		
	Cu	As	Fe
2	54.1	7.4	11.3
3	59.1	7.6	10.4
5	60.5	7	9
8	60.1	6.9	7.8
10	41.4	5.6	7.9

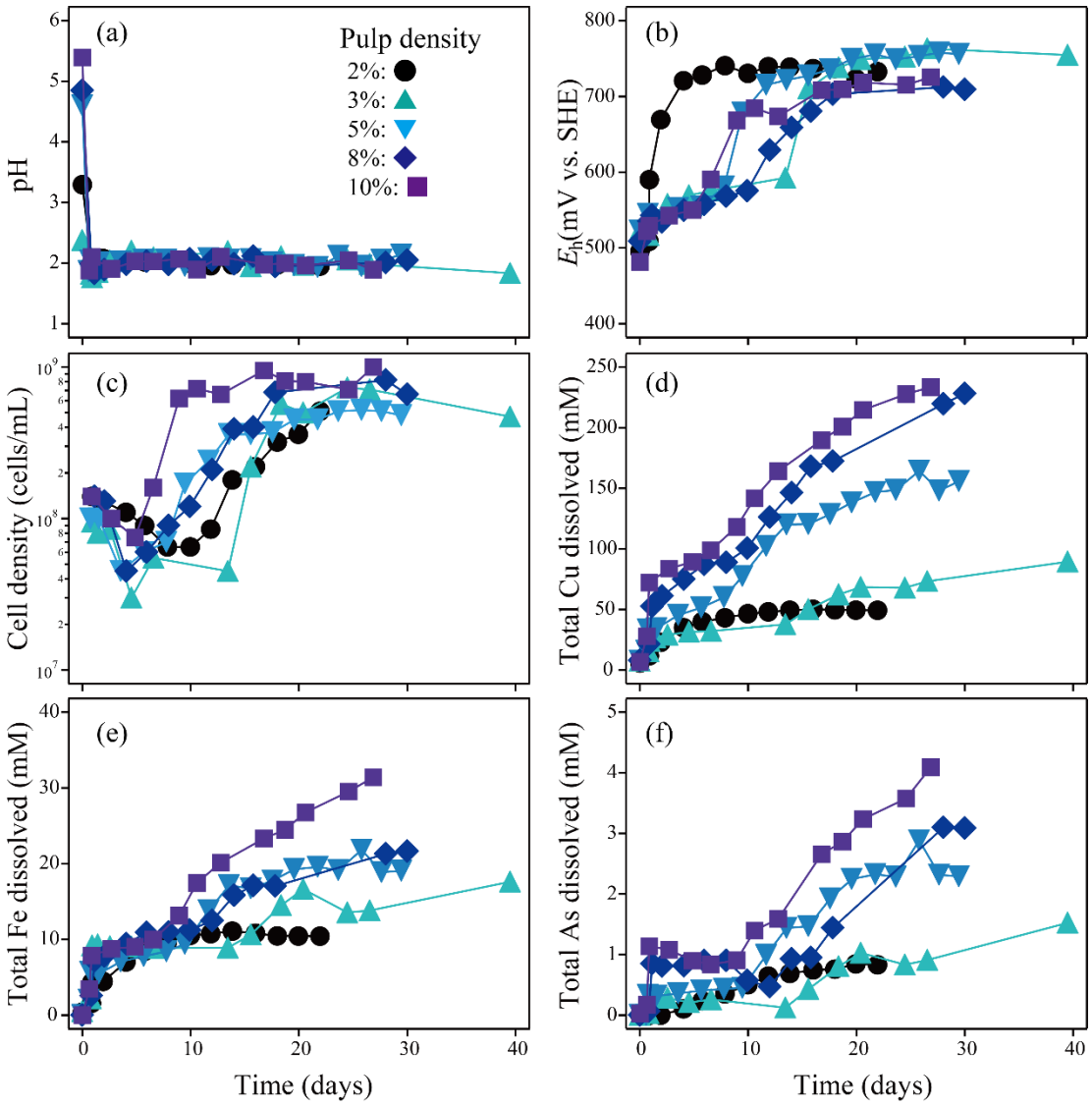

Fig. 7.1 Changes in pH (a), E_h (b), cell density (c), total soluble Cu concentration (d), total soluble Fe concentration (e), and total soluble As concentration (f) during bioleaching of D3 concentrate at the pulp density of 2% (●), 3% (▲), 5% (▼), 8% (◆), and 10% (■). Pre-grown culture was inoculated at day 1.

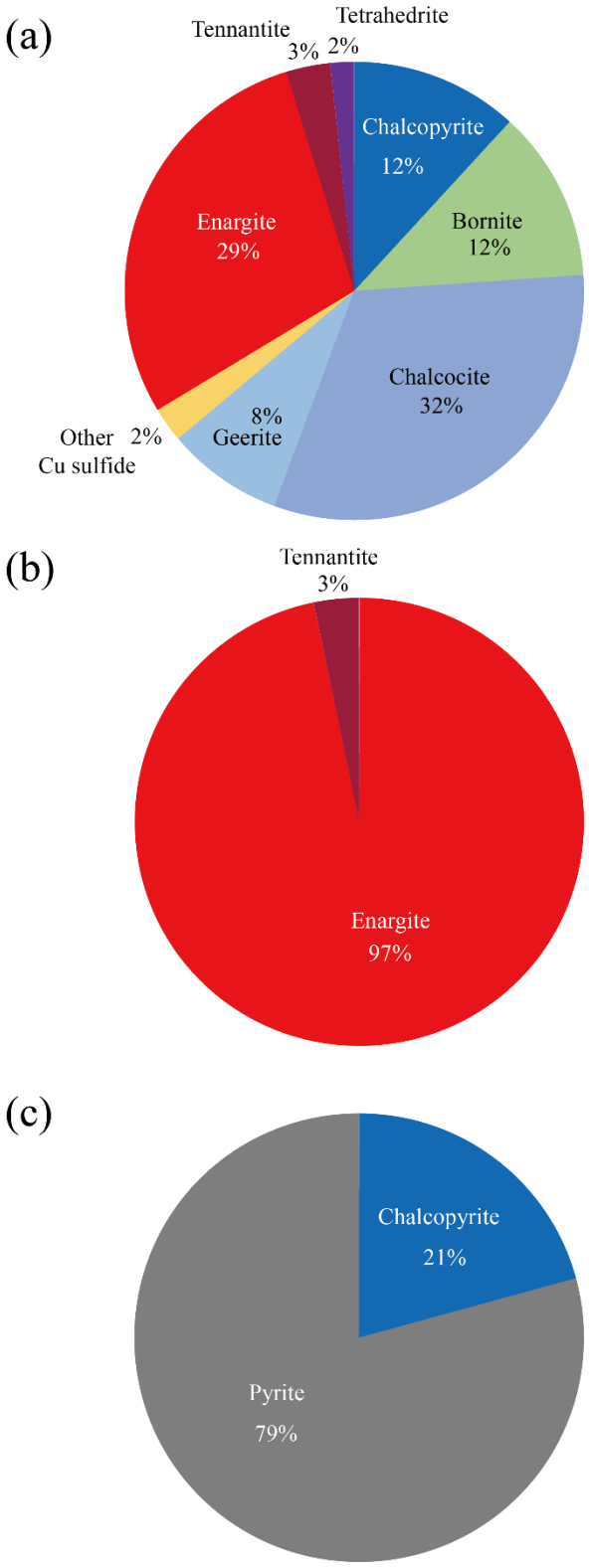

Fig. 7.2 Composition of Cu (a), Fe (b), and As (c) contents dissolved from each mineral in D3 concentrate.

7.3.2 Catalytic effect of AC on bioleaching of D3 concentrate

For the practical evaluation, AC-catalyzed bioleaching of copper sulfide at the pulp density of 10% were carried out in the stirred tank reactor and its catalytic effect was investigated. In the absence of AC, planktonic cell density actively increased more than 10^9 cells/mL, while long lag phase of cell growth was apparently seen in the culture with 0.5% AC addition (Fig. 7.3c). Considering the E_h-rise in this culture at the early stage of the experiment (Fig. 7.3b), however, larger amount of AC enabled adsorbing the majority of planktonic cells on its surface, possibly leading to the invisible increase of the cell density occurred on the AC surface. Consequently, cell density in any cultures reached at the same level in the late stage of the experiment, indicating that cell growth itself was hardly inhibited by the addition of AC. Even though slightly lower E_h was maintained by 0.05% AC addition compared to the culture without AC, almost similar trend in both cases suggest that 0.05% AC was insufficient to control the E_h to lower level (< 700 mV). The addition of 0.5% AC retained the lowered E_h less than 700 mV throughout the experiment with two-stage E_h increase (Fig. 7.3b): (i) relatively rapid E_h rise until day 10 (1st stage), followed by (ii) gradual re-increase of once-dropped E_h from day 10 to 30 (2nd stage). This two-stage E_h increase might be attributed to the presence of yeast extract, supplemented to support the initial cell growth. Heterotrophic Fe-oxidizer, *Am. ferrooxidans* ICP, *Sb. sibiricus* N1, *Acidiplasma* sp. Fv-Ap was likely activated by using yeast extract as a carbon source, which led to the rapid increase of E_h to 682 mV until day 10 (Fig. 7.3b). Once yeast extract was completely consumed for their growth, E_h was dropped to 631 mV in 3 days possibly due to (i) the deactivation of heterotrophic Fe-oxidizer and (ii) the E_h-lowering effect by sufficient amount of AC (0.5%). After this, heterotrophic Fe-oxidizer would switch their energy source to the organic metabolite produced by autotrophic S-oxidizer, *At. caldus* KU, resulting in the slower but steady increase of E_h. Since the activity of microorganism in reactor was rather higher than that in the flask, larger amount of AC (0.5%) was found necessary to maintain the lower E_h level compared to the bioleaching in the flask level.

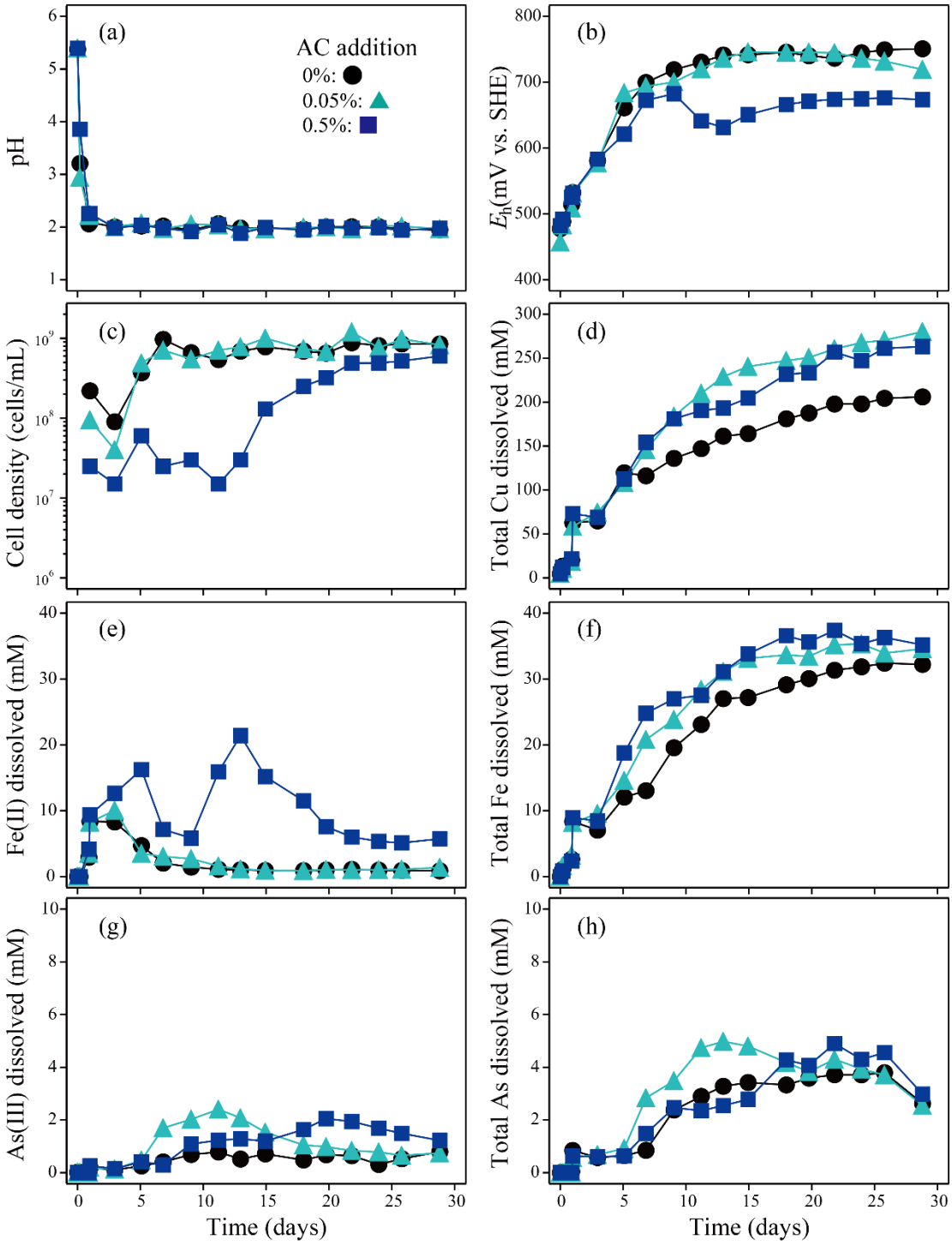

Fig. 7.3 Changes in pH (a), E_h (b), cell density (c), total soluble Cu concentration (d), Fe(II) concentration (e), total soluble Fe concentration (f), As(III) concentration (g) and total soluble As concentration (h) during bioleaching of D3 concentrate at the pulp density of 10% in the absence (●) or presence of 0.05% (▲) and 0.5% (w/v) (■) AC. Pre-grown culture was inoculated at day 1.

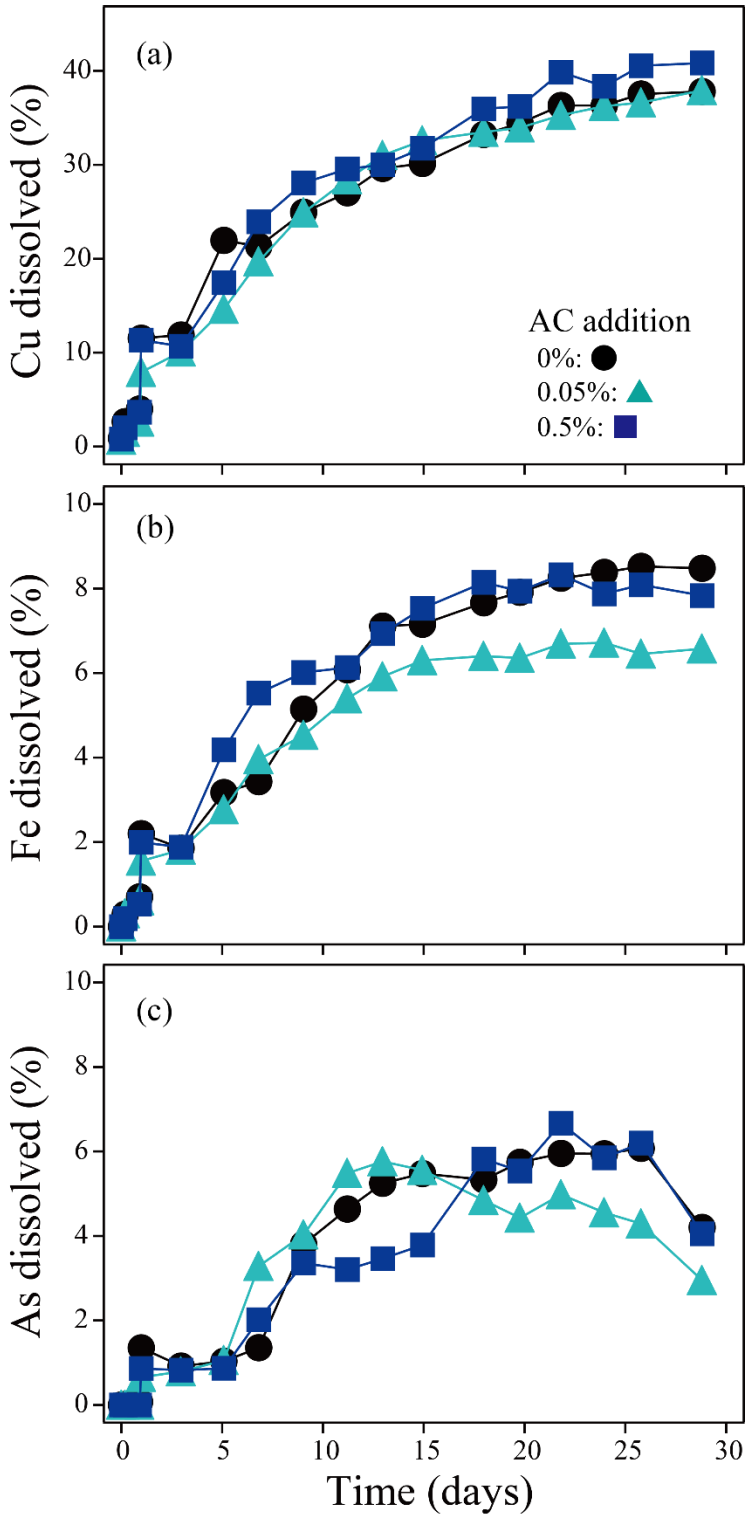

Fig. 7.4 Changes in the Cu (a), Fe (b), and As recovery (c) corrected by the solution volume during bioleaching of D3 concentrate at the pulp density of 10% in the absence (●) or presence of 0.05% (▲) and 0.5% (w/v) (■) AC. Pre-grown culture was inoculated at day 1.

In the presence of AC, higher Cu solubilization was observed (280 and 263 mM with 0.05 and 0.5% AC addition, respectively) than that without AC (205 mM) (Fig. 7.3d), while Cu recovery corrected by solution volume showed similar value in each cases (Fig. 7.4a): 38% (0% AC), 38% (0.05%), and 41% (0.5%). Although it seemed that the enhanced Cu dissolution was the results of the concentration of Cu ion due to the water evaporation, it was found that some part of leaching solid sank to the bottom of reactor, which would be unreacted with leaching solution throughout the experiment (defined as “unreacted residue”). As shown in Fig. 7.5, reacted part of solid residue (defined as “reacted residue”) were easily separated from the unreacted residue since the latter was firmly solidified at the bottom of reactor vessel.

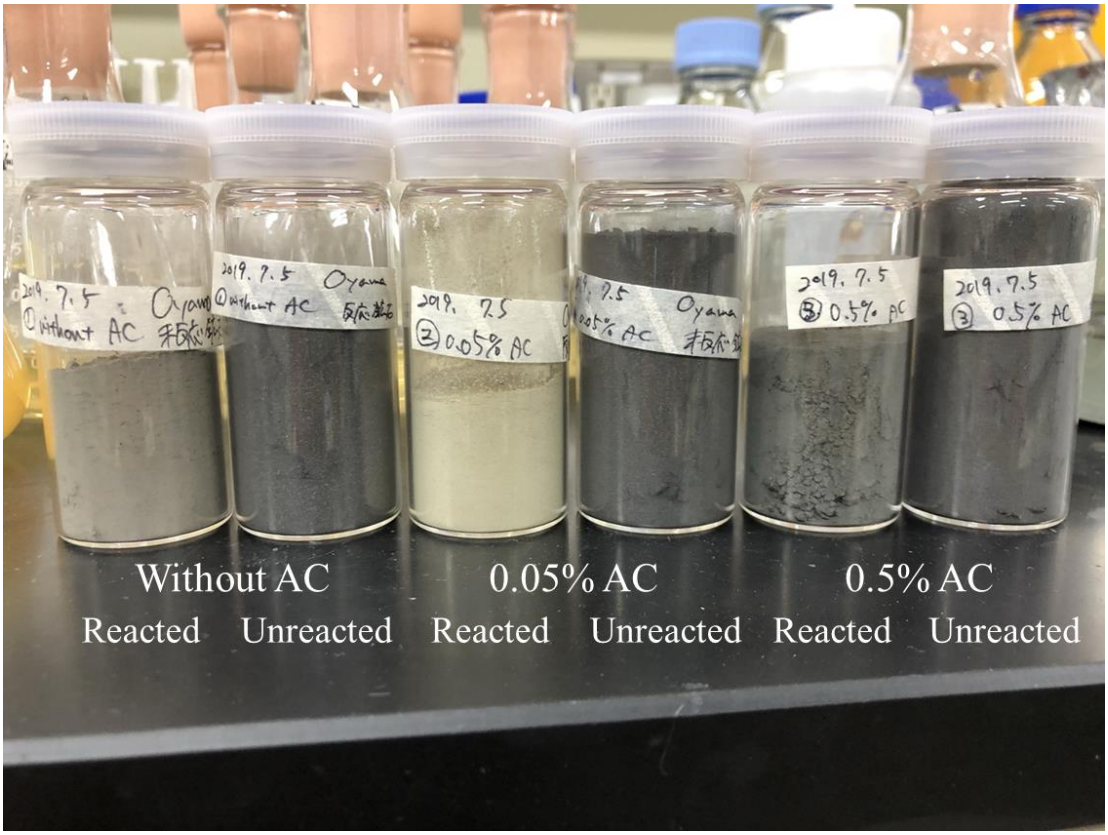

Fig. 7.5 Separately collected solid residue after 30 days of bioleaching of D3 concentrate in the absence or presence of 0.05% and 0.5% AC. Reacted residue: floated and well-mixed part of leaching reside with whiter color. Unreacted residue: settled and coagulated part of leaching residue with black color.

In order to eliminate the effect of unreacted solid from the consideration, Cu, Fe, and As recovery were re-corrected by the amount of unreacted residue (Fig. 7.6). The presence of AC realized the almost complete dissolution of copper sulfides regardless of AC amount: final Cu recovery improved from 80% (0% AC) to 100% (0.05% AC9 and 98% (0.5% AC). Contrary to slight contribution of AC to enargite dissolution (see chapter 5 and 6), it has been well-known that chalcopyrite dissolution is dramatically promoted by the presence of AC (Nakazawa et al., 1998; Zhang et al., 2007; Liang et al., 2010; Hao et al., 2018). This was confirmed by MLA results, where abundance of chalcopyrite was suddenly dropped by the addition of AC (16% (0% AC) to 3% (0.05%) and < 1% (0.5%); Table 7.2; Fig.7.7).

Hiroyoshi et al. (2000, 2001, 2002, 2007, 2008) reported that chalcopyrite dissolution is promoted at lower E_h rather than higher E_h via the transformation into chalcocite as an intermediate, followed by its dissolution to solubilize the Cu ion (Eqs. 7-4 and 7-5).

$$CuFeS_2 + 3Cu^{2+} + 4e^- = 2Cu_2S + Fe^{2+} \quad \text{(Eq. 7-4)}$$

$$Cu_2S = 2Cu^{2+} + S^0 + 4e^- \quad \text{(Eq. 7-5)}$$

The E_h when Eq. 7-4 and 7-5 occur were defined as E_c and E_{ox}, which are thermodynamically calculated by Eq. 7-6 and 7-7.

$$E_c\ (V) = 0.72 + 0.059 \log \frac{(a_{Cu^{2+}})^{0.75}}{(a_{Fe^{2+}})^{0.25}} \quad \text{(Eq. 7-6)}$$

$$E_{ox}\ (V) = 0.60 + 0.059 \log\ (a_{Cu^{2+}})^{0.5} \quad \text{(Eq. 7-7)}$$

where R, T, F, and a_i are gas constant (J/Kmol), temperature (K), faraday constant (C/mol), and the activities of species *I*, respectively. When E_h satisfied the optimal range, $E_{ox} < E_h < E_c$, the reactions of Eq. 7-4 and 7-5 occur at the same time, leading to faster chalcopyrite dissolution. Since E_c and E_{ox} are varied depending on Cu^{2+} and Fe^{2+} concentration, Okamoto et al (2004) introduced "E_{normal}" to normalize the optimal E_h range in any experimental condition, with the definition as below;

$$E_{normal} = (E - E_{ox}) / (E_c - E_{ox}) \quad \text{(Eq. 7-8)}$$

In this definition, optimal potential range for the enhanced chalcopyrite dissolution, $E_{ox} < E_h < E_c$, is set to be $0 < E_{normal} < 1$.

Fig. 7.8 shows the changes in E_{normal} during bioleaching of D3 concentrate in the absence or presence of AC. The results showed that E_{normal} value slightly exceed over 1 after day 10 in the absence of AC, while the presence of AC basically enabled controlling the E_{normal} into the optimal range, $0 < E_{normal} < 1$, throughout the experiment. This AC-catalyzed E_{normal} control would contributed to the enhanced chalcopyrite dissolution, resulting in the dropped abundance of chalcopyrite confirmed by MLA (Fig. 7.7). Although the catalytic effect of AC on the dissolution of easily soluble copper sulfide (bornite, chalcocite, and geerite) has been poorly investigated, the decrease in their proportion by the addition of AC from 6% (0% AC) to < 1% (0.5% AC) was likely the evidence that the presence of AC also catalytically facilitate the dissolution of them (Table 7.2; Fig. 7.7). This suggests that the dissolution of chalcocite formed by Eq. 7-4 also could be promoted by AC catalyst, probably leading to further enhancement of chalcopyrite dissolution. In summary, chalcopyrite dissolution would be dramatically enhanced by AC based on the following two mechanisms; (i) AC-catalyzed E_h-control achieved optimal E_{normal} range to facilitate the chalcopyrite transformation into easily soluble copper sulfide such as chalcocite, and (ii) the dissolution of chalcocite produced via chalcopyrite transformation is accelerate by AC.

Enargite dissolution was also greatly enhanced by the addition of AC: the proportion of enargite measured by MLA dropped from 24% (0% AC) to 7% (0.05%) and 6% (0.1%) (Table 7.2; Fig. 7.7). Although lowered E_h by the addition of 0.5% AC was assumed undesirable for the enargite dissolution (Fig. 7.3b), larger amount of AC would lead to high contact frequency between enargite and AC, possibly supporting the continuous enargite dissolution.

Overall, even though the condition of bioreactor operation must be further optimized, catalytic effect of AC was found useful to enhance the Cu solubilization during bioleaching of As-bearing copper concentrate even in the stirred tank reactor level.

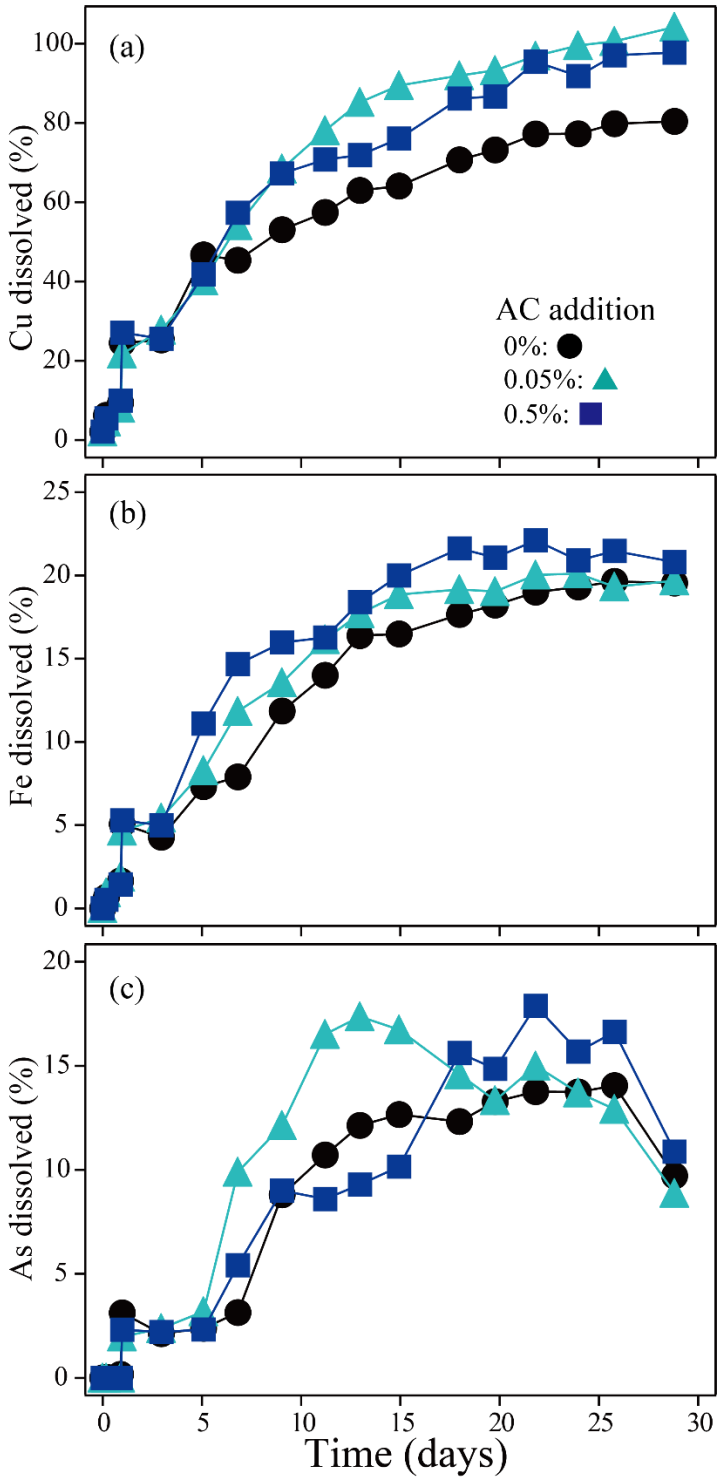

Fig. 7.6 Changes in the Cu (a), Fe (b), and As recovery (c) corrected by the solution volume and the amount of unreacted residue during bioleaching of D3 concentrate at the pulp density of 10% in the absence (●) or presence of 0.05% (▲) and 0.5% (w/v) (■) AC. Pre-grown culture was inoculated at day 1.

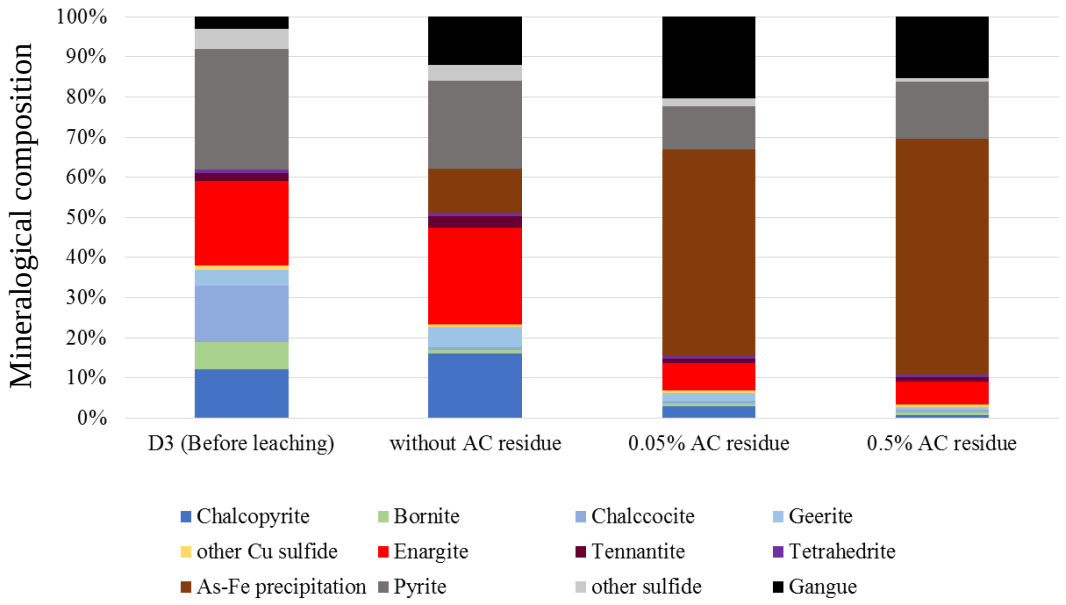

Fig. 7.7 MLA results of original D3 concentrate and bioleached reacted residue recovered on day 30 from cultures containing 0%, 0.05%, or 0.5% AC.

Table 7.2 Mineralogical composition of original D3 concentrate and bioleached reacted residue recovered on day 30 from cultures containing 0%, 0.05%, or 0.5% AC determined by MLA.

Mineral (wt%)	Original D3 concentrate	Without AC reacted residue	0.05% AC reacted residue	0.5%AC reacted residue
Chalcopyrite	12	16	3	<1
Bornite	7	1	<1	<1
Chalcocite	14	<1	<1	<1
Geerite	4	5	2	<1
other Cu sulfide	1	<1	<1	<1
Enargite	21	24	7	6
Tennantite	2	3	1	1
Tetrahedrite	1	<1	<1	<1
As-Fe precipitation	-	11	53	61
Pyrite	30	22	11	15
other sulfide	5	4	2	<1
Gangue	3	12	21	16

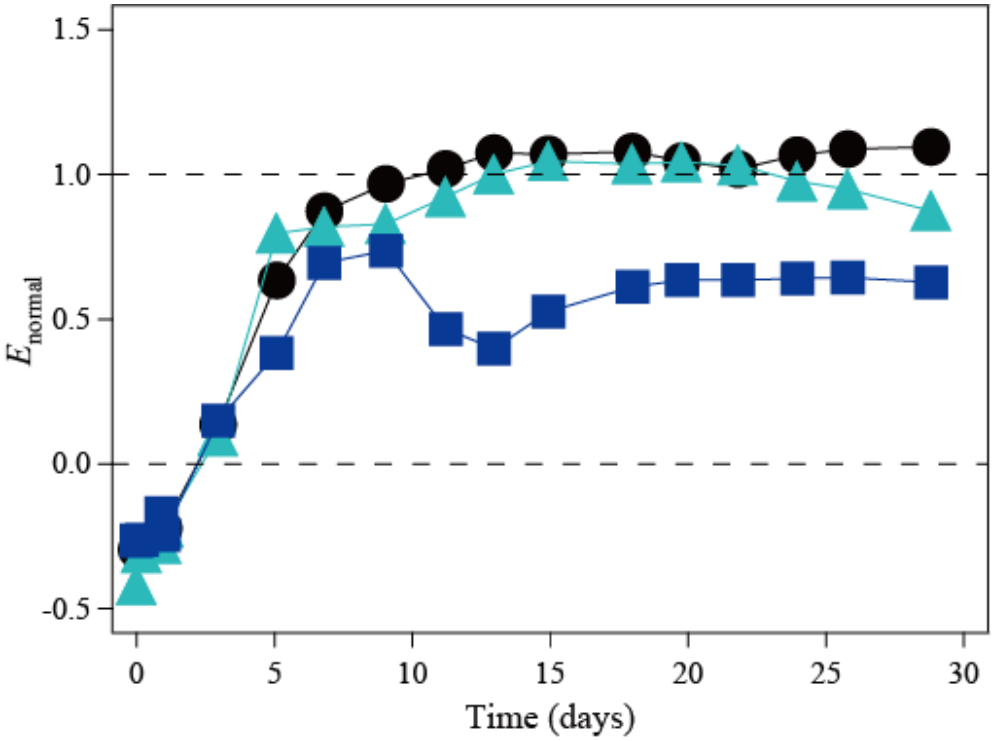

Fig. 7.8 Changes in the E_{normal} during bioleaching of D3 concentrate at the pulp density of 10% in the absence (●) or presence of 0.05% (▲) and 0.5% (w/v) (■) AC.

Contrary to the improved final Cu recovery by the addition of AC, both final Fe and As recovery reached to the similar values in any cultures at the end of the experiment, approximately 20% and 10%, respectively. Since 97% of As and 21% of Fe are derived from enargite and chalcopyrite dissolution, respectively, considering almost complete Cu extraction from the concentrate, it was expected that majority of Fe and As were immobilized in the solid phase, which led to their lower recovery. MLA results indeed revealed that As was co-precipitated with Fe, whose dominance became noticeable with the addition of AC (11%, 53%, and 61% in the presence of 0%, 0.05%, 0.5% AC, respectively; Table 7.2; Fig. 7.7). Based on XRD analysis, however, jarosite was found the only secondary mineral formed during bioleaching, but no As-bearing minerals (Fig. 7.9). Interestingly, fine particle (< 1 μm) composed of Fe, S, O, As and Cu were uniformly detected by SEM observation (Fig. 7.10). The composition of these fine particles indicates that Cu and As could be incorporated into the structure of jarosite, resulting in the formation of Fe-As precipitations. Previous study regarding the As immobilization as biogenic scorodite reported that increasing As-inclusion into ferric

sulfate structure gradually changed the color of precipitates from brownish orange to whitish pale green (Tanaka et al., 2018). Likewise, whiter color of reacted leaching residue obtained from the culture containing 0.05% AC proved that As-inclusion into jarosite structure indeed occurred, resulting in the immobilization of As as the Fe-As precipitates; note that blackish color of reacted residue obtained from the culture in the presence of 0.5% AC could be derived from the contamination of AC.

This facilitated Fe-As co-precipitation would be due to the relatively higher pH automatically maintained at around 2.0 throughout the experiment (Fig. 7.3a); Fe(III) is easily immobilized as jarosite at such pH, accompanying with co-immobilization of As. Since larger amount of As were theoretically once-solubilized by the addition of AC owing to the enhanced enargite dissolution, the resultant formation of Fe-As precipitates would be consequently facilitated (Fig. 7.7). These results suggested that, even though immobilization ratio was not able to be calculated, AC was also likely useful for the immobilization of once-dissolved As from enargite during bioleaching of As-bearing copper concentrate.

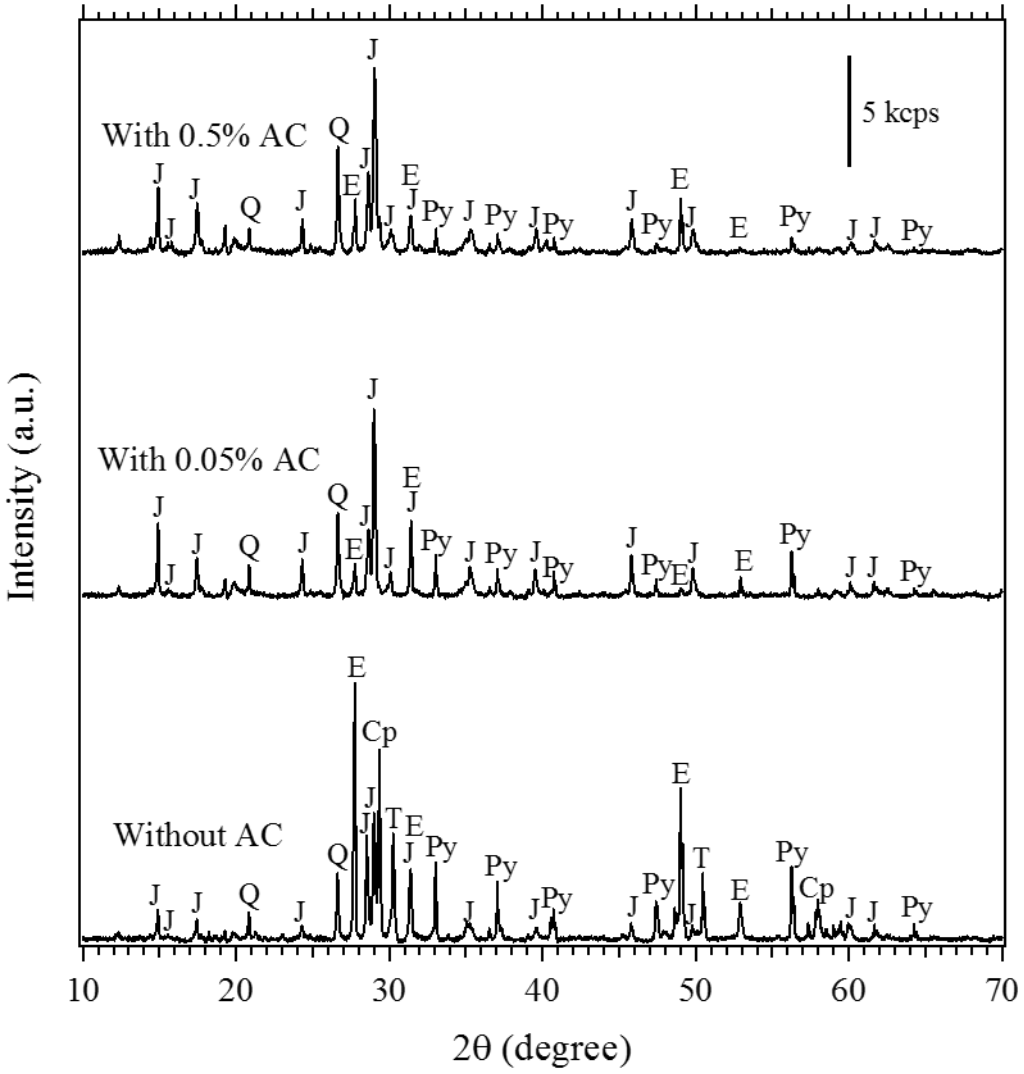

Fig. 7.9 X-ray diffraction patterns of bioleached residue recovered on day 30 from cultures containing 0%, 0.05%, or 0.5% AC. E: enargite (Cu_3AsS_4; PDF No. 00-035-0775), Py: pyrite (FeS_2; PDF No. 00-042-1340), Q: quartz (SiO_2; PDF No. 01-070-3755), J: jarosite ($K(Fe_3(SO_4)_2(OH)_6)$; PDF No. 01-076-0629), Cp: chalcopyrite ($CuFeS_2$; PDF No. 01-075-6866), Tennantite ($Cu_{12}As_4S_{13}$; PDF No. 01-074-1027).

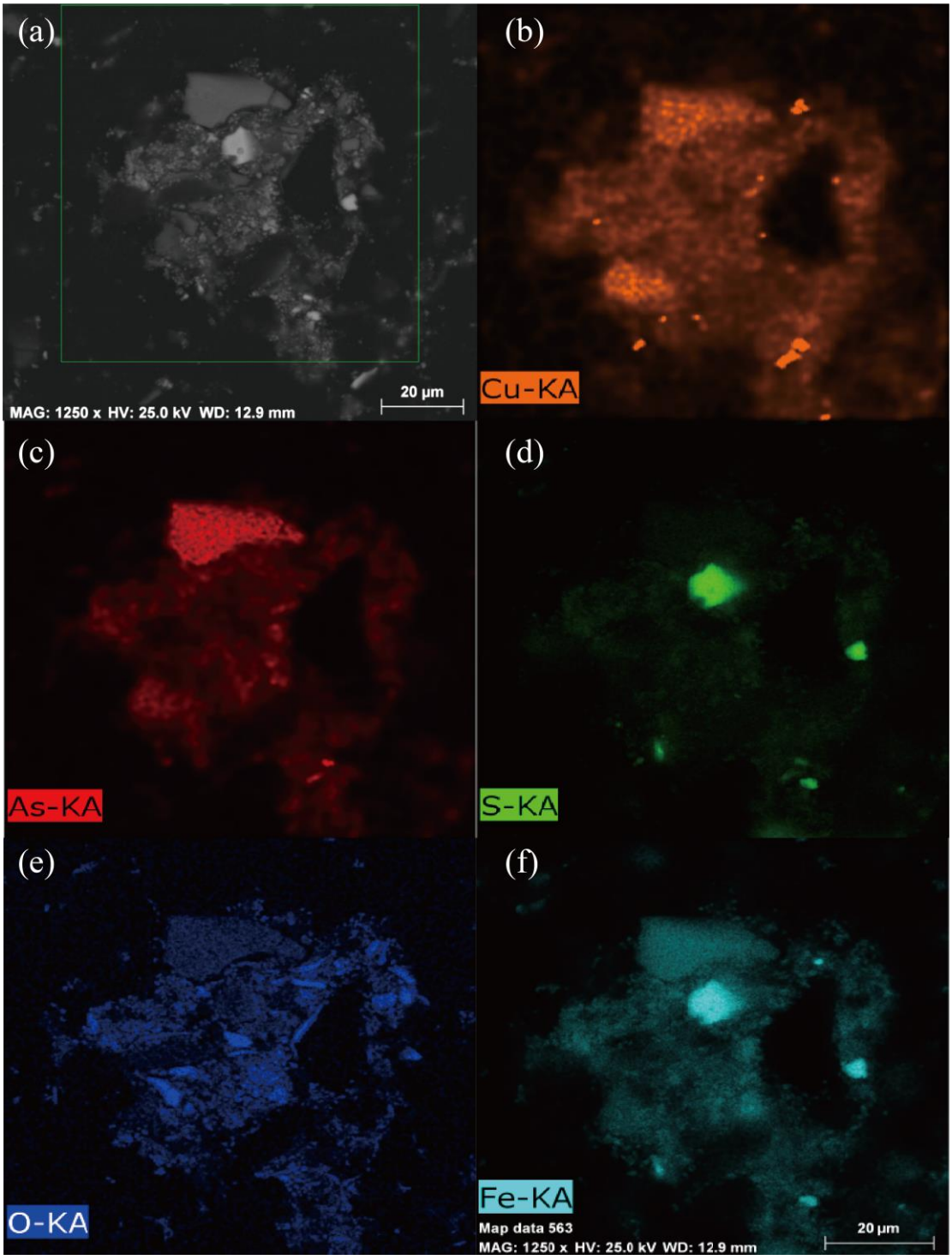

Fig. 7.10 SEM image (a) and elemental mapping (b-f) of reacted residue recovered at day 30 from the culture containing 0.5% AC: Cu (b), As (c), S (d), O (e), and Fe (f). Aggregation of ultrafine particle (< 1 μm) composed of Cu, As, S, O, and Fe was found.

7.4 Conclusions

AC-catalyzed bioleaching system was scaled up to stirred tank reactor in order to investigate the catalytic effect of AC on As-bearing copper concentrate at high pulp density. Pre-grown bioleaching cultures were subsequently transferred to the new media with higher pulp density, aiming to the gradual adaptation of moderate thermophile consortia to As-bearing copper concentrate. Finally, the pulp density successfully increased from 2% up to 10% with retaining the great cell activity. AC catalyst was indeed added for its evaluation to high pulp density culture, whereas the improvement of Cu recovery corrected by solution volume was hardly seen even in the presence of AC. Since the unreacted residue was found settled and solidified at the bottom of the reactor, the correction by solution volume as well as the amount of unreacted residue was carried out, leading to the more noticeable difference in final Cu recovery: 80%, 100%, and 98% in the presence of 0%, 0.05%, and 0.5% AC, respectively. This might be due to the enhanced chalcopyrite and enargite dissolution determined by MLA, where obvious disappearances of chalcopyrite and enargite by the addition of AC was observed. AC-catalyzed E_h-control and contact between AC and these minerals could offer the desirable condition for faster dissolution of these refractory minerals. The dissolution of easily soluble copper sulfide (chalcocite, geerite, bornite) was also facilitated by AC, which could indirectly contribute to the enhancement of chalcopyrite dissolution. XRD, SEM, and MLA results revealed that the presence of AC was also effective in promoting the As immobilization based on the co-precipitation with jarosite. Overall, the applicability of AC-catalyzed bioleaching to high pulp density of As-bearing copper concentrate was successfully confirmed.

References

1. Astudillo, C. and Acevedo, F., 2008. Adaptation of *Sulfolobus metallicus* to high pulp densities in the biooxidation of a flotation gold concentrate. Hydrometallurgy 92, 11-15.
2. Hao, X., Liu, X., Zhu, P., Chen, A., Liu, H., Yin, H., Qiu, G. and Liang, Y., 2018. Carbon material with high specific surface area improves complex copper ores' bioleaching efficiency by mixed moderate thermophiles. Minerals 8, 301.
3. Hiroyoshi, N., Miki, H., Hirajima, T. and Tsunekawa, M., 2000. A model for ferrous-promoted chalcopyrite leaching. Hydrometallurgy 57, 31-38.
4. Hiroyoshi, N., Miki, H., Hirajima, T. and Tsunekawa, M., 2001. Enhancement of chalcopyrite leaching by ferrous ions in acidic ferric sulfate solutions. Hydrometallurgy 60, 185-197.
5. Hiroyoshi, N., Arai, M., Miki, H., Tsunekawa, M. and Hirajima, T., 2002. A new reaction model for the catalytic effect of silver ions on chalcopyrite leaching in sulfuric acid solutions. Hydrometallurgy 63, 257-267.
6. Hiroyoshi, N., Kuroiwa, S., Miki, H., Tsunekawa, M. and Hirajima, T., 2007. Effects of coexisting metal ions on the redox potential dependence of chalcopyrite leaching in sulfuric acid solutions. Hydrometallurgy 87, 1-10.
7. Hiroyoshi, N., Kitagawa, H. and Tsunekawa, M., 2008. Effect of solution composition on the optimum redox potential for chalcopyrite leaching in sulfuric acid solutions. Hydrometallurgy 91, 144-149.
8. Liang, C.-L., Xia, J.-L., Zhao, X.-J., Yang, Y., Gong, S.-Q., Nie, Z.-Y., Ma, C.-Y., Zheng, L., Zhao, Y.-D. and Qiu, G.-z., 2010. Effect of activated carbon on chalcopyrite bioleaching with extreme thermophile *Acidianus manzaensis*. Hydrometallurgy 105, 179-185.
9. Ma, Y.-l., Liu, H.-c., Xia, J.-l., Nie, Z.-y., Zhu, H.-r., Zhao, Y.-d., Zheng, L., Hong, C.-h. and Wen, W., 2017. Relatedness between catalytic effect of activated carbon and passivation phenomenon during chalcopyrite bioleaching by mixed thermophilic Archaea culture at 65ºC. Transactions of Nonferrous Metals Society of China 27, 1374-1384.
10. Nakazawa, H., Fujisawa, H. and Sato, H., 1998. Effect of activated carbon on the bioleaching of chalcopyrite concentrate. International Journal of Mineral Processing 55, 87-94.
11. Okamoto, H., Nakayama, R., Hiroyoshi, N. and Tsunekawa, M., 2004. Redox

potential dependence and optimum potential of chalcopyrite leaching in sulfuric acid solutions. Journal of MMIJ 120, 592-599.

12. Tanaka, M., Sasaki, K. and Okibe, N., 2018. Behavior of sulfate ions during biogenic scorodite crystallization from dilute As(III)-bearing acidic waters. Hydrometallugy 180, 144-152.
13. Zhang, W.-M. and Gu, S.-F., 2007. Catalytic effect of activated carbon on bioleaching of low-grade primary copper sulfide ores. Transactions of Nonferrous Metals Society of China 17, 1123-1127.

Chapter 8

Conclusions

8.1 Conclusions

Slow dissolution kinetic of refractory primary copper sulfides such as chalcopyrite and enargite even in bioleaching process suggests the necessity of some reaction catalyst. Especially for enargite bioleaching system, less attention has been paid than that of chalcopyrite; hence, limited information about possible catalyst is available. Considering the serious increase in the As contamination in copper deposits, however, the exploitation of As-bearing copper mineral as a copper resource is urgently necessitated. Therefore, this thesis aimed to evaluate the candidate catalysts, silver and activated carbon, in enargite bioleaching for the development of Cu production process from As-bearing copper sulfides.

Firstly, silver catalyst was tested in bioleaching of enargite concentrate (**chapter 4**), which has been long recognized as a promising catalyst for the chalcopyrite leaching. Addition of Ag_2S as a silver catalyst enabled selective Cu dissolution from enargite while suppressing pyrite oxidation: at the highest Ag_2S concentration of 0.04%, Cu recovery reached 96%, while Fe dissolution was suppressed to reach only 29% by day 72. Lowered E_h level by Ag_2S addition (i) and high subjectivity of Ag_2S to Fe^{3+}-oxidation (ii) could be the reason of suppressed pyrite dissolution. Based on the results from the thermodynamic calculation and solid analyses, faster enargite dissolution proceeds via the formation of at least two types of secondary products (chalcocite, Cu_2S; trisilver arsenic sulfide, Ag_3AsS_4). Addition of Ag_2S thermodynamically and microbiologically contributed to lowering E_h during bioleaching, consequently satisfying E_{ox} (Cu_2S) < E_h < E_c (Ag^+) to enhance enargite dissolution via formation of chalcocite intermediate. Detection of trisilver arsenic sulfide (Ag_3AsS_4) and its intermediate layer $(Cu,Ag)_3AsS_4$ on the enargite surface indicated that Cu ion in the enargite lattice would be gradually substituted with Ag ion in the solution. Such secondary products did not impose a rate-limiting step, since the Ag-catalyzed bioleaching was shown to be controlled by a chemical surface reaction, rather than diffusion through product film, which was the case in the absence of Ag_2S. An economical and environmentally-friendly alternative catalyst possessing similar catalytic properties with silver was not found, while complete Ag-recovery as trisilver arsenic sulfide was thought one of the possibilities to implement this process into real operation.

Even though the strong catalytic ability of Ag was desirable for the Cu recovery from enargite, loss of A was inevitable, leading to the uneconomical process. This motivated us to search for the cheaper catalyst, which is certainly disposable after the leaching process. Since activated carbon has also been tested as a useful but cheaper catalyst in chalcopyrite bioleaching, its catalytic effect on enargite bioleaching was also evaluated (**chapter 5**). In the absence of AC, co-existing pyrite (FeS_2) in enargite concentrate began to rapidly solubilize at day 7, which was increasingly delayed by the addition of 0.1% and 0.2% AC to day 25 and 35, respectively. This was likely the result of the lowered E_h level via Fe^{3+}-reduction coupled with reduced inorganic sulfur compounds (RISCs)-oxidation on the AC surface acting as an electron-mediator. Real-time PCR analysis found that the abundance of S-oxidizing bacteria dropped in the presence of AC, proving that RISCs as an energy source for S-oxidizing bacteria were indeed consumed via the coupling reaction. While final Cu recovery was improved from 36% (0% AC) to 53% (0.2%), the electrochemical study suggested that this was not much contributed by the galvanic interaction between enargite and AC. A kinetic study using the shrinking core model revealed that AC addition let Cu solubilize slowly but steadily and continuously. Suppressed pyrite dissolution by AC addition was followed by suppressed Fe-passivation, which would contribute to steady enargite dissolution. Addition of AC also facilitated the As immobilization from 3.1 mM (0% AC at day 10) to 5.2 mM (0.1% AC at day 30), 7.0 mM (0.2% AC at day 40), and 6.9 mM (0.3% AC at day 60). EPMA analysis found that As was immobilized as ferric arsenate selectively on the enargite surface, while its re-solubilization was observed coincided with rapid pyrite dissolution. This observation implied that rapid supply of sulfate ion via pyrite dissolution might trigger the re-solubilization of As-precipitates. Based on the results obtained above, AC-catalyzed E_h-control played an important role in controlling pyrite dissolution, which is indirectly but strongly influential on steady enargite dissolution without Fe-passivation and stable As immobilization. Therefore, further investigation in the catalytic ability of AC was expected beneficial for the development of AC-catalyzed bioleaching system.

For the clarification of the fundamental catalytic ability of AC, various AC were compared in the abiotic experiment, followed by their application into the bioleaching experiment (**chapter 6**). The former experiment mainly aimed at the elucidation of the

property determining E_h-control ability of AC, while the latter was conducted to investigate if different AC properties affect on Cu solubilization from enargite. It was found that E_h-controlling ability of AC is determined by the structural property such as graphene and defect (edge) structure formed during the activation process, but not shape (powder or granular), specific surface area, and total pore volume. Due to the extremely high electric conductivity of graphene, AC with massive graphene structure would enable faster electron transfer for the coupling reaction that occurred on the AC surface. On the other hand, AC with plentiful defect structure is more advantageous in the oxidation reaction (e.g. Fe^{2+}- and tetrathionate-oxidation), since the abundant surface functional group in the defect structure might catalyze the H_2O_2 production, followed by its consumption for the oxidation reaction. Chemical-activated carbon was thought the best E_h-controlling AC due to its well-developed graphene structure, whilst the abundant defect structure in steam-activated carbon is undesirable for E_h-controlling catalyst. Even though the contribution of the galvanic effect was found negligibly small through the individual contact in **chapter 5**, extremely increased contact frequency by employing the powder AC could maximize the effect of galvanic interaction. As a result, slowed enargite dissolution by AC-catalyzed E_h-reduction was likely canceled out, resulting in the retention of faster enargite dissolution even under E_h-lowered condition by AC catalysis. This observation suggests that, therefore, finer AC must be used for the improvement of Cu solubilization from enargite. As a conclusion, powder AC made by chemical-activation process was found the best AC catalyst for bioleaching of enargite concentrate in terms of E_h-controlling ability and improvement of Cu solubilization.

Finally, AC-catalyzed bioleaching system was scaled up to stirred tank reactor targeting complex copper concentrate, D3 concentrate, at high pulp density for the practical evaluation of AC (**chapter 7**). Pre-grown bioleaching cultures were subsequently transferred to the new media with higher pulp density, aiming to the gradual adaptation of moderate thermophile consortia to complex copper concentrate. Consequently, the pulp density successfully increased from 2% up to 10% with retaining the great cell activity. AC catalyst was indeed added to high pulp density culture for its evaluation, whereas the improvement of Cu recovery corrected by solution volume was hardly seen. Since the unreacted residue was found settled and solidified at the bottom of the reactor,

the correction by solution volume as well as the amount of unreacted residue was carried out, resulting in the more noticeable difference in final Cu recovery: 80%, 100%, and 98% in the presence of 0%, 0.05%, and 0.5% AC, respectively. This might be due to the enhanced chalcopyrite and enargite dissolution determined by MLA, where obvious disappearances of chalcopyrite and enargite were observed. AC-catalyzed E_h-control and contact between AC and these minerals could offer the desirable condition for faster dissolution of these refractory minerals. The dissolution of easily soluble copper sulfide (chalcocite, geerite, bornite) was also facilitated by AC, which might indirectly contribute to the enhancement of chalcopyrite dissolution. XRD, SEM, and MLA results revealed that the presence of AC was also effective in promoting the As immobilization based on the co-precipitation with jarosite. In summary, the applicability of AC-catalyzed bioleaching to high pulp density of As-bearing complex copper sulfide was successfully confirmed.

Overall, the utility of catalyst (Ag and AC) in bioleaching of As-bearing copper concentrate has been successfully confirmed by the fundamental study, which was also scaled up to the practical level to provide the helpful information for the future implementation into a real mining operation. Whole findings in this work would provide us the new aspects and future direction for the further development of biomining technologies.

8.2 Recommendations for future work

In this work, two different As-bearing concentrates, enargite concentrate and D3 concentrate, were employed as the target samples. These samples were produced from the process to obtain high Cu-grade copper concentrate from As-bearing copper ore. The brief flowsheet of the process for the exploitation of As-bearing copper ore is described in Fig. 8.1. Unfortunately, since the current industrial technique is not capable of economic Cu production from As-bearing minerals, the repeated separations are conducted to minimize the As contamination in the final copper concentrate. Through this process, crushing and milling of ores are also repeated to improve mineral liberation for the following separation. This led to the production of extremely fine concentrate, which is not applicable to conventional bio-heap leaching due to the low water-flowage. Therefore, the development of the leaching process enabling copper production form fine concentrate is thought necessary. Stirred tank reactor, as was also employed in this work, is considered as one of the options, while further investigation regarding the agitation efficiency, aeration system, pH management, pulp density, and mechanical effect, is inevitable. Innovation of aeration system (e.g. installation of fine bubble technologies) could also provide a new aspect for the novel process to obtain the Cu from such fine concentrate.

Moreover, the effect of the presence of easily soluble copper sulfide (e.g. chalcocite, covellite, bornite) on the dissolution of refractory primary copper sulfide must be clarified. The dissolution behavior of complex copper sulfide has been less discussed, remaining uncertainties in the relationship between two types of minerals. The investigation on this would be beneficial to determine the appropriate concentrate, As bearing complex copper concentrate (e.g. D3 concentrate) or As-bearing copper concentrate (e.g. enargite concentrate) for bioleaching installation.

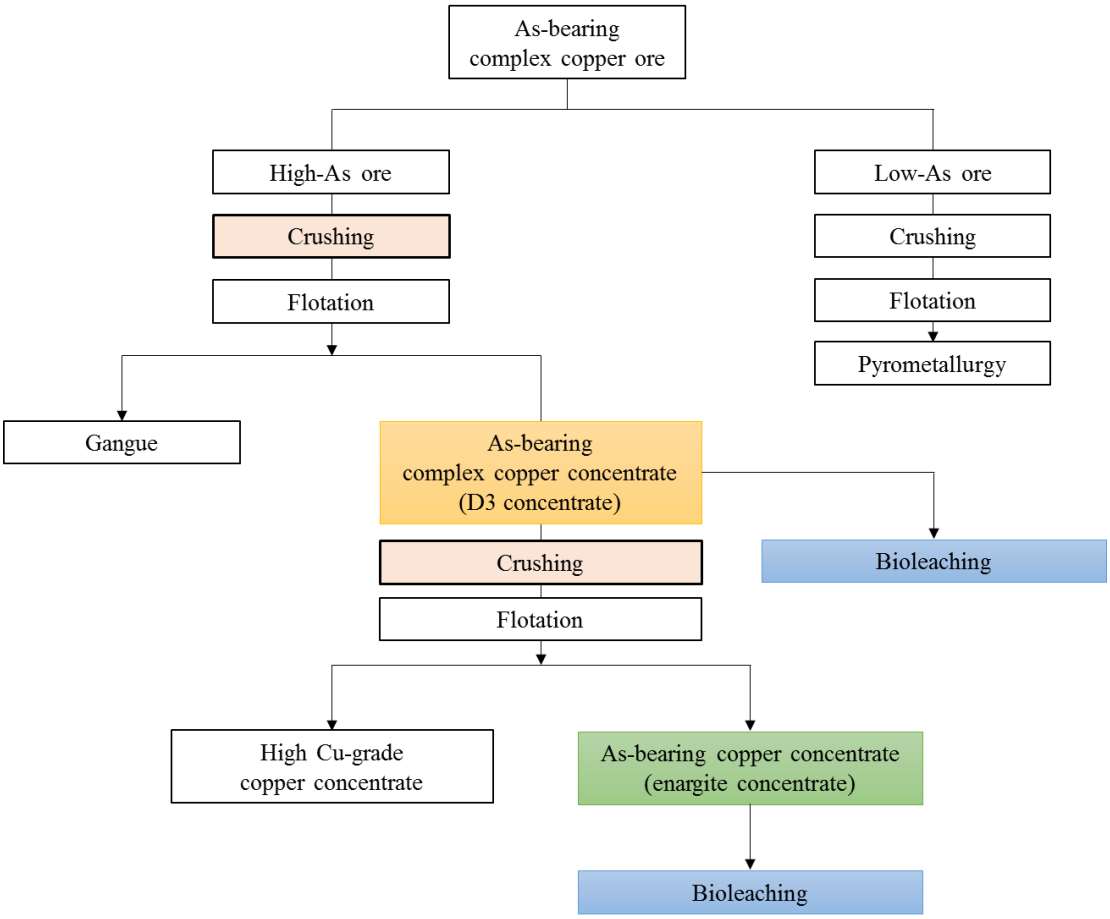

Fig. 8.1 Brief flowsheet of the exploitation process for As-bearing copper ores.

Regardless of its economic obstacle, Ag-catalyzed bioleaching is the possible option for the exploitation of As-bearing copper concentrate (e.g. enargite concentrate) as proposed in Fig. 8.2; note that the stirred tank reactor is employed under the assumption of fine concentrate. It is expected that economic loss would be reduced by (i) employing originally Ag-containing concentrate as a target material, (ii) re-using Ag-containing solid residue, and (iii) adding the waster Ag resources such as printed circuit board (PCB). As was found in chapter 4, separation of Ag as Ag_3AsS_4 is surely the promising Ag-recycling system, suggesting that the development of Ag-separation technique is the most important for the application of this process into real operation.

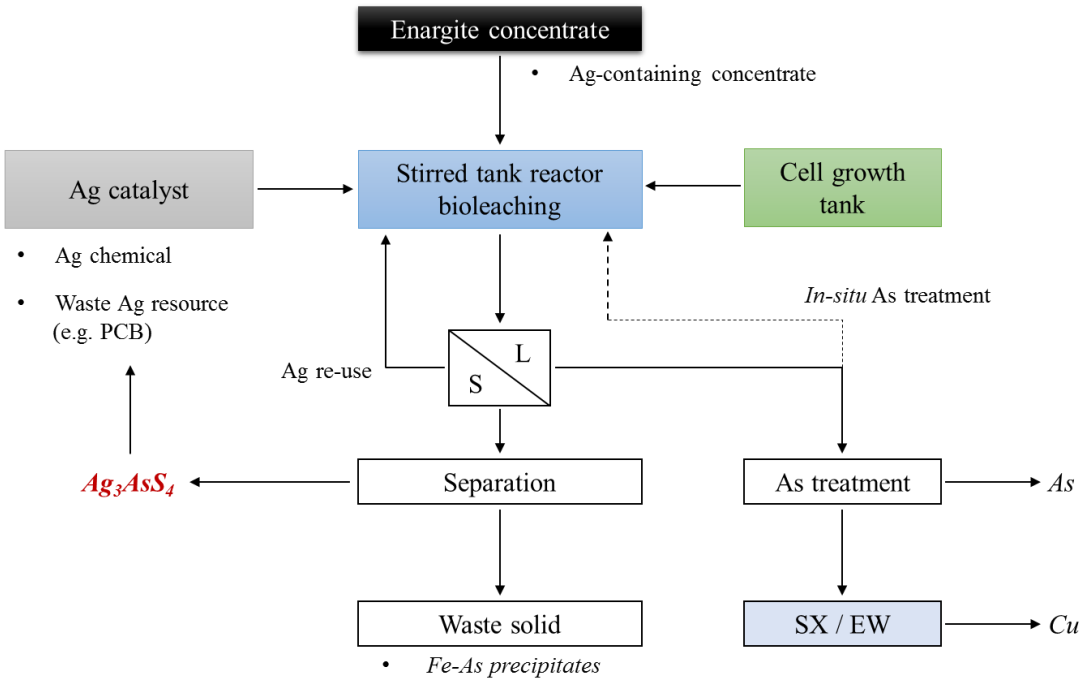

Fig. 8.2 Proposed flowsheet of Ag-catalyzed bioleaching of enargite concentrate.

In the AC-catalyzed bioleaching system, the basic concept of the process is similar to that in the presence of Ag; since AC is the more economical catalyst, the separation step is excluded (Fig. 8.3). The re-use of solid residue containing AC as the catalyst is, however, desirable for the low-cost process; this indicates that the investigation of repeatedly used AC in bioleaching provides us the valuable information. Based on the findings in this work, graphene structure was found a key factor controlling E_h behavior. This implies that graphite with high specific surface area could be replaceable with much stronger catalytic ability. Therefore, bioleaching of enargite concentrate using ultrafine graphite must also be tested for the further developed carbon-assisted bioleaching system.

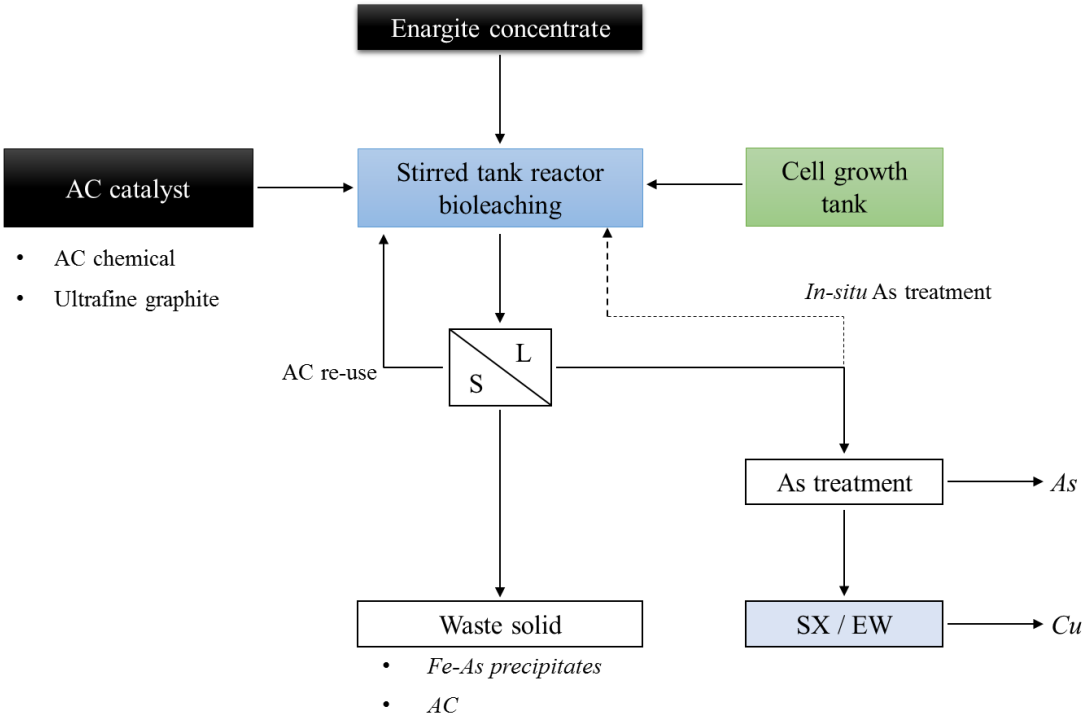

Fig. 8.3 Proposed flowsheet of AC-catalyzed bioleaching of enargite concentrate.

In both cases, As immobilization process still needs to be improved to achieve the selective leaching of Cu rather than As. Solubilized As is post-treated to be removed from the leachate, which is the reason of high-cost processing. In order to eliminate this post-treatment process, transferring the As-containing leachate back to the tank reactor is thought advantageous in *in-situ* As immobilization as Fe-As precipitates. Especially for AC-catalyzed bioleaching, circulation of As-containing leachate enables to gradually oxidize the As(III) to As(V), with former being mobile than the latter, which establishes the appropriate condition for further As immobilization. It is also expected that this circulation facilitates the aging of amorphous precipitates to highly crystalline scorodite ($FeAsO_4 \cdot 2H_2O$). Therefore, stable As immobilization would be achievable, realizing safety Cu production from As-bearing concentrate.

Acknowledgements

First of all, I would like to express my sincere gratitude to my supervisor, associate Prof. Naoko Okibe, for her warm supervision, supports and encouragement throughout my doctor's course. Almost 9 years have passed since I met her for the first time, she always put her efforts into giving me opportunities to improve my research skills. I could not finish this work without her help. I am really honored to be her PhD student.

Besides, I would like to thank Prof. Tsuyoshi Hirajima, Prof. Keiko Sasaki, and associate Prof. Hajime Miki for their kind advices and constant encouragements. They always showed me what the ideal researcher is. I also wish to acknowledge the secretary in our lab., Mrs. Makiko Semba, for her technical supports.

I would like to show my appreciation to Prof. Hiroaki Nakano from Department of Materials Science and Engineering, Kyushu University as a member of my thesis committee, for his important suggestions and invaluable comments.

My appreciation also goes to Dr. Sabrina Hedrich, Dr. Axel Schipper, Dr. Ruiyong Zhang from Bundesanstalt fur Geowissenschaften und Rohstoffe (BGR), Germany. Dr. Naoaki Kataoka and Mr. Ono from Swing Corporation for accepting me as an internship student and for taking care of me.

I would like to thank associate Prof. Maiko Nishibori (Department of Energy and Material Sciences, Kyushu University), associate Prof. Junichiro Ishibashi and Mr. Kazuhiko Shimada (Department of Earth and Planetary Sciences, Graduate School of Science, Kyushu University), for giving me a valuable opportunity of lab-rotation. My special thanks also go to assistant Prof. Takahiro Funatsu and Ms. Miwa Hirashima and Ms. Minako Matsue in Advanced Graduate Program in Global Strategy for Green Asia, for their kind supports.

I would like to express my appreciation to Advanced Graduate Program in Global Strategy for Green Asia. This educational program provided me with meaningful opportunities to learn and understand a relationship between technologies and society. I am also grateful for financial support provided by the program.

I would like to show my acknowledgment to JX Nippon Mining & Metals Corporation for kindly providing us with enargite concentrate.

The XAFS experiments were performed at Kyushu University Beamline (Saga-

LS/BL06) with the proposal of No. 2016IK003, 2016IIK013, and 2016IIIK006 under the supervision of associate Prof. Takeharu Sugiyama.

Many thanks to Lab. Members in Mineral Processing, Recycling and Environmental Remediation Laboratory as follows; Dr. Sayo Moriyama, Dr. Mohsen M. Farahat, Dr. Ahmed M. Elmahdy, Dr. Paulmanickam Koilraj, Dr. Widi Astuti, Dr. Mutia Dewi Yuniati, Dr. Wuhui Luo, Dr. Yusei Masaki, Dr. Atsunori Tayaoka, Dr. XiangChun Liu, Dr. Gde Pandhe Wisnu Suyantara, Dr. Binglin Guo, Dr. Intan Nurul Rizki, Dr. Masahito Tanaka, Dr. Santisak Kitjanukit, Dr. Kojo Twum Konadu, Dr. Chitiphon Chuaicham, Masaharu Koga, Masashi Maki, Shiori Morishita, Taichi Momoki, Osamu Ichikawa, Mari Yoshida, Yuken Fukano, Daisuke Nakayama, Hidekazu Matsuoka, Yu Takaki, Kenta Toshiyuki, Akinobu Iguchi, Katsutoshi Tsutsumi, Takahiro Matsumoto, Tsubasa Oji, Akihiro Inoue, Shugo Nagato, Kazuyoshi Oka, Melisa Pramesti Dewi, Yuta Era, Takeru Fukumori, Taigen Masuyama, Ryota Matsushita, Yusuke Hotta, Kyohei Takamatsu, Yuta Kamura, Yoshikazu Hayashi, Yu Hirayama, Yukihiro Muta, Tian Quanzhi, Ryohei Nishi, Haruki Noguchi, Shunsuke Imamura, Shingo Nakama, Shogo Nagano, Yu Tanaka, Yuya Komori, Yuta Orii, Yuna Watanabe, Kinato Yagi, Wang Mengmeng, Diego Moizes Mendoza Flores, Kohei Nonaka, Kaito Hayashi, Ryotaro Sakai, Zenta Shirozu, and Yuki Semoto. It was great pleasure to be together in the laboratory.

Last but not least, my great respect and gratitude go to my parents, Kumi Oyama and Eiji Oyama, for their affectionate support and encouragement.

March 2020, Keishi Oyama
Kyushu University
Fukuoka, Japan